ҚАЗАҚСТАН РЕСПУБЛИКАСЫ
ҒЫЛЫМ ЖӘНЕ ЖОҒАРЫ БІЛІМ МИНИСТРЛІГІ

SATBAYEV UNIVERSITY
МЕТАЛЛУРГИЯ ЖӘНЕ КЕН БАЙЫТУ ИНСТИТУТЫ

ISSN 2616-6445 (Online)
ISSN 2224-5243 (Print)
DOI 10.31643/2018/166445

Минералдық шикізаттарды кешенді пайдалану

3(334)

Комплексное Использование Минерального Сырья

Complex Use of Mineral Resources

ШІЛДЕ-ҚЫРКҮЙЕК 2025
JULY-SEPTEMBER 2025
ИЮЛЬ-СЕНТЯБРЬ 2025

ЖЫЛЫНА 4 РЕТ ШЫҒАДЫ
QUARTERLY JOURNAL
ВЫХОДИТ 4 РАЗА В ГОД

ЖУРНАЛ 1978 ЖЫЛДАН БАСТАП ШЫҒАДЫ
JOURNAL HAS BEEN PUBLISHING SINCE 1978
ЖУРНАЛ ИЗДАЕТСЯ С 1978 ГОДА

АЛМАТЫ - 2025

Редакция мекен жайы:
Металлургия және кен байыту институты
050010, Қазақстан Республикасы, Алматы қ., Шевченко к-сі, Уәлиханов к-нің қиылысы, 29/133,
Fax. +7 (727) 298-45-03, Tel. +7-(727) 298-45-02, +7 (727) 298-45-19
E mail: journal@kims-imio.kz, product-service@kims-imio.kz
http://kims-imio.com/index.php/main

«Минералдық шикізаттарды кешенді пайдалану» журналы ғылыми жұмыстардың негізгі нәтижелерін жариялау үшін Қазақстан Республикасы Білім және ғылым министірлігінің Білім және ғылым сапасын қамтамасыз ету комитеті ұсынған ғылыми басылымдар тізіміне енгізілген.
Меншік иесі: «Металлургия және кен байыту институты» АҚ

Журнал Қазақстан Республикасының Ақпарат және коммуникация министрлігінің Байланыс, ақпараттандыру және бұқаралық ақпарат құралдары саласындағы мемлекеттік бақылау комитетінде қайта тіркелген

2016 ж. 18 қазандағы № 16180-Ж Куәлігі

Address:
Institute of Metallurgy and Ore Beneficiation
29/133 Shevchenko Street, corner of Ch. Valikhanov Street, Almaty, 050010, Kazakhstan
Fax. +7 (727) 298-45-03, Tel. +7-(727) 298-45-02, +7 (727) 298-45-19
E mail: journal@kims-imio.kz, product-service@kims-imio.kz
http://kims-imio.com/index.php/main

The Journal "Complex Use of Mineral Resources" is included in the List of publications recommended by the Committee for Control in the Sphere of Education and Science of the Ministry of Education and Science of the Republic of Kazakhstan for the publication of the main results of scientific activities.
Owner: "Institute of Metallurgy and Ore Beneficiation" JSC

The Journal was re-registered by the Committee for State Control in the Sphere of Communication, Information and Mass Media of the Ministry of Information and Communication of the Republic of Kazakhstan.

Certificate № 16180-Ж since October 18, 2016

Адрес редакции:
Институт Металлургии и Обогащения
050010, Республика Казахстан, г. Алматы, ул. Шевченко, уг. ул. Валиханова, 29/133,
Fax. +7 (727) 298-45-03, Tel. +7 (727) 298-45-02, +7 (727) 298-45-19
E mail: journal@kims-imio.kz, product-service@kims-imio.kz
http://kims-imio.com/index.php/main

Журнал «Комплексное использование минерального сырья» включен в Перечень изданий, рекомендуемых Комитетом по контролю в сфере образования и науки Министерства образования и науки Республики Казахстан для публикации основных результатов научной деятельности.
Собственник: АО «Институт металлургии и обогащения»

Журнал перерегистрирован в Комитете государственного контроля в области связи, информатизации и средств массовой информации
Министерства информации и коммуникации Республики Казахстан
Свидетельство № 16180-Ж от 18 октября 2016 г.

Crossref

creative commons

DOI: 10.31643/2025/6445.23
Engineering and Technology

Effect of Infill Patterns and Print Orientation on the Mechanical Properties of Manufactured Polylactic Acid Parts

[1]Hamoud M., [2]Abdal-Aziz O., [1]Barakat A., [1]Gad A.

[1]Faculty of Engineering, Helwan University, Cairo, Egypt
[2]Department of Basic Science Engineering, Canadian International College, Giza, Egypt

** Corresponding author email: Omnia_mohsen@cic-cairo.com*

Received: *May 15, 2024*
Peer-reviewed: *May 20, 2024*
Accepted: *June 20, 2024*

ABSTRACT

The fused deposition modeling (FDM) technique produces function models of various thermoplastic polymers and is one of the most commonly utilized additive manufacturing (AM) technologies. The purpose of this research is to study how combining infill pattern (CIP) and printing orientation affects tensile characteristics and building time. Polylactic acid (PLA) was chosen as a material for the specimen's fabrication. The print orientations were the on-long-edge and flat orientations. Because the product is built along the z-axis, the short-edge (up-right) orientation was not considered, resulting in minimal strength. The combinations of the infill patterns called Concentric, Cross, Triangle, Zigzag, Rectilinear, Cubic, Honeycomb, and Grid were investigated with 70% infill density and 0.15 mm layer thickness with a layer-by-layer strategy. The result indicates that the printing orientation significantly affected the tensile strength, especially in CIP specimens. The on-long edge orientation of the CIP specimen had higher tensile strength. The specimen Concentric/Triangle has the highest tensile strength in flat and on-long edge orientations of 30 MPa and 33 MPa, respectively. Still, the building time in flat orientation was long (25 min.) while the printing time in on-long orientation was short (29 min.). The honeycomb/Triangle combination represents lower tensile strength in both orientations of 19 MPa for flat and 20 MPa for on-long edge, but the building time in both orientations was long (14 min and 35 min, respectively). As a result, the specimen with the CIP has greater tensile strength than the single-infill pattern specimen. It was additionally found that when the Triangular pattern was combined with other patterns, the tensile strength of those patterns improved. CIP specimens built in an on-edge orientation had a higher tensile strength than those built in a flat orientation. In the triangle infill pattern, when combined with other patterns, the tensile strength of some samples enhanced while the others improved, while others decreased.

Keywords: Fused deposition modeling (FDM), additive manufacturing (AM), Polylactic acid (PLA), layer-by-layer, printing orientation, Combined infill patterns (CIP), build orientation.

Information about authors:

Mohamed Hamoud Ahmed — *Assistant professor, Mechanical Engineering Department, Faculty of Engineering, Helwan University, Cairo, Egypt. Email: Dr_hamoud2015@h-eng.helwan.edu.eg*

Omnia Mohsen Mohamed Abdalaziz — *Assistant Lecturer, Mechanical Engineering Department, Faculty of Engineering, Canadian International College, Cairo, Egypt. Email: Omnia_mohsen@cic-cairo.com*

Azza Fathallah Mostafa Barakat — *Professor, Mechanical Engineering Department, Faculty of Engineering, Helwan University, Cairo, Egypt. Email: barakatazza@h-eng.helwan.edu.eg*

Ahmed Sobhi Mohamed Gad — *Dr., Mechanical Engineering Department, Faculty of Engineering, Helwan University, Cairo, Egypt. Email: a.sobhi.m@gmail.com*

Introduction

The additive manufacturing (AM) techniques are known as three-dimensional printing (3DP) technology. This method produces 3D objects with lightweight and complicated structures [1]. 3D printers have been used in various applications in recent years such as architectural configurations, prototype manufacturing, and medical applications. The AM techniques include FDM, digital light processing, laminated object manufacturing, and stereo lithography which depend on the material's types, the production tolerances, and the product's application [2]. The main disadvantage of these techniques is their longer production time and low part strength compared to other traditional manufacturing techniques. That is why they cannot be used for mass production. FDM technology is one of the greenest and most economical 3D printing processes since it produces functional prototypes that use different thermoplastic filaments as a starting material [3]. There are various types of thermoplastic filaments such as Acrylonitrile Butadiene Styrene (ABS), Polylactic acid (PLA), Nylon, Thermoplastic elastomer (TPE), High-Impact Polystyrene (HIPS), polypropylene (PP), and other thermoplastic polymer materials are available for

FDM method for different purposes. These filaments have been used as synthetic polymer components due to their processability, mechanical flexibility, physicochemical capabilities, and ability to withstand significant deformations [4]. In this way, the filaments are heated in the nozzle and are then dispensed on the printing plate layer-by-layer to produce the desired 3D structure [5]. This enables the manufacturing of complex products that are difficult to be modeled by subtractive processes. Such techniques are now used in industries to shorten the time and cost involved in product development [[6], [7]]. However, the FDM draws some significant disadvantages including poor mechanical qualities, surface finish, and inferior dimensional quality [8]. The quality of the product is attributed to process parameters such as layer thickness, infill pattern, infill density, nozzle temperature, build orientation, print speed, and raster angle [9]. Notably, various works studied the FDM specimen properties in association with the parameters of the printing process [10]. Chacon et al. investigated the impact of layer thickness, building orientations, and rate of feed on the PLA specimens' tensile strength with the FDM process [11]. They found that as the layer thickness of the specimen decreased, the resulting strength increased, while the strength varied significantly for the sample with a flat orientation. In addition, Durgun et al. explored the improvement of production cost and mechanical properties for the FDM process [12]. It had been concluded that the build orientation had a greater impact on surface roughness and the ABS polymer's strength than the raster orientations. Aloyaydi et al. studied how infill patterns affect FDM parts' compression strength [13]. The Grid type pattern showed the greatest compressive strength, while the Triangular pattern had higher impact energy. Further, Mishra et al. investigated the influence of FDM printing variables and the thickness of layers on the strength [14]. It was found that the strength of FDM parts increases as the wall layer increases. The influence of printing variables such as the air gap and raster angle on FDM's specimen strength has been examined by Ahn et al. [15]. They discovered that the air gap and raster angle significantly affect the strength. Wang et al. studied the PLA specimen's mechanical properties under various printing parameters using the 3D-printing process [16]. They concluded that the height of the layer influences the layer bonding of 3D-printed samples' strength. Yang et al. investigated five printing parameters to find out their effect on building time, strength, and surface roughness utilizing the analysis of variance test (ANOVA) [17]. They showed that the layer thickness and the nozzle diameter had the most impact on tensile strength and surface roughness. Sukindar et al. examined the nozzle diameter and the impact of pressure drop on product quality by comparing different extruder angles and diameters using finite element analysis (FEA) and testing procedures. In their work, the low strength in FDM-printed samples is considered a drawback that results from poor layer binding [18]. In addition, poor adhesion between layers is caused by temperatures or parameters that are not optimized. Furthermore, Moradi et al. worked on 3D-printed Honeycomb internal pattern samples with FDM technology [19]. Compared with other infill patterns, Honeycomb patterns showed a higher mechanical resistance. Besides, Akhoundi et al. examined the effect of binding and adhesion after printing, regarding various patterns such as concentric, rectilinear, Honeycomb, and Hilbert curves, on the strength of the final product [20]. The research focused on the infill pattern and infill percentage of 3D-printed PLA parts. Accordingly, Hanon et al. investigated the strength of PETG (polyethylene terephthalate-glycol) and PLA, comparing the two materials in a variety of building orientations (from +45° to -45°) using Honeycomb and Straight patterns [21]. Better elongation results were indicated by PETG which enhances the highest tensile strength possible value in Y orientation with a 0° raster direction. Also, they improve the flexural rigidity by decreasing its value below 10%. Moreover, Samykano et al. analyzed the parameters of the FDM utilizing an improved mathematical model [22]. Their findings indicated that the optimized parameters for ABS material were 80% density, 65° raster angle, and 0.5 mm thickness of layer. Li et al. proved that layer height is the main factor influencing the strength of bonding, followed by deposition velocity [23]. It was noticed that the infill rate has a negligible effect. The mechanical characteristics of the FDM parts employing standard laminate theory were explored by Casavola et al. [24]. Both Young's modulus and Ultimate Tensile Strength (UTS) decreased when the raster's angle increased from 0° to 90°, while samples at 45° showed mediate mechanical behaviors. Studying the effect of the raster angle on the strength, Rajpurohit et al. verified that a lower layer height and a 0° raster angle provide higher strength [25]. As well as the tensile strength increased as the raster width increased up to a point at which the tensile strength decreased. In the same manner, Dave et al. noticed higher tensile strength

of samples that were built into on-long edge and flat orientations with rectilinear and concentric infill patterns as compared to upright orientations [26]. Also, they confirmed that parts with Hilbert's curve infill patterns performed improved when oriented along the short edge compared to the long edge. In comparison with the strength of ABS monofilaments, Rodrigues et al. viewed degradation in the FDM specimens' strength due to the existence of losses and void of molecule's orientation throughout the extrusion procedure [27]. However, Lederle et al. performed material extrusion in an inert gas atmosphere and found that both ABS and nylon copolymer materials had been mechanically enhanced [28]. Utilizing different materials, Wu et al. compared various parameters of a specific material with those of the ABS specimen [29]. They utilized the polyether-ether-ketone (PEEK) specimens to be examined. The results ensure that the PEEK had good strength performance comparable with the ABS specimen as it recorded 114% higher compressive strength, 115% higher bending strength, and 108% higher tensile strength. Ziemian et al. reported greater fatigue life for 0° and + 45°/− 45° raster orientations under tension-tension fatigue testing when compared to transverse (90°) and diagonal (45°) raster orientation [30]. Witkin et al. investigated how the building orientations affected the thermal and mechanical properties of polyetherimide (ULTEM) specimens that were printed using FDM and found that the thermal expansion coefficient varied according to the orientation [31]. Alvarez et al. found that for hexagonal infill patterns, infill percentages ranging from 50% to 98% resulted in longer printing times and lower tensile strength [32]. Furthermore, Shih et al. found that PLA specimens, which were treated with cold plasma, had a higher strength of interlayer bonding than PLA samples that were left untreated. They also observed that the bonding strength had been adversely affected by the treatment time [33]. Lee et al. examined forced air cooling's effects on PLA specimens manufactured [34]. They concluded that using the FDM method and at greater airflow velocities conditions (5 m/s), a trade-off between the dimensional quality and the strength had occurred since the dimensional quality was improved while the mechanical strength was decreased. Bin Ishak et al. used material deposition for various building orientations in a single product in several planes [35]. For the upright printed samples, they observed developments in yield strength, modulus of elasticity, and (UTS). Currently, research has been presented about the impact of the combined infill pattern on the mechanical behavior of parts. In this line, Mohd Ariffin et al. combined (MIP) multiple infill patterns in a sample with different build orientations and found the effect on mechanical properties, as shown in Fig. 1 [36]. To design the patterns, they used CAD software which indicated that the FDM process was unable to combine patterns on its own. As a result, the Grid and Honeycomb patterns have the maximum ultimate tensile strength with the lightest weights, while the build orientation had significant effects on the mechanical characteristics.

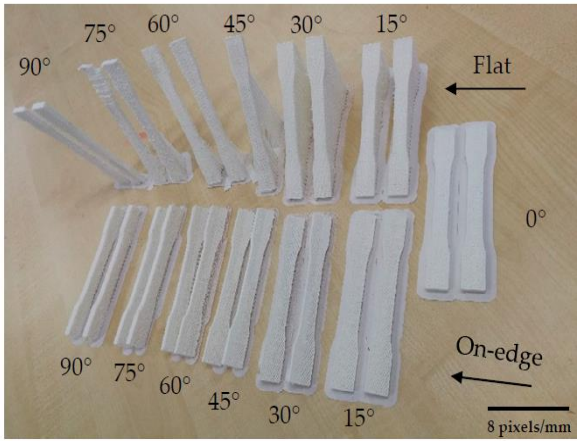

Fig. 1 - Set of classified layers and 3DP printed PLA samples

Similarly, Patel et al. studied the part's ultimate tensile strength with a combined infill pattern with different infill densities, and sequences of layer staking for various raster's orientations using the FDM technique, as shown in Fig. 2 [37]. While compared to single infill pattern samples, the results showed that the arrangements of combined infill and stacking of layer had a significant impact on the strength for the 45° raster's orientation.

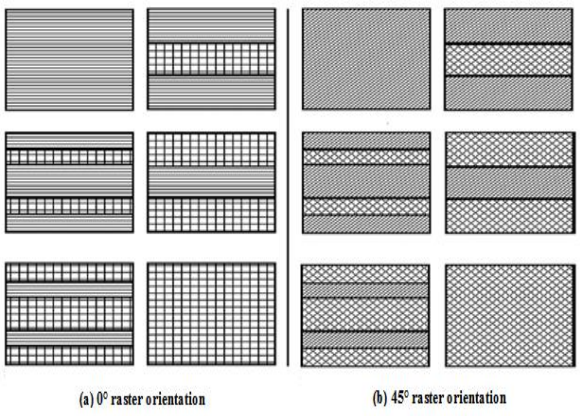

Fig. 2 - Various staking of layers for different infill densities and raster orientations.

However, Roger et al. used topological optimization in such a way the structural design of the 3D-built printed parts had been optimized, as shown in Figs. 3 and 4 [38]. They combined the heterogeneous infill types while printing the sample using the FDM technique to achieve their targeted properties.

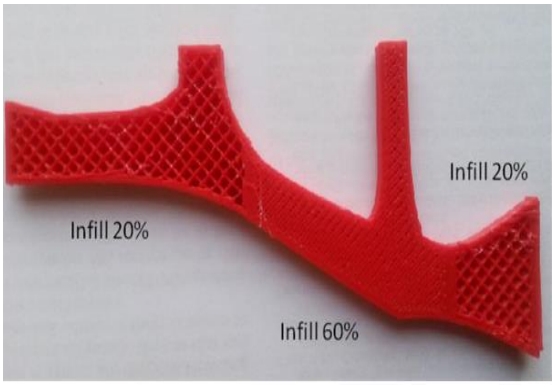

Fig. 3 - Inner rectilinear filling of the optimized structure with different densities

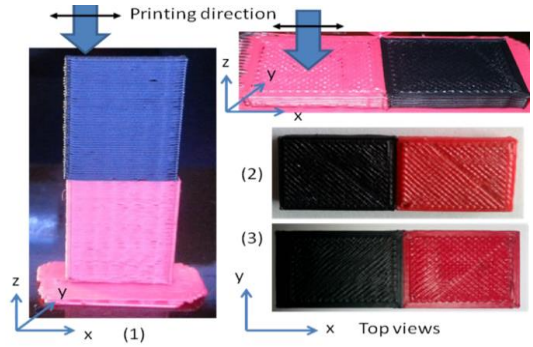

Fig. 4 - Bimaterial samples: (1) vertical printing, (2) horizontal printing with side-by-side parts, and (3) horizontal printing with side-by-side and interpenetrated layers at the interface

(a) Flat orientation (XY)

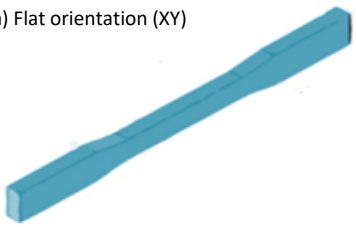

(b) On-long orientation (ZX)

Fig. 5 - 3DP printed tensile parts with different build orientations

Moreover, Naik et al. investigated the effects of raster angles on the UTS of multiple infill patterns (MIP) items produced with the FDM technique (Fig.5) [39]. The findings indicated that single-infill pattern samples had less tensile strength than MIP parts. Also, they found that MIP parts built-in on long orientation had high UTS/mass ratios and UTS.

Finally, Sajjad, R et al. examined the influence of combined infill strategies on the structural strength of single-build samples using FDM technology, as shown in Fig. 6 [3]. The experimental results have shown that the combinations of triangular and rectangular patterns led to 20%, 13%, 27%, and 4% increments in ratio of strength-to-weight compared with Triangular type, Rectilinear type, Rectangular type, and Honeycomb type single infill, respectively. In addition, along with minimal production cost, the rectangular infill combination with the Triangle patterns possessed the optimum strength-to-weight ratio.

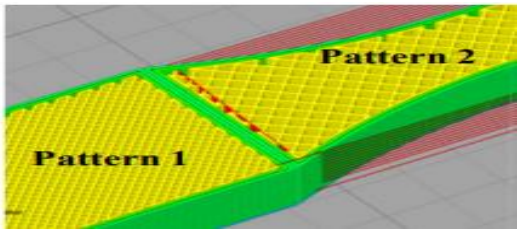

Individual infills	Possible combinations of filling patterns			
	Pattern 1	Pattern 2	Pattern 1	Pattern 2
Rectilinear	Rectilinear	Honeycomb	Honeycomb	Rectilinear
Triangle	Triangle	Rectangular	Rectangular	Triangle
Rectangular	Triangle	Honeycomb	Honeycomb	Triangle
Honeycomb	Rectangular	Honeycomb	Honeycomb	Rectangular

Fig. 6 - Printing of combinations of chosen infill patterns with various types of infill patterns

To the best of the author's knowledge, few studies have been accomplished on the effect of the combined infill patterns and some printing variables like building orientation on the tensile properties and 3D printing time of FDM products. There are requirements for a study on the effect of single and CIP on the tensile properties of FDM-printed PLA parts. Hence, in this study, experimental investigations were carried out to understand the impact of a CIP at different building orientations and infill patterns on the strength of FDM-printed PLA parts. To fabricate the specimens, a customized G-code file was prepared to print CIP specimens, and the uniaxial tensile tests were carried out to investigate mechanical responses in terms of tensile strength. It was noticed that the tensile strength for

some CIP specimens has been increased as well as the printing time has been decreased.

Experimental part

FDM-based printer and material

In this study, an open-source 3DP with the FDM technique was utilized for the samples' fabrication. The 3D printer had a print-bed of 500 × 500 × 500 mm^3. As shown in Fig. 7, the 3D printer may use several different thermoplastic materials such as PLA, ABS, and PEEK. In our work, the PLA material was selected because of its high modulus and strength. Also, the manufacturer specifications of the PLA filament and the 3DP parameters are presented in Table 1 and Table 2.

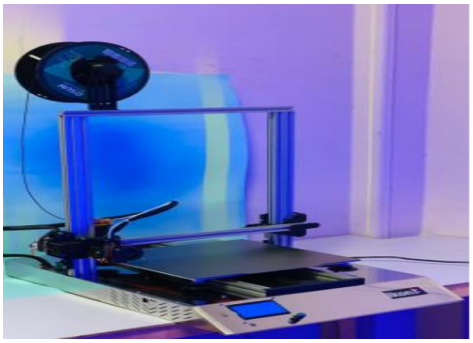

Fig.7 - Open source FDM 3D printer

Table 1 - PLA material properties by the manufacturer

Description	Typical value
Filament diameter	1.75 mm
Tensile Strength at Yield	65 MPa
Flexural modulus	2102 MPa
Flexural strength	75 MPa
Elongation at break	12 %
Density	1.25 g/cm^3
Printing temperature	205-225 ˚C
Melting temperature	115 ± 35 ˚C

Table 2 - Main printing parameters of the 3DP machine

Description	Value
Nozzle diameter	0.4 mm
Layer height	0.15 mm
Wall thickness	0.7 mm
Infill density	100 %
Print speed	60 mm/s
Printing temperature	200 ˚C
Build plate temperature	60 ˚C
Line width	0.35 mm

Experimental design for fabrication of specimens

Print orientations are the most significant process parameters affecting the quality of CIP products, among other printing parameters. The CIP specimens were designed and fabricated as dog bone shapes according to the ASTM D638 standard for tensile test measurement, as shown in Fig. 8. The build orientations of the part are defined by placing the specimen models concerning the x-axis. There were two print orientations were considered (flat and on-edge) with 70% infill density and 0.15 mm layer thickness using the layer-by-layer (LBL) printing strategy, as shown in Fig. 9. Since the part in the upright orientation is built along the z-axis, resulting in the minimum strength, this orientation was not considered. The CIP models were created using the Cura 3DP software, version 5.1.0, as shown in Fig 10. It consists of different layers of single infill patterns, which involve Concentric, Cross, Triangle, Zigzag, Rectilinear, Cubic, Honeycomb, and Grid pattern types, respectively, as shown in Fig 11.

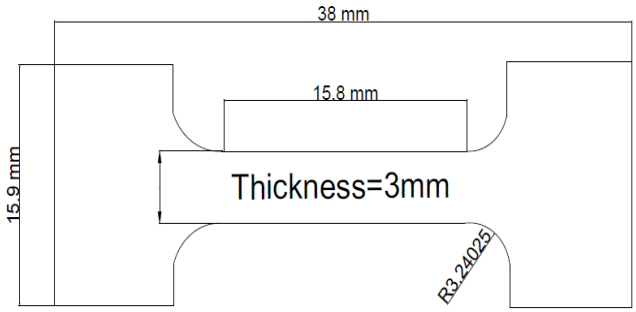

Fig.8 - Tensile specimen with dog bone shape (Dimensions were in mm)

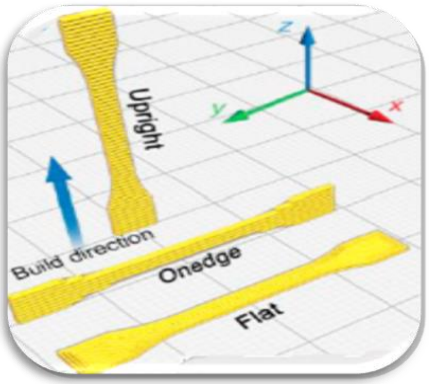

Fig. 9 - 3D-printed tensile specimens with different orientations

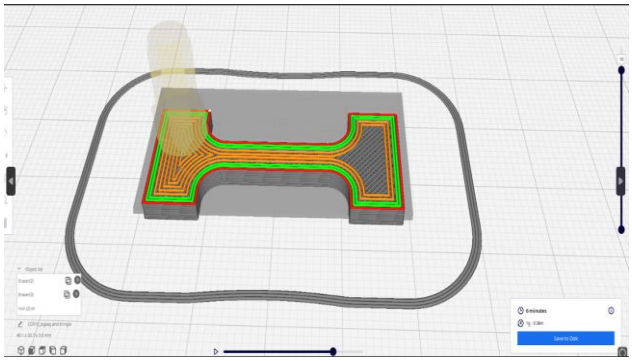

Fig. 10 - FDM 3D printer on Cura software

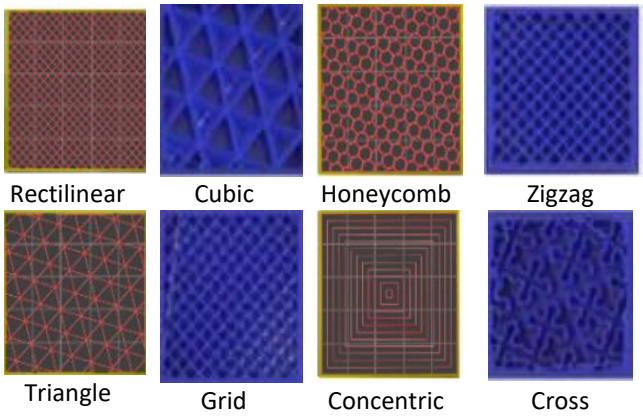

Fig. 11 - Infill patterns of the 3D printed PLA

Specimen fabrications

Based on the ASTM D638 standard, 3D models of the tensile specimen were designed in Solid Works. The models are exported in STL files format and transferred to the slicer software, where the whole cross-sections of the 3D models are converted to individual layers of a specific layer thickness with the adjustment of the process parameters then the files are exported in G-Code format which is assigned to a 3DP using PLA filaments. By considering CIP, the shell feature is used for printing the boundary of the parts, while for the inner sections.

Tensile test

Each specimen is tested using a Zwick/Roell Z010 tensile testing machine by the ASTM D638 standard; this machine is shown in Fig. 12. This machine has a load cell that can measure loads up to 10 kN. Additionally, it has built-in software that enables the recording, control of measured data, and monitoring. Between the two jigs, the tensile specimen (a dog bone) is gripped and tightened. To monitor and record the material deformation until the specimen fractures, the speed's crosshead is retained at 2 mm/min during the entire test. After that, the test is stopped, and the crosshead motion resumes, returning to its starting point. Through the data acquisition system, data test is collected from the software. The 3D-printed dog-bone specimens after mechanical testing are shown in Fig. 13.

Fig. 12 - 3D printed dog-bone specimens during testing using mechanical testing machine Zwick/ Roell Z010 according to ASTM D638.

Fig. 13 - The fractured 3D printed dog-bone specimens after testing using mechanical testing machine Zwick/ Roell Z010 according to ASTM D638

Results and Discussion

Results

In the present work, investigations were carried out to study the tensile behavior of CIP printed parts of different orientations. All of the experiments are carried out by the previously discussed experimental design and tested. In this section, the results obtained through the tensile test of the FDM samples with CIP are discussed.

Effect of the combined infill patterns and printing orientation on tensile strength

For studying the effect of the combined infill pattern on the strength and printing or building time of PLA samples, four samples were printed as a single infill pattern (Concentric, Cross, Triangle, and Zigzag), and then each two types of these patterns were combined. The six combined samples (Concentric/Cross, Concentric/Triangle, Concentric/Zigzag, Cross/Triangle, Cross/Zigzag, and Triangle/Zigzag) were obtained via the layer-by-layer printing strategy, which means layer infill type by layer of different infill types with flat and on-long edge orientations. Table 3 and Table 4 represent the results of tensile strength for different orientations of single and combined infill patterns. It was noted that the Triangle pattern improved significantly the strength of the sample. Thus, four other different patterns (Rectilinear, Cubic, Honeycomb, and Grid) were printed and combined with the Triangle pattern. Accordingly, four combined samples were obtained (Rectilinear/Triangle, Cubic/Triangle, Honeycomb/Triangle, and Grid/Triangle), and the effect of the Triangle pattern after combining them with on the tensile strength was studied as presented in Table 5.

Table 3 - Tensile strength of PLA samples printed with different types of single infill patterns

Infill type	Tensile strength (MPa)	
	Flat	On-long edge
Concentric	21	31
Triangle	25	28
Cross	15	25
Zigzag	29	30
Grid	10	25
Cubic	10	26
Honeycomb	12	29
Rectilinear	15	32

Table 4 - Tensile strength of combined PLA samples using different infill patterns

Combined infill type	Tensile strength (MPa)		3D printing infill
	Flat	On-long	
Concentric /Cross	25	28	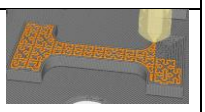
Concentric /Zigzag	27	30	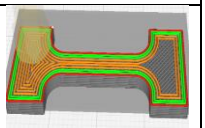
Concentric /Triangle	30	33	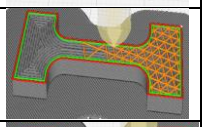
Triangle /Zigzag	22	31	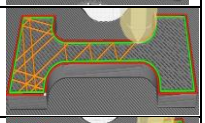
Triangle / Cross	23	29	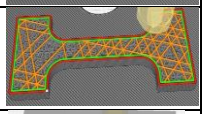
Cross / Zigzag	26	27	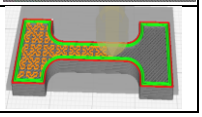

Table 5 - Tensile strength of PLA samples printed with Triangle pattern combined with different infill patterns

Combined infill type	Tensile strength (MPa)		3D printing infill
	Flat	On-long	
Triangle / Grid	21	24	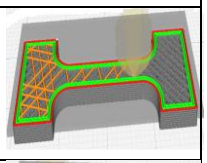
Triangle /Cubic	26	30	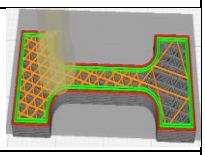
Triangle /Honeycomb	19	20	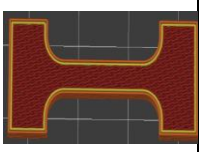
Triangle /Rectilinear	23	24	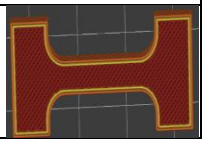

On the other hand, Fig. 14 shows the effect of different types of single infill patterns on the tensile strength of the PLA-printed samples at different orientations. In the case of the on-long orientation, a higher strength is observed for all samples than for

the other orientations. It is obvious that in the on-long edge orientation of the PLA samples printed with the single pattern, the Rectilinear infill pattern possessed the highest tensile strength (32 MPa), while in the flat orientation of the single pattern, the Zigzag pattern possessed the highest tensile strength (29 MPa), as shown in Fig. 14. On the other hand, the effect of different types of combined infill patterns on the tensile strength of the PLA-printed samples at different orientations is shown in Fig. 15. It was found that when some different patterns were combined, the strength of both infill patterns increased, such as Concentric/Triangle, Cubic/Triangle, and Concentric/Cross in the flat orientations, and Concentric/Triangle, Zigzag/Triangle, Cubic/Triangle, and Cross/Triangle in the on-long orientations. It was also found that the pattern that has high strength improves the pattern that has low strength when combining them, such as Concentric/Triangle, Concentric/Cross, Concentric/Zigzag, Cross/Zigzag, Cross/Triangle, Rectilinear/Triangle, Honeycomb/Triangle, Grid/Triangle, and Cubic/Triangle samples in flat orientations and Concentric/Triangle, Zigzag/Triangle, cubic/Triangle, Concentric/Cross, and Cross/Zigzag in on-long orientations, as shown in Fig. 15. It was also noted that when the Triangle infill pattern was combined with some patterns, some patterns improved while others decreased the tensile of the sample, as it was in Zigzag/Triangle with flat orientations and Grid/Triangle, Honeycomb/Triangle, and Rectilinear/Triangle with on-long orientation, as shown in Fig. 16.

Effect of the infill patterns and printing orientation on the building time of the PLA samples

Building time is an important parameter for the production of 3D-printed materials in industry. In this regard, the impact of printing orientations and the infill pattern of the FDM part on the building time was studied. Tables 6, 7, and 8 represent the results of the building time test for different orientations of single and combined infill patterns.

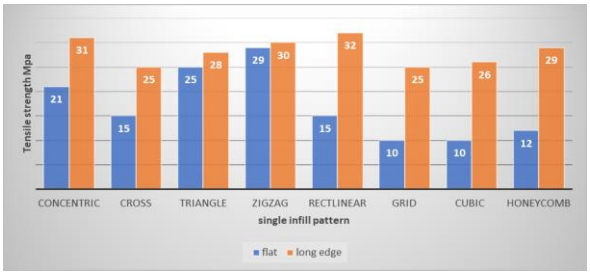

Fig. 14 - Effect of printing orientation on the tensile strength of PLA samples printed with different types of single infill patterns

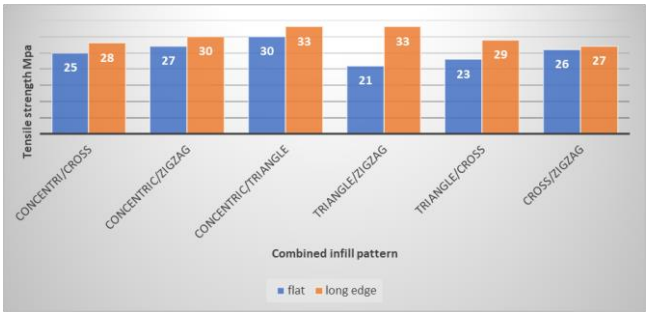

Fig. 15 - Effect of printing orientation on the tensile strength of PLA samples printed with different types of combined infill patterns

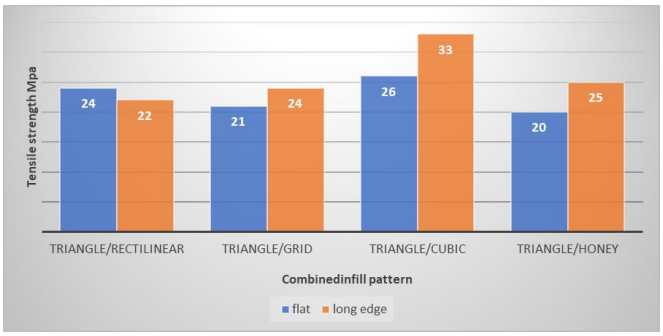

Fig. 16 - Effect of printing orientation on the tensile strength of PLA samples printed with Triangle combined with different types of infill patterns

Table 6 - Building time (min) of single PLA samples using different infill patterns printed orientation

Infill type	Building time (min)	
	Flat	On-long edge
Concentric	20	32
Triangle	18	31
Cross	22	33
Zigzag	18	30
Grid	13	25
Cubic	15	26
Honeycomb	12	29
Rectilinear	15	25

Table 7 - Building time (min) of combined PLA samples using different infill patterns printed orientation

Infill type	Building time (min)	
	Flat	On-long edge
Concentric/Cross	25	30
Concentric/Zigzag	26	28
Concentric/Triangle	25	29
Triangle/Zigzag	18	31
Cross/Triangle	20	32
Zigzag/Cross	17	32

Table 8 - Building time (min) of combined PLA samples using Triangle with different infill patterns printed orientation

Infill type	Building time (min)	
	Flat	On-long edge
Triangle/Grid	12	35
Triangle/Cubic	12	29
Triangle/Honeycomb	14	35
Triangle/Rectilinear	13	36

In the case of on-long orientation, a longer printing time is observed for all samples than for the other orientations. As seen from Fig. 17, for single infill patterns in the flat orientation, the Cross pattern had a longer time and the Honeycomb had a shorter time in the on-long orientation. As shown in Figs. 18 and 19, for the combined pattern, the Concentric/Zigzag pattern had a longer time in the flat orientation and Triangle/Rectilinear in the on-long orientation. Here it is interesting to note that there are samples that, when combined, the building time less than printing them individually, such as Concentric/cross, Concentric/Zigzag, Concentric/Triangle, Zigzag/Triangle, Cross/Triangle, and in on-long orientation, and Zigzag/Cross, Cubic/Triangle, Rectilinear/Triangle, and Grid/Triangle in flat orientation.

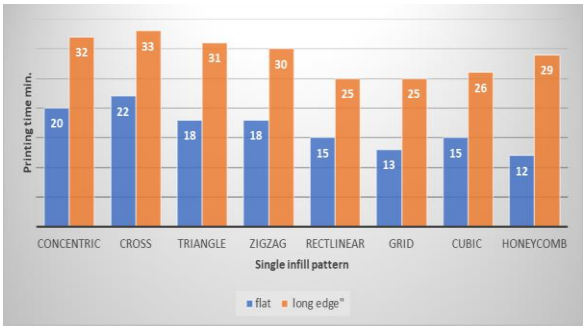

Fig. 17 - Effect of printing orientation of different single infill patterns on the building time of the PLA printed samples

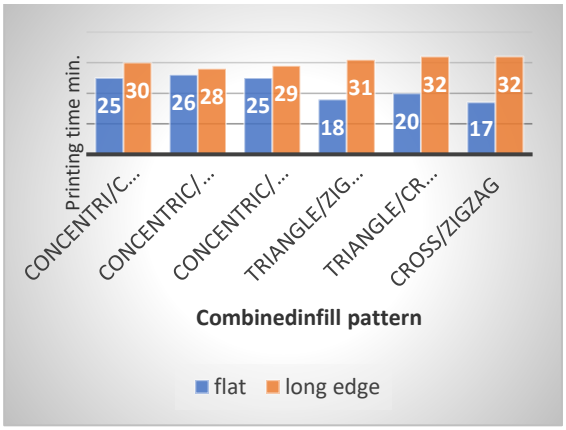

Fig. 18 - Effect of printing orientation of different combined infill patterns on the building time of the PLA printed samples

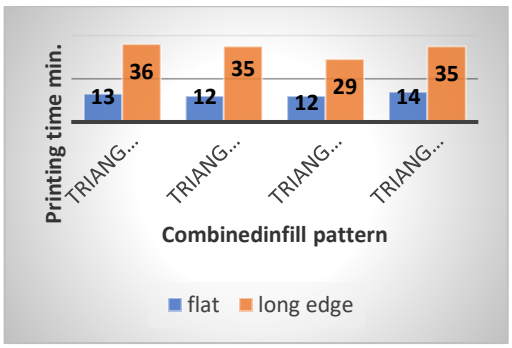

Fig. 19 - Effect of printing orientation of Triangle with different types of infill patterns on the building time of the PLA printed samples

Discussion

After deep research, it was found that not much research has been accomplished on the effect of the combined infill patterns and some printing variables like building orientation on the tensile properties and 3D printing time of FDM products. There are requirements for a study on the effect of single and CIP on the tensile properties of FDM-printed PLA parts. Hence, in this study, experimental investigations were carried out to understand the impact of a CIP at different building orientations and infill patterns on the strength of FDM-printed PLA parts.

In the case of the on-long orientation, a higher strength is observed for all samples than for the flat orientation due to vertically stacked layers and these layers are perpendicular to the applied force during the tensile test and have good adhesion of layers because each layer acts as a reinforcing element for the layers below and above it additionally it provides better structural integrity. In flat orientation, the applied force is parallel to the layers leading to weaker interlayer bonding, and interlayer boundaries may act as stress concentrators, making failure of the product.

In the on-long edge orientation of the single pattern, the Rectilinear infill pattern possessed the highest tensile strength because it offers good structural integrity and efficient material usage.

While in the flat orientation of the single pattern, the Zigzag pattern possessed the highest tensile strength. This is because of its interlocking Structure, increased Contact Area, and improved Layer Adhesion.

The PLA samples printed using a combination of Concentric and Triangle patterns possessed the highest strength in both orientations (flat and on-long) compared to their single counterparts. The synergistic improvement in the strength of the two

samples can be due to several factors: enhanced interlayer adhesion, increased surface area, improved load distribution, and structural integrity.

Moreover, its printing time decreased, particularly in the on-long orientation, and increased in the flat orientation as compared to its single counterparts.

When the Triangle and Cubic samples were combined and printed in the flat orientation, the strength of the two single samples improved because these patterns were regular and repetitive, they helped to distribute stress uniformly throughout the print, minimizing the concentration of stress points that could cause failure and the building time was the shortest in the combined sample. Similarly, printing on the on-long orientation.

In the case of combined Concentric and Cross samples, an improvement in the strength of the two singular samples was found since it maximizes the print strength in both the X and Y axes when printed on a flat orientation. This is important because forces acting on a flat surface are usually distributed in both directions, making reinforcement in both directions required to prevent deformation, twisting, and bending, however, the building time was longer in the combined sample. Whereas, in the on-long orientation, an improvement was found in the Cross sample only, but the building time of the combined sample was the shortest.

After combining the Triangle and Cross patterns, an improvement in the strength of the two samples was found, in the case of on-long orientation by creating an interlocking structure, promoting better layer adhesion, offering directional strength, optimizing material usage, ensuring uniform stress distribution, enhancing rigidity, and simplifying the printing process, and the building time of the combined sample was the shortest. However, in a flat orientation, the strength of the cross pattern was improved due to its combination with the concentric pattern, the building time was longer in the combined sample.

When the Triangle and Zigzag samples were combined, an improvement in the strength of the two samples was found, this is because the Zigzag infill design adds support in multiple directions and increases overall strength, while the Triangle infill pattern helps with stability and resistance to bending., in the case of on-long orientation, and the printing time of the combined sample was the shortest.

So we can conclude from these results that when combining the Triangle infill pattern with other patterns, the effect on tensile strength can depend on several factors:

i. Complementary Patterns: Some infill patterns may complement the Triangle infill pattern, resulting in improved tensile strength. For example, combining the Triangle infill with a perpendicular or diagonal pattern can enhance the overall structural integrity by providing additional reinforcement and reducing stress concentration points.

ii. Conflicting Patterns: When the Triangular infill pattern is combined with some other patterns that may not distribute the material effectively or provide adequate support, it could lead to decreased tensile strength. The interaction between these patterns can result in weak points or inconsistencies in the structure, reducing its overall mechanical performance.

Conclusions

In this study, the impact of combined infill patterns and printing orientations has been examined, concerning the tensile and building time characteristics of PLA-based 3D-printed objects. Based on the experimental findings, the following major conclusions are drawn:

The results showed that CIP specimens built in an on-edge orientation had a higher tensile strength than those built in a flat orientation.

The PLA samples printed using a combination of Concentric and Triangle patterns possessed the highest strength in both orientations (flat and on-long) compared to their single counterparts. The synergistic improvement in the strength of the two samples was found to be 30% and 16.7%, respectively, in the case of the flat orientation and 6% and 15%, respectively, in the case of the on-long orientation. Moreover, its printing time decreased, particularly in the on-long orientation, and increased in the flat orientation as compared to its single counterparts.

When the Triangle and Cubic samples were combined and printed in the flat orientation, the strength of the two single samples improved by 3.8% and 61.5%, respectively, and the building time was the shortest in the combined sample. Similarly, printing on the on-long orientation, both samples improved by 6.7% and 3%, respectively, and the building time was the shortest in the combined sample.

In the case of combined Concentric and Cross samples, an improvement in the strength of the two singular samples was found to be 16% and 40%,

respectively, when printed on flat orientation, however, the building time was longer in the combined sample. Whereas, in the on-long orientation, an improvement was found in the Cross sample only by 10.7%, but the building time of the combined sample was the shortest.

After combining the Triangle and Cross patterns, an improvement in the strength of the two samples was found to be 3.4% and 13.7%, respectively, in the case of the on-long orientation, and the building time of the combined sample was the shortest. However, in a flat orientation, improvement was found in the Cross sample only by 34.7%, but then again, the building time was longer in the combined sample.

When the Triangle and Zigzag samples were combined, an improvement in the strength of the two samples was found to be 9.7% and 3.2%, respectively, in the case of on-long orientation, and the printing time of the combined sample was the shortest.

The Triangle infill pattern, when combined with some other patterns, the tensile strength of some samples enhanced while the others improved, while others decreased.

The printed PLA samples with the combined patterns Zigzag/Triangle and Concentric/Zigzag in the flat orientation and Grid/Triangle, Honeycomb/Triangle, and Rectilinear/Triangle in the on-long orientation have the lowest tensile strength and the highest building time. So, it is not recommended for future work.

Research recommendations. With PLA material, the present work is only valid for uniaxial loading. The way forward of this research may include the implementation of the proposed strategies for combined loading, shear, and flexural by using the same or different printing materials.

CRediT author statement. All authors contributed to this study. **M. Hamoud**: Conceptualization, Methodology, Software. **O. Abdal-Aziz**: Data curation, Writing draft preparation. **A. Barakat**: Visualization, Investigation. **A. Gad**: Supervision, Software, Validation, Reviewing and Editing.

Research Finance. This research did not receive any specific grant from funding agencies in the public, commercial, or not-for-profit sectors.

Cite this article as: Hamoud M, Abdal-Aziz O, Barakat A , Gad A. Effect of Combined Infill Patterns and Print Orientation on the Mechanical Properties of Manufactured Polylactic Acid Parts. Kompleksnoe Ispolzovanie Mineralnogo Syra = Complex Use of Mineral Resources. 2025; 334(3):5-18. https://doi.org/10.31643/2025/6445.23

Өндірілетін полилактикалық қышқыл бөліктерінің механикалық қасиеттеріне толтыру үлгілері мен басып шығару бағытының әсері

[1]Hamoud M., [2]Abdal-Aziz O., [1]Barakat A., [1]Gad A.

[1]Faculty of Engineering, Helwan University, Cairo, Egypt
[2]Негізгі ғылыми инженерия бөлімі, Канада халықаралық колледжі, Гиза, Египет

Мақала келді: *15 мамыр 2024*
Сараптамадан өтті: *20 мамыр 2024*
Қабылданды: *20 маусым 2024*

ТҮЙІНДЕМЕ

Балқытылған тұндыру арқылы модельдеу (FDM) әдісі әртүрлі термопластикалық полимерлердің функционалдық үлгілерін шығарады және ең жиі қолданылатын қоспаларды өндіру (AM) технологияларының бірі болып табылады. Бұл зерттеудің мақсаты толтыру үлгісі (CIP) мен басып шығару бағытын біріктіру созылу сипаттамаларына және құрастыру уақытына қалай әсер ететінін зерттеу болып табылады. Үлгіні жасау үшін материал ретінде полилактикалық қышқыл (PLA) таңдалды. Баспа бағдарлары ұзын жиекті және жалпақ бағыттарда болды. Өнім z осі бойымен салынғандықтан, қысқа жиекті (жоғары оң жақ) бағдары ескерілмеді, бұл ең аз беріктікке әкеледі. «Концентрлік», «Крест», «Үшбұрыш», «Зигзаг», «Түз сызықты», «Кубтық», «Бал ұясы» және «Тор» деп аталатын толтыру үлгілерінің комбинациялары толтыру тығыздығы 70% және 0,15 мм қабат қалыңдығымен қабатты стратегиямен зерттелді. Нәтиже басып шығару бағытының, әсіресе CIP үлгілеріндегі созылу беріктігіне айтарлықтай әсер еткенін және CIP үлгісінің ұзын жиегі бағытының созылу беріктігі жоғары екенін көрсетеді. Concentric/Triangle (Концентрлік/Үшбұрыш) үлгісі сәйкесінше 30 МПа және 33 МПа кезінде жазық және ұзын жиек бағдарларында ең жоғары созылу беріктігіне ие болды, бірақ тегіс бағыттағы жинақтау уақыты ұзағырақ болды (25 минут), ал ұзын жиек бағдарында басып шығару уақыты қысқа болды (29 минут). Бал ұясы/үшбұрыш комбинациясы екі бағытта да төмен созылу беріктігін қамтамасыз етті: тегіс

	жиек үшін 19 МПа және ұзын жиек үшін 20 МПа, бірақ құрастыру уақыты екі бағытта да ұзағырақ болды (тиісінше 14 минут және 35 минут). Нәтижесінде, CIP үлгісі бір рет толтырылған үлгіге қарағанда үлкен созылу беріктігіне ие. Сонымен қатар, үшбұрышты өрнекті басқа өрнектермен біріктіргенде, сол өрнектердің созылу күші жақсарғаны анықталды. Шеттік бағдармен құрастырылған CIP үлгілері тегіс бағдармен жасалған үлгілерге қарағанда жоғары созылу беріктігіне ие болды. Кейбір басқа үлгілермен біріктірілген үшбұрышты толтыру үлгісінде кейбір үлгілердің созылу беріктігі жоғарылады, ал басқалары жақсарды, ал кейбіреулері төмендеді.
	Түйін сөздер: Балқытылған тұндыру арқылы модельдеу (FDM), қоспаларды өндіру (AM), полилактикалық қышқыл (PLA), қабат-қабат, басып шығару бағыты, аралас толтыру үлгілері (CIP), құрастыру бағыты.
Mohamed Hamoud Ahmed	***Авторлар туралы мәліметтер:*** *Ассистент профессор, машина жасау кафедрасы, инженерлік факультеті, Хелван университеті, Каир, Египет. Email: Dr_hamoud2015@h-eng.helwan.edu.eg*
Omnia Mohsen Mohamed Abdalaziz	*Канада халықаралық колледжі, инженерлік факультетінің машина жасау кафедрасының ассистент оқытушысы, Каир, Египет. Email: Omnia_mohsen@cic-cairo.com*
Azza Fathallah Mostafa Barakat	*Профессор, машина жасау кафедрасы, инженерлік факультеті, Хелван университеті, Каир, Египет. Email: barakatazza@h-eng.helwan.edu.eg*
Ahmed Sobhi Mohamed Gad	*Доктор, машина жасау бөлімі, инженерлік факультеті, Хелван университеті, Каир, Египет. Email: a.sobhi.m@gmail.com*

Влияние рисунков заполнения и ориентации печати на механические свойства деталей, изготовленных из полимолочной кислоты

[1]Hamoud M., [2]Abdal-Aziz O., [1]Barakat A., [1]Gad A.

[1]Faculty of Engineering, Helwan University, Cairo, Egypt
[2]Департамент фундаментальной инженерии, Канадский международный колледж, Гиза, Египет

Поступила: *15 мая 2024*
Рецензирование: *20 мая 2024*
Принята в печать: *20 июня 2024*

АННОТАЦИЯ

Метод моделирования наплавленным осаждением (FDM) позволяет создавать функциональные модели различных термопластичных полимеров и является одной из наиболее часто используемых технологий аддитивного производства (АП). Целью данного исследования является изучение того, как сочетание рисунка заполнения (CIP) и ориентации печати влияет на характеристики растяжения и время строительства. В качестве материала для изготовления образцов была выбрана полимолочная кислота (PLA). Ориентация печати была длинной и плоской. Поскольку изделие построено вдоль оси Z, ориентация короткого края (вверх-правая) не рассматривалась, что приводит к минимальной прочности. Комбинации рисунков заполнения под названием «Концентрический», «Крест», «Треугольник», «Зигзаг», «Прямолинейный», «Кубический», «Соты» и «Сетка» были исследованы с плотностью заполнения 70% и толщиной слоя 0,15 мм с послойной стратегией. Результат показывает, что ориентация печати оказала значительное влияние на прочность на разрыв, особенно в образцах CIP, а ориентация образца CIP вдоль длинной кромки имела более высокую прочность на разрыв. Образец Концентрик/Треугольник имеет самую высокую прочность на разрыв при плоской ориентации и ориентации по длинной кромке - 30 МПа и 33 МПа соответственно, но время наращивания при плоской ориентации было большим (25 минут), в то время как время печати при ориентации по длинной стороне был коротким (29 мин.). Комбинация «сота/треугольник» обеспечивает меньшую прочность на разрыв в обеих ориентациях: 19 МПа для плоской и 20 МПа для длинной кромки, но время сборки в обеих ориентациях было большим (14 минут и 35 минут соответственно). В результате образец с CIP имеет большую прочность на разрыв, чем образец с одним заполнением. Кроме того, было обнаружено, что при сочетании треугольного рисунка с другими узорами прочность на разрыв этих узоров улучшалась.

Образцы CIP, построенные с ориентацией по краю, имели более высокую прочность на разрыв, чем образцы, построенные с плоской ориентацией. В шаблоне заполнения «Треугольник» в сочетании с некоторыми другими шаблонами прочность на разрыв некоторых образцов увеличилась, в то время как у других улучшилась, а у других снизилась.

Ключевые слова: Моделирование наплавлением (FDM), аддитивное производство (AM), полимолочная кислота (PLA), послойное ориентация печати, комбинированные шаблоны заполнения (CIP), ориентация сборки.

Mohamed Hamoud Ahmed	***Информация об авторах:*** *Доцент кафедры машиностроения инженерного факультета Хелуанского университета, Каир, Египет. Email: Dr_hamoud2015@h-eng.helwan.edu.eg*
Omnia Mohsen Mohamed Abdalaziz	*Ассистент кафедры машиностроения, инженерный факультет, Канадский международный колледж, Каир, Египет. Email: Omnia_mohsen@cic-cairo.com*
Azza Fathallah Mostafa Barakat	*Профессор кафедры машиностроения инженерного факультета Хелуанского университета, Каир, Египет. Email: barakatazza@h-eng.helwan.edu.eg*
Ahmed Sobhi Mohamed Gad	*Доктор кафедры машиностроения инженерного факультета Хелуанского университета, Каир, Египет. Email: a.sobhi.m@gmail.com*

References

[1] Ryan KR, Down MP, Hurst NJ, Keefe EM, & Banks CE. Additive manufacturing (3D printing) of electrically conductive polymers and polymer nanocomposites and their applications. EScience. 2022; 2(4):365-381. https://doi.org/10.1016/j.esci.2022.07.003

[2] Gross BC, Erkal JL, Lockwood SY, Chen C, & Spence DM. Evaluation of 3D printing and its potential impact on biotechnology and the chemical sciences. 2014. https://pubs.acs.org/doi/full/10.1021/ac403397r

[3] Sajjad R, Butt SU, Saeed HA, Anwar MT, & Rasheed T. Impact of multiple infill strategy on the structural strength of single build FDM printed parts. Journal of Manufacturing Processes. 2023; 89:105-110. https://doi.org/10.1016/j.jmapro.2023.01.065

[4] Poojitha G, Talari P, Banoth S, & Kumar A. Effects of combined infill angle with a honeycomb pattern on the mechanical properties of HIPS and polypropylene in FDM process. Materials Today: Proceedings. 2023. https://doi.org/10.1016/j.matpr.2023.09.219

[5] Gohar S, Hussain G, Ali A, & Ahmad H. Mechanical performance of honeycomb sandwich structures built by FDM printing technique. Journal of Thermoplastic Composite Materials. 2023; 36(1):182-200. https://doi.org/10.1177/0892705721997892

[6] Bellini A, & Güçeri S. Mechanical characterization of parts fabricated using fused deposition modeling. Rapid Prototyping Journal. 2003; 9(4):252-264.

[7] Ismail KI, Yap TC, & Ahmed R. 3D-printed fiber-reinforced polymer composites by fused deposition modeling (FDM): fiber length and fiber implementation techniques. Polymers. 2022; 14(21):4659. https://doi.org/10.3390/polym14214659

[8] Karalekas D, & Antoniou K. Composite rapid prototyping: overcoming the drawback of poor mechanical properties. Journal of Materials Processing Technology. 2004; 153:526-530. https://doi.org/10.1016/j.jmatprotec.2004.04.019

[9] Farashi S, & Vafaee F. Effect of printing parameters on the tensile strength of FDM 3D samples: a meta-analysis focusing on layer thickness and sample orientation. Progress in Additive Manufacturing. 2022, 1-18.

[10] Torres J, Cole M, Owji A, DeMastry Z, & Gordon AP. An approach for mechanical property optimization of fused deposition modeling with polylactic acid via the design of experiments. Rapid Prototyping Journal. 2016; 22(2):387-404.

[11] Chacón J M, Caminero M A, García-Plaza E, & Núnez P J. Additive manufacturing of PLA structures using fused deposition modeling: Effect of process parameters on mechanical properties and their optimal selection. Materials & Design. 2017; 124:143-157. https://doi.org/10.1016/j.matdes.2017.03.065

[12] Durgun I, & Ertan R. Experimental investigation of FDM process for improvement of mechanical properties and production cost. Rapid Prototyping Journal. 2014; 20(3):228-235. https://doi.org/10.1108/RPJ-10-2012-0091

[13] Aloyaydi B, Sivasankaran S, & Mustafa A. Investigation of infill patterns on the mechanical response of 3D printed poly-lactic acid. Polymer Testing. 2020; 87:106557. https://doi.org/10.1016/j.polymertesting.2020.106557

[14] Mishra S B, & Mahapatra S S. Improvement in tensile strength of FDM-built parts by parametric control. Applied Mechanics and Materials. 2014; 592:1075-1079. https://doi.org/10.4028/www.scientific.net/AMM.592-594.1075

[15] Ahn S H, Montero M, Odell D, Roundy S, & Wright P K. Anisotropic material properties of fused deposition modeling ABS. Rapid prototyping journal. 2002; 8(4):248-257.

[16] Wang S, Ma Y, Deng Z, Zhang S, & Cai J. Effects of fused deposition modeling process parameters on tensile, dynamic mechanical properties of 3D printed polylactic acid materials. Polymer testing. 2020; 86:106483. https://doi.org/10.1016/j.polymertesting.2020.106483

[17] Yang L, Li S, Li Y, Yang M, & Yuan Q. Experimental investigations for optimizing the extrusion parameters on FDM PLA printed parts. Journal of Materials Engineering and Performance. 2019; 28:169-182.

[18] Sukindar N A, Ariffin MKA, Baharudin BHT, Jaafar CNA, & Ismail MIS. Analyzing the effect of nozzle diameter in fused deposition modeling for extruding polylactic acid using open-source 3D printing. J. Teknol. 2016; 78(10):7-15. https://doi.org/10.3390/polym12122792

[19] Moradi M, Meiabadi S, & Kaplan A. 3D printed parts with honeycomb internal pattern by fused deposition modeling; experimental characterization and production optimization. Metals and Materials International. 2019; 25:1312-1325.

[20] Akhoundi B, Behravesh AH. Effect of filling pattern on the tensile and flexural mechanical properties of FDM 3D printed products. Exp. Mech. 2019; 59:883-897.

[21] Hanon MM, Marczis R, Zsidai L. Anisotropy evaluation of different raster directions, spatial orientations, and fill percentage of 3D printed PETG tensile test specimens. Key Eng. Mater. 2019; 821:167-173. https://doi.org/10.4028/www.scientific.net/KEM.821.167

[22] Samykano M, Selvamani SK, Kadirgama K, Ngui WK, Kanagaraj G, Sudhakar K. Mechanical property of FDM printed ABS: Influence of printing parameters. Int. J. Adv. Manuf. Technol. 2019; 102:2779-2796. https://doi.org/10.1007/s00170-019-03313-0

[23] Li H, Wang T, Sun J, Yu Z. The effect of process parameters in fused deposition modeling on bonding degree and mechanical properties. Rapid Prototype J. 2018; 24:80-92. http://dx.doi.org/10.1108/RPJ-06-2016-0090

[24] Casavola C, Cazzato A, Moramarco V, Pappalettere C. Orthotropic mechanical properties of fused deposition modeling parts described by classical laminate theory. Mater Des. 2016; 90:453-458. https://doi.org/10.1016/j.matdes.2015.11.009

[25] Rajpurohit SR, Dave HK. Effect of process parameters on tensile strength of FDM printed PLA part. Rapid Prototyp J. 2018; 24:1317-1324. http://dx.doi.org/10.1108/RPJ-06-2017-0134

[26] Dave HK, Patadiya NH, Prajapati AR, Rajpurohit SR Effect of infill pattern and infill density at varying part orientation on tensile properties of fused deposition modeling-printed poly-lactic acid part. P I Mech Eng C-J Mec. 2019. https://doi.org/10.1177/0954406219856383

[27] Rodriguez JF, Thomas JP, Renaud JE. Mechanical behavior of acrylonitrile butadiene styrene (ABS) fused deposition materials: Experimental investigation. Rapid Prototyp J. 2001; 7:148-158.

[28] Lederle F, Meyer F, Brunotte GP, Kaldun C, Hübner EG. Improved mechanical properties of 3D-printed parts by fused deposition modeling processed under the exclusion of oxygen. Prog Addit Manuf. 2016; 1:3-7. https://doi.org/10.1007/s40964-016-0010-y

[29] Wu W, Geng P, Li G, Zhao D, Zhang H, Zhao J. Influence of layer thickness and raster angle on the mechanical properties of 3D-printed PEEK and a comparative mechanical study between PEEK and ABS. Materials. 2015; 8:5834-5846. https://doi.org/10.3390/ma8095271

[30] Ziemian S, Okwara M, Ziemian CW. Tensile and fatigue behavior of layered acrylonitrile butadiene styrene. Rapid Prototyp J. 2015; 21:270-278. http://dx.doi.org/10.1108/RPJ-09-2013-0086

[31] Zaldivar RJ, Witkin DB, McLouth T, Patel DN, Schmitt K, Nokes JP. Influence of processing and orientation print effects on the mechanical and thermal behavior of 3D-Printed ULTEM® 9085 Material. Addit Manuf. 2017; 13:71-80. https://doi.org/10.1016/j.addma.2016.11.007

[32] Alvarez C, Kenny L, Lagos C, Rodrigo F, Aizpun M. Investigating the influence of infill percentage on the mechanical properties of fused deposition modeled ABS parts. Ing Invest. 2016; 36:110-116. http://dx.doi.org/10.15446/ing.investig.v36n3.56610

[33] Shih CC, Burnette M, Staack D, Wang J, Tai BL. Effects of cold plasma treatment on interlayer bonding strength in FFF process. Addit Manuf. 2019; 25:104-111. https://doi.org/10.1016/j.addma.2018.11.005

[34] Lee CY, Liu CY. The influence of forced-air cooling on a 3D printed PLA part manufactured by fused filament fabrication. Addit Manuf. 2019; 25:196-203. https://doi.org/10.1016/j.addma.2018.11.012

[35] Bin Ishak I, Fleming D, Larochelle P. Multiplane fused deposition modeling: a study of tensile strength. Mech Based Des Struct Mach. 2019; 47:1-16. https://doi.org/10.1080/15397734.2019.1596127

[36] Lalegani Dezaki M, & Mohd Ariffin M K A. The Effects of Combined Infill Patterns on Mechanical Properties in FDM Process. Polymers. 2020; 12(12):2792. https://doi.org/10.3390/polym12122792

[37] Dave H K, Patel B H, Rajpurohit S R, Prajapati A R, & Nedelcu D. Effect of multi-infill patterns on tensile behavior of FDM printed parts. Journal of the Brazilian Society of Mechanical Sciences and Engineering. 2021; 43(1). https://doi.org/10.1007/s40430-020-02742-3

[38] Roger F, Krawczak P. 3D-printing of thermoplastic structures by FDM using heterogeneous infill and multi-materials: An integrated design-advanced manufacturing approach for factories of the future. CFM 2015 - 22ème Congrès Français de Mécanique. 2015.

[39] Naik M, Thakur D, & Chandel S. An insight into the effect of printing orientation on tensile strength of multi-infill pattern 3D printed specimen: Experimental study. Materials Today: Proceedings. 2022; 62:7391. https://doi.org/10.1016/j.matpr.2022.02.305

Crossref
DOI: 10.31643/2025/6445.24
Engineering and Technology

Methods for purifying table salt from the Bakhyt-Tany deposit

[1]Urazkeldiyeva D.A., [1]Kadirbayeva A.A., [2]Minakovsky A.F., [1]Sarypbekova N.K., [1*]Smailov B.M.

[1]M.Auezov South Kazakhstan Research University, Shymkent, Kazakhstan
[2]Belarusian State Technological University, Minsk, Belarus

** Corresponding author email: baha_uppr@mail.ru*

Received: *April 4, 2024*
Peer-reviewed: *May 8, 2024*
Accepted: *June 21, 2024*

ABSTRACT
This article discusses modern methods of purifying table salt from the Bakhyt-Tany deposits. Currently, the demand for various methods of production and processing of table salt is increasing. Therefore, high-quality purification of table salt and its effective use is one of the urgent tasks. As an object of study, salts were taken from the Bakhyt-Tany deposit, located in the Sozak district of the Turkestan region. The main goal of the scientific work is to study methods for purifying and processing sodium chloride from impurities. Modern analytical methods were used during scientific research. To determine the physicochemical properties of table salt, PEM JSM 6610 LV, X-ray microanalysis Inca Energy-450, energy dispersive system-fluorescence spectroscopy, IR-Fourier spectrometer were chosen. As a result of the research work, it turned out that using only the lime-soda method itself, it is possible to purify salt from calcium and magnesium ions up to 90-93%. It has been established that when using the phosphate method of purifying a saline solution, the degree of purification from calcium and magnesium ions increases to 95-97%. To further increase the degree of purification, it was recommended to first purify the solution using the lime-soda method, and then purify the solution using the phosphate method. It has been established that with this method the degree of purification can be increased to 99%.

Keywords: sodium chloride, brines, table salt, salt purification methods, sodium phosphate.

Information about authors:

Dilbar Urazkeldiyeva Abdikhmidovna — *PhD doctoral student, The higher School of chemical engineering and biotechnology, M.Auezov South Kazakhstan University, Shymkent, Kazakhstan. Email: urazkeldieva.97@list.ru*

Kadirbayeva Almagul Akkopeykyzy — *Candidate of technical sciences, Assistant Professor, The higher School of chemical engineering and biotechnology, M.Auezov South Kazakhstan University, Shymkent, Kazakhstan. Email: diac_2003@mail.ru*

Minakouski Aliaksandr — *Candidate of Technical Sciences, Docent, Departament of science, Belarusian State Technological University, Minsk, Belarus. E-mail: sashmin@mail.ru*

Sarypbekova Nursulu Koshenovna — *Candidate of chemical sciences. Docent. The higher School of chemical engineering and biotechnology, M.Auezov South Kazakhstan University, Shymkent, Kazakhstan. Email: nurislam_kar@mail.ru*

Smailov Bakyt Matkarimovich — *PhD doctor, Department of scientific research, M.Auezov South Kazakhstan University, Shymkent, Kazakhstan. Email: Baha_uppr@mail.ru*

Introduction

Every country in the world mines and processes table salt to some extent. The main producers of table salt in the CIS countries are enterprises in Russia, Belarus, Ukraine, Kazakhstan and Turkmenistan [[1], [2]]. The technologies used in the production of table salt in these countries depend primarily on the type and nature of the salt deposit, its geographical location, the quality of raw materials and the presence of various impurities, as well as on consumer requirements to salt quality [[3], [4]]. Currently, the production of table salt is based on various methods of its extraction and processing, and the world market is growing by an estimated 1% per year. At the same time, the technogenic impact on the environment is also growing, which makes its negative contribution to the deterioration of its condition [[5], [6], [7]]. There are several traditional methods to purify sodium chloride from unwanted ions, and they include lime-soda method, barium carbonate method and so on. The lime-soda method is difficult to achieve high purity of salt, and barium is a highly toxic element and barium sulfate compounds can lead to the development of pneumoconiosis [9]. Sodium phosphate is mainly used for water softening, to precipitate calcium and magnesium ions from solution. The advantages of

the phosphate method are that phosphate compounds are widely used by the food industry, and in small quantities are not dangerous to human health. The article considers lime-soda and phosphate methods of salt purification from calcium and magnesium ions. The purity of salt and reagents is one of the most important criteria in production. The lime-soda method has long been known as a purification method, but a multi-stage purification system is required to obtain high purity salt [[9], [10]].

Also disadvantages of already existing methods of salt purification from undesirable ions are multistage process, application of concentrated hydrochloric acid for treatment of sodium chloride solution, which at further evaporation and centrifugation causes corrosion of equipment; at the same time additional washing of NaCl crystals from acid by expensive high-purity water is required, which together with multistage process significantly increases the cost of the process of table salt purification [[7], [8]].

Although NaCl can be purified to any desired degree, it is associated with certain costs that increase the cost of the product. Thus, it is very important to provide purification in the most practical way [[11], [12]]. Therefore, the aim of this paper is to study the peculiarities of table salt production and to analyze its main environmental impacts.

Salt lakes of Bakhyt-Tany deposit located on the territory of Suzak district of Turkestan region (Figure 1) were taken for study as raw materials. The deposit is located far from the settlements of tasty village at a distance of 15 km to the north of the field. Lake Bakhyt-Tany is a continental dry self-sedimenting lake with developed new-sedimentation and old-sedimentation. Its composition is chloride, without root salt. The surface area of the lake is 1.87 km². The surface is flat, smooth with traces of mining. Near the banks, the surface is swollen, broken by cracks, along which liquid silt protrudes, forming rolls up to 5-8 cm high on the surface. The thickness of new sediment is mainly from 3 to 15 cm. The thickness of old sediment is from 11 to 47 cm, including the average thickness of 0.2 m for Block B and 0.25 m for Block C1. The thickness of garnet is 0.78-1.0 m. The average thickness of the salt deposit is 1.26 m - 0.93 m. In general, the salt deposit is a stratum gradually wedging out to the lake periphery.

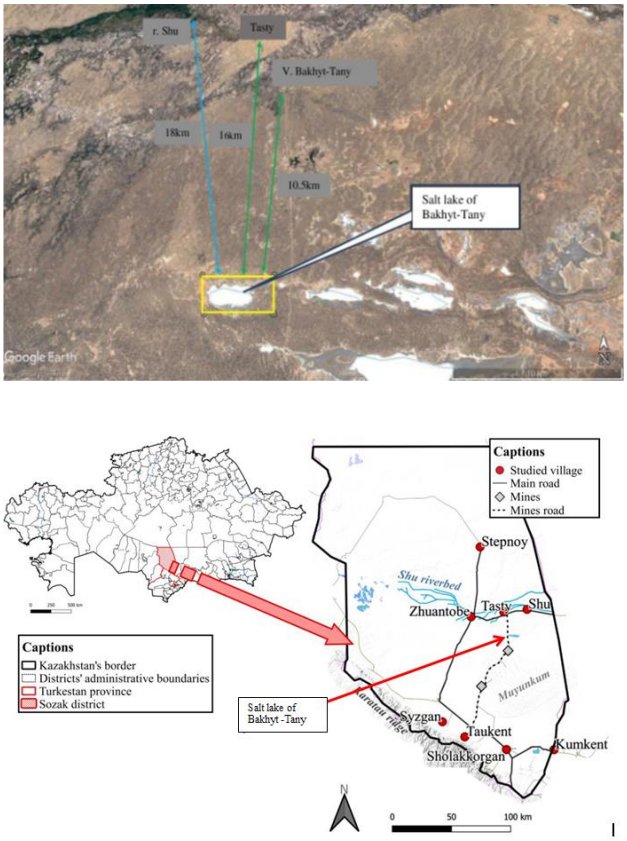

Figure 1 - Location of the lake of the Bakhyt-Tany deposit

The ground aquifer lies at a depth of 2 to 5 meters. The chemical composition of water is sulfate-chloride, rarely sulfate. Mineralization varies from 2 to 10 g/l. Water availability of the horizon is low. Within Bakhyt-Tany deposit ground waters were not opened by excavations of 2.5 m. The annual capacity of the enterprise is taken taking into account the need to develop commercial salt reserves for the Contract period, i.e. 25 years. Industrial reserves of salt deposit as of 01.01.2016 are 1349.6 thousand tons or 811 thousand m³ in the sum of categories B+C1 [6]. The purpose of this work is to study the methods of processing and purification of sodium chloride from impurities.

Experimental part

To conduct the study from the deposit Bakhyt-Tany were taken samples of sodium salt mineral, the depth of sampling 50 cm. Chemical analysis of samples was carried out according SS 13685-84 [13].

Methods of analysis. For determination of sulfate ions we used the method of barium sulfate turbiometry, for determination of calcium and magnesium ions we used titration with EDTA

(Tab.1), Elemental analysis was carried out by means of energodispersive X-ray fluorescence spectroscopy on energy dispersive microanalysis system INCA Energy 450, installed on scanning electron microscope JSM 6610 LV, JEOL, Japan (Fig.2-3. Tab.2). The error of determination - 0.01 %. A JSM 6610 LV scanning electron microscope, JEOL, Japan, was used to study the microstructure of the samples (Fig.3). The accelerating voltage was 20 kV. The imaging mode was secondary electrons. Chemical analysis of the sample was carried out according to SS-sodium chloride.

X-ray diffractometer Dron - 4-07 was used to obtain X-ray diffractometric analysis. With a tube with a cobalt anode (Fig.4). Diffractometer imaging mode:

- sweep speed 2 deg/min;
- tube operating parameters: 30 kV, 20 mA.

IR analysis of the sample was carried out by a FTIR spectrometer NEXUS E.S.P. (Thermo Scientific, USA) (Fig.5).

As a result of the research the chemical composition of the salt of Bakyt-Tany lake was determined using scanning electron microscope LEO 912 AB OMEGA (Carl Zeiss SMT AG Oberckochen, Germany) and SEM JEOL JSM. The elemental composition of sodium salt is given in Table 1.

Experimental methodology. To purify the brine from impurities using the lime-soda method, a saturated salt solution with a concentration of 315 g/l was prepared. The solution was prepared at a temperature of 80-100 ^{0}C so that all salt dissolved. After that we added sodium carbonate and calcium hydroxide calculated in advance by chemical reactions. The obtained mixture was stirred continuously for 10-15 min in the thermostat, then the mixture was allowed to stand for 30 min at room temperature and passed through a filter. Insoluble salt residue and insoluble calcium and magnesium compounds remained on the filter as a precipitate. The composition of the precipitate on the filtrate is shown in Figure 5. We determined the content of calcium and magnesium ions in the filtered brine by titration method. The obtained NaCl solution is sent for management and drying of the target product.

To purify the brine from impurities by phosphate method, a stoichiometric amount of sodium phosphate is added to the saturated solution to precipitate Ca and Mg salts. The mixture is stirred and kept at room temperature for 30 minutes. The resulting solution is then sedimented. Extracted in the solid phase from the saturated solution of NaCl impurity ions of calcium and magnesium, formed in the interaction with sodium phosphate, filtered, washed. Then the clarified NaCl solution is directed to the management and drying of the target product [[15], [16], [17]].

The discussion of the results

According to the results of the study the moisture content of the samples was 0.6-1%. According to the obtained results the approximate salt composition of halite mineral was calculated: $CaSO_4$ –2.5%, $MgSO_4$ –0.18%, $MgCl_2$ – 0.37%,NaCl – 88.4%. The mineral contains up to 2 % wt. % of insoluble residue, which does not allow to use it for production of table salt without preliminary desliming.

Table 1 - Results of chemical analysis of sodium salt of Bakhyt-Tany deposit

Ions	Mg^{2+}	Ca^{2+}	Cl^-	SO_4^{2-}	Na^+	Insolub. residue
Content, %	0.28	0.880	53.4	1.83	35.3	1.17-2

Insoluble residue of salt has two phases: the first is clay insoluble mass, the second is transparent crystals of insoluble calcium sulfate.

After determining the composition of table salt, the purification method was selected. Due to the fact that the composition of the natural mineral is similar to table salt, the physicochemical properties were studied to obtain sodium chloride used in food and soda ash production by removing calcium, magnesium ions and mechanical additives from the mineral [[18], [19]].

Table 2 - Elemental composition of sodium salt of Bakyt-Tany deposit

Element	O	Na	Mg	S	Cl	Ca	Total
Spectr 1	10.4	32.37	1.16	1.26	53.04	1.77	100
Spectr 2	3.74	38.78	0.42	0.15	56.42	0.48	100
Spectr 3	7.53	31.87	0.81	0.31	58.88	0.60	100
Total, %	7.22	34.34	0.80	0.57	56.11	0.95	100

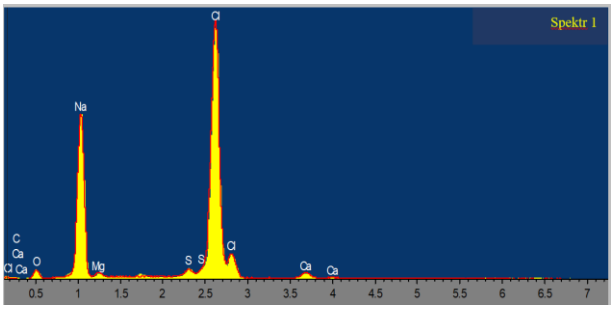

Figure 2 - Spectrogram of elements of natural sodium salt of the Bakhyt-Tany deposit

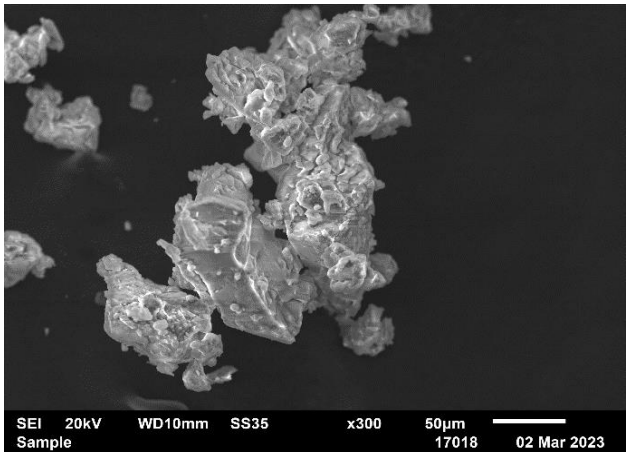

Figure 3 - Micrographs of the surface of the natural sodium salt of the Bakhyt-Tany deposit

The very high intensity of sodium and chlorine pickers in the figure compared to other elements indicates that the sample contains a higher proportion of sodium and chlorine.

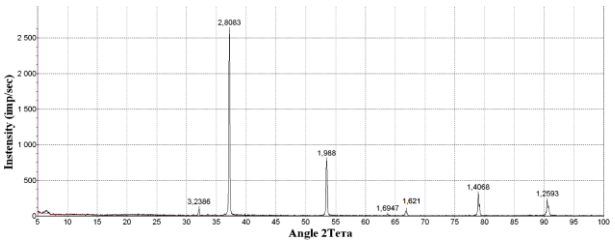

Figure 4 – Results of the XRD of the natural sodium salt of the Bakhyt Tany deposit

Reflexes: 3.24; 2.81; 1.99, 1.69; 1.62; 1.41; 1.26 Å - NaCl (Hyalite) - ASTM-5-628. All the intense and non-intense peaks in the X-ray radiograph of the salt sample belong to sodium chloride. The rest of the sodium mineral seodyniums in the composition of the salt are very low in content, below 2 %. Therefore, they are not visible in the X-ray diagram. All these data, including XRD, elemental analysis, chemical analysis, indicate a very high content of sodium chloride in the natural sodium mineral of the Bakhyt-Tany deposit.

Based on literature sources, several methods have been selected to purify salt from impurities and ions. There are several traditional methods of purifying sodium chloride from unwanted ions, these include lime-soda method, barium carbonate method, etc. The purity of salt and reagents is one of the most important criteria in production. The lime-soda method has long been known as a purification method, but a multi-stage purification system is required to obtain high purity salt. The following reactions occur in the brine:

$$CaCl_2 + Na_2CO_3 \rightarrow 2NaCl + CaCO_3 \quad (1)$$
$$CaSO_4 + Na_2CO_3 \rightarrow Na_2SO_4 + CaCO_3 \quad (2)$$
$$MgCl_2 + Na_2CO_3 \rightarrow 2NaCl + MgCO_3 \quad (3)$$
$$MgSO_4 + Na_2CO_3 \rightarrow Na_2SO_4 + MgCO_3 \quad (4)$$
$$MgCl_2 + 2NaOH \rightarrow 2NaCl + Mg(OH)_2 \quad (5)$$
$$MgSO_4 + 2NaOH \rightarrow Na_2SO_4 + Mg(OH)_2 \quad (6)$$

Figure 5 shows the IR analysis of the sludge on the filter after cleaning by the lime-soda method. The figure shows that the most intense peaks 1427, 878,716 cm^{-1} are characteristic for calcium carbonate, and in the region of 3200 - 3700 cm^{-1} absorption of OH-groups.

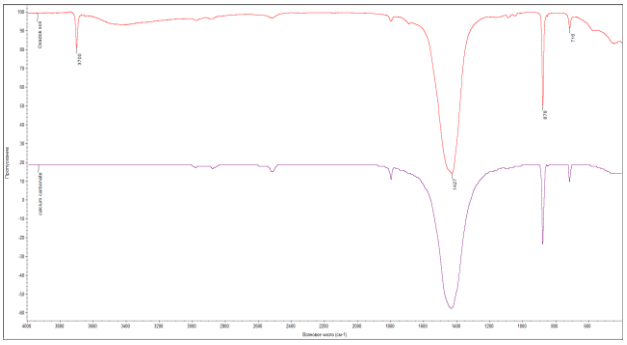

Figure 5 - IR analysis of the sludge on the filter after treatment with the lime-soda method

The phosphate treatment method is very advantageous because calcium and magnesium phosphates precipitate in the solution, which can be used in fertilizer production.

$$3CaCl_2 + 2Na_3PO_4 \rightarrow 6NaCl + Ca_3(PO_4)_2 \quad (7)$$
$$3CaSO_4 + 2Na_3PO_4 \rightarrow 3Na_2SO_4 + Ca_3(PO_4)_2 \quad (8)$$
$$3MgCl_2 + 2Na_3PO_4 \rightarrow 6NaCl + Mg_3(PO_4)_2 \quad (9)$$
$$3MgSO_4 + 2Na_3PO_4 \rightarrow 3Na_2SO_4 + Mg_3(PO_4)_2 \quad (10)$$

The soda-lime and phosphate methods were used for sodium chloride purification at the Bakhyt-Tany field. Only 90-93% of calcium and magnesium ions were removed from the brine using only the soda-lime method itself. When the cleaning reagents sodium carbonate and calcium hydroxide were added over 50%, the degree of purification increased to 94-98%.

When only phosphate method of solution cleaning was used, the degree of cleaning from calcium-magnesium ions increased up to 95-97% [[20], [22]]. To further increase the degree of purification, it was recommended to first purify the solution with the lime-soda method, and then purify the solution with the phosphate method. With this method, the purification degree can be increased up to 99%. The advantage of the method is that it reduces the consumption of cleaning reagents, does not require additional heating or reheating, the process is not multistage. Table 3 shows the degree of solution purification from calcium and magnesium ions by different methods.

Table 3 - The degree of solution purification from calcium and magnesium ions by different methods

No	Method	Degree of purification,%	
		Ca^+	Mg^+
1	Lime-soda	90	93
2	Lime-soda lime, in excess	93-94	97-98
3	Phosphate	96-97	94-95
4	lime soda and phosphate	99	99

Conclusions

The obtained results allow us to conclude that the natural salt mineral of the Bakhyt-Tany deposit contains a high concentration of sodium chloride and a small number of impurities.

Thus, the obtained results, including XRF, elemental analysis, chemical analysis, indicate a very high content of sodium chloride in the natural sodium mineral of the Bakhyt-Tany deposit. In the article lime-soda and phosphate method of salt purification from calcium and magnesium ions are considered.

Only 90-93% of calcium and magnesium ions were removed from the brine using the soda-lime method alone. When sodium carbonate and calcium hydroxide cleaning reagents were added over 50% in excess, the degree of purification increased to 94-98%. When only phosphate method of solution cleaning was used, the degree of cleaning from calcium-magnesium ions increased up to 95-97%. It was found that this method can increase the degree of purification up to 99% [[19], [20]].

***CRediT author statement*: D.Urazkeldiyeva:** Methodology, formal analysis, investigation, Data writing, Original draft preparation, writing– review and editing. **A. Kadirbayeva:** Data curation, Writing draft preparation. **A. Minakovsky:** Resources, supervision. **N.Sarypbekova:** Investigation. **B. Smailov:** Reviewing and Editing.

Conflicts of Interest. On behalf of all authors, the correspondent author declares that there is no conflict of interest.

Cite this article as: Urazkeldiyeva DA, Kadirbayeva AA, Minakovsky AF, Sarybekova NK, Smailov BM. Methods for purifying table salt from the Bakhyt-Tany deposit. Kompleksnoe Ispolzovanie Mineralnogo Syra = Complex Use of Mineral Resources. 2025; 334(3):19-25. https://doi.org/10.31643/2025/6445.24

Бақыт-Таңы кен орнындағы ас тұзын тазарту әдістері

[1]Уразкелдиева Д.А., [1]Кадирбаева А.А., [2]Минаковский А.Ф., [1]Сарыпбекова Н.К., [1*]Смайлов Б.М.

[1]М. Әуезов атындағы Оңтүстік Қазақстан зерттеу университеті, Шымкент, Қазақстан
[2]Беларусь Мемлекеттік технологиялық университеті, Минск, Беларусь

ТҮЙІНДЕМЕ

Бұл мақалада Бақыт-Таңы кен орнының ас тұзын тазартудың заманауи әдістері қарастырылған. Қазіргі кезде ас тұзын өндіру және оны өңдеудің әртүрлі әдістеріне деген сұраныс артып отыр. Сол себепті аз тұзын жоғары дәрежеде тазалау және оны тиімді пайдалану өзекті мәселелердің бірі болып табылады. Аз тұзын тазалау үшін зерттеу нысаны ретінде Түркістан облысындағы Созақ ауданының аумағында орналасқан Бақыт-

Мақала келді: *4 сәуір 2024*
Сараптамадан өтті: *8 мамыр 2024*
Қабылданды: *21 маусым 2024*

Таңы кен орнының тұзды көлдері алынды. Ғылыми жұмыстың негізгі мақсаты – аз тұзын, яғни натрий хлоридін қоспалардан тазарту және өңдеу әдістерін зерттеу. Ғылыми зерттеу жүргізу кезінде заманауи талдау әдістері қолданылды. Ас тұзының физика-химиялық қасиеттерін анықтау үшін PEM JSM 6610 LV, рентгендік микроанализ Inca Energy-450, энергетикалық дисперсиялық жүйе - флуоресцентті спектроскопия, ИҚ-Фурье спектрометрі таңдалды. Ғылыми-зерттеу жұмыстарының нәтижесінде әкті-содалы әдістің өзін ғана қолданғанда тұзды кальций мен магний иондарынан 90-93%-ға дейін тазартуға болатындығы анықталды. Тұзды ерітіндіні тазалау үшін фосфатты әдіс қолданып, кальций магний иондарынан тазалау дәрежесі 95-97% дейін өсетіндігі анықталды. Тазалау дәрежесін одан әрі арттыру үшін ерітіндіні алдымен әкті-содалы әдіспен тазартып, кейін ертіндіні фосфатты әдіспен тазарту ұсынылды. Бұл әдіс арқылы тазалау дәрежесін 99% дейін жоғарылатуға болатыны анықталды.

Түйін сөздер: натрий хлориді, тұзды ерітінділер, ас тұзы, тұздарды тазарту әдістері, натрий фосфаты.

Авторлар туралы ақпарат:

Уразкелдиева Дилбар Абдихамидовна — *PhD докторант, Химиялық инженерия және биотехнология жоғарғы мектебі, М. Әуезов атындағы Оңтүстік Қазақстан зерттеу университеті, Шымкент, Қазақстан. E-mail: urazkeldieva.97@list.ru*

Қадірбаева Алмагүл Ақкөпейқызы — *Техника ғылымдарының кандидаты, қауымдастырылған профессор, Химиялық инженерия және биотехнология жоғарғы мектебі, М. Әуезов атындағы Оңтүстік Қазақстан зерттеу университеті, Шымкент, Қазақстан. E-mail: diac_2003@mail.ru*

Александр Минаковский — *Техника ғылымдарының кандидаты, доцент, Ғылым департаменті, Беларусь Мемлекеттік технологиялық университеті, Минск, Беларусь. E-mail: sashmin@mail.ru*

Сарыпбекова Нурсулу Кошеновна — *Химия ғылымдарының кандидаты, доцент, Химиялық инженерия және биотехнология жоғарғы мектебі, М. Әуезов атындағы Оңтүстік Қазақстан зерттеу университеті, Шымкент, Қазақстан. E-mail: nurislam_kar@mail.ru*

Смайлов Бакыт Маткаримулы — *PhD доктор, ғылыми зерттеу департаменті, М. Әуезов атындағы Оңтүстік Қазақстан зерттеу университеті, Шымкент, Қазақстан. E-mail: Baha_uppr@mail.ru*

Методы очистки поваренной соли из месторождения Бакыт-Таны

[1]Уразкелдиева Д.А., [1]Кадирбаева А.А., [2]Минаковский А.Ф., [1]Сарыпбекова Н.К., [1*]Смайлов Б.М.

[1]Южно-Казахстанский исследовательский университет имени М. Ауезова, Шымкент, Казахстан
[2]Белорусский Государственный технологический университет, Минск, Беларусь

Поступила: *4 апреля 2024*
Рецензирование: *8 мая 2024*
Принята в печать: *21 июня 2024*

АННОТАЦИЯ

В данной статье рассмотрены современные методы очистки поваренной соли месторождений Бахыт-Таны. В настоящее время возрастает спрос на различные способы производства и переработки поваренной соли. Поэтому качественная очистка поваренной соли и ее эффективное использование является одной из актуальных задач. В качестве объекта исследования для были взяты соли из месторождений Бакыт-Таны, расположенного на территории Созакского района Туркестанской области. Основная цель научной работы – изучение методов очистки и переработки хлорида натрия от примесей. В ходе научных исследований использовались современные аналитические методы. Для определения физико-химических свойств поваренной соли были выбраны PEM JSM 6610 LV, рентгеновский микроанализ Inca Energy-450, энергодисперсионная система-флуоресцентная спектроскопия, ИК-Фурье-спектрометр. В результате исследовательской работы выяснилось, что при использовании только самого известково-содового метода можно очистить соль от ионов кальция и магния до 90-93%. Установлено, что при использовании фосфатного метода очистки солевого раствора степень очистки от ионов кальция и магния увеличивается до 95-97%. Для дальнейшего повышения степени очистки рекомендовалось сначала очищать раствор известково-содовым методом, а затем очищать раствор фосфатным методом. Установлено, что данным методом степень очистки можно повысить до 99%.

Ключевые слова: хлорид натрия, рассолы, поваренная соль, методы очистки солей, фосфат натрия.

Информация об авторах:

Уразкелдиева Дилбар Абдихамидовна — *PhD докторант, Высшая школа химической инженерии и биотехнологии, Южно-Казахстанский исследовательский университет имени М. Ауезова, Шымкент, Казахстан. E-mail: urazkeldieva.97@list.ru*

Кадирбаева Алмагул Аккопейкызы — *Кандидат технических наук, ассоцированный профессор, Высшая школа химической инженерии и биотехнологии, Южно-Казахстанский исследовательский университет имени М. Ауезова, Шымкент, Казахстан. E-mail: diac_2003@mail.ru*

Александр Минаковский	*Кандидат технических наук, доцент, Департамент науки, Белорусский Государственный технологический университет, Минск, Беларусь. E-mail: sashmin@mail.ru*
Сарыпбекова Нурсулу Кошеновна	*Кандидат химических наук, доцент. Высшая школа химической инженерии и биотехнологии, Южно-Казахстанский исследовательский университет имени М. Ауезова, Шымкент, Казахстан. E-mail: nurislam_kar@mail.ru*
Смайлов Бакыт Маткаримулы	*PhD доктор, Департамент научных исследований, Южно-Казахстанский исследовательский университет имени М. Ауезова, Шымкент, Казахстан. E-mail: Baha_uppr@mail.ru*

References

[1] Bishimbayev VK, Amreev DD, Kapsalyamov BA, Gapparova KM, Sarsenov A. Analız rynka súlfata natrıa ı ıssledovanıe vozmojnostı ego polýchenıa ız súlfatnıkov mestorojdenıa Jaksykylysh [Analysis of the sodium sulfate market and study of the possibility of its production from sulfate rocks of the Zhaksykylysh deposit]. Bulletin of Science of Southern Kazakhstan. 2019; 1(5):58-65. (in Rus).

[2] Desyatov AV, Kruchinina NE, Novikov SV. Glýbokaıa pererabotka mıneralızovannyh shahtnyh vod s polýcheníem krıstalıcheskogo súlfata natrıa [Deep processing of mineralized mine water to produce crystalline sodium sulfate. Advances in chemistry and chemical technology]. 2016; 9:96-99. (in Rus).

[3] Ren Z, Wei X, Li R, Wang W, Wang Y, Zhou Z. Highly selective extraction of lithium ions from salt lake brines with sodium tetraphenylborate as co-extractant, Separation and Purification Technology. 2021; 269:118756. https://doi.org/10.1016/j.seppur.2021.118756

[4] Cipolletta G, Lancioni N, Akyol Ç, Eusebi AL, Fatone F. Brine treatment technologies towards minimum/zero liquid discharge and resource recovery: State of the art and techno-economic assessment, Journal of Environmental Management. 2021; 300:113681. https://doi.org/10.1016/j.jenvman.2021.113681

[5] Zhang X, Ren Y, Ping L, Ma H, Liu C, Wang Y, Kong L, Shen W. Solid-liquid equilibrium for the ternary systems and atmospheric pressure, J. Chem. Eng. 2014; 12:3969-3974. https://doi.org/10.1021/je500854m

[6] Anarbayev AA, Khegay R, Spabekova R, and etc. Investigation of the process of lithium chloride extraction from brine of the salt lakes of the aral sea region. International Journal of Innovative Technology and Exploring Engineering. 2019; 8(7):2235-2238.

[7] Shen Y, Linnow K, Steiger M. Crystallization behavior and damage potential of Na_2SO4 –NaCl mixtures in porous building materials. Cryst. Growth Des. 2020; 20(9):5974-5985. http://dx.doi.org/10.1021/acs.cgd.0c00671

[8] Ren Z, Wei X, Li R, Wang W, Wang Y, Zhou Z. Highly selective extraction of lithium ions from salt lake brines with sodium tetraphenylborate as co-extractant. Separation and Purification Technology. 2021; 269:118756. http://dx.doi.org/10.1016/j.seppur.2021.118756

[9] Pat. 2495825 C01B 3/14 RU. Sposob ochistki khlorida natriya [Method of purification of sodium chloride]. Fakeev AA, Polishchuk OM, Mursky GL. Opubl. 20.10.2013, 29. (in Russ.).

[10] Pat. 1428 C01D 3/08 KG. Sposob ochıstkı solányh porod ot prımesnyh ıonov [A method for cleaning salt rocks from impurity ions] Kochkorova ZB, Kalchaeva BSh, Murzubraimov BM, Satybaldiev AS. Opubl. 30.03.2012 (in Russ.).

[11] Khalil A, Mohammed S, Hashaikeh R, Hilal N. Lithium recovery from brine: Recent developments and challenges. Desalination. 2022; 528:115611. http://dx.doi.org/10.1016/j.desal.2022.115611

[12] Section "Environmental Protection" for the project "Extraction of lake salt from the Bakhyt-Tany deposit in the Sozak district, Turkestan region", Shymkent, 2022 https://cloud.mail.ru/public/WuDV/DUyDS59W6

[13] GOST P 51574-2000. Common salt. Test methods. Publishing House of Standards, Moscow. (in Russ).

[14] Li Zhu, YuLong Ma, ShaoYing Ge, YuYu Wang. Solid-liquid phase equilibria of the quaternary system. The Journal of Chemical Thermodynamics. 2022; 165:106658. https://doi.org/10.1016/j.jct.2021.106658

[15] Anarbayev AA, Khegay R, Spabekova R, Kabylbekova BN, Dmitrevsky BA. Studying the process of lithium chloride extraction from the brine. News Nat. Acad. Sci. RK. 2020; 1(439):99-105. http://dx.doi.org/10.32014/2020.2518-170X.12

[16] Shen W, Ren Y, Sun J. Solid-liquid phase equilibrium and phase diagram for the reciprocal quaternary system – Science Direct, Fluid Phase Equilib. 2016; 429:196-204. https://doi.org/10.1016/j.fluid.2016.09.005

[17] Kadirbayeva AA, Kaldybayeva G, Iskakova T, Raiymbekov EB. As tuzynyng kuramyn zhane oni tazalaudi zertteu [Study of the composition of table salt and its purification]. Bulletin KazNTU. 2017; 3(121):605-609. (in Kaz.).

[18] Anarbayev AA, Ormanova GM, Kabylbekova BN, Vysotskaya NA, Kucharov BK. Regularities of interaction of calcium chloride of distiller liquid with natural sodium sulfate. Rasayan J. Chem. 2020; 13(4):2173-2180. http://dx.doi.org/10.31788/RJC.2020.1345888

[19] Xu Zhao, Qi Zhang, Haihong Wu, Xiaocui Hao, Liang Wang, Xiping Huang. Extraction of Lithium from Salt Lake Brine. Progress in Chemistry. 2017; 29(7):796-808. (In Chinese). https://doi.org/10.7536/PC170313

[20] Dahmardeh H, Akhlaghi Amiri HA, Nowee SM. Evaluation of mechanical vapor recompression crystallization process for treatment of high salinity wastewater. Chemical Engineering and Processing - Process Intensification. 2019; 145:107682. http://dx.doi.org/10.1016/j.cep.2019.107682

[21] Xingguo Luo, Xingbin Li, Chang Wei, Zhigan Deng, Ye Liu, Minting Li, Sanqiang Zheng, Xing Huang. Recovery of NaCl and Na_2SO4 from high salinity brine by purification and evaporation. Desalination. 2022; 530:115631. http://dx.doi.org/10.1016/j.desal.2022.115631

[22] Myerson A, Erdemir D & Lee A. (Eds.). Handbook of Industrial Crystallization (3rd ed.). Cambridge: Cambridge University Press. 2019. http://dx.doi.org/10.1017/9781139026949

Crossref

creative commons

DOI: 10.31643/2025/6445.25
Engineering and Technology

The effect of Sodium Dodecyl Sulfate on Polysulfone membrane for Pb (II) ions removal in an aqueous solution

[1]Nurul Qistina Ismail, [1*]Abdul Hafidz Yusoff, [1]Noor Fazliani Shoparwe, [2]Nur Nabihah Yusof, [3]Muhammad Noorazlan, [1]Nadiah Ameram, [4]Mohammad M. Fares

[1] Universiti Malaysia Kelantan, Jeli 17600, Kelantan, Malaysia
[2] School of Physics, Universiti Sains Malaysia, 11800 USM, Penang, Malaysia
[3] University Pendidikan Sultan Idris, 35900 Tanjong Malim, Perak, Malaysia
[4] Jordan University of Science & Technology, P.O. Box 3030, 22110, Irbid, Jordan

** Corresponding author email: hafidz.y@umk.edu.my*

Received: *December 12, 2023*
Peer-reviewed: *February 20, 2024*
Accepted: *June 24, 2024*

ABSTRACT

An unsustainable level of contamination increase is driven by industrialization, population growth and growth in developing countries. Contamination of heavy metal ions in wastewater such as Pb (II) are non-biodegradable and poses a serious threat to human health and other living things. One of the major methods for treating heavy metals contamination is by chemical precipitation. However, it produced hazardous sludge that requires further treatment and used a significant quantity of chemicals during the heavy metals treatment process due to its low impact on the environment. As a result, a membrane filtration method as an alternative treatment for treating heavy metals in wastewater has been investigated. In this study, the membranes were fabricated using the wet phase inversion method approach by incorporating polysulfone (PSF) polymer with dimethylacetamide (solvent) and inclusion of different concentrations of sodium dodecyl sulfate (SDS) (M1= 0 wt%, M2= 0.5 wt%, M3= 1.0 wt%, M4= 1.5 wt%, M5= 2.0 wt%). The fabricated membranes were tested to remove 50 mg/L Pb (II) ions in aqueous solution. Scanning electron microscopy (SEM) was used to investigate the morphological structures of membranes. Moreover, the structural characteristics of fabricated membranes were evaluated according to these parameters; contact angle, porosity and mean pores radius. Furthermore, the performance of the membrane was also evaluated for permeation and rejection flux by using dead-end cell filtration. The results indicate that the M4 membrane with 1.5 wt% SDS had the highest rejection rate (90.52%) for Pb (II) ions. This is likely due to the presence of macrovoids and a porous structure, as shown by SEM analyses. Other supporting evidence includes a lower contact angle (63.91°), higher water uptake (43.58%), higher porosity (85.21%), and a lower mean pore radius (6 nm) for the M4 membrane. The fouling mechanism model suggests that the complete blocking observed in the experimental data indicates that porous blockage occurred on the membrane's surface during the absorption of Pb (II) ions. In conclusion, compared to the pure membrane, it becomes evident that the addition of SDS into the membrane solution enhanced the properties of the membranes. The M4 membrane with a composition of 1.5 wt% concentration SDS demonstrated optimal filtration for removing Pb (II) ions in a water treatment process due to excellent properties mentioned above.

Keywords: polysulfone; sodium dodecyl sulfate; lead; membrane filtration; phase inversion.

Information about authors:

Nurul Qistina Ismail — *Postgraduate Students at Gold, Rare Earth and Material Technopreneurship Centre (GREAT), Faculty of Bioengineering and Technology, Universiti Malaysia Kelantan, 17600 UMK kampus Jeli, Kelantan. Email: nurulqistinaa98@gmail.com*

Abdul Hafidz Yusoff — *Associate Professor at Gold, Rare Earth and Material Technopreneurship Centre (GREAT), Faculty of Bioengineering and Technology, Universiti Malaysia Kelantan, 17600 UMK kampus Jeli, Kelantan. Email: hafidz.y@umk.edu.mu*

Noor Fazliani Shoparwe — *Dr. Gold, Rare Earth and Material Technopreneurship Centre (GREAT), Faculty of Bioengineering and Technology, Universiti Malaysia Kelantan, 17600 UMK kampus Jeli, Kelantan. Email: fazliani.s@umk.edu.my*

Nur Nabihah Yusof — *Dr., School of Physics, Universiti Sains Malaysia, 11800 USM, Penang, Malaysia. Email: nurnabihah7@usm.my*

Muhammad Noorazlan — *Dr., Physics Department, Faculty of Science and Mathematics, Universiti Pendidikan Sultan Idris, Tanjung Malim, Perak, 35900, Malaysia. Email: azlanmn@fsmt.upsi.edu.my*

Nadiah Ameram — *Dr, Gold, Rare Earth and Material Technopreneurship Centre (GREAT), Faculty of Bioengineering and Technology, Universiti Malaysia Kelantan, 17600 UMK kampus Jeli, Kelantan. Email: nadiah@umk.edu.my*

Mohammad, M. Fares — *Professor, Department of Applied Chemistry, Jordan University of Science & Technology, P.O. Box 3030, 22110, Irbid, Jordan. Email: fares@just.edu.jo*

Introduction

The aquatic species that are harmed by the hazardous contaminant discharged in wastewater can make ordinary waterways unsuitable for drinkable water sources. The heavy metals that contaminate water supplies are harmful to humans and other living things [[1], [2]]. In this paper, we are focusing on removal of heavy metals contamination in synthetic wastewater.

The majority of heavy metals contamination comes from industrial effluent, including from mining, metal finishing, fertilizer production, electroplating and petroleum refineries [[1], [2], [3]]. The example for heavy metals are arsenic, cobalt, chromium, copper, nickel, lead, titanium, strontium and mercury. Even at low metal ion concentrations, almost all heavy metals are harmful to humans a living thing. Excessive exposure to heavy metals may cause a variety of diseases such as osteoporosis, cardiovascular problems, and gastrointestinal and renal toxicity [4]. Additionally, these heavy metals are nonbiodegradable, which makes them more challenging to remove from water surfaces. Therefore, the measurement and understanding to control the heavy metals contamination in wastewater are essential.

Chemical precipitation is a common method for treating water. However, this method created a significant volume of hazardous sludge that needed to be treated later and required the application of several chemicals for their treatment before they could be properly disposed [[5], [6], [7]]. Therefore, a focus is being placed on an innovative membrane filtering technology treatment since it offers a sustainable and low-energy process for removing Pb (II) ions.

The primary structural chain of polysulfone (PSF) is mostly made up of benzene rings connected by sulfonyl (-SO2-), ether (-O-) and isopropylidene (-C(CH3)2-) groups [8]. The researchers are interested in PSF polymeric membranes because of their exceptional stability, high mechanical strength and excellent thermal properties [[8], [9]]. However, the PSF membrane's hydrophobic characteristics affect a number of its potential and make it less effective in the water purification process [[8], [10], [11]]. Furthermore, PSF membranes have minimal water flow and can significantly increase membrane fouling because of their hydrophobicity [[12], [13], [14]]. Hence, to improve the hydrophilicity feature in PSF membrane, it is crucial to amend hydrophilicity modification [[15], [16], [17]]. Therefore, the inclusion of PEG as a hydrophilic inorganic nanomaterial was used as an additives.

In this study, we aimed to enhance the ability of the PSF membrane by altering the surface of PSF with SDS anionic surfactant to have better removal of Pb (II) ions. Due to the existence of hydrophobic interactions, it should be highlighted that the alkyl chain of the surfactant is a significant feature that substantially determines the adsorption behaviour and the structure of the adsorbed layer [[18], [19]]. The amphiphilic nature of SDS surfactant allows it to aggregate and form micelles at a certain concentration (referred to as the critical micelle concentration (CMC)) as well as to adsorb at interfaces of polymer chains and modify their characteristics [20]. SDS surfactant is used in remediation technologies based on the aforementioned strengths. Specifically, the capacity to assemble at interfaces promotes the desorption and mobility of contaminants, whereas their ability to micellize and incorporate the contaminants into aggregations makes it much easier to remove and further separate contaminants that have been trapped inside micelles [[21], [22]].

To preserve river ecosystems and ensure the long-term survival of both human and aquatic life, a sustainable wastewater treatment process using membrane filtration is suggested in this study. This research used PSF as polymeric membrane mixes with different concentrations of SDS (0.5, 1.0, 1.5, 2.0 wt%) in preparation of membrane dope solution via phase inversion method. This study aims to investigate the influence of SDS as an ionic surfactant in developing the morphology properties and performance of the membranes.

Experimental part

2.1. Material

The polysulfone (PSF) ($C_{27}H_{24}Cl_2O_4S$), polyethylene glycol (PEG) ($C_{2n}H_{4n+2}O_{n+1}$) and sodium dodecyl sulfate (SDS) ($CH_3(CH_2)_{11}OSO_3Na$) were purchased from Sigma-Aldrich (United States, American). Dimethylacetamide (DMAc) (C_4H_9NO) and lead nitrate ($(PbNO_2)_3$) were from Merck (Selangor, Malaysia) and distilled water.

2.2. Fabrication of PSF/GO membrane

The wet phase inversion method was used to prepare the fabricated membrane solution. Table 1 is a summary of the dope solutions composition. The requisite amount of PEG was put into the media bottle containing DMAc solution and the mixture was agitated until homogenous at 60^oC before PSF

were added. The solution continues agitated for 8 hours. To verify there were no air bubbles in the mixed solution, the solution was left undisturbed at room temperature for at least 1 hour. The casting membrane was cast by feeding dope solution onto a casting blade with 250 m thickness. The solution then was drawn with a consistent pace on a glass plate. The glass plate containing the casting membrane was immersed in a coagulation batch containing distilled water overnight before cutting to a small circle size of 5x5 cm for storage.

Table 1 - Fabricated PSF membrane dope solution

Membrane		Composition (wt %)			
		PSF	***PEG***	***DMAc***	***SDS***
M1	PURE PSF	16	10	74	0
M2	SDS 0.5	16	10	73.5	0.5
M3	SDS 1.0	16	10	73	1.0
M4	SDS 1.5	16	10	72.5	1.5
M5	SDS 2.0	16	10	72	2.0

Notes: PSF=Polysulfone, PEG=Polyethylene glycol, DMAc= Dimethylacetamide, SDS= sodium dodecyl sulfate

2.3. Characterization of fabricated membrane

2.3.1. SEM analysis

SEM was employed by HITACHI TM3000 to examine the cross section of morphology membranes. The membranes were submerged into a nitrogen liquid to be frozen for 5 to 10 minutes. After being shattered, the membrane structure was preserved. At 10 and 25 kV, the images were captured under extremely high vacuum conditions.

2.3.2. Contact Angle

The hydrophilicity of the membrane was evaluated using contact angle goniometer. The membrane samples were placed on glass slide with double tape. The micro syringe was used to drop 10 µl of methylene blue solution onto the membrane surfaces at room temperature. Thereafter, the images of water droplet with membrane surface were analyses by ImageJ.JS images software [20].

2.3.3. Water uptake

The water uptake test was performed to evaluate the amount of water absorbed by fabricated membranes. The wet membranes were weighed using analytical balance before dried up in an oven at 60°C for 24 hours to measure dry membrane weight. The water uptake measurements of three membrane samples were averaged. Equation 1 below was used to calculate the water uptake of the samples [20];

$$\%\ uptake = \left(\frac{w_1 - w_2}{w_2}\right) \times 100 \qquad (1)$$

Where W_1 indicated the weight of wet state membrane (g) and W_2 indicated the weight of dry state membrane (g).

2.3.4. Porosity

An analytical balance was used to measure the wet weight while the membrane is wet. The dry membrane weight value was taken by drying a membrane in an oven for 24 hours at 60°C. An averaged value of three membrane samples were recorded. The following equation used to evaluate the porosity using the data taken [20];

$$Porosity, \varepsilon = \frac{\frac{w_1 - w_2}{\rho_w}}{\frac{w_1 - w_2}{\rho_w} + \frac{w_2}{\rho_m}} \times 100\% \qquad (2)$$

Where, W_1 indicated the weight of wet state membrane (g), W_2 indicated the weight of dry state membrane (g), ρ_w is the density of distilled water (0.998 g/mL) and ρ_m is the density of polymer (PSF = 1.24 g/mL)

2.3.5. Mean Pore Radius

The mean pore radius of the membranes is determined based on the membrane porosity and pure water flux values. The Guereout–Elford–Ferry equation was used to calculate the mean pore radius [20];

$$rm = \sqrt{\frac{(2.9 - 1.75\varepsilon) \times 8\eta l Q}{\varepsilon \times A \times \Delta P}} \qquad (3)$$

Where η is the water viscosity (8.9 x 10^{-4} Pa.s), l is the membrane thickness (m), Q is the volume of permeate water per unit time (m^3/s), A is the membrane area (m^2), and ΔP is the operational pressure (Pa).

2.4. Performance Studies for Humid Acid Removal

2.4.1. Permeation flux

This process was performed using a dead-end cell membrane module as shown in Figure 1. The membrane was cut 5x5 cm into a circle shape to fit in the flat sheet membrane separation unit. The procedure was done by passing feed through the membrane. The 2 bar pressure reservoir is used in the membrane. The permeation flux was calculated using the equation below [20];

$$J_w = \frac{V}{A \cdot \Delta t} \quad (4)$$

Where J_w is the pure water flux (PWF), V is the permeate volume, Δt is the permeate time (h) and A is the area of membrane (m^2).

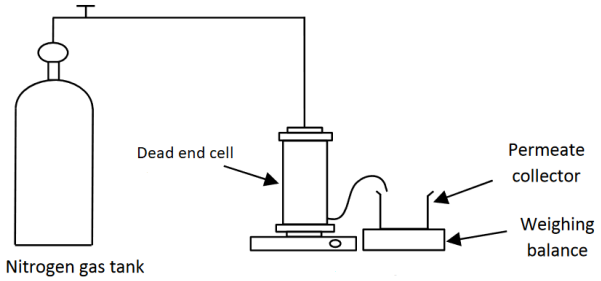

Figure 1 - Dead-end cell membrane module for permeation testing diagram.

2.4.2. Rejection test

For the rejection test, Pb (II) ions aqueous solution was used as a solute to analyse the solute rejection membranes. The permeate for Pb (II) ions was measured with Induced Coupled Plasma Optical Emission Spectroscopy (ICP-OES Agilent 1100) at 187 nm wavelength. The solute rejection is defined as [21];

$$\%R = \left(1 - \frac{C_\rho}{C_f}\right) \times 100 \quad (5)$$

Where, C_p is the Pb (II) ions concentration in the permeate and C_f is the Pb (II) ions concentration in the feed.

2.5. Fouling and kinetic studies

2.5.1 Fouling study

The fouling analysis of each membrane involves three stages. The first stage, lasting for 30 minutes, focuses on measuring the pure water flux ($JWF2$). The second stage involves aqueous filtration of Pb (II) ions, and the third stage, also lasting for 30 minutes, involves washing the membrane with distilled water ($JWF2$). The average values obtained after these three stages are measured and used to determine the membrane's fouling resistance. In this analysis, equations (6) and (7), as described by [20], are utilized to calculate the relative flux reduction (RFR) and fouling resistance ratio (FRR).

$$RFR\ (\%) = \left(1 - \frac{J_{TS}}{J_{WF}}\right) X\ 100\% \quad (6)$$

Where, RFR was relative flux reduction, J_{TS} was Pb (II) ions permeate flux and J_{WF} was the initial pure water flux.

$$FRR\ (\%) = \frac{J_{WF2}}{J_{WF}} X\ 100\% \quad (7)$$

Where FRR was the fouling resistance ratio and J_{WF2} was the pure water flux after the washing step.

2.5.2. Kinetic studies

Hermia's blocking models were utilized to analyze the experimental data and identify the predominant fouling mechanism in this filtration process. The fouling equations for complete blocking (8), standard blocking (9), intermediate blocking (10), and cake filtration (11) mechanisms are provided in Table 2.

Table 2 - Four types of fouling mechanisms and their equations

Fouling mechanism	Equations	
Complete blocking, b	$J = J_0 e^{-k_b t}$	(8)
Standard blocking, s	$J = \frac{J_0}{\left(1 + \frac{k_s J_0}{2} t\right)^2}$	(9)
Intermediate blocking, i	$J = \frac{J_0}{1 + k_i J_0 t}$	(10)
Cake filtration, c	$J = \frac{J_0}{\left(1 + 2k_C J_0^2 t\right)^{\frac{1}{2}}}$	(11)

Notes;
J_0 – initial flux,
t – time taken (min),
k – fouling parameter for each fouling mechanism

Results and Discussion

3.1. Characterization of PSF/SDS membrane

3.1.1. SEM analysis

Scanning electron microscopy was used to photograph membrane morphology. The membrane revealed as the concentration of SDS increases, the membrane morphology transformed to a thin skin layer, finger-like porous and macrovoids upon analysis of the cross-sectional structure membrane. As seen in Figure 2, the pure membrane, M1 has a thick dense layer and a sponge structure with few isolated close-end drop-like pores. In fabricated membranes, the M2 membrane with total 0.5 wt% of SDS concentration displayed the drop-like holes were displaced by irregular porous and larger macrovoids at the bottom of the cross-section

surfaces, yet, the sponge sections are still present. Moreover, finger-like structures that potentially increase water permeability emerged in the M3 membrane at the top layers and the larger macrovoid in the bottom layer. Furthermore, at membrane with concentrations 1.5 wt% and 2.0 wt% SDS (M4 and M5), the formation of a narrow finger-like structure became more elongated and had an enormous channel of macrovoids.

The interaction of PSF-SDS complex attributed to the suppresses in the development of finger like structure in the interlayer. In addition, the free micelles that may separate from polymer chains during the immersion process might result in enormous macrovoids inside the membrane structure. Moreover, the rapid demixing of the membrane solution leads to the creation of the porous structure with finger-like macrovoids while the delayed demixing of the membrane solution leads to the bicontinuous sponge-like structure. The slower rate exchange of solvent and nonsolvent during the phase inversion process leads to smaller pores and a spongy structure and more drop-like pores which can change the membrane permeability, in contrast to rapid exchange rate solvent and nonsolvent resulted in larger pores, more finger-like pores structures as well as more channel available.

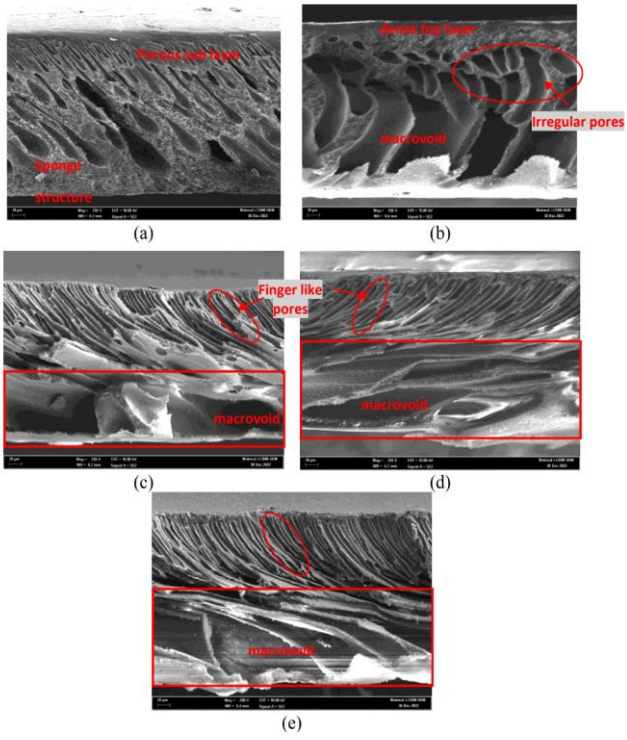

Figure 2 - The SEM analyses for cross-section (x250) morphology on fabricated membrane (**a**= pure PSF; **b**= 0.5 wt%; **c**= 1.0 wt%; **d**= 1.5 wt%; **e**= 2.0 wt%)

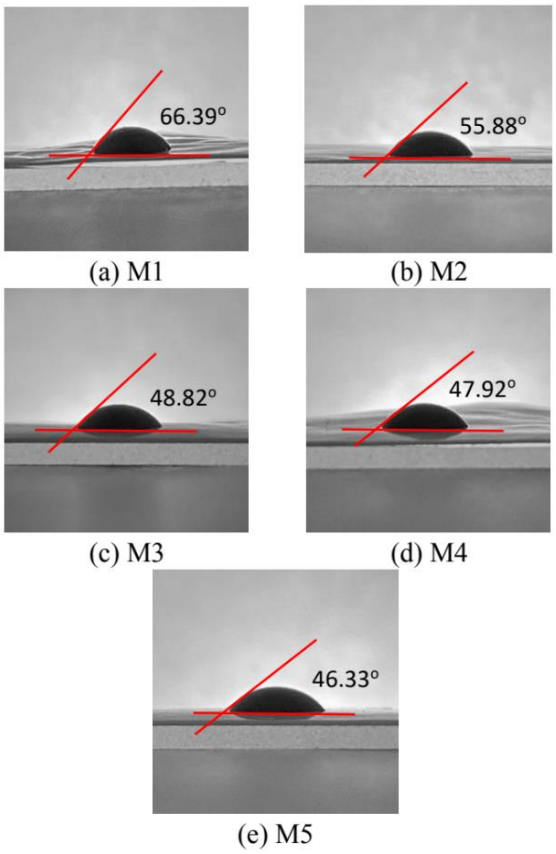

Figure 3 - The images of contact angle for all fabricated membranes (M1= pure PSF; M2= 0.5 wt%; M3= 1.0 wt%; M4= 1.5 wt%; M5= 2.0 wt%)

3.1.2. Physical evaluations on fabricated membranes

Table 3 summarizes the contact angle, porosity and mean pore radius of the fabricated membrane. The angle that forms between water droplets and membrane surfaces is known as contact angle. The membrane's hydrophilicity may be assessed by measuring contact angle. The membranes were referred to as hydrophilic if the contact angle measurement was >90° and vice versa [21]. Figure 3 shows the images of the contact angle for each fabricated membrane. Results show the pure membrane M1 had the highest value 66.39° of contact angle than other membranes which revealed the characteristic of PSF membrane as a hydrophobic polymer. Among the fabricated membranes, the M5 membrane with 2.0 wt% of SDS concentration has the lowest contact angle value of 46.33° which indicates that the membrane surface has the highest hydrophilicity. This result showed the addition of hydrophilic inorganic compound, PEG and hydrophilic surfactant, SDS giving an effect on the membrane surface properties. The O-H hydroxyl group facilitates the linkage of hydrogen

bonds between water molecules on the membrane surface, which increases the membrane hydrophilicity [[22], [23]]. The increment of SDS concentration causes the membrane surface to become more hydrophilic. Therefore, the overall contact angle for all the membranes was arranged in descending order M1> M2> M3> M4> M5 with value 66.39^{o}> 55.88^{o}> 48.82^{o}> 47.92^{o}> 46.33^{o}, respectively.

Studying water uptake is a dependable method to gain insights into the hydrophilic properties of a membrane. The level of hydrophilicity on the membrane surface greatly influences the amount of water absorbed and if the polymer contains macrovoids. The research findings indicate that an increase in SDS inclusion leads to higher water uptake by the membrane. Generally, measuring water uptake aligns with porosity. An increase in membrane porosity strongly suggests a corresponding increase in water uptake, indicating a greater hydrophilicity of the membrane surface.

The modification of membrane morphology was quantified by calculation of membrane porosity. The overall porosity value increased with an increase in SDS concentration. The porosity value for M1, M2, M3, M4 and M5 were 73.35%, 83.33%, 84.48%, 85.21% and 85.30%, respectively. According to the findings, the pure membrane M1 had a lower porosity value than other membranes treated with SDS. this demonstrated the inclusion of SDS modified the structure and morphology of the membrane. This conclusion has been proved by FESEM analysis that have been discussed in Figure 2 above.

Furthermore, the mean pore radius value for pure membrane (M1) was much smaller (3 nm) than the membrane containing SDS. This is due to the hydrophobic characteristic of polymeric PSF that enable the prevention of water to passing through the pure membrane and give effect on membrane permeability. Among the membranes treated with SDS, the pore size was improved with increasing SDS concentration to 1.0 wt%. However, the pore size started to decrease at 1.5 wt% concentration of SDS. This is because of the delay in demixing of solvent and non-solvent during the immersion phase due to the presence of the PSF/SDS complex which enhanced the finger-like structure in the sub-layer membrane. As a consequence, the pore size on the membrane surface decreases. Based on other study, the decreasing in membrane pore size enables in high rejection of solutes [20].

Table 3 - Summary of contact angle, water uptake, porosity and mean pore radius of fabricated membrane.

Membranes	Contact angle (^{o})	Water uptake (%)	Porosity (%)	Mean pore radius (nm)
M1	66.39	33.29	73.35 ± 0.09	3
M2	55.88	39.01	83.33 ± 0.09	8
M3	48.82	41.28	84.48 ± 0.04	10
M4	47.92	43.58	85.21 ± 0.15	6
M5	46.33	44.22	85.30 ± 0.07	7

Notes; M1= pure PSF, M2= 0.5 wt% of SDS, M3= 1.0 wt% of SDS, M4= 1.5 wt% of SDS, M5= 2.0 wt% of SDS.

3.2. Membrane performance studies

3.2.1. Permeation flux

Table 4 displays the summary of membrane performance on permeability testing. The comparison of permeation flux for pure water flux (PWF) and Pb (II) ions flux was also present in Table 4. The PWF was testing by dead-end cell filtration with 2 bar pressure in a nitrogen atmosphere. Results showed the PWF for pure membrane exhibited the lowest flux due to the hydrophobic characteristic of the polymer membrane. Among fabricated membranes, the PWF increased when the amount of SDS concentration increased at a total of 1.0 wt% SDS. However, the water flux rate appeared to deceases in the concentration of 1.5 wt% and 2.0 wt% SDS. Water flux rates can be arranged in descending order for all the membranes M3>M2>M5>M4>M1 with water flux rates 20.46>13.60>9.83>6.19>1.66 g/m^{2}h, respectively.

The increase of water flux after the addition of SDS in membrane dope solution is due to the hydrophilicity improvement on the fabricated membrane surface. Meanwhile, the decrease of water flux at SDS with high concentration can be related to the size of the mean pore radius on the membrane surface as shown in Table 4. The smaller pore size gives an effect on the lack of water flow permeating through the membrane at one time. According to FESEM analyses on the cross-section morphology that were shown in Figure 2, the images displayed the narrow finger like structure on M4 and M5 which indicated the reason for the permeability rates of water flux through the membrane.

The Pb (II) ions feed aqueous solution were tested at 2 bar pressure in a nitrogen atmosphere

and displayed a similar sequence with PWF flux. The pure PSF membrane has the lowest Pb (II) ions flux 1.61 g/m^{2}h, followed by M4< M5< M2< M3 with Pb (II) ions flux of 3.06< 9.13< 10.95< 19.88 g/m^{2}h, respectively. The addition of SDS to PSF membrane dope solution gives the formation of finger-like pores and macro-void structure on the morphology of the membrane. Hence, we can conclude the addition of SDS to the fabricated membrane increases membrane water flux better than the pure membrane, M1.

Table 4 - Summary of PWF, Pb (II) ions flux, Pb (II) ions concentration (ppm) and Pb (II) ions rejection after filtration process using dead end cell for fabricated membranes

Membrane	PWF flux (g/m²h)	Pb (II) ions flux (g/m²h)	Pb (II) ions concentration (ppm)	Pb (II) ions Rejection (%)
M1	1.66	1.61	44.72	10.56
M2	13.20	10.95	23.49	53.02
M3	20.46	19.88	26.63	46.74
M4	6.19	3.06	4.74	90.52
M5	9.83	9.13	11.24	77.52

Notes; PWF= Pure Water Flux, PB= Lead, M1= pure PSF, M2= 0.5 wt% of SDS, M3= 1.0 wt% of SDS, M4= 1.5 wt% of SDS, M5= 2.0 wt% of SDS.

3.2.2. Rejection

The Pb (II) ions rejection of fabricated membranes was shown in Figure 4. The membrane treated with SDS removed more Pb (II) ions compare to a pure membrane. Among the fabricated membrane, the rejection of Pb (II) ions increased when the amount of SDS concentration increased at a total of 1.5 wt% SDS (M4). However, after the SDS concentration is increases to 2.0 wt% (M5), the rejection of Pb (II) ions became slightly decreases. The M4 membrane had the maximum removal of 90.52% for Pb (II) rejection compared to other membranes even though it had a lower penetration flux. This is due to the production of the PSF-SDS complex and the deposition of the SDS polarisation layer that stops it from passing through the membrane [22]. Despite having a higher SDS concentration, the M5 membrane had lower Pb (II) removal than the M4 membrane. This is because, at 2.0 wt% of SDS concentration, the micelles deform close to the membrane surface, allowing metal ion-containing micelles to pass through the membrane and resulting in having a lower removal performance than the M4 membrane. The rejection of Pb (II) ions was followed by M1<M3<M2<M5<M4 with rejection values of 10.56<46.74<53.02<77.52<90.52 per cent rejection.

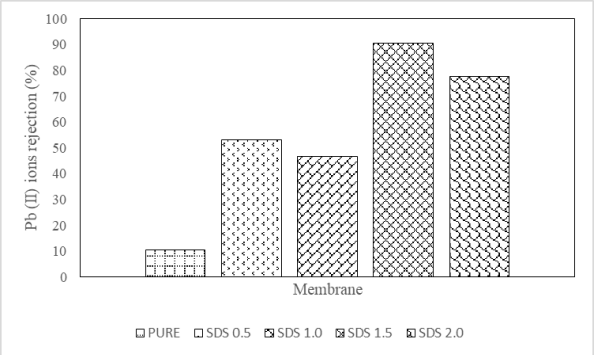

Figure 4 - The Pb (II) ions rejection for fabricated membranes (M1= pure PSF; M2= 0.5 wt%; M3= 1.0 wt%; M4= 1.5 wt%; M5= 2.0 wt%)

.

3.3 Fouling and kinetic studies

3.3.1 Fouling studies

A study was conducted to examine membrane fouling, which is a drawback in membrane filtration. In this analysis, the reversible fouling ratio (RFR) and flux recovery ratio (FRR) were investigated. A higher RFR value indicated a larger accumulation of Pb (II) ions on the membrane surface, which then adsorbed onto the membrane pore [20]. Additionally, a lower FRR value indicated a higher susceptibility to membrane fouling. The fouling analysis of all the produced membranes is illustrated in Figure 5.

According to Figure 5, the membrane containing SDS has better resistance to fouling compared to the pure membrane. Among the membranes tested, the M4 membrane has the highest RFR value (33.57%), indicating a higher deposition of Pb (II) ions on its surface. Previous research has shown that membrane fouling can be influenced by factors such as surface morphology, roughness, and hydrophobicity [20]. Membranes with higher porosity are more prone to pore clogging, resulting in lower permeation flux and increased fouling. The RFR values for the M1, M2, M3, M4, and M5 membranes are approximately 55.20%, 13.00%, 14.46%, 33.57%, and 26.34%, respectively.

After thoroughly rinsing the membrane with distilled water, the secondary water flux was measured. The membrane's morphology can impact the FRR values, as the Pb (II) ions can easily get trapped on the membrane's surface and pores, making it difficult to clean the membrane. The FRR values for M1, M2, M3, M4, and M5 were 44.47%, 87.43%, 81.24%, 73.54%, and 72.96%, respectively. Except for the pure membrane, M1, the FRR values

were higher than the RFR values. This could be attributed to the formation of a micellar gel layer due to the increased SDS concentration. The adsorption of Pb (II) ions onto the SDS gel layer effectively removed the ions, while particle aggregation led to larger micelles and higher FRR levels [21].

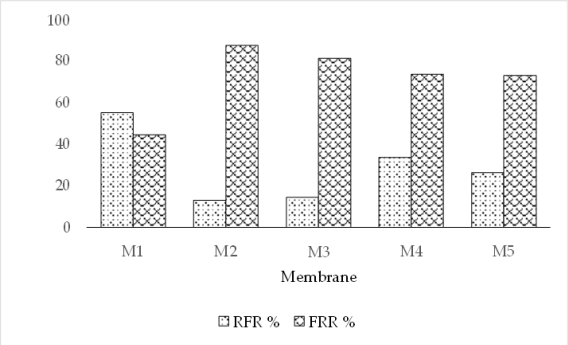

Figure 5 - Membrane fouling for reversible fouling ratio (RFR) and flux recovery ratio (FRR)

Conclusions

In this study, the PSF polymer membrane was fabricated with different concentrations of SDS (0.5 wt%, 1.0 wt%, 1.5 wt% and 2.0 wt%) and DMAc solvent. Our results suggest the addition of SDS into the membrane solution enhanced the properties of the membranes. The results show that fabricated M4 membrane with the addition of 1.5% of SDS had greater results for Pb (II) removal from aqueous solution with 90.52% rejection due to the presence of macrovoids and a porous structure, as shown by SEM analyses. In addition, the fouling mechanism model suggests that the complete blocking observed in the experimental data indicates that porous blockage occurred on the membrane's surface during the absorption of Pb (II) ions.

Acknowledgements. The authors would like to thank GREAT Research Centre, Faculty of Bioengineering and Technology, Universiti Malaysia Kelantan and the School of Materials and Mineral Resources Engineering, Universiti Sains Malaysia for facilitating laboratory and adequate technician assistance for this research. Prof Mohammad M. Fares wishes to acknowledge Jordan University for Science & Technology, project number 20220858 for financial support and facilities.

This work was supported by Universiti Malaysia Kelantan, UMK Matching Research Grant Scheme, [grant number R/MTCH/A1300/00692A/003/2021/00947], [R/JUST/A1300/01684A/010/2023/01209] and JUST Grant number 20220858

***CRediT author statement*:** The experiments were carried out by **N.Q.I.**; the samples were handled by **N.N.Y.**; the results were analyzed and checked by **M.N.** and **N.A.**; the experiments were intended by **N.F.S.** and **M.M.F.**, **A.H.Y.** supervised the project, checked the overall articles, and processed the paper submission. All authors have read and agreed to the published version of the manuscript

Conflicts of interest. The corresponding author states that there is no conflict of interest.

Cite this article as: Nurul Qistina Ismail et al. The effect of Sodium Dodecyl Sulfate on Polysulfone membrane for Pb (II) ions removal in an aqueous solution. Kompleksnoe Ispolzovanie Mineralnogo Syra = Complex Use of Mineral Resources. 2025; 334(3):26-36. https://doi.org/10.31643/2025/6445.25

Су ерітіндісінде Pb (II) иондарын жою үшін натрий додецил сульфатының полисульфонды мембранаға әсері

[1]Nurul Qistina Ismail, [1*]Abdul Hafidz Yusoff, [1]Noor Fazliani Shoparwe, [2]Nur Nabihah Yusof, [3]Muhammad Noorazlan, [1]Nadiah Ameram, [4]Mohammad, M. Fares

[1] Малайзия Келантан университеті, Джели 17600, Келантан, Малайзия
[2] Физика мектебі, Сайнс Малайзия Университеті, 11800 USM, Пенанг, Малайзия
[3] Пендикан Сұлтан Идрис университеті, 35900 Tanjong Malim, Перак, Малайзия
[4] Иордания ғылым және технология университеті, Ирбид, Иордания

Мақала келді: *12 желтоқсан 2023*
Сараптамадан өтті: *20 ақпан 2024*
Қабылданды*: 24 маусым 2024*

ТҮЙІНДЕМЕ

Ластану деңгейінің өсуіне индустрияландыру, халық санының өсуі және дамушы елдердегі даму себеп болады. Pb (II) сияқты ауыр металдар иондарымен ластанған ағынды сулар биологиялық ыдырамайды және адам денсаулығына және басқа да тіршілік иелеріне үлкен қауіп төндіреді. Ауыр металдармен ластанумен күресудің негізгі әдістерінің бірі химиялық тұндыру болып табылады. Дегенмен, бұл әдісті қолданғанда ары қарай өңдеуді қажет ететін қауіпті лай пайда болады. Қоршаған ортаға әсерінің төмен болуына байланысты ауыр металдарды өңдеу процесінде химиялық заттар көп пайдаланылады. Осыған байланысты ағынды сулардағы ауыр металдарды тазартудың балама әдісі ретінде мембраналық фильтрация әдісі зерттелді. Бұл зерттеуде мембраналар диметилацетамидпен (еріткіш) полисульфонды (ПСФ) полимерді және натрий додецил сульфатының (SDS) әртүрлі концентрациясын қосу арқылы ылғал фазалық инверсия әдісін қолдана отырып жасалды (M1 = 0 масса %, M2 = 0,5 масса %, M3= 1,0 масса %, M4= 1,5 масса %, M5= 2,0 масса %). Дайындалған мембраналар сулы ерітіндідегі 50 мг/л Pb (II) иондарын жою үшін сынақтан өтті. Сканерлеуші электронды микроскоп (SEM) мембраналардың морфологиялық құрылымдарын зерттеу үшін пайдаланылды. Сонымен қатар, дайындалған мембраналардың құрылымдық сипаттамалары – жанасу бұрышы, кеуектілік және орташа кеуектер радиусы сияқты параметрлерге сәйкес бағаланды. Сонымен қатар, мембрананың өнімділігі тұйық жасушаларды фильтрациялау арқылы өткізгіштік және қабылдамау ағыны бойыншада бағаланды. Нәтижелер салмағы 1,5% SDS бар M4 мембранасында Pb (II) иондары үшін ең жоғары қабылдамау жылдамдығы (90,52%) болатынын көрсетті. Бұл FESEM талдаулары көрсеткендей, макрооидтардың және кеуекті құрылымның болуына байланысты болуы мүмкін. Басқа растайтын дәлелдер төменгі жанасу бұрышын (63,91^0), жоғары суды сіңіруді (43,58%), жоғары кеуектілікті (85,21%) және M4 мембранасының төменгі орташа кеуек радиусын (6 нм) қамтиды. Ластану механизмінің моделі эксперименттік деректерде байқалған толық блоктаудың Pb (II) иондарын сіңіру кезінде мембрана бетінде кеуекті бітелу пайда болғанын көрсетеді. Қорытындылай келе, таза мембранамен салыстырғанда, мембраналық ерітіндіге SDS қосу мембраналардың қасиеттерін жақсартатыны анықталды. Құрамы салмағы 1,5% SDS концентрациясы бар M4 мембранасы жоғарыда айтылған қасиеттерге байланысты суды тазарту процесінде Pb (II) иондарын жою үшін оңтайлы фильтрлейтінін көрсетті.

Түйін сөздер: полисульфон, натрий додецил сульфаты, қорғасын, мембраналық фильтрация, фазалық инверсия.

Авторлар туралы ақпарат:

Nurul Qistina Ismail *Алтын, сирек жер және материалдық технологиялар орталығының магистрі (GREAT), биоинженерия және технология факультеті, Малайзия университеті Келантан, 17600 UMK kampus Jeli, Келантан. Email: nurulqistinaa98@gmail.com*

Abdul Hafidz Yusoff *Алтын, сирек жер және материалдық технология орталығының (GREAT) доценті, биоинженерия және технология факультеті, Малайзия университеті Келантан, 17600 UMK kampus Jeli, Келантан. Email: hafidz.y@umk.edu.mu*

Noor Fazliani Shoparwe *Доктор, Алтын, сирек жер және материалдық технология орталығы (GREAT), биоинженерия және технология факультеті, Малайзия университеті Келантан, 17600 UMK kampus Jeli, Келантан. Email: fazliani.s@umk.edu.my*

Nur Nabihah Yusof *Доктор, физика мектебі, Сайнс Малайзия Университеті, 11800 USM, Пенанг, Малайзия. Email: nurnabihah7@usm.my*

Muhammad Noorazlan *Доктор, Физика бөлімі, ғылым және математика факультеті, Университет Пендидикан Султан Идрис, Танжунг Малим, Перак, 35900, Малайзия. Email: azlanmn@fsmt.upsi.edu.my*

Nadiah Ameram *Доктор, Алтын, сирек жер және материалдық технология орталығы (GREAT), биоинженерия және технология факультеті, Малайзия университеті Келантан, 17600 UMK kampus Jeli, Келантан. Email: nadiah@umk.edu.my*

Mohammad, M. Fares *Иордания ғылым және технология университетінің қолданбалы химия кафедрасының профессоры, П.О. Қорап 3030, 22110, Ирбид, Иордания. Email: fares@just.edu.jo*

Влияние додецилсульфата натрия на полисульфоновую мембрану для удаления ионов Pb(II) в водном растворе

[1]Nurul Qistina Ismail, [1*]Abdul Hafidz Yusoff, [1]Noor Fazliani Shoparwe, [2]Nur Nabihah Yusof, [3]Muhammad Noorazlan, [1]Nadiah Ameram, [4]Mohammad M. Fares

[1] Университет Малайзии Келантан, Джели 17600, Келантан, Малайзия
[2] Школа физики, Университет Сайнс Малайзия, 11800 USM, Пенанг, Малайзия
[3] Университет Пендидикан Султан Идрис, 35900 Танджонг Малим, Перак, Малайзия
[4] Иорданский университет науки и технологий, Ирбид, Иордания

Поступила: *12 декабря 2023*
Рецензирование: *20 февраля 2024*
Принята в печать: *24 июня 2024*

АННОТАЦИЯ

Неустойчивый рост уровня загрязнения обусловлен индустриализацией, ростом населения и ростом развивающихся стран. Загрязнения сточных вод ионами тяжелых металлов, таких как Pb (II), не поддаются биоразложению и представляют серьезную угрозу для здоровья человека и других живых существ. Одним из основных методов борьбы с загрязнением тяжелыми металлами является химическое осаждение. Однако на нем образовывался опасный ил, требующий дальнейшей обработки, и использовалось значительное количество химикатов в процессе очистки от тяжелых металлов из-за его низкого воздействия на окружающую среду. В результате был исследован метод мембранной фильтрации как альтернативный метод очистки сточных вод от тяжелых металлов. В этом исследовании мембраны были изготовлены с использованием метода инверсии влажной фазы путем включения полимера полисульфона (PSF) с диметилацетамидом (растворителем) и включения различных концентраций додецилсульфата натрия (SDS) (M1 = 0 мас.%, M2 = 0,5 масс. %, M3= 1,0 масс. %, M4= 1,5 масс. %, M5= 2,0 масс. %. Изготовленные мембраны были протестированы на удаление 50 мг/л ионов Pb(II) в водном растворе. Сканирующую электронную микроскопию (СЭМ) использовали для исследования морфологической структуры мембран. Кроме того, по этим параметрам оценивались структурные характеристики изготовленных мембран; контактный угол, пористость и средний радиус пор. Кроме того, характеристики мембраны также оценивали по потоку проникновения и отторжения с использованием тупиковой клеточной фильтрации. Результаты показывают, что мембрана M4 с 1,5 мас.% ДСН имела самый высокий уровень отторжения (90,52%) ионов Pb (II). Вероятно, это связано с наличием макропустот и пористой структуры, как показали анализы FESEM. Другие подтверждающие данные включают меньший угол контакта (63,91°), более высокое поглощение воды (43,58%), более высокую пористость (85,21%) и более низкий средний радиус пор (6 нм) для мембраны M4. Модель механизма загрязнения предполагает, что полная блокировка, наблюдаемая в экспериментальных данных, свидетельствует о том, что закупорка пор произошла на поверхности мембраны при поглощении ионов Pb(II). В заключение, по сравнению с чистой мембраной становится очевидным, что добавление ДСН в раствор мембраны улучшило свойства мембран. Мембрана M4 с содержанием ДСН 1,5 мас.% продемонстрировала оптимальную фильтрацию для удаления ионов Pb(II) в процессе водоочистки благодаря отличным свойствам, упомянутым выше.

Ключевые слова: полисульфон, додецилсульфат натрия, вести, мембранная фильтрация, инверсия фазы.

Информация об авторах:

Nurul Qistina Ismail — *Магистр Центра технологического предпринимательства в области золота, редких земель и материалов (GREAT), факультета биоинженерии и технологий, Университет Малайзии Келантан, 17600 кампус UMK Джели, Келантан. Email: nurulqistinaa98@gmail.com*

Abdul Hafidz Yusoff — *Доцент Центра технологического предпринимательства в области золота, редких земель и материалов (GREAT), факультет биоинженерии и технологий, Университет Малайзии Келантан, 17600 UMK кампус Джели, Келантан. Email: hafidz.y@umk.edu.mu*

Noor Fazliani Shoparwe — *Доктор, Центр технологического предпринимательства редкоземельных металлов и материалов (GREAT), факультет биоинженерии и технологий, Университет Малайзии Келантан, 17600 UMK кампус Джели, Келантан. Email: fazliani.s@umk.edu.my*

Nur Nabihah Yusof — *Доктор философии, Школа физики, Университет Сайнс Малайзия, 11800 USM, Пенанг, Малайзия. Email: nurnabihah7@usm.my*

Muhammad Noorazlan — *Доктор физических наук, факультет естественных наук и математики, Пендидиканский университет Султана Идриса, Танджунг Малим, Перак, 35900, Малайзия. Email: azlanmn@fsmt.upsi.edu.my*

Nadiah Ameram — *Доктор, Центр технологического предпринимательства редкоземельных металлов и материалов (GREAT), факультет биоинженерии и технологий, Университет Малайзии Келантан, 17600 UMK кампус Джели, Келантан. Email: nadiah@umk.edu.my*

Mohammad, M. Fares — *Профессор кафедры прикладной химии Иорданского университета науки и технологий, П.О. Box 3030, 22110, Ирбид, Иордания. Email: fares@just.edu.jo*

References

[1] Singh J, Sharma M, and Basu S. Heavy metal ions adsorption and photodegradation of remazol black XP by iron oxide/silica monoliths: Kinetic and equilibrium modelling, Advance Powder Technology. 2018; 29(9):2268-2279. https://doi.org/10.1016/j.apt.2018.06.011

[2] Kolbasov A, Sinha-Ray S, Yarin A L, and Pourdeyhimi B. Heavy metal adsorption on solution-blown biopolymer nanofiber membranes, Journal Membrane Science. 2017; 530:250–263. https://doi.org/10.1016/j.memsci.2017.02.019

[3] Xu M, Hadi P, Chen G, and McKay G. Removal of cadmium ions from wastewater using innovative electronic waste-derived material, Journal Hazardous Material. 2014; 273:118-123. https://doi.org/10.1016/j.jhazmat.2014.03.037

[4] Vardhan K H, Kumar P S, and Panda R C. A review on heavy metal pollution, toxicity and remedial measures: Current trends and future perspectives, J. Mol. Liq. 2019; 290:111197. https://doi.org/10.1016/j.molliq.2019.111197

[5] Azimi A, Azari A, Rezakazemi M, and Ansarpour M. Removal of Heavy Metals from Industrial Wastewaters: A Review, ChemBioEng Rev. 2017; 4(1):37-59. https://doi.org/10.1002/cben.201600010

[6] Chaemiso T D. Removal Methods of Heavy Metals from Laboratory Wastewater, J. Nat. Sci. Res. 2019; 9(2):36-42. https://doi.org/10.7176/jnsr/9-2-04

[7] Chandra Joshi N, Sharma R, and Singh A. Biosorption: A Review on Heavy Metal Toxicity and Advances of Biosorption on Conventional Methods, J. Chem. Chem. Sci. 2017; 7(9):714-724. www.chemistry-journal.org

[8] Chukov D, Nematulloev S, Zadorozhnyy M, Tcherdyntsev V, Stepashkin A, and Zherebtsov D. Structure, mechanical and thermal properties of polyphenylene sulfide and polysulfone impregnated carbon fiber composites, Polymers (Basel). 2019; 11(4). https://doi.org/10.3390/polym11040684

[9] Abd Hamid S, Shahadat M, and Ismail S. Zeolite–polysulfone-based adsorptive membrane for removal of metal pollutants, Chem. Pap. 2021; 75(9):4479-4492. https://doi.org/10.1007/s11696-021-01668-x

[10] Shokri E, Yegani R, and Akbarzadeh A. Novel adsorptive mixed matrix membranes by embedding modified montmorillonite with arginine amino acid into polysulfones for As(V) removal, Appl. Clay Sci. 2017; 144:141-149. https://doi.org/10.1016/j.clay.2017.05.011

[11] Benkhaya S, et al. Polysulfone/Polyetherimide Ultrafiltration composite membranes constructed on a three-component Nylon-fiberglass-Nylon support for azo dyes removal: Experimental and molecular dynamics simulations, Colloids Surfaces A Physicochem. Eng. Asp. 2021; 625:126941. https://doi.org/10.1016/j.colsurfa.2021.126941

[12] Gao Y, Li B, Zhong L, Zhang L, and Ding Z. Effect of nano-amphiphilic cellulose as a modifier to PSf composite membranes, Vacuum. 2014; 107:199-203. https://doi.org/10.1016/j.vacuum.2014.01.029

[13] Ibrahim G P S. et al. Novel, one-step synthesis of zwitterionic polymer nanoparticles via distillation-precipitation polymerization and its application for dye removal membrane, Sci. Rep. 2017; 7(1):1-16. https://doi.org/10.1038/s41598-017-16131-9

[14] Ibrahim G P S. et al. Performance intensification of the polysulfone ultrafiltration membrane by blending with copolymer encompassing novel derivative of poly(styrene-co-maleic anhydride) for heavy metal removal from wastewater. Chem. Eng. J. 2018; 353:425-435. https://doi.org/10.1016/j.cej.2018.07.098

[15] Khajouei M, Najafi M, and Jafari S A. Development of ultrafiltration membrane via in-situ grafting of nano-GO/PSF with anti-biofouling properties, Chem. Eng. Res. Des. 2019; 142:34-43. https://doi.org/10.1016/j.cherd.2018.11.033

[16] Fainerman V B, Mobius D, and Miller R. Surfactants: Chemistry, Interfacial Properties, Applications. 2001.

[17] Mao X, Jiang R, Xiao W, and Yu J. Use of surfactants for the remediation of contaminated soils: A review, J. Hazard. Mater. 2015; 285:419-435. https://doi.org/10.1016/j.jhazmat.2014.12.009

[18] Fernández E, Benito J M, Pazos C, and Coca J. Ceramic membrane ultrafiltration of anionic and nonionic surfactant solutions, Journal Membrane Science. 2005; 246(1):1-6. https://doi.org/10.1016/j.memsci.2004.04.007

[19] Peyravi M, Rahimpour A, Jahanshahi M, Javadi A, and Shockravi A. Tailoring the surface properties of PES ultrafiltration membranes to reduce the fouling resistance using synthesized hydrophilic copolymer, Microporous Mesoporous Material. 2012; 160:114-125. https://doi.org/10.1016/j.micromeso.2012.04.036

[20] Shoparwe N F, Kee L C, Otitoju T A, Shukor H, Zainuddin N, and Makhtar M M Z. Removal of humic acid using 3-methacryloxypropyl trimethoxysilane functionalized MWCNT Loaded TiO_2/PES hybrid membrane, Membranes (Basel). 2021; 11(9):721. https://doi.org/10.3390/membranes11090721

[21] Ariono D, Khoiruddin, Prabandari D, Wulandari R, and Wenten I G. Preparation and characterization of polysulfone/PEG heterogeneous ion exchange membrane for reverse electrodialysis (RED), J. Phys. Conf. Ser. 2017; 877(1). https://doi.org/10.1088/1742-6596/877/1/012075

[22] Folgado E, Ladmiral V, and Semsarilar M. Towards permanent hydrophilic PVDF membranes. Amphiphilic PVDF-b-PEG-b-PVDF triblock copolymer as membrane additive, Eur. Polym. J. 2020; 131:109708. https://doi.org/10.1016/j.eurpolymj.2020.109708

[23] Toosi M R, Emami M R S, and Hajian S. Dynamic filtration and static adsorption of lead ions in aqueous solution by use of blended polysulfone membranes with nano size MCM-41 particles coated by polyaniline, Environ. Sci. Pollut. Res. 2018; 25(20):20217-20230. https://doi.org/10.1007/s11356-018-2236-3

Crossref

DOI: 10.31643/2025/6445.26

Engineering and technology

Effect of soapstock in the composition of modified additive for improving strength characteristics of concrete structures

[1,2]Dyussembinov D.S., [1,2]Lukpanov R.E., [1,2*]Altynbekova A.D., [1,2]Zhantlesova Zh.B., [3] Talal Awwad

[1] Solid Research Group LLP, Astana, Kazakhstan
[2] L.N. Gumilyov Eurasian National University, Astana, Kazakhstan
[3] Damascus University, Damascus, Syria

** Corresponding author email: kleo-14@mail.ru*

Received: *March 25, 2024*
Peer-reviewed: *April 2, 2024*
Accepted: *July 9, 2024*

ABSTRACT

The article presents the results of research on the influence of soapstock used in the composition of two-component modified additive. Standard tests of beam samples for flexural and compressive strength, and standard cubic samples for water absorption and frost resistance were performed. Tests were performed for samples with different contents of soapstock (Sp): 5, 7.5, 10 and 12.5 % by weight of cement, microsilica and phosphogypsum. The strength measurements of the beam samples showed that the maximum effect concerning the increase in material strength was achieved at 5% of the soapstock content. However, it should be noted that the subsequent decrease in strength with increasing concentration of soapstock is not significant, up to Sp=10% does not exceed 1%. Thus, the optimal concentration of soapstock, at which the maximum effect on the strength of the material will be achieved, is 5-10%. The obtained curve of dependence of water absorption change on the soapstock concentration showed the optimal gradient of water absorption, which corresponds to Sp=10%. With further increase of soapstock, the decrease of water absorption index is not significant. Tests on frost resistance showed that the maximum resistance to cyclic freezing is observed in samples with Sp=10%, further increase reduces frost resistance. The regularity in the increase of frost resistance with increasing concentration of soapstock is logical because with each increase in concentration, the hydrophobization of the material increases. However, if the hydrophobicity of samples with Sp=12.5%, although not significantly, still increases about Sp=10%, the frost resistance decreases.

Keywords: foam concrete, two-component modified additive, technological scheme, soapstock, strength properties, water absorption, frost resistance.

Information about authors:

Dyussembinov Duman Serikovich — *Senior Researcher, Solid Research Group LLP, Astana, Kazakhstan. C.t.s., Associate Professor, Department of Technology of Industrial and Civil Construction, L.N. Gumilyov Eurasian National University, Astana, Kazakhstan. Email: dusembinov@mail.ru*

Lukpanov Rauan Ermagambetovich — *Scientific Supervisor, Solid Research Group LLP, Astana, Kazakhstan. PhD, Professor, Department of Technology of Industrial and Civil Construction, L.N. Gumilyov Eurasian National University, Astana, Kazakhstan. Email: rauan_82@mail.ru*

Altynbekova Aliya Doszhankyzy — *Researcher, Solid Research Group LLP, Astana, Kazakhstan. Senior lecturer, Department of Technology of Industrial and Civil Construction, L.N. Gumilyov Eurasian National University, Astana, Kazakhstan. Email: kleo-14@mail.ru*

Zhantlesova Zhibek Beisembayevna — *Junior researcher, Solid Research Group LLP, Astana, Kazakhstan. PhD. Student, Department of Technology of Industrial and Civil Engineering, L.N. Gumilyov Eurasian National University, Astana, Kazakhstan. Email: zhibek81@mail.ru*

Talal Awwad — *Professor of Department of Geotechnical Engineering, Damascus University, Damascus, Syria. E-mail: dr.awwad.gfce@gmail.com*

Introduction

The application of new materials and technologies in production is a key factor in the development of the construction industry, bringing innovation and rethinking the way materials are created and used. Special attention is paid to concrete construction, where innovative approaches contribute to the formation of more efficient, durable and sustainable structures. The production of construction materials plays an important role in the economy, providing raw materials for the industry and significantly influencing the overall output. New materials and

production methods are being actively researched in this area, including the development of more environmentally friendly processes. One example of such innovation is the recycling of anthropogenic waste into construction composites, which helps to reduce environmental impact and increase the sustainability of building materials [[1], [2], [3], [4]].

In modern construction, guaranteeing the strength and durability of materials is an integral part of creating reliable and sustainable structures. In this context, foam concrete occupies a special place among a variety of building materials used in various industries. Due to its lightness, excellent thermal insulation properties and high degree of resistance to destruction, foam concrete is widely used for the construction of various building structures and products. However, despite its many advantages, there is considerable potential for further improvement of the properties and characteristics of this material through the use of various additives and innovative technologies [[5], [6], [7]].

Cellular materials such as foamed concrete play a key role in modern construction due to their high thermal insulation and applicability in building construction. It not only contributes to environmental improvement, but also saves resources as improved thermal insulation helps to reduce the consumption of fuel, energy and natural materials. However, the foam concrete production process faces the problem of the short life of the foam. Various stabilization methods are used to increase the durability of foam concrete, among which modified additives are particularly promising. These additives help to increase the stability of the foam and extend its service life [[8], [9], [10], [11]].

A wide range of modified additives and their application methods provide an opportunity to optimize foam strengthening, which ultimately leads to improved quality and reliability of foam concrete structures. Rapid development in this area of research pushes the construction industry towards innovative solutions that contribute not only to reducing the negative environmental impact but also to improving energy efficiency, which is an important aspect in today's environmentally oriented construction practice [[12], [13]].

A large part of the transformation of concrete as an important building material is determined by the use of various additives that can improve its physical and mechanical properties [[14], [15]]. These additives can be carefully selected according to the specific needs and technological application of concrete. For example, some additives are aimed at increasing the setting or curing rate of concrete, while others are designed to increase its strength, reduce water absorption, improve frost resistance and provide other desired characteristics [[16], [17], [18], [19]]. The use of properly selected additives plays a key role in creating concrete structures that meet high requirements for strength, durability and resistance. The results obtained correlate well with similar studies conducted in the field of foam concrete [[20], [21], [22], [23]]. In these works, comprehensive studies of the physical and mechanical properties of foam concrete were carried out, including comparative analysis of different variants of compositions. These studies not only confirm the obtained results, but also provide valuable data on the technical characteristics of foam concrete under different conditions and with different compositions.

This article details the process of development and application of a modified additive, which has a plasticizing effect to significantly improve the characteristics and functionality of foam concrete as a building material. The additive is developed taking into account the peculiarities and requirements of foam concrete production, which allows to achieve a higher level of quality and efficiency of its application.

In the composition of the additive it is supposed to use industrial wastes, exactly the following components: microsilica (Ms further), phosphogypsum (PhG further) soapstock (Sp further), post-alcohol bard (PaB further), as well as caustic soda.

Microsilica - waste from metallurgical production, delivered from TNK Kazchrome JSC. The chemical composition is as follows: SiO_2: 90-92%; Al_2O_3: 0.6-0.8%; Fe_2O_3: 0.4-0.7%; CaO: 0.4-0.9%; MgO: 0.8-1.0%; Na_2O: 0.6-0.8%; K_2O: 1.2-1.4%; C: 0.9-1.2%; S: 0.2-0.3%. To increase the strength properties of concrete, microsilica, which is a finely dispersed medium of active minerals, is introduced into its composition.

Post-alcohol bard - waste from alcohol production, delivered from Aydabul distillery JSC. PaB has the following composition: crude protein - 2.0%, non-fatty substances - 3.0%, fat - 0.5%,

cellulose - 0.5%. For its better mixing and plasticization, post-alcohol bard, which is essentially a surface active additive, is introduced into the composition.

Phosphogypsum - waste from phosphoric acid production, delivered from Kazphosphate LLP. The composition includes: - calcium sulfate dihydrate ($CaSO_4*2H_2O$) not less than 70 %; - water-soluble phosphates not more than 0.3 %; - fluoride compounds (in terms of fluorine) not more than 0.25 %; - water (H_2O) not more than 26 %. For mineralogical balance, phosphogypsum is introduced into the concrete mix as a result of the addition of microsilica, which includes up to 95% silicon oxide.

Soapstock - waste from refined oil production, delivered from Altec Ltd. The use of soapstock in the composition of concrete contributes to its volumetric hydrophobization due to the fact that it is represented by a fatty acid composition.

Caustic soda (NaOH) – stabilizer, delivered from Kaustik JSC. The additive also contains a small amount of caustic soda, which is necessary for leaching of soapstock and slowing down the process of its oxidation.

The result is a hydrophobic concrete with increased strength. The main purpose of this additive is to improve the hydrophilicity of the cement, which promotes more efficient moisture penetration and reduces the need for water to mix the foam concrete mass. This will lead to a more homogeneous structure of the foam concrete, which is an important factor in its quality and strength. In addition, the additive will help reduce the number of micropores in the cell walls of the foam concrete, which will provide a better porous structure for the material, improving its properties.

The study aims to evaluate the effect of each of the above-mentioned component of the additive. However, this paper will present the results of the third stage of the study, namely the effect of soapstock on the transformation processes of concrete, exactly on its strength, water absorption and frost resistance. Cement-sand mixture with 20% inclusion of microsilica and 15% content of phosphogypsum by weight of cement was presented as a reference sample. The technological composition of the reference sample was obtained from the results of the first and second stages of the study, the effect of microsilica and phosphogypsum on the quality of concrete.

Experimental technique

The proposed additive is a composite mixture of industrial waste consisting of a liquid and a solid phase. The solid phase (component 1, K1), in turn, is represented by a dry mixture of microsilica, phosphogypsum and neutralized soapstock, and the liquid phase (component 2, K2) - by post-alcohol bard.

To increase the strength properties of concrete, microsilica, which is a finely dispersed medium of active minerals, is introduced into its composition. For its better mixing and plasticization, post-alcoholic bard, which is essentially a surface active additive, is introduced into the composition. For mineralogical balance, phosphogypsum is introduced into the concrete mix as a result of the addition of microsilica, which includes up to 95% silicon oxide. The use of soapstock in the composition of concrete contributes to its volumetric hydrophobization due to the fact that it is represented by a fatty acid composition. The additive also contains a small amount of caustic soda, which is necessary for leaching of soapstock and slowing down the process of its oxidation. Ultimately, we obtain hydrophobic concrete with increased strength.

Figure 1 shows the technological scheme of production of the modified additive. The technological process of production includes two subsequent stages of production. At the first stage preparation of the dry component of the additive is carried out in the process of grinding, drying and mixing of microsilica and phosphogypsum. Grinding of components is necessary to obtain a homogeneous fine-dispersed medium, to obtain their maximum activity in the process of hydration of concrete. Drying is necessary for the qualitative selection of components by weight and exclusion of unaccounted water in the composition of the additive. In the second stage, the liquid component of the additive is prepared, exactly mixing of soapstock with post-alcohol bard and their subsequent neutralization by acidity.

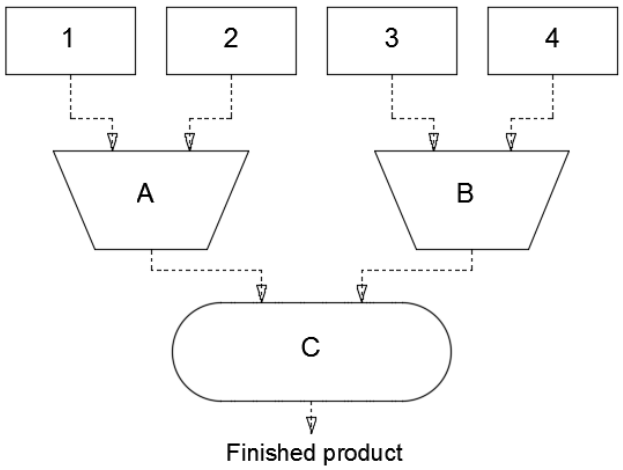

1 – Microsilica
2 – Phosphogypsum
3 – Soapstock and caustic soda
4 – Post-alcohol bard
A, B – Mixer
C – Rotary Dispergator

Stage 1: (preparation of dry component): mixing of microsilica with phosphogypsum in mixer A.
Stage 2: (preparation of the liquid component): mixing in mixer B of soapstock, caustic soda and post-alcohol bard.

Figure 1 - Technological stage of additive production

Table 1 - Variable compositions of mixtures

Stages	Content of components by weight, g							
	Sand	Cement	Ms	PhG	Sp	NaOH	PaB	Water
Reference	1500	500	0	-	-	-	-	200
Stage 1	1500	450	50	-	-	-	-	200
	1500	425	75	-	-	-	-	200
	1500	400	100	-	-	-	-	200
	1500	375	125	-	-	-	-	200
Stage 2	1500	450		50	-	-	-	200
	1500	425		75	-	-	-	200
	1500	400		100	-	-	-	200
	1500	375		125	-	-	-	200
Stage 3	1500	475.0			24.750	0.250	-	200
	1500	462.5			37.125	0.375	-	200
	1500	450.0			49.500	0.500	-	200
	1500	437.5			61.875	0.625	-	200
Stage 4	1500	500					5	195
	1500	500					10	190
	1500	500					15	185
	1500	500					20	180

Table 2 – Variable compositions of the studied mixtures

Sample	Content of components by weight, g							
	Sand	Cement	Ms	PhG	Sp	NaOH	PaB	Water
Reference	1500	340	85	75	-	-	-	200
Sp=5%	1500	323	81	71	25	0.25	-	200
Sp=7.5%	1500	315	79	69	37	0.38	-	200
Sp=10%	1500	306	77	68	50	0.50	-	200
Sp=12.5%	1500	298	74	66	62	0.63	-	200

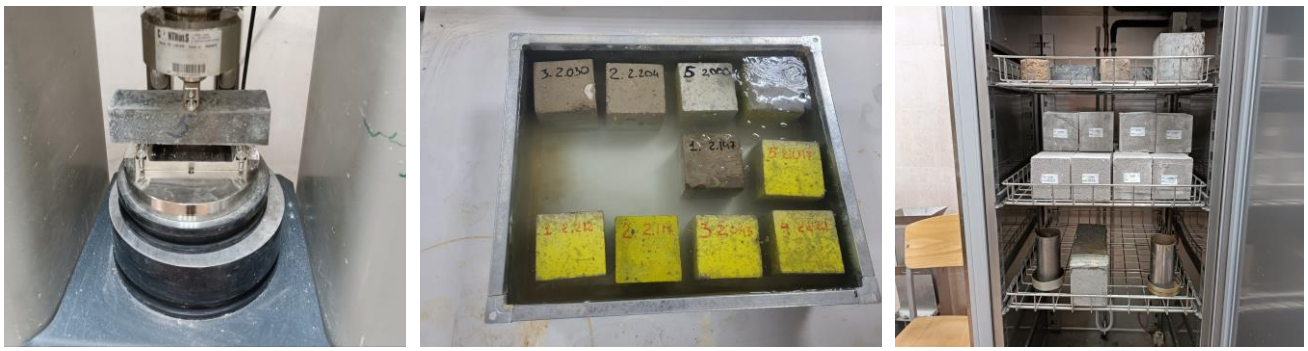

Figure 2 - Conducting laboratory tests

Table 1 shows the variation compositions of the mixtures of each stage of the study. Table 2 shows the variation compositions of the mixtures of the third stage of the study, exactly the compositions with different contents of soapstock (hereinafter - Sp).

The ratio of microsilica to cement is 10, 15, 20 and 25% by weight. The ratio of phosphogypsum to microsilica to cement is 10, 15, 20 and 25% by weight. The ratio of soapstock to caustic soda with respect to microsilica with phosphogypsum and cement is 5.0, 7.5, 10.0, and 12.5% by weight. The ratio of post-alcohol bard to water is 2.5, 5.0, 7.5, and 10% by weight. Variable substitution of soapstock with caustic soda (for stabilization) from 5.0 to 12.5 % (2.5 % multiplicity) by weight of cement, microsilica and phosphogypsum. The ratio of the latter is fixed, is 20 % of microsilica by weight of cement and 15 % of phosphogypsum by weight of microsilica with cement (according to previously conducted studies).

Evaluation of strength parameters of samples in compression and bending of sample beams was carried out according to the standard method of GOST 30744-2001 [24] (Figure 2). Comparison of strength of samples of variable composition was performed to evaluate the optimal composition of the modified additive and to assess its performance. Comparison of strength values of samples with and without the additive will allow to evaluate the influence of the additive components on concrete modification and its transformation in terms of strength improvement. Evaluation of the samples for water absorption capacity of the compared concrete samples was performed according to GOST 12730.3-2020 [25] (Figure 2). Comparison of water absorption of concrete will allow to give an assessment of the serviceability of concrete with the use of modified additive, primarily related to the service life of the material. The hydrophobicity of the material will characterize its resistance to the damaging effects of water during service life, as well as its improvement in frost resistance (taking into account the mechanics of frost resistance testing). Evaluation of samples for frost resistance of concrete samples was carried out according to GOST 10060-2012 [26] (Figure 2). Comparison of frost resistance indices of variation types of concrete is also related to the assessment of the serviceability of the material, evaluation of its durability. The sequence of cyclic freezing and thawing of the samples was performed under the condition of reducing the number of cycles, i.e. as the cycles increase, the terms of control measurements were reduced (from 50 to 25 cycles). Control measurements of strength and mass were performed: at 50, 100, 150, 175, 175, 200, 225 and 250 cycles.

Results and Discussion

Figure 3 shows the results of strength measurements at 28 days of the bar samples. Figure 3A shows the results of partial and average strength values at different concentrations of soapstock, and Figure 3B shows the statistical values of coefficients of variation and comparison as a percentage of reference sample.

According to the measurement results (Figure 3A), the partial strength values of reference samples range from 55.56 to 58.39MPa, the average is 56.53MPa. The partial strength values of samples with Sp=5% content range from 55.65 to 58.19MPa, the average is 56.91MPa. For samples with Sp=7.5% content, the strength ranges from 55.28 to 59.11MPa, with an average of 56.88MPa. The same values for samples with Sp=10% content range from 54.79 to 57.35PMa, with an average of 56.37MPa. In samples with Sp=12.5% content, the strength from 51.63 to 56.49PMa, with an average of 56.61MPa. The samples with soaptock content of 5, 7.5 and 10% have similar strength values to the

reference sample, according to the curves of Figure 1B, the difference being 0.69, 0.61 and -0.30%, respectively. The samples with 12.5% soapstock content have strength values different from the reference sample, the difference is -5.45%. The latter indicates the negative influence of soapstock at its high content in the concrete mixture. Further strength reduction from increasing the amount of soapstock and caustic soda $Na(OH)_2$ leads to an increase in the composition of alkali and fatty acids, which after the release of fatty acids reduce the activity of the cement hydration process, and alkali subsequently interacting with portlandites increase the process of internal corrosion of concrete. The evaluation of the coefficients of variation suggests that the high concentration of soapstock reduces the stability of concrete structures, as evidenced by the increase in the variation of these partial strength values. Thus, the influence of soapstock on the strength of concrete was not revealed, moreover, its high concentration negatively affects the strength of concrete.

To obtain the most accurate statistical value of reference sample strength, 21 partial values of cubic (not beam samples) strength (cumulative from the entire set of tests) were used. The large number of samples allowed to determine as accurately as possible the mathematical expectation of strength values, relative to which the loss of strength will be made. The latter becomes permissible because the influence of soapstock on strength increase is not observed, and the strength reduction at a high concentration of soapstock (more than 10%), in the context of frost resistance tests, does not affect the analysis of the results. Figure 4 shows the distributions of the partial strength values concerning the Gaussian diagram constructed from the results of the obtained partial strength values. For the convenience of comparing the data with the private values (auxiliary axis on the diagram), the probability density was corrected relative to unity. This correction does not change the quality of the curve but calibrates the scale of the Gaussian diagram to the private strength values. For information, the partial strength values are shown in the diagram of Figure 4 on the right: for ease of perception, all partial strength values have been sorted from smaller to larger.

The average strength of the 21 measurements was 66.38 MPa, the squared deviation was 0.97 and the coefficient of variation was 1.45%. The coefficient of variation, with a large number of tests, allows subsequent adjustments to be made for strength losses. Given a coefficient of variation of 1.45%, strength losses up to ±1.45% can be attributed to statistical error. Therefore, loss of strength was assumed to be effective when the values of the percentage of strength change (loss of strength) exceeded the values of the coefficient of variation reference sample.

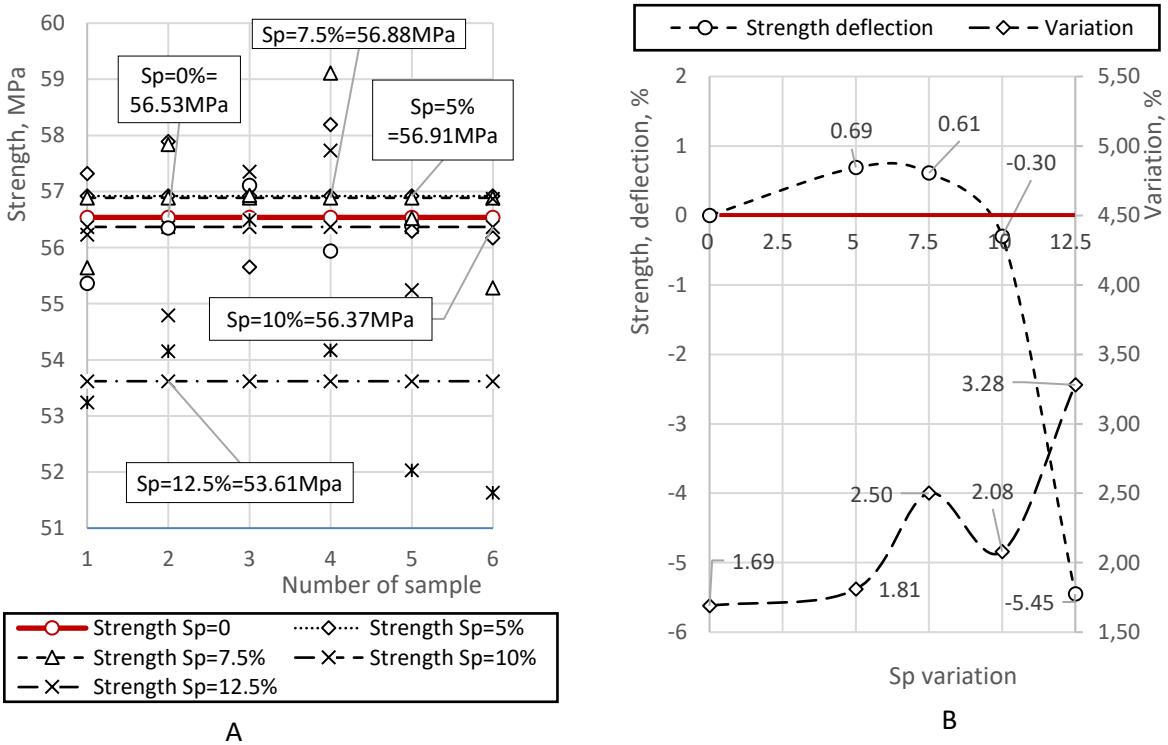

Figure 3 - Strength graphs of samples at 28 days of age

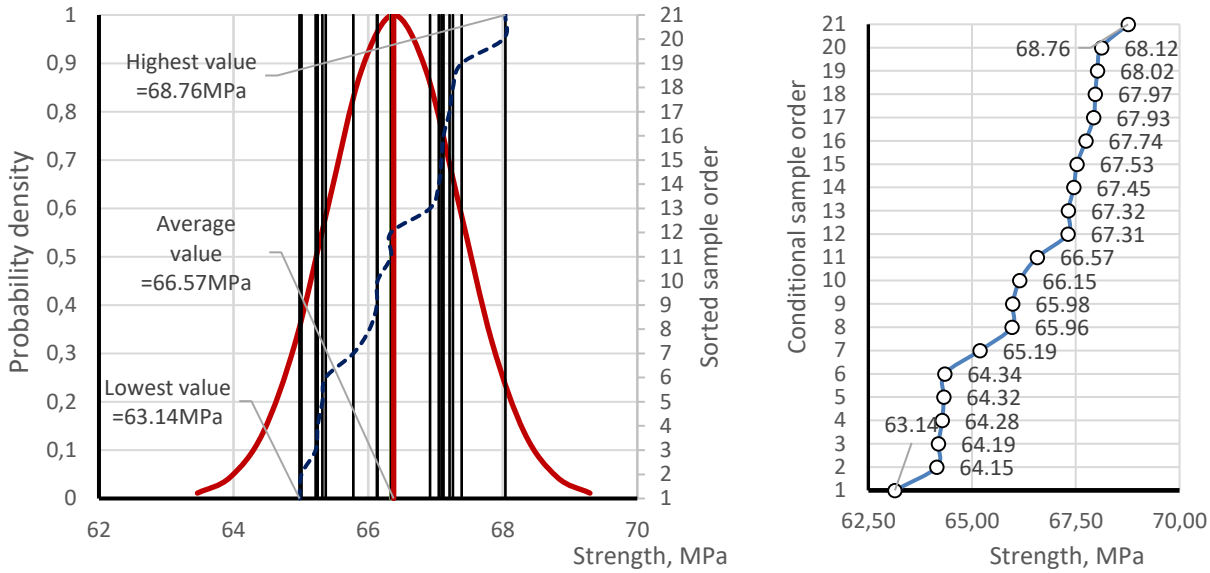

Figure 4 - Distribution of individual strength values

Figures 5-9 show plots of strength loss and mass loss as a result of cyclic freezing and thawing of cubic samples with variation inclusion of soapstock (Sp). Figure 5-9A shows absolute partial values of strength loss, and Figure 5-9B shows mass loss and their corresponding coefficients of variation.

The variation of strength sample from freezing cycles from 50 to 200 varies from 62.32 to 55.20 MPa. The maximum strength reduction corresponds to the maximum number of cycles, and the appreciable strength reduction occurs from 100 cycles. Thus, coefficients of variation increase with increasing number of cycles, varying in the range of 2.45-12.78%. The variation in strength values of samples with a minimum percentage of Sp=5.0% varies from 65.38 to 60.44 MPa, and a decrease in strength is also observed from 100 cycles. The coefficients of variation have a similar pattern as the reference samples, ranging from 3.03 to 8.75%. The variation of strength values of samples with Sp=7.5% varies from 66.45 to 62.17 MPa, while the strength reduction already occurs from 125 cycles, and the increment of variation coefficients is from 1.53 to 6.82%. In samples with a percentage of Sp=10.0%, a noticeable decrease in strength values occurs from 150 cycles, with a variation of strength values from 66.12 to 62.94%, and the coefficient of variation from 3.41 to 5.69. In samples with a maximum percentage of Sp=12.5%, the decrease in strength values occurs from 125 cycles, with variation in strength values from 63.33 to 58.13%, and coefficients of variation from 2.31 to 7.83%. However, the samples with maximum Sp content show an overall strength reduction relative to the reference sample, on average by 4.8%, indicating the negative effect of Sp on the strength performance of concrete, at their high concentration.

The mass reduction curves of the samples are generally similar to the strength curves. The reduction of reference samples varies from 2388 to 2231 grams, with an initial decrease in mass observed at 100 cycles. Similarly, as with strength, an increase in the coefficients of variation (for all Sp variations) from 1.36 to 9.23% is observed with an increasing number of cycles. For samples with Sp=5.0%, the variation in loss ranges from 2366 to 2264 grams, the initial decrease is also at 100 cycles, and the coefficients of variation increase from 1.36 to 7.12%. The samples with Sp=7.5% showed a loss in mass from 2375 to 2268 grams, but appreciable loss was observed at 125 cycles, and the coefficients of variation increased from 1.36 to 6.42%. For samples with Sp=10.0%, mass loss starts from 150 cycles, ranges from 2362 to 2309 grams, and coefficients of variation vary from 1.36 to 4.54%. The samples with maximum content with Sp=12.5 have losses ranging from 2397 to 2296 grams, with coefficients of variation varying from 1.36 to 6.39%. The onset of mass loss is observed at both 50 and 125 cycles, with mass loss at 100 cycles being negligible, quantitatively close to reference samples. The instability of the results indicates the negative effect of Sp in high concentration on the quality of concrete.

Analysis of the coefficients of variation in both cases indicates a decrease in the stability of the strength (and mass) results with increasing freezing cycles, but their quantitative index depends on the quantitative change in strength (and mass) relative to the initial one (corresponding to 0 cycles). The latter is confirmed by the lowest values of the coefficients of variation in samples with Sp=10.0%, which exhibit the least loss of strength. Quantitatively, the coefficient of variation of strength in samples with Sp=10.0% is 2.24 times less than in reference samples, and in relation to other variations of Sp, in 1.11-1.53 times. The coefficient of variation of masses in samples with Sp=10.0% is 2.14 times less than in reference sample, and in relation to other variations of Sp, in 1.17-1.67 times.

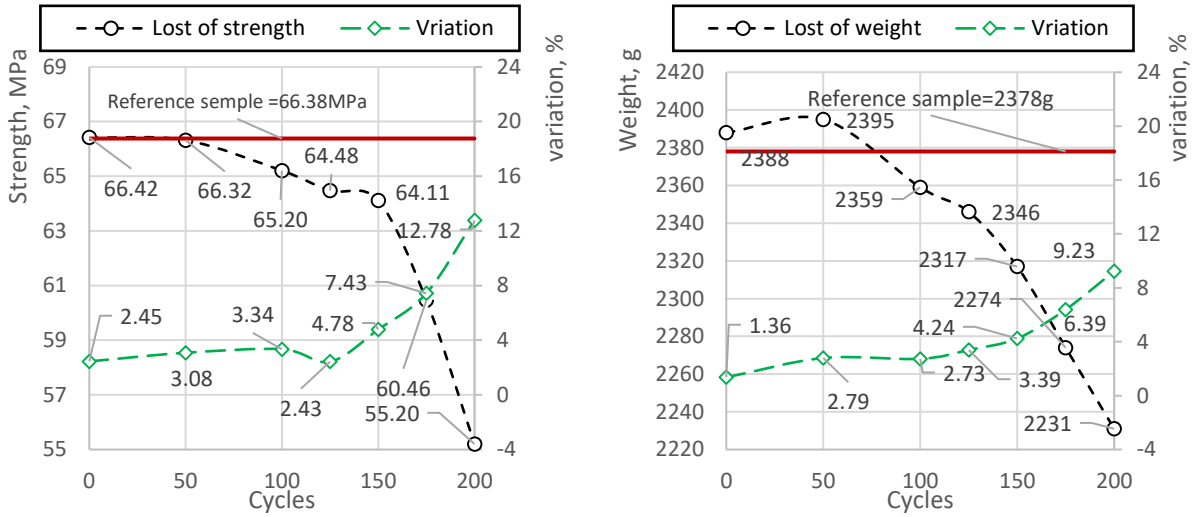

A B

Figure 5 - Strength and mass loss at Sp=0%

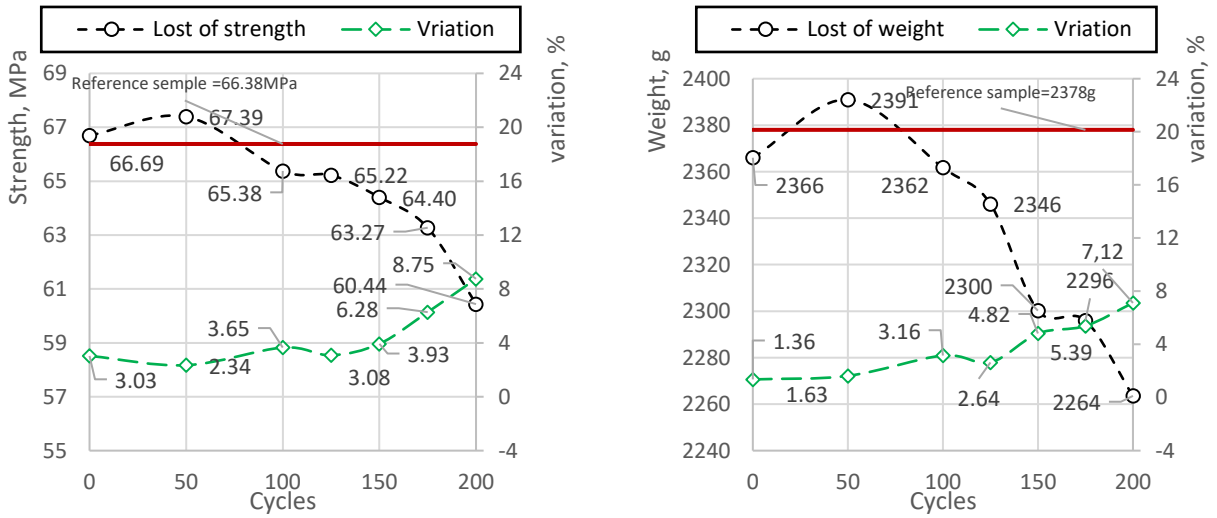

A B

Figure 6 - Strength and mass loss at Sp=5.0%

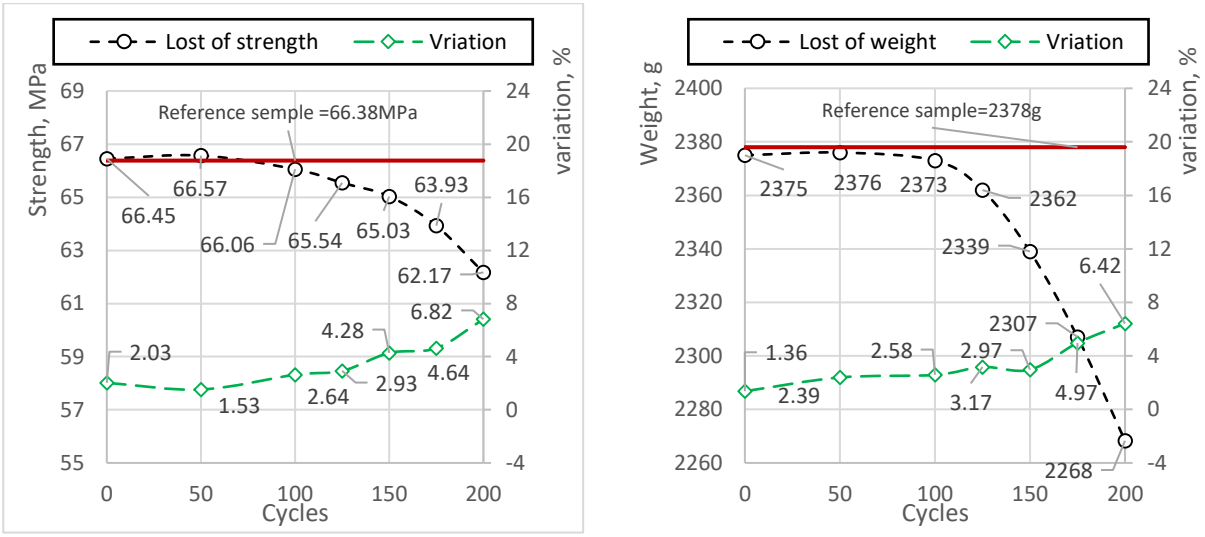

Figure 7 - Strength and mass loss at Sp=7.5%

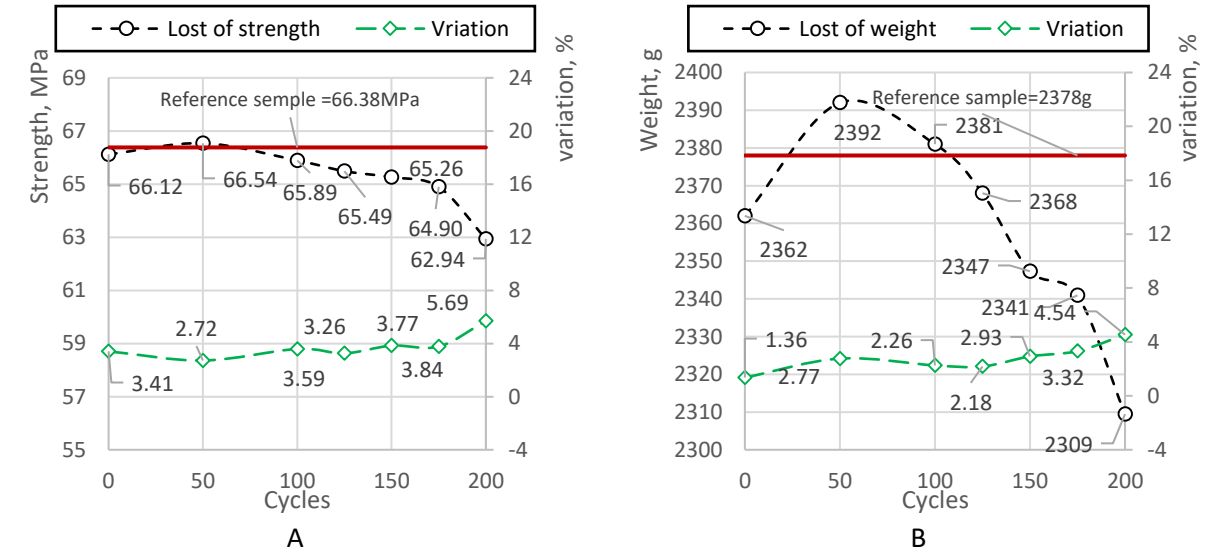

Figure 8 - Strength and mass loss at Sp=10.0%

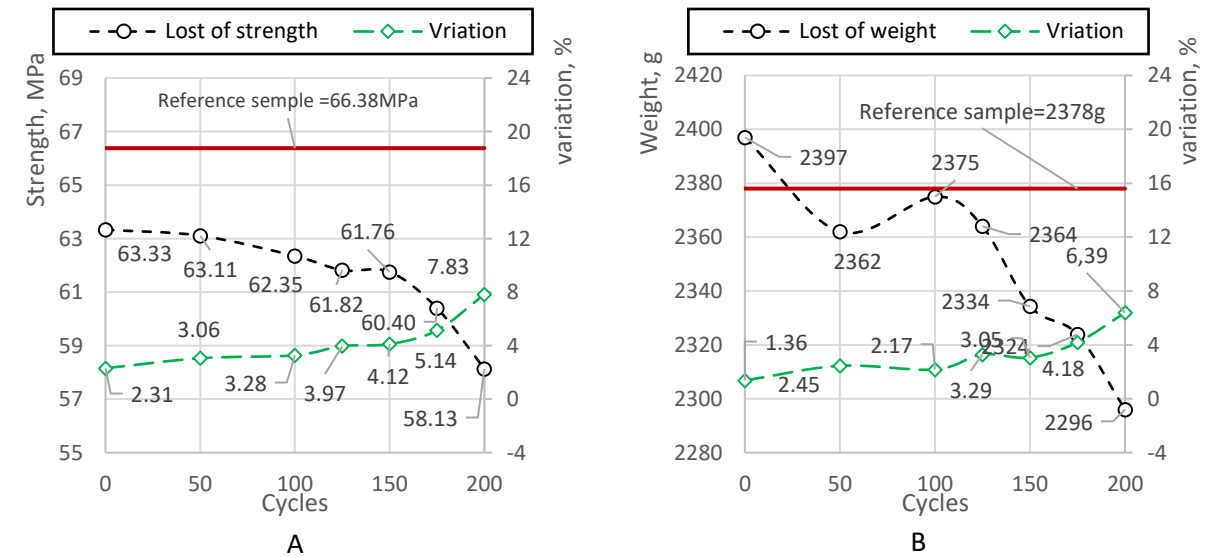

Figure 9 - Strength and mass loss at Sp=12.5%

Figure 10 shows comparisons of strength and mass losses in percentages as a function of soapstock content in the sample. (Figure 10A is a comparison of strength loss and Figure 10B is a comparison of mass loss). The comparison charts relative to the reference sample (red curve) show both qualitative and quantitative changes in mass and strength of the samples. The diagrams also show the numerical values of maximum losses corresponding to 200 cycles.

The curves in Figure 10 clearly show the effect of soapstock on the durability of concrete, relative to its resistance to cyclic freezing. The average value of maximum strength loss of reference samples in percentage terms is 16.84% and mass loss is 6.18% on average. For samples with Sp=5% content, the maximum strength loss is 8.95% and the maximum mass loss is 4.81%. For samples with Sp=7.5%, the same values are 6.34% in strength and 4.61% in mass. For samples with Sp=10.0%, the same values are 5.69% in strength and 2.88% in weight. For samples with maximum Sp=12.5%, the strength is 7.83% and weight is 3.45%. Thus, the maximum resistance to cyclic freezing was found in samples with Sp=10.0%. In case of loss of strength and mass, frost resistance in relation to reference samples increases by 50% (150/100), and in relation to other variations of Sp, by from 20 (125/100) to 50% (150/100).

Figure 11 shows the results of water absorption measurements of samples with different Sp contents.

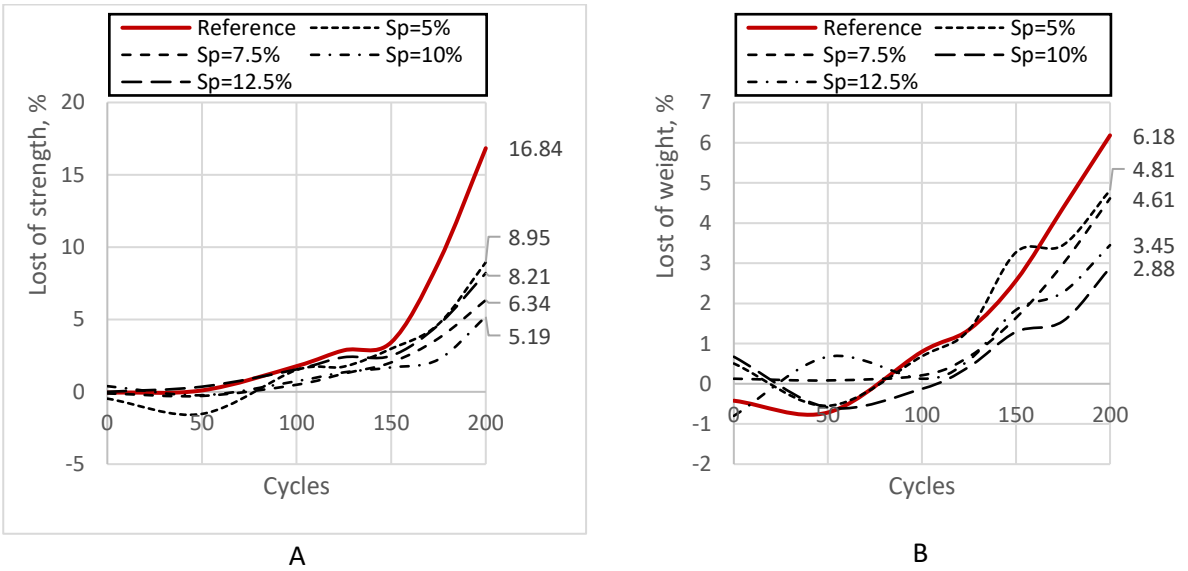

Figure 10 - Comparison of maximum strength and mass loss

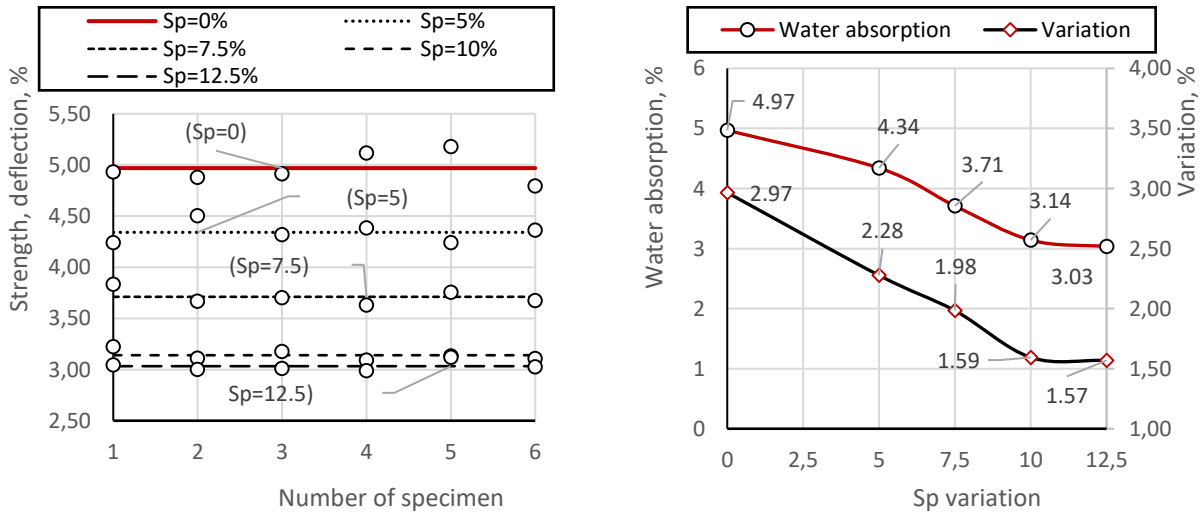

Figure 11 - Water absorption results

Figure 11A shows the private water absorption values and their corresponding averages. The straight lines in the diagram correspond to the average water absorption value of each type, in order to visualize the deviations of the private values from the average value. Figure 11B shows comparisons of the average water absorption values of samples with different Sp contents and their corresponding coefficients of variation.

According to the results, the average of the six water absorption measurements of the reference sample was 4.97%, with a variation from 4.79 to 5.18%. For samples with Sp=5%, water absorption varies from 4.24 to 4.51%, with an average of 4.34%. For samples with Sp=7.5% water absorption ranges from 3.63 to 3.83%, with an average of 3.71%. For Sp=10% from 3.09 to 3.22%, with an average of 3.14%. For Sp=12.5% from 2.99 to 3.12%, the mean is 3.03%. With each increase in the percentage of soapstock, there is a decrease in water absorption capacity. Relative to the reference samples, the decrease is: for Sp=5% samples, the decrease is 12.6%; for Sp=7.5% samples, the decrease is 25.3%; for Sp=10% samples, the decrease is 36.8%; for Sp=12.5% samples, the decrease is 39.0%. The decrease in water absorption relative to a linear increase in soapstock content (multiple of 2.5%), is not linear: up to 10% soapstock content there is a rapid decrease in water absorption, after - a sharp decline. Numerically, the increments are: 12.6, 14.5, 15.4, 3.4% from each subsequent addition of soapstock (2.5%). The sharp decline in water absorption indicates a decrease in the efficiency of hydrophobizing effect of soapstock on the material at its high concentration. Analysis of the coefficients of variation showed a high degree of convergence of private values of all variations, including reference samples: the coefficients of variation range from 1.57 to 2.97%. The variation of the results decreases with increasing concentration of soapstock, i.e. the maximum stability of the results logically corresponds to the maximum hydrophobization of the samples.

Conclusion

Based on the results of the tests performed, the following generalized conclusions can be drawn:

Standard tests of beam samples for flexural and compressive strength, and standard cubic samples for water absorption and frost resistance were performed. Tests were performed for samples with different soapstock (Sp) contents: 5, 7.5, 10 and 12.5 % by weight of cement, microsilica and phosphogypsum.

Measurements of the strength of the beam samples showed that the maximum effect concerning the increase in the strength of the material is achieved at 5% of the soapstock content. However, it should be noted that the subsequent decrease in strength with increasing concentration of soapstock is not significant, up to Sp=10% does not exceed 1%. Thus, the optimal concentration of soapstock, at which the maximum effect on the strength of the material will be achieved, is 5-10%.

Tests on frost resistance showed that the maximum resistance to cyclic freezing is observed in samples with Sp=10%, further increase reduces frost resistance. The regularity in the increase of frost resistance with increasing concentration of soapstock is logical, because with each increase in concentration, the hydrophobization of the material increases. However, if the hydrophobicity of samples with Sp=12.5%, although not significantly, still increases about Sp=10%, the frost resistance decreases. The latter is because the high concentration of soapstock leads to a decrease in the structural strength of the material, since fatty acids in the composition of soapstock harm the strength set of concrete, as fatty acids in the water-soluble state (due to the use of caustic alkali NaOH) when getting into the cement mortar are evenly distributed, and after the setting of alkali pass into the active phase of cement binder, subsequently releasing fatty acids that form a hydrophobic structure. Large amounts of fatty acids reduce the adsorption of moisture and thus limit the hydration process.

The obtained curve of dependence of water absorption change on the concentration of soapstock showed the optimal gradient of water absorption, which corresponds to Sp=10%. With further increase of soapstock, the decrease of water absorption index is not significant.

Conflict of interest. The corresponding author declares that there is no conflict of interest.

CRediT author statement. All authors contributed to this study. **D. Dyussembinov**: Conceptualization, Methodology, Software. **R. Lukpanov**: Data curation, Writing draft preparation. **Zh. Zantlesova**: Visualization, Investigation. **R. Lukpanov**: Supervision. E. **Talal Awwad**: Software, Validation. **A. Altynbekova**: Reviewing and Editing.

Acknowledgements. This research was funded by the science committee of the Ministry of Education and Science of Kazakhstan (Grant № AP13068424).

Cite this article as: Dyussembinov DS, Lukpanov RE, Altynbekova AD, Zhantlesova ZhB, Talal Awwad. Investigation of soapstock influence on physical and mechanical properties used as a part of two-component modified additive. Kompleksnoe Ispolzovanie Mineralnogo Syra = Complex Use of Mineral Resources. 2025; 334(3):37-50. https://doi.org/10.31643/2025/6445.26

Бетон конструкцияларының беріктік сипаттамаларын жақсарту үшін модификацияланған қоспаның құрамындағы соапстоктың әсері

[1,2] Дюсембинов Д.С.,[1,2]Лукпанов Р.Е., [1,2]Алтынбекова А.Д., [1,2]Жантлесова Ж.Б., [3] Talal Awwad

[1] ЖШС «Solid Research Group», Астана, Қазақстан
[2] Л.Н. Гумилев атындағы Еуразия ұлттық университеті, Астана, Қазақстан
[3] Дамаск университеті, Дамаск, Сирия

Мақала келді: *25 наурыз 2024*
Сараптамадан өтті: *2 сәуір 2024*
Қабылданды: *9 шілде 2024*

ТҮЙІНДЕМЕ

Мақалада екі компонентті модификацияланған қоспаның бөлігі ретінде қолданылатын соапсток әсерін зерттеу нәтижелері берілген. Арқалық үлгілерге иілу және қысу беріктігі бойынша және суды сіңіру және аязға төзімділік бойынша стандартты кубтық үлгілерге стандартты сынақтар жүргізілді. Сынақтар соапстоктың әр түрлі мөлшерлеріне (Sp): цемент, микрокремний және фосфогипс салмағы бойынша 5, 7,5, 10 және 12,5% болатын үлгілер үшін жүргізілді. Арқалық үлгілердің беріктігін өлшеу материалдың беріктігін арттыру тұрғысынан максималды әсерге құрамында соапстоктың мөлшері 5% болғанда қол жеткізілетінін көрсетті. Алайда, соапстоктың концентрациясы жоғарылағанда беріктіктің кейінгі төмендеуі көп болмайтынын атап өткен жөн, Sp=10% дейін ол 1% аспайды. Осылайша, материалдың беріктігіне қатысты максималды әсерге қол жеткізілетін соапстоктың оңтайлы концентрациясы 5-10% құрайды. Суды сіңіру өзгерістерінің соапсток концентрациясына тәуелділігінің алынған қисығы Sp=10% сәйкес келетін су сіңірудің оптималды градиентін көрсетті. Соапстокты көбейткеннен суды сіңіру айтарлықтай төмендемейді. Аязға төзімділік сынақтары Sp=10% үлгілерде циклдік тоңазытуға максималды төзімділік байқалатынын көрсетті, ал кейінгі жоғарылау аязға төзімділікті төмендетеді. Соапсток концентрациясының жоғарылауымен аязға төзімділіктің жоғарылауының заңдылықтары қисынды, өйткені концентрация артқан сайын материалдың гидрофобизациясы артады. Дегенмен, Sp=12,5% үлгілердің гидрофобтылығы айтарлықтай болмаса да, Sp=10%-ға қатысты жоғарыласа, аязға төзімділік төмендейді.

Түйін сөздер: көбік бетон, пенобетон, екі компонентті модификацияланған қоспа, технологиялық схема, соапсток, беріктік қасиеттері, су сіңіргіштігі, аязға төзімділігі

Авторлар туралы ақпарат:

Дюсембинов Думан Серикович — *Аға ғылыми қызметкер, «Solid Research Group» ЖШС, Астана, Қазақстан. Т.ғ.к., доцент, «Өнеркәсіптік және азаматтық құрылыс технологиясы» кафедрасы, Л.Н.Гумилев атындағы ЕҰУ, Астана, Қазақстан. Email: dusembinov@mail.ru*

Лукпанов Рауан Ермагамбетович — *Ғылыми жетекші, «Solid Research Group» ЖШС, Астана, Қазақстан. PhD, Профессор, «Өнеркәсіптік және азаматтық құрылыс технологиясы» кафедрасы, Л.Н.Гумилев атындағы ЕҰУ, Астана, Қазақстан. Email: rauan_82@mail.ru*

Алтынбекова Алия Досжанкызы — *Ғылыми қызметкер, «Solid Research Group» ЖШС, Астана, Қазақстан. Аға оқытушы, «Өнеркәсіптік және азаматтық құрылыс технологиясы» кафедрасы, Л.Н.Гумилев атындағы ЕҰУ, Астана, Қазақстан. E-mail: kleo-14@mail.ru*

Жантлесова Жибек Бейсембаевна — *Кіші ғылыми қызметкер, «Solid Research Group» ЖШС, Астана, Қазақстан. PhD докторант, «Өнеркәсіптік және азаматтық құрылыс технологиясы» кафедрасы, Л.Н.Гумилев атындағы ЕҰУ, Астана, Қазақстан. E-mail: zhibek81@mail.ru*

Talal Awwad — *Дамаск университетінің геотехника кафедрасының профессоры, Дамаск, Сирия. E-mail: dr.awwad.gfce@gmail.com*

Влияние соапстока в составе модифицированной добавки для улучшения прочностных характеристик бетонных конструкций

[1,2] Дюсембинов Д.С.,[1,2]Лукпанов Р.Е., [1,2]Алтынбекова А.Д., [1,2]Жантлесова Ж.Б., [3] Talal Awwad

[1] ТОО «Solid Research Group», Астана, Казахстан
[2] Евразийский национальный университет им. Л.Н. Гумилева, Астана, Казахстан
[3]Дамасский университет, Дамаск, Сирия

Поступила: *25 марта 2024*
Рецензирование: *2 апреля 2024*
Принята в печать: *9 июля 2024*

АННОТАЦИЯ

В статье представлены результаты исследования влияния соапстока, применяемая в составе двухкомпонентной модифицированной добавки. Были выполнены стандартные испытания образцов-балочек на прочность при изгибе и при сжатии, стандартных кубических образцов на водопоглощение и морозостойкость. Испытания выполнены для образцов с разным содержанием соапстока (Sp): 5, 7.5, 10 и 12.5 % по массе цемента, микрокремнезема и фосфогипса. Измерение прочности образцов-балочек показали, что максимальный эффект относительно увеличения прочности материала достигается при 5% содержании соапстока. Однако стоит отметить, что последующее снижение прочности при увеличении концентрации соапстока не значительно, до Sp=10% не превышает 1%. Таким образом оптимальная концентрация соапстока, при которой будет достигнут максимальный эффект относительно прочности материала, составляет 5-10%. Полученная кривая зависимости изменения водопоглощения от концентрации соапстока показала оптимальный градиент водопоглощения, которому соответствует Sp=10%. При последующем увеличении соапстока, снижение показателя водопоглощения не существенно. Испытания на морозостойкость показали, что максимальная стойкость к циклическому замораживанию наблюдается у образцов с Sp=10%, последующее увеличение снижает морозостойкость. Закономерность в увеличении морозостойкости при увеличении концентрации соапстока логична, поскольку с каждым увеличением концентрации растет гидрофобизация материала. Однако, если гидрофобность образцов с Sp=12.5% хоть и не существенно, но все же растет по отношению к Sp=10%, то морозостойкость снижается.

***Ключевые слова*:** пенобетон, двухкомпонентная модифицированная добавка, технологическая схема, соапсток, прочностные показатели, водопоглощение, морозостойкость.

Информация об авторах:

Дюсембинов Думан Серикович — *Старший научный сотрудник, ТОО «Solid Research Group», Астана, Казахстан. К.т.н., Доцент, Кафедра «Технология промышленного и гражданского строительства», ЕНУ им. Л.Н.Гумилева, Астана, Казахстан. Email: dusembinov@mail.ru*

Лукпанов Рауан Ермагамбетович — *Научный руководитель, ТОО «Solid Research Group», Астана, Казахстан. PhD, Профессор, Кафедра «Технология промышленного и гражданского строительства», ЕНУ им. Л.Н.Гумилева, Астана, Казахстан. Email: rauan_82@mail.ru*

Алтынбекова Алия Досжанкызы — *Научный сотрудник, ТОО «Solid Research Group», Астана, Казахстан. Старший преподаватель, Кафедра «Технология промышленного и гражданского строительства», ЕНУ им. Л.Н.Гумилева, Астана, Казахстан. E-mail: kleo-14@mail.ru*

Жантлесова Жибек Бейсембаевна — *Младший научный сотрудник, ТОО «Solid Research Group», Астана, Казахстан. PhD докторант, Кафедра «Технология промышленного и гражданского строительства», ЕНУ им. Л.Н.Гумилева, Астана, Казахстан. E-mail: zhibek81@mail.ru*

Talal Awwad — *Профессор кафедры геотехники Дамасского университета, Дамаск, Сирия. E-mail: dr.awwad.gfce@gmail.com*

References

[1] Raj A, Sathyan D, Mini KM. Physical and functional characteristics of foam concrete: A review. Construction and Building Materials. 2019; 221:787-799.

[2] Liu J, Ge T, Wu Y, Chen R. Effect of Sand-to-Cement Ratio on Mechanical Properties of Foam Concrete. Buildings. 2022; 12(11):1969. https://doi.org/10.3390/buildings12111969

[3] Vishavkarma A, Harish KV. Tension and bond characteristics of foam concrete for repair applications. Case Studies in Construction Materials. 2024; 20:e02767.

[4] Liu J, Ren Y, Chen R, Wu Y, Lei W. The Effect of Pore Structure on Impact Behavior of Concrete Hollow Brick, Autoclaved Aerated Concrete and Foamed Concrete. Materials. 2022; 15(12):4075. https://doi.org/10.3390/ma15124075

[5] Chica L, Alzate A. Cellular concrete review: New trends for application in construction. Construction and building materials. 2019; 200:637-647.

[6] Gencel O, Nodehi M, Hekimoğlu G, Ustaoğlu A, Sarı A, Kaplan G, Bayraktar OY, Sutcu M, Ozbakkaloglu T. Foam Concrete Produced with Recycled Concrete Powder and Phase Change Materials. Sustainability. 2022; 14(12):7458. https://doi.org/10.3390/su14127458

[7] Moussadik A, El Fadili H, Saadi M, & Diouri A. Lightweight aerated concrete based on activated powders of coal gangue and fly ash. Construction and Building Materials. 2024; 417:135333. https://doi.org/10.1016/j.conbuildmat.2024.135333

[8] Liu P, Luo A, Liu L, Li Y, Zhang S, Zhi W, & Yu Z. Study on the preparation and performances analysis of lightweight high strength ceramsite aerated concrete. Journal of Materials Research and Technology. 2023; 25:6672-6683.

[9] Fu Y, Wang X, Wang L, Li Y. Foam Concrete: A State-of-the-Art and State-of-the-Practice Review. Advances in Materials Science and Engineering. 2020: 1-25. https://doi.org/10.1155/2020/6153602

[10] Gołaszewski J, Klemczak B, Smolana A, Gołaszewska M, Cygan G, Mankel C, Peralta I, Röser F, Koenders EAB. Effect of Foaming Agent, Binder and Density on the Compressive Strength and Thermal Conductivity of Ultra-Light Foam Concrete. Buildings. 2022; 12(8):1176. https://doi.org/10.3390/buildings12081176

[11] Zhang Y, Jiang Y, Ling TC. Use of CO2 as a controlled foam stabilizer to enhance pore structure and properties of foamed concrete. Cement and Concrete Composites. 2024; 145:105356. https://doi.org/10.1016/j.cemconcomp.2023.105356

[12] Fu Y, Wang X, Wang L, Li Y. Foam Concrete: A State-of-the-Art and State-of-the-Practice Review. Advances in Materials Science and Engineering. 2020: 1-25. https://doi.org/10.1155/2020/6153602

[13] Zhou H, Zhao X, Wang X, Song T, Liu H, & Zhang H. Elevated temperature properties of foam concrete: Experimental study, numerical simulation, and theoretical analysis. Construction and Building Materials. 2024; 411:134393. https://doi.org/10.1016/j.conbuildmat.2023.134393

[14] Cui ZD, Zhang L J, Fan KK, & Yuan L. Coupling effect of freezing-thawing cycles and dynamic loading on the accumulative deformation and microstructure of foam concrete. Materials and Structures. 2024; 57(6):136. https://doi.org/10.1617/s11527-024-02409-8

[15] Han Y, Zhou M, Wang J, Tian Y, & Wang X. Optimization of coal-based solid waste ceramsite foam concrete mix proportions and performance study. Construction and Building Materials. 2024; 416:135226. https://doi.org/10.1016/j.conbuildmat.2024.135226

[16] Bie Y, Ba S, Chen S. Studies on foamed concrete micropores and their effects on stress distribution and heat conduction. Journal of Building Engineering. 2024; 87:109152. https://doi.org/10.1016/j.jobe.2024.109152

[17] Dang J, Tang X, Xiao J, Duan Z, & Han A. Role of recycled brick powder and alkaline solution on the properties of eco-friendly alkali-activated foam concrete. Journal of Cleaner Production. 2024; 436:140381. https://doi.org/10.1016/j.jclepro.2023.140381

[18] Vishavkarma A, Venkatanarayanan HK. Assessment of pore structure of foam concrete containing slag for improved durability performance in reinforced concrete applications. Journal of Building Engineering. 2024; 86:108939. https://doi.org/10.1016/j.jobe.2024.108939

[19] Liu Y, Zhao Z, Amin M N, Ahmed B, Khan K, Arifeen SU, & Althoey F. Foam concrete for lightweight construction applications: A comprehensive review of the research development and material characteristics. Reviews on Advanced Materials Science. 2024; 63(1):20240022. https://doi.org/10.1515/rams-2024-0022

[20] Lukpanov R, Dyussembinov D, Altynbekova A, Yenkebayev S, & Zhumagulova A. Investigation of Effect of Proposed Two-Stage Foam Injection Method and Modified Additive on Workability of Foam Concrete. Materials. 2024; 17(9):2024. https://doi.org/10.3390/ma17092024

[21] Lukpanov RE. et al. Assessment of the physical and mechanical characteristics of sand for the production of foam concrete using the two-stage foam injection method. Kompleksnoe Ispolzovanie Mineralnogo Syra= Complex use of mineral resources. 2025; 332(1):5-18. https://doi.org/10.31643/2025/6445.01

[22] Lukpanov R, et al. Optimal concentration of post-alcohol bard and microsilica in cement-sand mixtures determination. Kompleksnoe Ispolzovanie Mineralnogo Syra=Complex use of mineral resources. 2024; 330(3):92-103. https://doi.org/10.31643/2024/6445.33

[23] Lukpanov R, et al. Complex modified additive for concrete based on industrial waste. Magazine of Civil Engineering. 2022; 115(7):11507. https://doi.org/10.34910/MCE.115.7

[24] Interstate Standard GOST 30744-2001. Cements. Test methods using polyfractional sand. 2002, 1-36.

[25] Interstate Standard GOST 12730.3-2020. Concretes. Method of determination of water absorption, 2021, 1-3.

[26] Interstate Standard GOST 10060-2012. Concretes. Methods for determination of frost-resistance, 2014, 1-19.

Crossref
DOI: 10.31643/2025/6445.27
Engineering and technology

Modeling the influence of technological parameters of the magnetron sputtering process using the Caroline D12C system on the proportion of nanocrystallites in the structure of thin silicon films

[1]Tolubaev K.S., [1]Zhautikov B.A., [1*]Zobnin N.N., [2]Dairbekova G.S., [1]Kabieva S.K., [3] Al-Kasasbeh R.T.

[1] Karaganda Industrial University, Temirtau, Kazakhstan;
[2] Satpayev University, Almaty, Kazakhstan;
[3]University of Jordan, Amman, Jordan

** Corresponding author email: zobninnn@mail.ru*

Received: *July 5, 2024*
Peer-reviewed: *July 9, 2024*
Accepted: *July 12, 2024*

ABSTRACT
The experimental dependence of the fraction of nano-sized modification of silicon in thin films obtained by magnetron sputtering on the main technological indicators of the process - specific power on the target, pressure in the working chamber, pulsation frequency of the voltage supplied to the target - has been studied. The data was processed using the method of multiple correlation-regression analysis and a corresponding mathematical model was obtained that describes the experimental dependence. It has been established that the specific power at the target does not significantly affect the fraction of nanosilicon in the film. The voltage frequency on the target has only a positive effect and is therefore limited only by the technical capabilities of the sputtering equipment. The pressure in the working chamber has an optimal value because in the mathematical model for this factor there are both positive and negative coefficients. When analyzing the model by calculation, it was found that the largest proportion of nanosilicon in the film, 75.06%, is achieved at a voltage frequency on the target of 100 Hz and pressure in the working chamber of 1.9 Pa. These data are preliminary due to the limited number of experiments.

Keywords: Nanosized silicon, magnetron sputtering, Caroline D12C, film, mathematical modeling, correlation-regression analysis, target.

Information about authors:

Tolubayev Kanat — *Doctoral student, Karaganda Industrial University, Temirtau, Kazakhstan. Email: kanat.tolubayev@tttu.edu.kz*

Zhautikov Bakhyt — *Doctor of Technical Sciences, Professor, Karaganda Industrial University, Temirtau, Kazakhstan. Email: bakhyt_zhautikov@mail.ru*

Zobnin Nikolai — *Candidate of Technical Sciences, Karaganda Industrial University, Temirtau, Kazakhstan. Email: zobninnn@mail.ru*

Dairbekova Guldana — *PhD, Satbayev University, Almaty, Kazakhstan. Email: guldana.01.02.91@mail.ru*

Kabiyeva Sauke — *Candidate of Chemical Sciences, Associate Professor, Karaganda Industrial University, Temirtau, Kazakhstan. Email: kabieva.s@mail.ru*

Al-Kasasbeh Riad — *PhD, Professor, University of Jordan, Amman, Jordan. Email: riad_alkasasbeh@bau.edu.jo*

Introduction

One of the newest applications for thin-film silicon structures is the production of anodes for commercial lithium-ion batteries (LIBs). During the introduction of lithium into nanosilicon, intermetallic compounds are formed Li_xSi_y. In the Li_{12} Si_7 compound, for every 7 silicon atoms, there are 12 lithium atoms, respectively, the volume of lithium is 2.17 times greater than the volume of silicon. The ability to intercalate lithium also influences the high theoretical specific capacity of silicon-based LIB anodes – 4140 mAh/g, which significantly exceeds the values for graphite (372 mAh/g) [[1], [2], [3]]. The literature substantiates that crystalline silicon cannot be used as a negative electrode material, since it is destroyed when lithium is introduced due to an increase in the volume of the crystal cell [[4], [5], [6]]. In this regard, when creating thin-film silicon anodes, it is important to control and influence the ratio of the main polymorphic states of silicon (crystalline, amorphous and nanocrystalline forms) in the finished products. In this case, it is necessary to strive to reduce the proportion of the crystalline form of silicon and increase the proportion of

amorphous silicon or nanocrystals [[7], [8], [9]]. The ratio of various polymorphic phases of silicon in thin films can be changed by changing the main technological parameters of sputtering - specific power on the target, pressure in the working chamber, and pulsation frequency of the voltage supplied to the target. In this regard, modeling magnetron sputtering has become relevant to predict the polymorphism of thin silicon films and optimize the process.

Methodology

The most productive of the currently existing equipment options, the Caroline D12C system, was chosen to conduct experimental studies. The Caroline D12C vacuum deposition system (Figure 1) is intended for small- and medium-scale production and research in the field of thin film deposition using magnetron and thermal sputtering. The technical characteristics of the system are given in Table 1 [10].

Table 1 - Technical characteristics of the Caroline D12C magnetron sputtering system [10]

Number of substrates processed per 1 cycle (pcs.)	12pcs. Ø100 mm. 24 pcs. 60x48
Starting pressure in the working chamber, Pa	10^{-3}
Flow rate of working gases supplied to the chamber through one channel (l/hour)	0÷9
Quantity of supplied (non-aggressive) gases up to (pcs.)	3
Number of thermal evaporators up to (pcs.)	2
Number of magnetrons (pcs.)	1÷4
Type of magnetrons for film deposition	Pulse high frequency
Operating current of magnetrons, adjustable (A)	0.5÷23
Operating voltage of magnetrons (V)	300÷650
Target material and size: metals, alloys, silicon (composite targets not directly cooled can be used), mm	Ø 100×4÷12
Working pressure in the vacuum chamber, Pa	0.1 ÷ 3.0
Witness resistance control range (kOhm)	0.2÷20
Resistance measurement error (%)	±3
Recommended substrate heating temperature, °C	10÷550
Substrate temperature instability (%)	±15
Limit residual pressure in the working chamber, (Pa)	$2x10^{-4}$
Time to prepare the installation for operation, taking into account the "overclocking" of the cryopump, no longer (min.)	110
Weight with power and control stand, kg.	Up to 2250

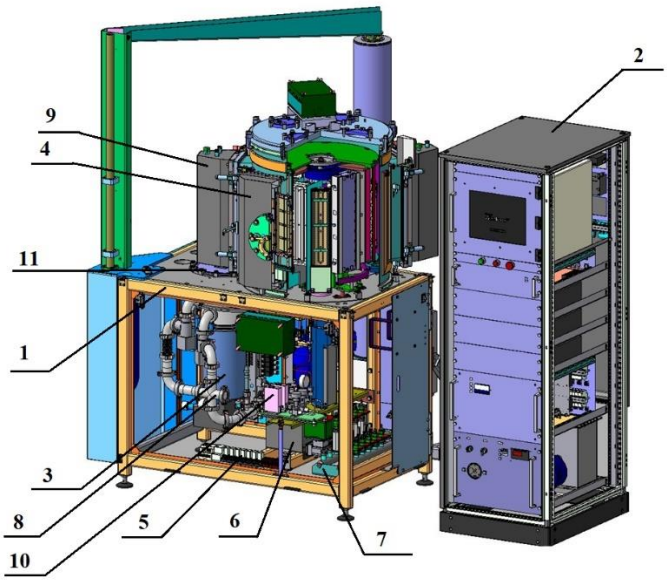

Fig. 1 - Diagram of the Caroline D12C magnetron sputtering system [6] 1 - technological module, 2 - control cabinet, 3 - fore-vacuum pump, 4 - working chamber, 5 - vacuum system, 6 - pneumatic equipment panel, 7 - water block, 8 - hydraulic equipment block, 9 - lifting and turning mechanism, 10 - gas supply panel, 11 – shutter

The system includes a process module (1), a control cabinet (2) and a foreline pump (3) (Figure 1). The main part of the technological module is the working chamber (4) with technological and internal chamber devices. These elements are installed on a plate, which is fixed in a frame structure. Devices to ensure the operation of the system are located under the supporting structure. The vacuum system (5), as part of the cryogenic pump, is installed on the plate below. The shutter (11) separates the vacuum system from the working chamber. The pneumatic equipment panel (6) is designed to distribute compressed air among the pneumatic actuators. The water block (7) ensures the distribution of water cooling to individual parts of the system. The hydraulic unit (8) is designed to create pressure in the hydraulic cylinder of the lifting and turning mechanism. Lift and rotate mechanism (9) for opening and rotating the chamber cover. The gas supply panel (10) is installed isolated from the housing on a special bracket under the stove.

When preparing samples of silicon films, the following technological parameters of the magnetron sputtering process were varied:

1) Specific power on targets. The variation was carried out in the maximum possible range from 1 to 100 W/cm^2, taking into account the available technical capabilities of modern production equipment;

2) Operating pressure in the spray chamber. Chamber pressure is regulated by changing the amount of inert gas supplied to the chamber. The pressure control range was from 0.5 to 3.0 Pa. It was assumed that increasing the gas flow rate would promote better sputtering of the silicon flow from the target to the substrate and the formation of silicon nanoparticles, as well as improved heat removal from condensing particles to avoid coalescence on the substrate;

3) The frequency of the voltage pulses applied to the target. At carrying out experiments applied constant (without pulse) voltage and two voltage frequency options were 20 and 100 kHz.

Silicon crystals were used as targets for magnetron sputtering. To produce silicon crystals, we used TCR-5C-1k/t equipment manufactured by Techno Search Corporation (Japan). The crystals were grown according to the Czochralski method using commercial high-purity silicon of SoG-Si grade 6-7N.

A preliminary assessment of the film morphology was carried out using the ELLIPS-1891 spectral ellipsometer designed for precision measurements of the thickness of thin films, the optical parameters of thin-film structures and the spectral dependences of the optical constants of the surfaces of various materials (metals, semiconductors, dielectrics, etc.). When the uniform morphology of the silicon film was revealed and the absence of a substrate surface not covered by the film, further determination of the thickness of the resulting film was carried out using a Jeol JSM-6490LA scanning electron microscope with a magnification range of up to 300,000 times.

The ratio of various polymorphic states of silicon in the film was assessed using Raman spectroscopic analysis on a Horiba system Jobin – Yvon HR800UV (France).

Results and Discussions

During the study, six silicon films were obtained under different technological conditions of magnetron sputtering. Each of the resulting films was studied using Raman spectroscopy and electron microscopy at several different points. This test showed the uniformity of polymorphism across the entire surface of each film, which indicates the advantage of magnetron sputtering technology over the CVD method in terms of ensuring film uniformity. The technological parameters of spraying and the results obtained are presented in Table 2.

Table 2 - Technological parameters of deposition and the proportion of polymorphic modifications in the structure of silicon films

# experience	Magnetron sputtering parameters and results					
	Specific power at the target, W/cm^2 (X1)	Pressure, Pa (X2)	Voltage frequency, kHz (X3)	Proportion of polymorphic state, volume. %		
				A	C	n-C (Y)
1	1	0.5	0	76.1	23.9	0
2	50	0.5	0	56.2	43.8	0
3	50	2.0	0	49.4	5.0	45.6
4	100	3.0	0	2.8	82.1	15.9
5	50	2.0	20	34.2	1.8	64.0
6	50	3.0	100	58.7	5.4	35.9

A – amorphous, C – crystalline, n-C – nanocrystalline

Figure 2 shows micrographs of two types of films that were obtained during the experiments. The first type of films (Figure 2 a), obtained in experiments No. 1-2, do not contain nano-sized silicon, the second type of films (Figure 2 b), obtained in experiments No. 3-6, contains it in varying quantities. Films similar to those presented in Figure 2a were previously obtained by the authors of [11].

Structures similar to Figure 2b were obtained by the authors of, however, the diameter of these structures (about 5 μm) is much larger than those obtained in this work (20-100 nm) [12]. They can be defined more as microtubes rather than nanofibers as in our case. At a higher magnification of microtubes, it was established that at the nano level, these tubes are represented by spherical nanocrystallites with a diameter of 100-150 nm [12]. These structures are also described by theoretical researchers. One of the options for a visual description of nanosilicon is the statement that this polymorphic structure has a spherical shape with a diameter of 3-10 nm [13]. The same data is provided from other sources regarding the size of silicon nanospheres - 3.5-20 nm [14]. However, the authors did not provide the corresponding microphotographs. Results most similar to the image in Figure 2b were obtained by a number of authors [[15], [16], [17], [18], [19], [20], [21]]. However, unlike these studies, we were able to obtain thinner fibres, which, when interwoven, formed a cellular porous structure at the microlevel. In addition, previous studies did not address the question of what is the proportion of silicon nanocrystallites in the structure of the resulting material. Are there, and in what quantities, amorphous and crystalline structures? Also, no works were found in which the influence of technological parameters of the industrial deposition process on the shape of nanocrystallites and their proportion in the composition of thin films was studied.

The preliminary data obtained (Table 1) were subjected to mathematical processing using the method of multiple correlation-regression analysis with the inclusion of linear, quadratic and cubic terms of the regression model, excluding paired and triple interactions between factors. As a result, a regression model (formula 1) was obtained that relates the parameters of magnetron sputtering (X1, X2, X3) with the fraction of nanosilicon in the composition of the resulting silicon film (Y).

$$Y = -30.7846 + 62.897 \times X2 + 0.2277 \times X3 - 5.3108 \times X2^2 \quad (1)$$

The resulting model is characterized by the following statistical characteristics:

Dispersion of inadequacy (S^2) = 49.8456

Reduced sum of squares = 3275.6 from 3375.3

F-ratio = 21.905

Multiple correlation coefficient = 0.9851

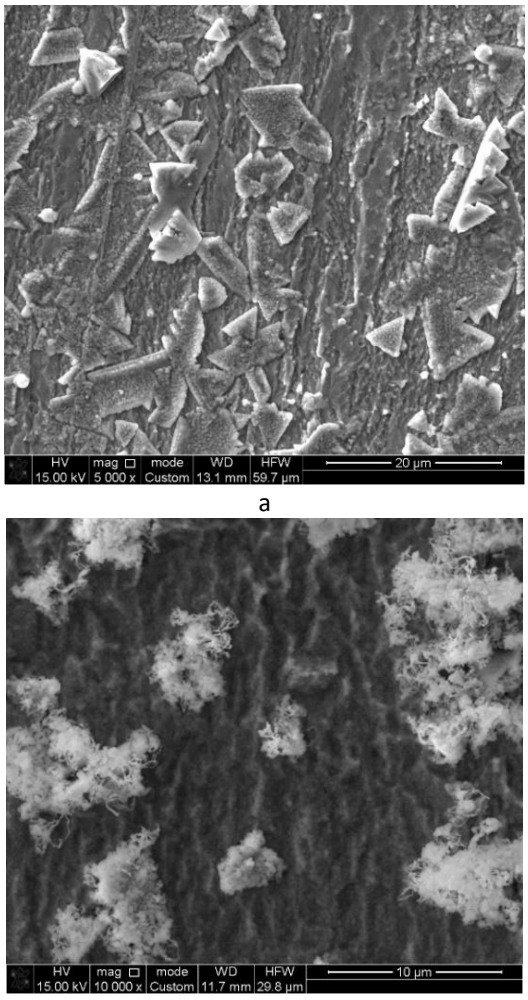

Fig. 2 - Microphotographs of the surface of a thin silicon film of magnetron sputtering
a – first type, b – second type

Table 3 presents an assessment of the adequacy of the data found by calculation using the resulting model. As can be seen from the table data, the maximum relative deviation of the calculated data from the experimental values is 15.18%. In combination with the above statistical characteristics of the model, this indicates a high level of adequacy of the resulting model of the magnetron sputtering process.

Table 3 - Assessment of the adequacy of the model of magnetron sputtering of silicon on a copper substrate

# Experiment	Proportion of nanosilicon in the film (Y), %		Deviation	
	Calculation	Experiment	Absolute	%
1	0.00	0.00	0.00	0.00
2	0.00	0.00	0.00	0.00
3	45.60	52.52	-6.92	15.18
4	15.90	14.51	1.38	8.71
5	64.00	57.07	6.92	10.82
6	35.90	37.28	-1.38	3.86

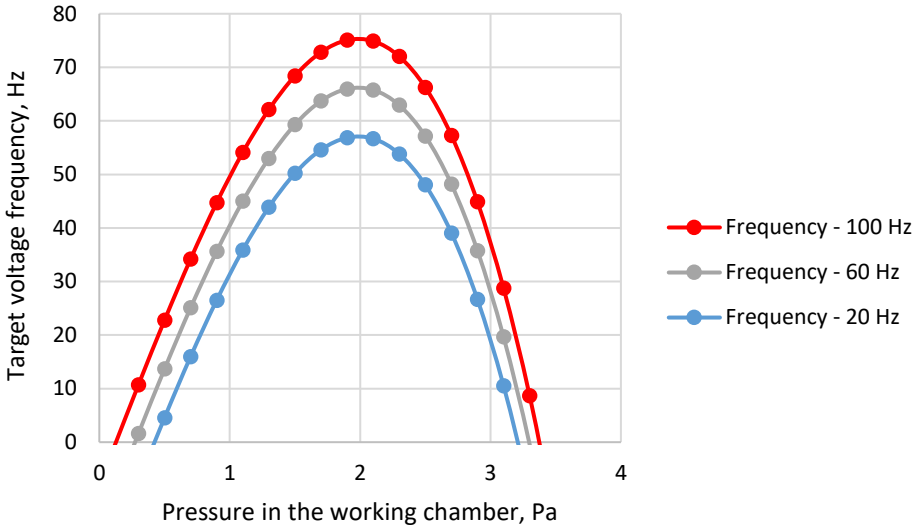

Fig.3 - **Calculated** graph of the dependence of the fraction of nanosilicon in the film on the pressure in the working chamber at different voltage frequencies on the target

When analyzing the resulting model, the assumption is confirmed that the specific power at the target (X1) does not significantly affect the fraction of nanosilicon in the film. The voltage frequency on the target has only a positive effect and is therefore limited only by the technical capabilities of the sputtering equipment. The pressure in the working chamber must be at its optimal value, because in the model for factor X2 there are both positive and negative coefficients.

Figure 3 shows a graph of the dependence of the fraction of nanosilicon in the film on the pressure in the working chamber, calculated using the model obtained here, at different voltage frequencies on the target.

In accordance with Figure 3, the largest proportion of nanosilicon in the film, 75.06%, is achieved at a voltage frequency on the target of 100 Hz and a pressure in the working chamber of 1.9 Pa. Of course, it should be understood that due to data limitations, this result may not be accurate. To improve the process model and clarify the optimal values of technological parameters of magnetron sputtering, more experimental data are needed.

Conclusions

In the process of studying magnetron sputtering of silicon films, it was found that the greatest influence on increasing the proportion of nano silicon in the film composition is exerted by an increase in the pressure in the working chamber and the frequency of voltage pulses on the target. An increase in the specific power at the target leads to a reduction in the proportion of the amorphous phase and an increase in the crystalline phase, but this indicator does not affect the increase in the proportion of nanocrystalline silicon. Increasing the pressure in the working chamber and the voltage frequency helps to increase the proportion of nanosilicon. However, there is probably a limit to these parameters, beyond which a further increase in their values reduces the share of nanosilicon. The silicon film obtained under experimental conditions acquires a porous cellular structure resulting from

the interweaving of silicon nanofibers. Based on experimental data, a correlation-regression model of the process of magnetron sputtering of silicon on a copper substrate was constructed with a high level of adequacy within the limits of the experiments. Using the obtained model, preliminary optimal parameters of the sputtering process were calculated. The calculated maximum fraction of nanosilicon in the film - 75.06%, is achieved at a voltage frequency on the target of 100 Hz and pressure in the working chamber of 1.9 Pa. Additional experiments are needed to identify more accurate optimal values of magnetron sputtering parameters and to test the resulting silicon films as anodes of lithium-ion batteries.

CRediT author statement: **K.Tolubaev**: Preparation and implementation of the magnetron sputtering process, generalization of the research results. **B.Zhautikov**: Growing silicon crystals to prepare a target for a magnetron. **N.Zobnin**: Mathematical data processing and establishment of a model of the magnetron sputtering process, working with the resulting model to optimize the process. **G.Dairbekova**: Electron microscopy of silicon film samples obtained by magnetron sputtering. **S. Kabieva**: Raman spectroscopy and interpretation of the obtained spectra. **R. Al-Kasasbeh**: deconvolution of the Raman spectra of silicon nanofilms, comparison of the results obtained with available literature sources.

Cite this article as: Tolubaev KS, Zhautikov BA, Zobnin NN, Dairbekova GS, Kabieva SK, Al-Kasasbeh RT. Modeling the influence of technological parameters of the magnetron sputtering process using the Caroline D12C system on the proportion of nanocrystallites in the structure of thin silicon films. Kompleksnoe Ispolzovanie Mineralnogo Syra = Complex Use of Mineral Resources. 2025; 334(3):51-58. https://doi.org/10.31643/2025/6445.27

Магнетронды шашырату процесінің технологиялық параметрлерінің Caroline D12C жүйесіндегі жұқа кремний қабықшаларының құрылымындағы нанокристаллиттер үлесіне әсерін модельдеу

[1]Толубаев Қ.С., [1]Жаутиков Б.А., [1*]Зобнин Н.Н., [2]Даирбекова Г.С., [1]Кабиева С.К., [3] Al-Kasasbeh R.T.

[1] Қарағанды индустриялық университеті, Теміртау, Қазақстан
[2] Сәтбаев университеті, Алматы, Қазақстан
[3]Иордания университеті, Амман, Иордания

Мақала келді: *5 шілде 2024*
Сараптамадан өтті: *9 шілде 2024*
Қабылданды: *12 шілде 2024*

ТҮЙІНДЕМЕ

Магнетронды бүрку әдісімен алынған жұқа пленкалардағы кремнийдің нано өлшемді модификациясының үлесінің процестің негізгі технологиялық көрсеткіштеріне - нысанадағы меншікті қуатқа, жұмыс камерасындағы қысымға, нысанаға берілетін кернеудің пульсация жиілігіне эксперименттік тәуелділігі зерттелді. Деректер бірнеше корреляциялық-регрессиялық талдау әдісімен өңделді және эксперименттік тәуелділікті сипаттайтын сәйкес математикалық модель алынды. Нысанадағы меншікті қуат пленкадағы нано кремнийдің үлесіне айтарлықтай әсер етпейтіні анықталды. Нысанаға кернеу жиілігі тек оң әсер етеді, сондықтан тек бүрку жабдықтарының техникалық мүмкіндіктерімен шектеледі. Жұмыс камерасындағы қысымның оңтайлы мәні бар, өйткені математикалық модельде бұл фактор оң және теріс коэффициенттерге ие. Модельді есептеу арқылы талдау кезінде пленкадағы нано кремнийдің ең үлкен үлесі 75,06% 100 Гц нысанадағы кернеу жиілігінде және 1,9 Па жұмыс камерасындағы қысымда қол жеткізілетіні анықталды. Бұл деректер эксперименттердің шектеулі санына байланысты алдын ала берілген түрі болып табылады.

Түйін сөздер: Нано өлшемді кремний, магнетронды бүрку, Caroline D12C, пленка, математикалық модельдеу, корреляциялық-регрессиялық талдау, нысан.

Авторлар туралы мәліметтер:

Толубаев Қанат — *Докторант, Қарағанды индустриялық университеті, Теміртау, Қазақстан. Email: kanat.tolubayev@tttu.edu.kz*

Жаутиков Бахыт Ахатович — *Техника ғылымдарының докторы, профессор, Қарағанды индустриялық университеті, Теміртау, Қазақстан. Email: bakhyt_zhautikov@mail.ru*

Зобнин Николай Николаевич — *Техника ғылымдарының кандидаты, Қарағанды индустриялық университеті, Теміртау, Қазақстан. Email: zobninnn@mail.ru*

Даирбекова Гулдана Сиюндыковна — *PhD, Сәтбаев университеті, Алматы, Қазақстан. Email: guldana.01.02.91@mail.ru*

Кабиева Сауле Казжановна	*Химия ғылымдарының кандидаты, доцент, Қарағанды индустриялық университеті, Теміртау, Қазақстан. Email: kabieva.s@mail.ru*
Al-Kasasbeh Riad	*PhD, профессор, Иордания университеті, Амман, Иордания. Email: riad_alkasasbeh@bau.edu.jo*

Моделирование влияния технологических параметров процесса магнетронного распыления на системе Caroline D12C на долю нанокристаллитов в структуре тонких пленок кремния

[1]Толубаев К.С., [1]Жаутиков Б.А., [1*]Зобнин Н.Н., [2]Даирбекова Г.С., [1]Кабиева С.К., [3] Al-Kasasbeh R.T.

[1] Карагандинский индустриальный университет, Темиртау, Казахстан
[2] Сатпаев университет, Алматы, Казахстан
[3]Университет Иордании, Амман, Иордания

Поступила: *5 июля 2024*
Рецензирование: *9 июля 2024*
Принята в печать: *12 июля 2024*

АННОТАЦИЯ

Изучена экспериментальная зависимость доли наноразмерной модификации кремния в тонких плёнках, полученных методом магнетронного напыления от основных технологических показателей процесса - удельной мощности на мишени, давления в рабочей камере, частоте пульсации напряжения, подаваемого на мишень. Данные обработаны методом множественного корреляционно-регрессионного анализа и получена соответствующая математическая модель, описывающая экспериментальную зависимость. Установлено, что удельная мощность на мишени не влияет существенным образом на долю нано кремния в плёнке. Частота напряжения на мишени влияет только положительным образом и потому ограничивается только техническими возможностями оборудования напыления. Давление в рабочей камере имеет оптимальное значение, т.к. в математической модели при этом факторе имеются как положительные, так и отрицательные коэффициенты. При анализе модели расчётным путём установлено, что наибольшая доля нано кремния в плёнке 75,06% достигается при частоте напряжения на мишени 100 Гц и давлении в рабочей камере 1,9 Па. Эти данные предварительные в силу ограниченного количества экспериментов.

Ключевые слова: Наноразмерный кремний, магнетронное напыление, Caroline D12C, плёнка, математическое моделирование, корреляционно-регрессионный анализ, мишень.

Информация об авторах:

Толубаев Канат	*Докторант, Карагандинский индустриальный университет, Темиртау, Казахстан. Email: kanat.tolubayev@tttu.edu.kz*
Жаутиков Бахыт Ахатович	*Доктор технических наук, профессор, Карагандинский индустриальный университет, Темиртау, Казахстан. Email: bakhyt_zhautikov@mail.ru*
Зобнин Николай Николаевич	*Кандидат технических наук, Карагандинский индустриальный университет, Темиртау, Казахстан. Email: zobninnn@mail.ru*
Даирбекова Гулдана Сиюндыковна	*PhD, Сатпаев университет, Алматы, Казахстан. Email: guldana.01.02.91@mail.ru*
Кабиева Сауле Казжановна	*Кандидат химических наук, доцент, Карагандинский индустриальный университет, Темиртау, Казахстан. Email: kabieva.s@mail.ru*
Al-Kasasbeh Riad	*PhD, Профессор, Иорданский университет, Амман, Иордания. Email: riad_alkasasbeh@bau.edu.jo*

References

[1] Bergmann RB, Werner JH. The future of crystalline silicon films on foreign substrates. Thin Solid Films. 2002; 403:162-169. https://doi.org/10.1016/S0040-6090(01)01556-5

[2] Chan CK, Peng H, Liu G, McIlwrath K, Zhang XF, Huggins RA, Cui Y. High-performance lithium battery anodes using silicon nanowires. Nature nanotechnology. 2008; 3(1):31-35. https://doi.org/10.1038/nnano.2007.411

[3] Yao W, Zou P, Wang M, Zhan H, Kang F, Yang Ch. Design principle, optimization strategies, and future perspectives of anode-free configurations for high-energy rechargeable metal batteriesю Electrochemical Energy Reviews. 2021; 4:601-631. https://doi.org/10.1007/s41918-021-00106-6

[4] Nussupov KK, Beisenkhanov NB, Zharikov SK, et al. Structure and composition of silicon carbide films synthesized by ion implantation. Phys. Solid State. 2014; 56:2307-2321. https://doi.org/10.1134/S1063783414110237

[5] Xin Chen, Chuankai Fu, Yuanheng Wang, Jiaxin Yan. Recent advances of silicon-based solid-state lithium-ion batteries. 2024; 19:100310. https://doi.org/10.1016/j.etran.2023.100310

[6] Karimi Z, Sadeghi A, Ghaffarinejad A. The comparison of different deposition methods to prepare thin film of silicon-based anodes and their performances in Li-ion batteries. Journal of Energy Storage. 2023; 72:108282. https://doi.org/10.1016/j.est.2023.108282

[7] Golubev VG, Davydov VYu, Medvedev AV, Pevtsov AB, Feoktistov NA. Raman spectra and electrical conductivity of silicon films with a mixed amorphous-crystalline composition: determination of the volume fraction of the nanocrystalline phase. Solid State Physics. 1997; 39(8):1348-1353. https://doi.org/10.1134/1.1130042

[8] Sharma M, Panigrahia J, Komaralaa VK. Nanocrystalline silicon thin film growth and application for silicon heterojunction solar cells: a short review. Nanoscale advances. 2021; 12:3373-3383. https://doi.org/10.1039/d0na00791a

[9] Lin H, Yang M, Ru X, Wang G, Yin S, Peng F, et al. Silicon heterojunction solar cells with up to 26.81% efficiency achieved by electrically optimized nanocrystalline-silicon hole contact layers. Nature Energy. 2023; 8:789-799. https://doi.org/10.1038/s41560-023-01255-2

[10] Automatic installation of magnetron and thermal coating "Caroline D12A" [Electronic resource] "Caroline D12A" Electronic training manual. URL: https://ipsiras.ru/Lab/CKPO/Nanofot/CarolineD12A.htm

[11] Mazinov A, Shevchenko A, Bahov V. Quantum Interactions of Optical Radiation with the Defect Centres in the Tails of the Forbidden Band of Amorphous Materials. Optica Applicata. 2014, 44. https://doi.org/10.5277/oa140213

[12] Mazinov S, Shevchenko AI, Voskresensky VM. BULLETIN of the L N Gumilyov Eurasian National University Mathematics Computer Science Mechanics Series. 2019.

[13] Goli M, González–Vélez H. Autonomic Coordination of Skeleton-Based Applications over CPU/GPU Multi-Core Architectures. International Journal of Parallel Programming. 2016; 45(2):203-224. https://doi.org/10.1007/s10766-016-0419-4

[14] Shkunov M N, Österbacka R, Fujii A, Yoshino K, Vardeny Z V. Laser Action in Polydialkylfluorene Films: Influence of Low-Temperature Thermal Treatment. Applied physics letters. 1999; 74(12):1648-1650. https://doi.org/10.1063/1.123642

[15] Chan C K, Peng H, Liu G, McIlwrath K, Zhang X F, Huggins R A, Cui Y. High-Performance Lithium Battery Anodes Using Silicon Nanowires. Nature Nanotechnology. 2007; 3(1):31-35. https://doi.org/10.1038/nnano.2007.411

[16] Wang X-L, Han W-Q. Graphene Enhances Li Storage Capacity of Porous Single-Crystalline Silicon Nanowires. ACS Applied Materials & Interfaces. 2010; 2(12);3709-3713. https://doi.org/10.1021/am100857h

[17] Li X, Zhi L. Managing Voids of Si Anodes in Lithium Ion Batteries. Nanoscale. 2013; 5(19):8864. https://doi.org/10.1039/c3nr03197g

[18] Ranganath Teki, Moni Kanchan Datta, Krishnan R, Parker T E, Lu T-M, Kumta P N, Nikhil Koratkar. Nanostructured Silicon Anodes for Lithium Ion Rechargeable Batteries. Small. 2009; 5(20):2236-2242. https://doi.org/10.1002/smll.200900382

[19] Syed Abdul Ahad, Kennedy T, Geaney H. Si Nanowires: From Model System to Practical Li-Ion Anode Material and Beyond. ACS energy letters. 2024; 9(4):1548-1561. https://doi.org/10.1021/acsenergylett.4c00262

[20] Imtiaz S, Amiinu I S, Storan D, Kapuria N, Geaney H, Kennedy T, Ryan K M. Dense Silicon Nanowire Networks Grown on a Stainless-Steel Fiber Cloth: A Flexible and Robust Anode for Lithium-Ion Batteries. Advanced Materials. 2021; 33(52):2105917. https://doi.org/10.1002/adma.202105917

[21] Collins G A, Kilian S, Geaney H, Ryan K M. A Nanowire Nest Structure Comprising Copper Silicide and Silicon Nanowires for Lithium-Ion Battery Anodes with High Areal Loading. Small. 2021; 17(34):2102333. https://doi.org/10.1002/smll.202102333

Crossref

creative commons

DOI: 10.31643/2025/6445.28

Metallurgy

Physical and chemical study of manganese dioxide sorbent after sorption of lithium from brines

Abdulvaliyev R.A., Karshyga Z.B., *Yersaiynova A.A., Yessengaziyev A.M., Orynbayev B.M., Kvyatkovskaya M.N.

Institute of Metallurgy and Ore Beneficiation JSC, Satbayev University, Almaty, Kazakhstan

** Corresponding author email: a.yersaiynova@stud.satbayev.university*

Received: *May 30, 2024*
Peer-reviewed: *June 23, 2024*
Accepted: *July 15, 2024*

ABSTRACT

The article presents the results of the study for the synthesized manganese dioxide sorbent after its saturation with lithium from brine. The sorbent was previously prepared. For this purpose the mixture of manganese oxide compounds was kept with lithium hydroxide in a wet state at 125 °C, calcinated at 450 °C and then the precursor was treated with dilute hydrochloric acid. The process intended to saturate the sorbent with lithium was performed by putting it in contact with a lithium-containing brine with a pH of 8.77 at T = 40°C for 24 hours in four cycles. The sorbent after saturation was studied using X-ray phase and thermal analysis methods. X-ray phase analysis showed that lithium-containing phases are represented by such compounds as $Li(Li_{0.17}Mn_{0.83})_2O_4$ and $Li_{0.78}Mn_{1.88}O_4$. The results of thermal analysis show the possibility of phases to be in the sorbent after saturation $LiMn_2O_4$ and $Li_{1,3}Mn_2O_4$ phases. The study results showed that ion-exchange interaction takes place between the lithium-ion from the brine and the proton from the manganese-oxide spinel composition to a greater extent during sorption. Besides, the redox nature of the interaction is present during the sorption of lithium. All lithium intercalation reactions proceed topotactically without significant changes in the main structure of the original sorbent.

Keywords: lithium, brine, sorbent, manganese dioxide, sorption, exchange capacity.

Information about authors:

Karshyga Zaure Baitaskyzy — *Ph.D., Leading Researcher, Institute of Metallurgy and Ore Beneficiation JSC, Satbayev University, Shevchenko str., 29/133, 050010, Almaty, Kazakhstan. Email: z.karshyga@satbayev.university*

Abdulvaliyev Rinat Anvarbekovich — *Candidate of Technical Sciences, Head of the Laboratory of Alumina and Aluminium of the Institute of Metallurgy and Ore Beneficiation JSC, Satbayev University, Shevchenko str., 29/133, 050010, Almaty, Kazakhstan. Email: rin-abd@inbox.ru*

Yersaiynova Albina Abatkyzy — *Ph.D. student, Leading Engineer, Institute of Metallurgy and Ore Beneficiation JSC, Satbayev University, Shevchenko str., 29/133, 050010, Almaty, Kazakhstan. Email: a.yersaiynova@stud.satbayev.university*

Yessengaziyev Azamat Muratovich — *Ph.D., Head of the Laboratory of Titanium and Rare Refractory Metals of the Institute of Metallurgy and Ore Beneficiation JSC, Satbayev University, Shevchenko str., 29/133, 050010, Almaty, Kazakhstan. Email: a.yessengaziyev@satbayev.university*

Orynbayev Bauyrzhan Munarbaiuly — *Ph.D. student, Leading Engineer, Institute of Metallurgy and Ore Beneficiation JSC, Satbayev University, Shevchenko str., 29/133, 050010, Almaty, Kazakhstan. Email: Bauyrzhan.Orynbayev@stud.satbayev.university*

Kvyatkovskaya Marina Nikolayevna — *Researcher, Institute of Metallurgy and Ore Beneficiation JSC, Satbayev University, Shevchenko str., 29/133, 050010, Almaty, Kazakhstan. Email: kmn_55@mail.ru*

Introduction

Lithium plays a key role in the advancement of energy storage technologies, electric mobility and wireless devices. It effectively addresses such significant problems as environmental pollution, climate change and fossil fuel shortages [[1], [2]].

Global emissions of carbon dioxide (CO_2) produced by fossil fuels increased and reached the highest level in history between 2021 and 2022 [[3], [4]].

Currently, we are intensely experiencing climate change every year - floods, forest fires, droughts and other major disasters due to the release of CO_2 gas and other gases into the atmosphere in large quantities. In this regard, international organizations intend to switch to renewable energy sources in order to reduce the spread of greenhouse gases and to reduce the load of fossil fuels [5]. The main human activity that produces CO_2 emissions is the combustion of fuels (coal, natural gas and oil) used to generate electricity and vehicles [[6], [7]].

One of the best solutions is to replace traditional modes of transport with electric vehicles to prevent the depletion of oil and gas reserves around the world, as well as environmental, economic and geopolitical problems. The main component of electric vehicles is lithium-ion batteries.

Lithium-ion batteries (LIBs) are popular power sources in various applications due to their high energy density, efficiency, reliability and variety of electrode configurations. Recently, there has been a steady trend towards the development of a new generation of lithium-ion batteries with increased capacity and energy density, intended for electric vehicles (EV), hybrid electric vehicles (HEV), space objects and autonomous electronic devices (for example, hybrid solar panels) [[8], [9], [10], [11], [12]].

Lithium is very relevant in the production of high-tech equipment [13]. The need for lithium is expected to increase in the coming decades with increase in demand for electric vehicles and renewable energy. According to McKinsey & Company forecasts, the demand for lithium-ion batteries will increase by 4,700 TWh by 2030, leading to the rapid development of lithium mining [14].

Currently, it is recommended to use various mineral raw materials and industrial wastes to extract strategically important metals [[15], [16], [17], [18], [19]]. Lithium is extracted mainly from hydromineral raw materials (brines), hard rocks, and also from waste lithium batteries [20]. Each of these sources has its advantages and disadvantages. One of the most attractive raw materials for lithium sources is natural brines since they require lower environmental and economic costs compared to mining from hard rocks. Brines contain dissolved lithium ions which can be extracted with the use of various methods such as evaporation, precipitation, liquid-liquid extraction, sorption and membrane methods [[21], [22], [23], [24], [25]]. One promising method is the sorption of lithium from brines. Methods for the sorption of lithium from brines can be performed with the use of both organic and inorganic sorbents. Cation exchangers based on sulfo groups and based on amino groups can effectively sorb lithium and can also be effective for the extraction of lithium from solutions, especially under certain pH conditions. But organic ion exchangers have selectivity not only for lithium but also for other ions. It can complicate the separation and purification of recovered lithium and also result in the formation of organic waste which may require special disposal or treatment methods increasing the environmental burden of the process [26]. The synthesis and application of highly selective inorganic sorbents for lithium is a current scientific direction [[27], [28]].

Lithium-ion sieves (LIS) are considered one of the most promising materials for lithium recovery from low-lithium brines due to their high adsorption capacity and excellent lithium selectivity. Studies confirm manganese oxide (LMO) and titanium oxide (LTO) sorbents as effective methods for lithium recovery from brines [[29], [30], [31]].

Currently, there are two main classifications of LTO-type LIS: layered structures based on H_2TiO_3 and spinel structures based on $H_4Ti_5O_{12}$ [32]. The structure of H_2TiO_3 is explained by the main layered structure of the H_2TiO_3 precursor, similarly, the spinel structure of $H_4Ti_5O_{12}$ is derived from the spinel structure of its precursor - $Li_4Ti_5O_{12}$. Titanium-based lithium-ion sieves have attracted attention due to their theoretical superior adsorption capacity but the practical adsorption capacity observed after extraction of lithium from brine or seawater is often lower [33].

Lithium-ion oxides based on spinel-type manganese oxide are currently the most popular selective sorbents. The scientists developed sorbents on such oxide-based manganese as λ-MnO_2, $MnO_2{\cdot}0.3H_2O$ and $MnO_2{\cdot}0.5H_2O$ from the precursors $LiMn_2O_4$, $Li_{1.33}Mn_{1.67}O_4$ ($Li_4Mn_5O_{12}$) and $Li_{1.6}Mn_{1.6}O_4$ ($Li_2Mn_2O_5$) [[34], [35]]. These sorbents have excellent adsorption capacity; for example, sorbents made from precursors have the following sorption capacity: $LiMn_2O_4$ - 39.9 mg/g, $Li_4Mn_5O_{12}$ - 59 mg/g, and the sorbent from the precursor $Li_{1.6}Mn_{1.6}O_4$ has high capacity of 72.3 mg/g [36]. The advantage is their high selectivity for lithium, which avoids the sorption of other ions present in the solution [[37], [38]]. The specific adsorption of lithium relative to other coexisting ions occurs due to the unique ability of lithium ions in aqueous solution to selectively maneuver through layered gaps and occupy exchange sites relative to such competing ions as K^+, Na^+, Ca^{2+} and Mg^{2+}. This selectivity is due to the large ionic radii of ions such as K^+ (0.138 nm), Na^+ (0.102 nm) and Ca^{2+} (0.100 nm), in contrast to Li+ (0.074 nm), which makes them unable to cross narrow channels [39]. Although Mg^{2+} (0.072 nm) has a similar ionic radius to Li^+, its significantly higher free energy of hydration

compared to Li prevents its dehydration, thereby limiting its access to exchange sites [[28], [40]].

The study examined the conditions for obtaining a lithium-manganese precursor and its acid treatment, as well as the sorption characteristics and sorption capacity of the synthesized sorbent [41].

It is of great interest to study the composition of the saturated manganese dioxide sorbent to clarify and obtain additional information regarding the process of lithium sorption from brine.

Experimental part

Materials. Lithium hydroxide monohydrate $LiOH \cdot H_2O$ brand “puriss.”; hydrochloric acid HCl qualification “puriss.”; Mn_2O_3 “puriss. spec.”, MnO “puriss.”, brine from oil and gas fields.

Preparation of manganese dioxide sorbent. The preparation of sorbents consisted of three stages: 1) holding in an oven with treatment of a mixture of manganese oxide compounds and lithium hydroxide in an aqueous environment at 125 °C for 13 hours until dry at the end; 2) calcination of the processed product in a muffle furnace SNOL 7.2/1300 at 450 °C for 6 hours; 3) acid treatment of the precursor with dilute hydrochloric acid (0.5 mol/dm^3) at 40 °C with stirring for 24 hours.

Methodology and analysis methods. *Experimental procedure.* Sorption with saturation of manganese dioxide sorbent was performed under static conditions in a 3 dm^3 glass, with a VELP Scientifica LS F201A0151 (Italy) mechanical stirrer installed above it, providing a fixed number of revolutions. The constant temperature was maintained with the use of an Aizkraukles TW 2.02 water bath thermostat (ELMI, Latvia). A given amount of sorbent was transferred into a glass filled with a given volume of brine, set to a given temperature and stirred for a certain time to carry out sorption. The solution was separated from the sorbent by decantation, and then contact of the sorbent with a fresh portion of brine was ensured after sorption. Saturation of the sorbent upon contact with fresh portions of brine was performed in 4 cycles. The saturated sorbent was washed and dried after sorption.

Determination of the capacity of sorbents. Static exchange capacity is calculated by the formula:

$$\mathrm{SEC} = \frac{(C_0 - C_e) \cdot V}{m}$$

where, SEC – static exchange capacity; C_0 – metal concentration in the initial solution, mg/dm^3; C_e – residual equilibrium concentration of metal in the solution, mg/dm^3; V – solution volume, dm^3; m – a mass of dry sorbent, g.

Analysis methods. The quantitative content of the studied elements in brines is determined with the use of an Optima 8300DV atomic emission spectrometer with inductively coupled plasma and a SHIMADZU atomic absorption spectrophotometer type AA-7000 (Japan). X-ray phase analysis (XPA) was performed on a D8 ADVANCE diffractometer "BRUKER AXS GmbH", (Germany) Cu–Kα radiation, PDF-2 database of the International Center for Diffraction Data ICDD (USA).

Thermal analysis of the saturated sorbent sample was performed with the use of an STA 449 F3 Jupiter simultaneous thermal analysis device. Before heating, the furnace space was evacuated (evacuated per cent level ~ 92 %) and then purged with inert gas for 5 minutes. Heating was performed at a rate of 15°C/min. in an atmosphere of highly purified argon. Cooling was performed at a rate of 17 °C/min. The total volume of incoming gas was maintained within 50 ml/min. The results obtained with the STA 449 F3 Jupiter were processed with the use of the NETZSCH Proteus software.

Results and Discussion

The manganese dioxide sorbent for lithium sorption was synthesized according to the conditions presented above and may have a composition close to $MnO_2 \cdot nH_2O$; the process presumably occurs via the ion exchange mechanism. X-ray phase analysis (XRD) of the sorbent and its precursors is shown in Figure 1 (a, b, c). As can be seen from Figure 1a, lithium manganese oxide (LMO) was formed with the composition $LiMnO_2$ with an orthorhombic crystal lattice structure (space group Pmnm) as a result of holding a mixture of oxide compounds of manganese (II), (III) and lithium hydroxide in a wet state in a drying oven at 125 °C for 13 hours until it was dry. The oxidation of manganese present in the trivalent state to tetravalent with the transformation of the main phase of the LMO $LiMnO_2$ to $Li_{1,6}Mn_{1,6}O_4$ occurs with further calcination of the resulting LMO at 450 °C for 6 hours. It represents a face-centred cubic system

(space group Fd3m) with a lattice constant of 8.14 Å (Figure 1 c). It can be noted that the main phase of the resulting sorbent is represented by manganese (IV) dioxide as a result of acid treatment of the precursor after calcination; the diffraction pattern retained the cubic structure with only a slight decrease in the constant lattice to 8.036 Å (Figure 1 c). It may indicate that the acid treatment with the extraction of lithium from the precursor proceeds topotactically with the preservation of the cubic structure of the crystal lattice [42].

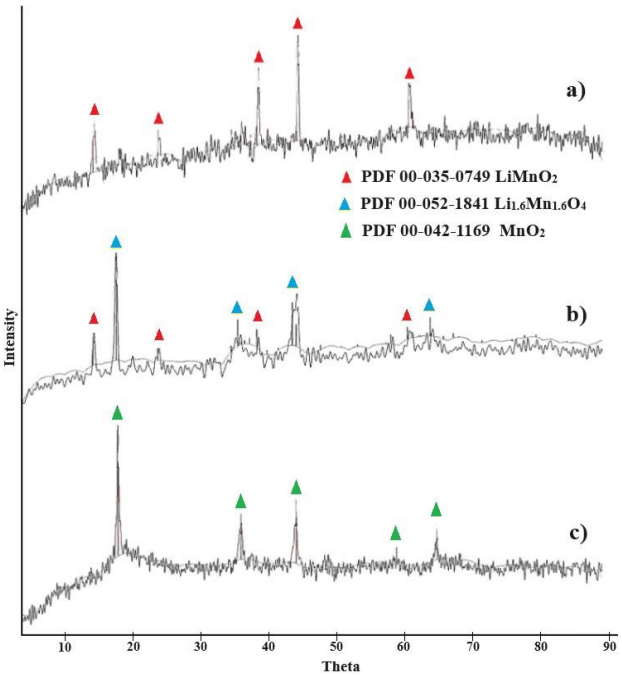

Figure 1 - Diffraction patterns of lithium-manganese oxide of the first stage of processing (a), precursor after calcination (b), and sorbent (c).

As can be seen from Figure 1 b, some part of underoxidised orthorhombic $LiMnO_2$ also remains after calcination. Orthorhombic $LiMnO_2$ adopts an ordered rock salt structure consisting of zigzag sheets of edge-sharing MnO_6 octahedra, separated by octahedrally coordinated lithium ions (Figure 2). According to work [43] the delithiation reactions which occur between orthorhombic $LiMnO_2$ and acid depend on the physical form of the material. On exposure to acid, a single crystal of $LiMnO_2$ was observed to undergo a delithiation reaction as described in reaction (1) to form a phase of composition MnO_2:

$$2\ LiMnO_2 + 2\ H^+ \rightarrow MnO_2 + 2\ Li^+ + H_2 \quad (1)$$

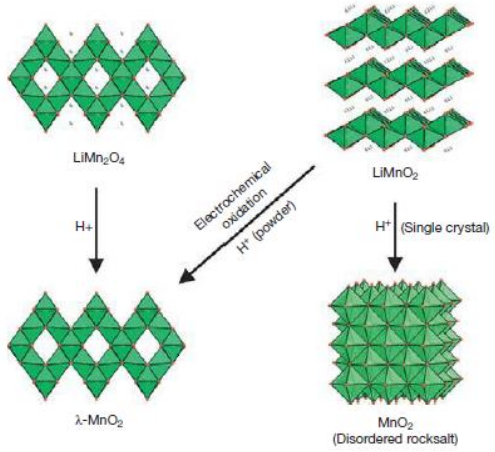

Figure 2 - Delithiation of $LiMn_2O_4$ and $LiMnO_2$ leads to the formation of new metastable polymorphs of MnO_2 [43].

In contrast, the reaction between powder samples of orthorhombic $LiMnO_2$ and acid proceeds via a combination of disproportionation and ion exchange as shown in reactions (2) and (3) [[43], [44]]:

$$3LiMnO_2 + 4\ \gamma H^+ \rightarrow Li_{3-2\gamma}Mn_{3-\gamma}O_{6-2\gamma} + \gamma Mn^{2+} + 2\gamma Li^+ + +2\gamma H_2O \quad (2)$$

$$LiMnO_2 + xH^+ \rightarrow Li_{1-x}H_xMnO_2 + xH^+ \quad (3)$$

In this case, the deintercalation reaction drives migration of the manganese cations so that they adopt the λ-MnO_2 network of delithiated $LiMn_2O_4$, which shares a common oxide ion lattice with the rock salt structure.

Transformation of the orthorhombic $LiMnO_2$ to the spinel-type lithium manganese oxide has been explained by researchers in the works [[45], [46]]. A delithiated orthorhombic $LiMnO_2$ structure is unstable; lithium extraction from the zig-zag layers is accompanied by a migration of manganese cations into some of the octahedral sites left vacant by the extracted lithium to yield a stable spinel-type structure.

Lithium extraction from the zig-zag channels causes a displacement of 50% of the manganese ions into neighbouring octahedra left vacant by the extracted lithium ions. These displacements generate the 3:1 spinel ratio of manganese ions in alternate layers between the close-packed oxygen planes.

Thus, the obtained sorbent, represented according to XRD, spinel structure of MnO_2, can have both $MnO_2 \cdot nH_2O$ and λ-MnO_2 phases in its composition. Additional information can be obtained after saturation of the sorbent, which should result in lithium

intercalation with the formation of lithium-manganese phases.

The saturation of the sorbent with lithium was carried out by contacting it with a lithium-containing brine containing: 38,32 mg/dm^3 Li; 10,14 g/dm^3 Ca; 2,29 g/dm^3 Mg; 27,26 g/dm^3 Na; 0,824 g/dm^3 K; 0,335 g/dm^3 Al.

The saturation process of 4 g of sorbent was performed in four cycles while maintaining the following conditions in each cycle: T = 40°C; duration 24 hours; brine volume 2.8 dm^3, brine pH 8.77. In this case, the total capacity of the sorbent for lithium for all cycles was 20.44 mg/g. The sorbent, after its saturation with lithium, was studied using instrumental analysis methods.

Study of the saturated sorbent composition. The manganese dioxide sorbent was studied by X-ray phase analysis after saturation by providing contact with brine. Figure 3 shows a diffraction pattern of a saturated sorbent.

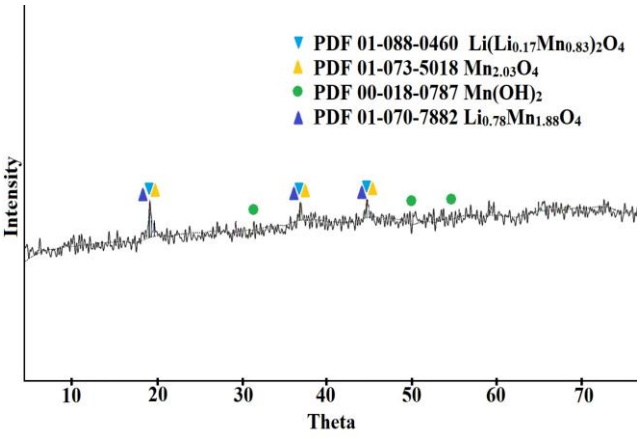

Figure 3 – Diffraction pattern of saturated sorbent

It can be seen according to the XRD data in Figure 3 that new lithium-containing oxide phases were formed on the sorbent during the sorption of lithium from brine, i.e., lithium-manganese oxides - mostly $Li(Li_{0.17}Mn_{0.83})_2O_4$, stoichiometrically equivalent to the $Li_{1.34}Mn_{1.66}O_4$, compound, and in slightly smaller quantities of $Li_{0.78}Mn_{1.88}O_4$. Both phases have a cubic Fd3m crystal lattice structure with a lattice constant of 8.14 Å for $Li(Li_{0.17}Mn_{0.83})_2O_4$ and 8.18 Å for $Li_{0.78}Mn_{1.88}O_4$. The sample also contains oxide $Mn_{2.03}O_4$ and manganese hydroxide $Mn(OH)_2$. It can be noted that the valence of manganese in the $Li(Li_{0.17}Mn_{0.83})_2O_4$ phase is close to four, i.e., when this compound was formed during the interaction of the sorbent with lithium from the brine, the valence of manganese did not change. It indicates that the process of lithium sorption mainly occurred through the ion exchange mechanism in this case, and not with the participation of valence forces due to the exchange of electrons between the sorbent and the brine [47]. Chitrakar et al. built a phase diagram containing of lithium manganese oxides and their delithiated products [42] (Figure 4). The diagram shows a compound of $Li_{1.33}Mn_{1.67}O_4$ composition, and it is almost similar to the $Li(Li_{0.17}Mn_{0.83})_2O_4$ phase obtained in a saturated sorbentin composition. According to the diagram, the reactions of lithium extraction and incorporation to form the delithiated oxide product $MnO_2{\cdot}0.31H_2O$ and lithium-manganese oxide $Li_{1.33}Mn_{1.67}O_4$, respectively, can occur in both directions.

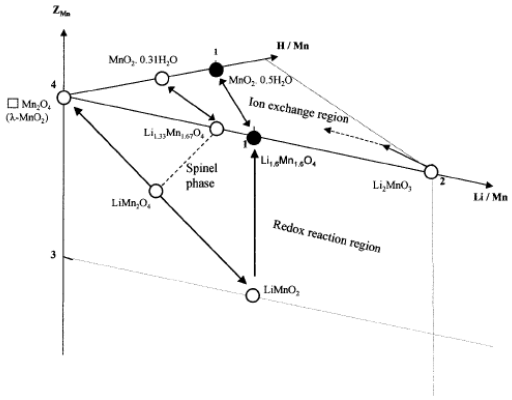

Figure 4 – Phase diagram of lithium manganese oxides and their delithiated products [42]

However, the formation of the $Li(Li_{0.17}Mn_{0.83})_2O_4$ phase obtained as a result of saturation can be represented under the expected reaction:

$$1.34\ Li^+ + 1.66\ (MnO_2{\cdot}0.4H_2O) \rightarrow Li(Li_{0.17}Mn_{0.83})_2O_4 + 1.34\ H^+ \quad (4)$$

In this case, the expected composition of the sorbent before its saturation with lithium, calculated by equation (4), can be represented as $MnO_2{\cdot}0.4H_2O$. A sorbent of similar composition was obtained by the authors of from a precursor with the composition of $Li_4Mn_5O_{12}$, i.e. from $Li_{1.33}Mn_{1.67}O_4$ [48].

Lithium sorption from brine also partially occurs with the formation of the $Li_{0.78}Mn_{1.88}O_4$ phase. The $Li_{0.78}Mn_{1.88}O_4$ phase has manganese with both valence +4 and +3. The formation of this compound may was influenced by the presence of the $Mn(OH)_2$ phase in the sorbent. Its presence led to the

formation of lithium-manganese oxide, accompanied by a coproportionation reaction. The expected reaction can be imagined:

$$0.78\ Li^+ + 1.73\ (MnO_2 \cdot 0.4H_2O) + 0.15\ Mn(OH)_2 \rightarrow Li_{0.78}Mn_{1.88}O_4 + 0.78\ H^+ + 0.452\ H_2O \quad (5)$$

or

$$0.78\ Li^+ + 1.73\ MnO_2 + 0.15\ Mn(OH)_2 + 0.24\ H_2O \rightarrow Li_{0.78}Mn_{1.88}O_4 + 0.78\ H^+ \quad (6)$$

At the same time, the $Li_{0.78}Mn_{1.88}O_4$ phase is close in composition to the $LiMn_2O_4$ spinel with a cubic crystal structure belonging to the Fd3m space group. Lithium ions occupy position 8a of tetrahedra in this structure. Mn^{3+} and Mn^{4+} ions are randomly distributed over the positions of 16d octahedra with a molar ratio of 1:1, and oxygen anions occupy positions of 32e face-centred cubes [43]. The approximately cubic, close-packed array of oxide ions includes an MnO_6 octahedron connected in three dimensions by common edges. On the other hand, the unit cell of $LiMn_2O_4$ can be considered a complex cubic structure: 32 oxygen atoms and 16 manganese atoms occupy half-positions of the octahedral interstitial site (16d), and the remaining half-positions (16c) are free. Here, 8 lithium atoms occupy 1/8 of the tetrahedral interstitial site (8a). Li^+ can be intercalated/deintercalated in the three-dimensional network of vacant octahedra and octahedral interstices along the 8a-16c-8a-16c channel, which is the structural basis of Li^+ intercalation/deintercalation in $LiMn_2O_4$ spinel [49]. Hunter in his work proposed a redox mechanism for the topotactic extraction of lithium from $LiMn_2O_4$ and defined the resulting spinel-type manganese oxide as λ-MnO_2 [50]:

$$4(Li)[Mn^{III}Mn^{IV}]O_4 + 8H^+ \rightarrow 3(\square)[Mn^{IV}_2]O_4 + 4Li^+ + 2Mn^{2+} + 4H_2O \quad (7)$$

where () are tetrahedral positions 8a; [] – octahedral positions 16d; □ – vacant positions.

In turn, the authors proposed a redox mechanism for the introduction of Li^+ into the dioxide structure when they studied the adsorption properties of λ-MnO_2 with the extraction of lithium from the aqueous phase [51]:

$$(\square)[Mn^{IV}_2]O_4 + nLiOH \rightarrow (Li_n\square_{1-n})[Mn^{III}_nMn^{IV}_{2-n}]O_4 + (n/2)H_2O + (n/4)O_2 \quad (8)$$

Besides, the author found during the study that spinels have 2 types of Li^+ extraction/incorporation reaction centres - redox-type centers and ion-exchange-type centres [51]. The proportions of each type can be assumed from the values of the Li/Mn molar ratio and the total valence of manganese in spinel. Ion exchange-type centres are predominantly formed at temperatures below 500 °C, while redox-type centres are formed at higher temperatures. Extraction/incorporation reactions of Li^+ occur predominantly with ion-exchange-type centres.

As it can be seen from equation (8), the reaction proceeds by interaction with LiOH; the extraction of lithium for manganese dioxide took place from a chloride-type brine upon saturation of the resulting sorbent in this study. At the same time, the pH of the brine was slightly alkaline and amounted to 8.77, and the brine contained hydroxyl ions in the composition of LiOH required for the possible occurrence of this reaction.

However, the researchers indicate that centres of the redox type are formed predominantly at temperatures of 500 °C and above [51]. The precursors were calcined at 450 °C in the present study, as noted above, and the $Li_{0.78}Mn_{1.88}O_4$ phase was present in a small amount according to the XRD of the saturated sorbent. Its formation could also be influenced by the presence of $Mn(OH)_2$ (reaction 5 or 6).

A thermal analysis of the saturated sorbent was performed; the thermograms are presented in Figure 5. As can be seen from the results of the above studies, an exothermic effect with a peak at 471.4 °C appeared on the DTA curve; well-pronounced endothermic effects with maximum development at 1084.2 °C and 1155.3 °C can also be noted. The dDTA curve recorded additional endothermic effects with extremes at 386.9 °C, 513.1 °C, 602.6 °C, 835.2 °C, 943.6 °C. Minima can be noted at 526.2 °C, 584.5 °C, 1011 °C on the DTG curve.

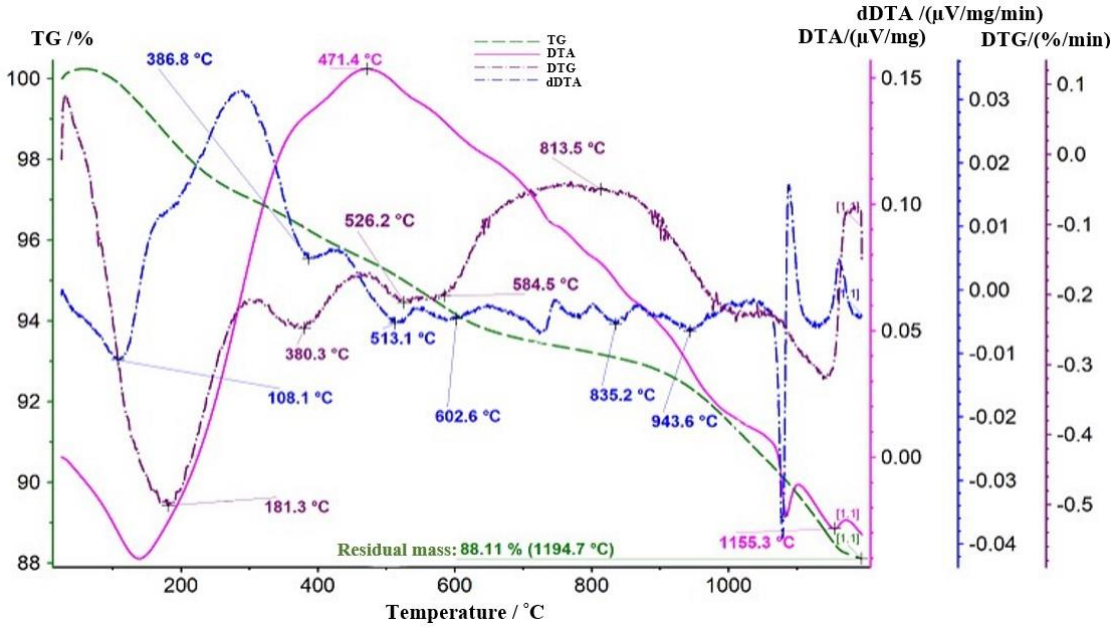

Figure 5 – Thermogram of the sorbent sample after saturation

The exothermic effect with a peak at 471.4 °C in the DTA curve may be a manifestation of the crystallization of the synthesized manganese dioxide gel. The combination of endothermic effects with extremes at 386.9 °C and 943.6 °C on the dDTA curve and an endothermic effect with maximum development at 1,155.3 °C on the DTA curve may reflect the presence of manganite - MnOOH. The first effect is associated with dehydration and the formation of pyrolusite or ß-kurnakite (ß-Mn_2O_3). Pyrolusite can transform into ß-Mn_2O_3 in the region of 500 – 600 °C. In the region of the development of the second effect (943.6 °C), ß-Mn_2O_3 decomposes with the formation of ß-Mn_3O_4. The latter effect reflects the reversible polymorphic transformation of ß-Mn_3O_4 into γ-Mn_3O_4. Considering separately the peaks of 1,084.2 °C and 1,155.3 °C on the DTA curve, we can assume the presence of α-Mn_3O_4. The first peak reflects the transition of α-Mn_3O_4 into ß-Mn_3O_4, the second – the reversible polymorphic transformation of ß-Mn_3O_4 into γ-Mn_3O_4.

Buzanov provides thermograms of $LiMn_2O_4$, $Li_{1,3}Mn_2O_4$ [52]. It can be assumed that the endothermic effect with an extremum at 835.2 °C reflects the decomposition of the $LiMn_2O_4$ phase. The peak of decomposition was recorded at 846 °C in the source. In superposition, with a stretch, a combination of the endothermic effect with an extremum at 602.6 °C on the dDTA curve (on the DTG curve it corresponds to a minimum at 584.5 °C) with the above-mentioned endothermic effect 835.2 °C (on the DTG curve it corresponds to a very weak minimum at 813.5 °C) may be a manifestation of the decomposition of $Li_{1,3}Mn_2O_4$. The thesis indicates temperatures of 613 °C and 823 °C.

It is not possible to unambiguously state the presence of γ-MnO_2 in a sample. The combination of endothermic effects at 602.6 °C, 943.6 °C on the dDTA curve and 1155.3 °C on the DTA curve can be interpreted as both a manifestation of ß-MnO_2 and a manifestation of γ-MnO_2.

As the results of thermal analysis show, the presence of phases of lithium-manganese oxides - $LiMn_2O_4$ and $Li_{1,3}Mn_2O_4$ is assumed in a sample of a saturated sorbent, in addition to the possible phases of manganite MnOOH, α-Mn_3O_4, ß-MnO_2 or γ-MnO_2. The detection of LMO phases indicates the sorption of lithium from brine with intercalation of lithium into the composition of the synthesized manganese-oxide spinels with the formation of these compounds.

Conclusions

The results of the studies showed that the sorption of lithium from brine on a synthesized manganese-oxide sorbent occurs with the formation of new lithium-containing phases. X-ray phase analysis showed the presence of phases in the sorbent after its saturation with lithium of $Li(Li_{0.17}Mn_{0.83})_2O_4$ and $Li_{0.78}Mn_{1.88}O_4$. The formation of the first phase occurs without a change in the

valence of manganese. It may indicate the ion-exchange nature of the interaction during the sorption of lithium from brine. And the formation of the second phase that occurs with a change in the valence of part of the manganese, indicates the redox nature of the interaction during sorption. The possibility of the presence of $LiMn_2O_4$ and $Li_{1,3}Mn_2O_4$, phases in the sorbent after saturation, formed due to redox reactions, is also indicated by the results of thermal analysis. In general, an ion exchange interaction takes place between a lithium ion from the brine and a proton from the manganese oxide spinel composition during sorption. All lithium intercalation reactions proceed topotactically without significant changes in the main structure of the original sorbent.

Conflicts of interest. On behalf of all authors, the corresponding author states that there is no conflict of interest.

CRediT author statement: ***Z.*** **Karshyga**: Conceptualization, Visualization, Writing draft preparation, Investigation, Methodology. **R. Abdulvaliyev**: Supervision. **A. Yersaiynova**: Reviewing and Editing, Investigation, Methodology, Data curation. **A. Yessengaziyev**: Validation. **B. Orynbayev**: Software. **M. Kvyatkovskaya**: Methodology.

Acknowledgements. This work was supported by the Science Committee of the Ministry of Science and Higher Education of the Republic of Kazakhstan (No. BR18574018).

Cite this article as: Abdulvaliyev RA, Karshyga ZB. Yersaiynova AA, Yessengaziyev AM, Orynbayev BM, Kvyatkovskaya MN. Physical and chemical study of manganese dioxide sorbent after sorption of lithium from brines. Kompleksnoe Ispolzovanie Mineralnogo Syra = Complex Use of Mineral Resources. 2025; 334(3):59-69. https://doi.org/10.31643/2025/6445.28

Тұзды ерітінділерден литийді сорбциялағаннан кейін алынған марганец диоксиді сорбентін физика-химиялық зерттеу

Абдулвалиев Р.А., Қаршыға З.Б., Ерсайынова А.А., Есенгазиев А.М., Орынбаев Б.М., Квятковская М.Н.

Металлургия және кен байыту институты АҚ, Сәтбаев университеті, Алматы, Қазақстан

Мақала келді: *30 мамыр 2024*
Сараптамадан өтті: *23 маусым 2024*
Қабылданды: *15 шілде 2024*

ТҮЙІНДЕМЕ

Мақалада марганец диоксиді негізінде синтезделген сорбенттің тұзды ерітіндідегі литиймен қанықканнан кейінгі зерттеу нәтижелері берілген. Алдын ала дайындалған сорбент: марганец оксиді қосылыстары мен литий гидроксидін 125 °С температурада ылғалды күйде ұстаудан, оларды 450 °С күйдіруден және одан әрі сұйылтылған тұз қышқылымен прекурсорды қышқылдық өңдеуден тұрады. Сорбентті литиймен қанықтыру процесі pH 8,77 литий бар тұзды ерітіндімен 24 сағат бойы қанықтыру арқылы жүргізілді, қанығудан кейінгі сорбент рентгендік фаза және термиялық талдау әдістері көмегімен зерттелді. Рентгендік фазалық талдау нәтижесінде $Li(Li_{0.17}Mn_{0.83})_2O_4$ и $Li_{0.78}Mn_{1.88}O_4$ құрамында литий бар фаза қосылыстары анықталды. Термиялық талдау нәтижелері қанықканнан кейін сорбентте $LiMn_2O_4$ және $Li_{1,3}Mn_2O_4$ фазаларының болатындығын көрсетті. Зерттеу нәтижелері бойынша сорбция кезінде тұзды ерітіндідегі литий ионы мен марганец-оксидті шпинельді құрамның протоны арасында ион алмасу әрекеттесуінің көбірек болатынын көрсетті. Сонымен қатар, литий сорбциясы кезінде әрекеттесудің тотығу-тотықсыздану сипаты бар. Литийдің барлық интеркалация реакциялары бастапқы сорбенттің негізгі құрылымында елеулі өзгерістерсіз топотактикалық түрде жүреді.

Түйін сөздер: литий, тұзды ерітінді, сорбент, марганец диоксиді, сорбция, алмасу көлемі.

Авторлар туралы ақпарат:

Қаршыға Зәуре Байтасқызы — *Ph.D., жетекші ғылыми қызметкер, Металлургия және кен байыту институты АҚ, Сәтбаев университеті, Шевченко көш., 29/133, 050010, Алматы, Қазақстан. Email: z.karshyga@satbayev.university*

Абдулвалиев Ринат Анварбекович — *Техника ғылымдарының кандидаты, сазтопырақ және алюминий зертханасының меңгерушісі, Металлургия және кен байыту институты АҚ, Сәтбаев университеті, Шевченко көш., 29/133, 050010, Алматы, Қазақстан. Email: rin-abd@inbox.ru*

Ерсайынова Альбина Абатқызы — *Ph.D. студент, жетекші инженер, Металлургия және кен байыту институты АҚ, Сәтбаев университеті, Шевченко көш., 29/133, 050010, Алматы, Қазақстан. Email: a.yersaiynova@stud.satbayev.university*

Есенгазиев Азамат Муратович	*Ph.D., титан және сирек қиын балқитын металдар зертханасының меңгерушісі, Металлургия және кен байыту институты АҚ, Сәтбаев университеті, Шевченко көш., 29/133, 050010, Алматы, Қазақстан. Email: a.yessengaziyev@satbayev.university*
Орынбаев Бауыржан Мұнарбайұлы	*Ph.D. студент, жетекші инженер, Металлургия және кен байыту институты АҚ, Сәтбаев университеті, Шевченко көш., 29/133, 050010, Алматы, Қазақстан. Email: Bauyrzhan.Orynbayev@stud.satbayev.university*
Квятковская Марина Николаевна	*Ғылыми қызметкер, Металлургия және кен байыту институты АҚ, Сәтбаев университеті, Шевченко көш., 29/133, 050010, Алматы, Қазақстан. Email: kmn_55@mail.ru*

Физико-химическое исследование сорбента диоксида марганца после сорбции лития из рассолов

Абдулвалиев Р.А., Қаршыға З.Б., Ерсайынова А.А., Есенгазиев А.М., Орынбаев Б.М., Квятковская М.Н.

АО Институт металлургии и обогащения, Satbayev University, Алматы, Казахстан

Поступила: *30 мая 2024*
Рецензирование: *23 июня 2024*
Принята в печать: *15 июля 2024*

АННОТАЦИЯ

В статье представлены результаты исследований по изучению синтезированного сорбента диоксида марганца после насыщения его литием из рассола. Предварительно был подготовлен сорбент, что заключалось в выдержке смеси оксидных соединений марганца с гидроксидом лития во влажном состоянии при 125 ℃, прокаливании при 450 ℃ и дальнейшей кислотной обработке прекурсора разбавленной соляной кислотой. Процесс насыщения сорбента литием проводился посредством его контактирования в четыре цикла с литийсодержащим рассолом с pH 8,77 при T = 40˚C, продолжительности 24 ч. Сорбент после насыщения был изучен с применением рентгенофазового и термического методов анализа. Рентгенофазовый анализ показал, что литийсодержащие фазы представлены соединениями $Li(Li_{0.17}Mn_{0.83})_2O_4$ и $Li_{0.78}Mn_{1.88}O_4$. Результаты термического анализа указывают на возможность присутствия в сорбенте после насыщения фаз $LiMn_2O_4$ и $Li_{1,3}Mn_2O_4$. Результаты исследований показали, что в большей степени при сорбции имеет место ионообменное взаимодействие между ионом лития из рассола и протоном из состава марганцево-оксидной шпинели. Помимо этого, присутствует при сорбции лития окислительно-восстановительный характер взаимодействия. Все реакции интеркаляции лития протекают топотактически без существенных изменений основной структуры исходного сорбента.

Ключевые слова: литий, рассол, сорбент, диоксид марганца, сорбция, обменная емкость.

Қаршыға Зәуре Байтасқызы	***Информация об авторах:*** *Ph.D., ведущий научный сотрудник, АО Институт металлургии и обогащения, Satbayev University, ул. Шевченко, 29/133, 050010, Алматы, Казахстан. Email: z.karshyga@satbayev.university*
Абдулвалиев Ринат Анварбекович	*Кандидат технических наук, заведующий лабораторией глинозема и алюминия, АО Институт металлургии и обогащения, Satbayev University, ул.Шевченко, 29/133, 050010, Алматы, Казахстан. Email: rin-abd@inbox.ru*
Ерсайынова Альбина Абатқызы	*Ph.D. студент, ведущий инженер, АО Институт металлургии и обогащения, Satbayev University, ул.Шевченко, 29/133, 050010, Алматы, Казахстан. Email: a.yersaiynova@stud.satbayev.university*
Есенгазиев Азамат Муратович	*Ph.D., заведующий лабораторией титана и редких тугоплавких металлов, АО Институт металлургии и обогащения, Satbayev University, ул.Шевченко, 29/133, 050010, Алматы, Казахстан. Email: a.yessengaziyev@satbayev.university*
Орынбаев Бауыржан Мұнарбайұлы	*Ph.D. студент, ведущий инженер, АО Институт металлургии и обогащения, Satbayev University, ул.Шевченко, 29/133, 050010, Алматы, Казахстан. Email: Bauyrzhan.Orynbayev@stud.satbayev.university*
Квятковская Марина Николаевна	*Научный сотрудник, АО Институт металлургии и обогащения, Satbayev University, ул.Шевченко, 29/133, 050010, Алматы, Казахстан. Email: kmn_55@mail.ru*

References

[1] Rowan TH, Andrew H, Frances W, Evi P, Robert Pl, Jordan JL. Life cycle assessment and water use impacts of lithium production from salar deposits: Challenges and opportunities. Resources, Conservation and Recycling. 2024; 207:107554. https://doi.org/10.1016/j.resconrec.2024.107554

[2] Weishang J, Jingfang Zh, Luojia Zh, Hao Zh, Wei Z, Liping W. Lithium-rich alloy as stable lithium metal composite anode for lithium batteries. eScience. 2024, 100266. https://doi.org/10.1016/j.esci.2024.100266

[3] Friedlingstein P, et al. Global Carbon Budget 2022. Earth System Science Data. 2022; 14(11):4811-4900. https://doi.org/10.5194/essd-14-4811-2022

[4] The National Energy Report Kazenergy 2023. Kazakhstan Association of Oil, Gaz and Energy Sector Organizations, Kazenergy. https://www.kazenergy.com/en/operation/ned/2177/,2023.

[5] The United Nations Framework Convention On Climate Change, https://unfccc.int/process-and-meetings/what-is-the-united-nations-framework-convention-on-climate-change.

[6] Environmental Protection Agency. Overview of Greenhouses gases. https://www.epa.gov/ghgemissions/overview-greenhouse-gases.

[7] Shukla PR, Skea J, Slade R, Fradera R, Pathak M, Alaa AK, Malek B, Renee VD, Hasija A, et al. Climate Change 2022 Mitigation of Climate Change Working Group III Contribution to the Sixth Assessment Report of the Intergovernmental Panel on Climate Change. Cambridge: Cambridge University Press. 2022.

[8] Yang J, Xia B, Shang Y, Huang W, Mi C. Improved Battery Parameter Estimation Method Considering Operating Scenarios for HEV/EV Applications. Energies. 2017; 10(1):5. https://doi.org/10.3390/en10010005

[9] Stroe DI, Swierczynski M, Stroe AI, Knudsen KS. Generalized Characterization Methodology for Performance Modelling of Lithium-Ion Batteries. Batteries. 2016; 2(4):37. https://doi.org/10.3390/batteries2040037

[10] Chen Z, Li X, Shen J, Yan W, Xiao R. A Novel State of Charge Estimation Algorithm for Lithium-Ion Battery Packs of Electric Vehicles. Energies. 2016; 9(9):710. https://doi.org/10.3390/en9090710

[11] Gao J, Zhang Y, He H. A Real-Time Joint Estimator for Model Parameters and State of Charge of Lithium-Ion Batteries in Electric Vehicles. Energies. 2015; 8(8):8594-8612. https://doi.org/10.3390/en8088594

[12] Bharathidasan M, Indragandhi V, Vishnu S, Michał J, Zbigniew L. A review on electric vehicle: Technologies, energy trading, and cyber security. Energy Reports. 2022; 8:9662-9685. https://doi.org/10.1016/j.egyr.2022.07.145

[13] Marcinov V, Klimko J, Takacova Z, Piroskova J, Miskufova A, Sommerfeld M, Dertmann C, Friedrich B, Orac D. Lithium Production and Recovery Methods: Overview of Lithium Losses. Metals. 2023; 13(7):1213. https://doi.org/10.3390/met13071213

[14] Battery 2030: Resilient, sustainable and circular. https://www.mckinsey.com/industries/automotive-and-assembly/our-insights/battery-2030-resilient-sustainable-and-circular#/

[15] Kenzhaliyev B, Surkova T, Berkinbayeva A, Amanzholova L, Mishra B, Abdikerim B, Yessimova D. Modification of Natural Minerals with Technogenic Raw Materials. Metals. 2022; 12:1907. https://doi.org/10.3390/met12111907

[16] Basudev S. Recovery and recycling of lithium: A review. Separation and Purification Technology. 2017; 172:388-403. https://doi.org/10.1016/j.seppur.2016.08.031

[17] Garcia LV, Ho YC, Myo Thant MM, Han DS, Lim JW. Lithium in a Sustainable Circular Economy: A Comprehensive Review. Processes. 2023; 11(2):418. https://doi.org/10.3390/pr11020418

[18] Mahran GMA, Gado MA, Fathy WM, ElDeeb AB. Eco-Friendly Recycling of Lithium Batteries for Extraction of High-Purity Metals. Materials. 2023; 16:4662. https://doi.org/10.3390/ma16134662

[19] Stopic S, Friedrich B. Advances in Understanding of the Application of Unit Operations in Metallurgy of Rare Earth Elements. Metals. 2021; 11:978. https://doi.org/10.3390/met11060978

[20] Meng F, McNeice J, Zadeh SS, Ghahreman A. Review of Lihium Production and Recovery from Minerals, Brines, and Lithium-Ion Batteries. Mineral Processing and Extractive Metallurgy Review. 2021; 42(2):123-141. https://doi.org/10.1080/08827508.2019.1668387

[21] Ye Zh, Yuehua H, Li W, Wei S. Systematic review of lithium extraction from salt-lake brines via precipitation approaches. Minerals Engineering. 2019; 139:105868. https://doi.org/10.1016/j.mineng.2019.105868

[22] Xianhui L, Yinghui M, Weihua Q, Senlin Sh, Chuyang YT, Jianxin L. Membrane-based technologies for lithium recovery from water lithium resources: A review. Journal of Membrane Science. 2019; 591:117317. https://doi.org/10.1016/j.memsci.2019.117317

[23] Ziller S, Von Bulow JF, Dahl SL. A fast sol - gel synthesis leading to highly crystalline birnessites under non-hydrothermal conditions. Dalton Transactions/ 2017; 46(14):4582-4588. https://doi:10.1039/c7dt00109f

[24] Xiaorong M, Yue J, Jiaming L, Zhengmeng S, Zhenpeng W. Electrochemical recovery of lithium from brine by highly stable truncated octahedral $LiNi_{0.05}Mn_{1.95}O_4$. Chemical Engineering Science. 2024; 283:119400. https://doi.org/10.1016/j.ces.2023.119400

[25] Tangkas IWCWH, Sujoto VSH, Astuti W. et al. Synthesis of Titanium Ion Sieves and Its Application for Lithium Recovery from Artificial Indonesian Geothermal Brine. J. Sustain. Metall. 2023; 9:613-624. https://doi.org/10.1007/s40831-023-00664-7

[26] Pratima M, Pandey BD, Mankhand TR. Extraction of lithium from primary and secondary sources by pre-treatment, leaching and separation: A comprehensive review. Hydrometallurgy. 2014; 150:192-208. https://doi.org/10.1016/j.hydromet.2014.10.012

[27] Adam S, Salman S, David M, Alan VC, Silvia R, Carmen AV, José MC, Daniel SA. Lithium recovery from hydraulic fracturing flowback and produced water using a selective ion exchange sorbent. Chemical Engineering Journal. 2021; 426:1385-8947. https://doi.org/10.1016/j.cej.2021.13071

[28] Qian Ch, Zhijie Ch, Hongqiang L, Bing-Jie N. Advanced lithium ion-sieves for sustainable lithium recovery from brines. Sustainable Horizons. 2024; 9:100093. https://doi.org/10.1016/j.horiz.2024.100093

[29] Yasin O, Zahra N, Mahmoud N, Nasrin Sh, Morteza A, Khatereh P, Amir R. Recent advances in nanomaterial development for lithium ion-sieving technologies. Desalination 2022; 529:115624. https://doi.org/10.1016/j.desal.2022.115624

[30] Shulei W, Xin Ch, Ying Zh, Yang Zh, Shili Zh. Lithium adsorption from brine by iron-doped titanium lithium ion sieves. Particuology. 2018; 41:40-47. https://doi.org/10.1016/j.partic.2018.02.001

[31] Snydacker DHI, Hegde V, Aykol M, Wolverton C, Computational Discovery of Li-M-O Ion Exchange Materials for Lithium Extraction from Brines. Chemistry of Materials. 2018; 30:6961. https://10.1021/acs.chemmater.7b03509

[32] Salman S, Bernd GL, Daniel SA. Metal oxide sorbents for the sustainable recovery of lithium from unconventional resources. Applied Materials Today. 2020; 19:100638. https://doi.org/10.1016/j.apmt.2020.100638

[33] Murphy O, Haji MN. A review of technologies for direct lithium extraction from low Li^+ concentration aqueous solutions. Frontiers in Chemical Engineering. 2022; 4. https://doi.org/10.3389/fceng.2022.1008680

[34] Chitrakar R, Kahon H, Miyai Y, and Ooi K. Recovery of Lithium from Seawater Using Manganese Oxide Adsorbent ($H_{1.6}Mn_{1.6}O_4$) Derived from $Li_{1.6}Mn_{1.6}O_4$. 2001; 40:2054-2058.

[35] Ryu T, Haldorai Y, Rengaraj A, Shin J, Hong HJ, Lee GW, Han YK, Huh YS, Chung KS. Recovery of Lithium Ions from Seawater Using a Continuous Flow Adsorption Column Packed with Granulated Chitosan-Lithium Manganese Oxide. Industrial & Engineering Chemistry Research. 2016; 55(26):7218-7225. http://dx.doi.org/10.1021/acs.iecr.6b01632

[36] Sun YS, Xiang L, Xiufeng R, Chunxi H, Yuan Zh, Weiping T. Improved structural stability and adsorption capacity of adsorbent material $Li_{1.6}Mn_{1.6}O_4$ via facile surface fluorination. Colloids and Surfaces A: Physicochemical and Engineering Aspects. 2021; 629:127465. https://doi.org/10.1016/j.colsurfa.2021.127465

[37] Popov GV. Sovremennyye metody i sredstva izvlecheniya litiya iz teplonositeley geotermalnykh mestorozhdeniy [Modern methods and means of attracting lithium from coolants of geothermal deposits]. Mining information and analytical bulletin. Scientific and technical journal. 2015; 63:256-260. (in Russ.).

[38] Luofeng L, Hongwei Zh, Yushan Zh, Dongmei C, Xinhua Zh. Lithium extraction from seawater by manganese oxide ion sieve MnO_2*$0.5H_2O$. Colloids and Surfaces A: Physicochemical and Engineering Aspects. 2015; 468:280-284. https://doi.org/10.1016/j.colsurfa.2014.12.025

[39] Klugman IY. Osobennosti iona litiya [Features of lithium ion]. Questions of applied physics: Interuniversity scientific collection. 2020; 27:71-79. (in Russ.)

[40] Gelfman M, Kovalevich O, Yustratov V. Kolloidnaya khimiya [Colloidal chemistry]. SPb.: Lan. 2010, 336. (in Russ.).

[41] Lukman N, Gita, AS, Diah S, Amien W. Synthesis and Characterization of Lithium Manganese Oxide with Different Ratio of Mole on Lithium Recovery Process from Geothermal Fluid of Lumpur Sidoarjo. J. Mater. Sci. Chem. Eng. 2015; 3:56–62.

[42] Chitrakar R, Kanoh H, Miyai Y, Ooi K. A New Type of Manganese Oxide ($MnO_2 \cdot 0.5H_2O$) Derived from $Li_{1.6}Mn_{1.6}O_4$ and Its Lithium Ion-Sieve Properties. Chem. Mater. 2000; 12:3151-3157.

[43] Hayward M. 2.15 - Soft Chemistry Synthesis of Oxides. Reference Module in Chemistry, Molecular Sciences and Chemical Engineering. Comprehensive Inorganic Chemistry II. 2nd.ed. From Elements to Applications. 2013.

[44] Tang W, Kanoh H, Ooi K. Lithium ion extraction from orthorhombic $LiMnO_2$ in ammonium peroxodisulfate solutions. J. Solid State Chem. 1999; 142(1):19-28.

[45] Gummow RJ, Liles DC, Thackeray MM. Lithium extraction from orthorhombic lithium manganese oxide and the phase transformation to spinel. Mat. Res. Bull. 1993; 28:1249-1256.

[46] Chitrakar R, Sakane K, Umeno A, Kasaishi Sh, Takagi N, Ooi K. Synthesis of orthorhombic $LiMnO_2$ by solid-phase reaction under steam atmosphere and a study of its heat and acid- treated phases. Journal of Solid State Chemistry. 2002; 169: 66-74.

[47] Ho YS, McKay G. Pseudo-second order model for sorption processes. Process Biochemistry. 1999; 34:451-465.

[48] Xiao J, Nie X, Sun S, Song X, Li P, Yu J. Lithium ion adsorption-desorption properties on spinel $Li_4Mn_5O_{12}$ and pH-dependent ion-exchange model. Adv. Powder Technol. 2015; 26:589-594.

[49] Xin X, Yongmei Ch, Pingyu W, Khaled G, Kaiying W, Ting H, Hertanto A, Maohong F. Extraction of lithium with functionalized lithium ion-sieves. Progress in Materials Science. 2016; 84:276-313.

[50] Hunter JC. Preparation of a New Crystal Form of Manganese Dioxide: λ-MnO_2. Journal of Solid State Chemistry. 1981; 3:142-147.

[51] Feng Q, Miyai Y, Kanoh H, Ooi K. Li^+ Extraction/Insertion with Spinel-Type Lithium Manganese Oxides. Characterization of Redox-Type and Ion-Exchange-Type Sites. Langmuir. 1992; 8:1861-1867.

[52] Buzanov GA. Fazovyye ravnovesiya s uchastiyem tverdykh rastvorov v sisteme Li-Mn-O. [Phase equilibria involving solid solutions in the Li-Mn-O system]. Moscow: Russion science academy. 2016. (in Russ.).

Crossref

creative commons

DOI: 10.31643/2025/6445.29
Metallurgy

Silicon Refining by Growing Crystallites in a Hypereutectic Melt of Aluminum with Silicon

Protopopov A.V., Protopopov M.A., Suleimenov E.A., *Altynbekov R.F.

M. Auezov South Kazakhstan University, Shymkent, Kazakhstan

** Corresponding author email: rustik2030@inbox.ru*

Received: *January 19, 2024*
Peer-reviewed: *March 18, 2024*
Accepted: *July 15, 2024*

ABSTRACT

Silicon is an essential chemical element that plays a very important role in life support on our planet. There is no single area of life on Earth where this most common chemical element is not present; its content is 27-30% of the mass of the Earth's crust. The most common form of its presence in the earth's crust is silicon dioxide, that is, silica. Silica is the main raw material source for semiconductor silicon for modern electrical engineering (production of diodes, transistors, photocells, and integrated circuits). Silicon is widely used in special materials science (alloying special steels, refining melts, and producing aluminum-silicon alloys (silumins). Reducing the cost of high-purity silicon can be achieved by reducing the temperature of the refining process of technical silicon. This scientific work examines the implementation of refining silicon in eutectic silicon melts with aluminum. Crystallization of silicon in hypereutectic melts below the liquidus temperature of the Si-Al phase equilibrium system occurs through the formation of silicon crystallization nuclei from clusters on the surface of the crystallizer - electrodes (rods) made of silicon with a temperature, which is below the temperature of the hypereutectic melt liquidus. The article describes methods for obtaining high-purity silicon and provides scientific justification for the implementation of such a task. The proposed method for producing high-purity silicon has so far been little studied and is of scientific and economic interest, since it can be carried out at relatively low temperatures, for example below 900°C. An important feature of eutectic melts is the stoichiometric content of components, which was the reason for the assumption of the molecular structure of eutectic melts. Eutectic molecules are, in our opinion, compounds of silicon and aluminum clusters.

Keywords: silicon, aluminum, cluster, crystallite, liquation, crystallization.

Information about authors:

Protopopov Anatoly Vsevolodovich — *Doctor of Technical Sciences, Professor, Head of the Laboratory "High-Temperature Synthesis of Composite Materials and Metallurgical Processes" of M. Auezov South Kazakhstan University, Tauke Khan Avenue 5, 160000, Shymkent, Kazakhstan. Email: awprotopopow@mail.ru*

Protopopov Maksim Anatolevich — *Researcher at the Laboratory «High-Temperature Synthesis of Composite Materials and Metallurgical Processes» of M. Auezov South Kazakhstan University, Tauke Khan Avenue 5, 160000, Shymkent, Kazakhstan. Email: promax80@gmail.com*

Suleimenov Erkinbek Ayataevich — *Candidate of technical sciences, Researcher at the Laboratory "High-Temperature Synthesis of Composite Materials and Metallurgical Processes" of M. Auezov South Kazakhstan University, Tauke Khan Avenue 5, 160000, Shymkent, Kazakhstan. Email: erkinbek.suleimenov@gmail.com*

Altynbekov Rustem Feliksovich — *Candidate of Technical Sciences, Associate Professor, Head of the Department of the Center for Scientific and Analytical Information of M. Auezov South Kazakhstan University, Tauke Khan Avenue 5, 160000, Shymkent, Kazakhstan. Email: rustik2030@inbox.ru*

Introduction

Silicon is the most important chemical element on our planet. There is not a single area of life on the Earth where this most common component is present, its content amounts to 27-30% of the mass of the Earth's crust [[1], [2], [3], [4]]. The most common form is silicon dioxide–silica. Silica is the main raw material source for semiconductor silicon for modern electrical engineering (production of diodes, transistors, photocells, and integrated circuits). Silicon is widely used in special materials science (alloying special steels, refining melts, and producing aluminum-silicon alloys (silumins). The growing need for high-purity silicon for photovoltaic energy converters, caused by the development of "Green Energy", served as the basis for the search and the development of effective technologies for refining metallurgical silicon to the level of "Solar" quality silicon, that is, with a Silicon content of 99.9999%. Without such a degree of purification of silicon from impurities, it is impossible to obtain

photovoltaic energy converters with a high efficiency for efficient solar batteries.

Silicon refining using a hypereutectic melt of aluminum and silicon is a process that is used to remove impurities and improve the quality of silicon, especially in the production of silicon single crystals for the semiconductor industry. Here's how it works:

1. Preparation of raw materials: First it is necessary to prepare the raw materials. This may be metal silicon, which contains impurities such as aluminum, iron, and other metals. A mixture of aluminum and silicon is also suitable.

2. Melting: A mixture of silicon and aluminum is heated to a temperature beyond the melting point of silicon. This ensures the formation of a hypereutectic liquid, which can interact with silicon, but not aluminum.

3. Separation: In a hypereutectic liquid, silicon dissolves while aluminum remains unchanged. This allows aluminum and other impurities to be removed from the silicon. The separation occurs due to differences in the solubility of aluminum and silicon in a given liquid.

4. Cooling and crystallization: After separation, the silicon begins to crystallize within the liquid. This can happen by slowly cooling the mixture. Silicon crystals can be produced as single crystals or polycrystals, depending on the process.

5. Silicon extraction and processing: The resulting silicon crystals are then removed from the melt and further processed and purified to improve their quality.

This process produces purer silicon suitable for semiconductors and other high-tech industries. It is important to note that it can be resource and energy-intensive, and its effectiveness depends on the exact conditions and process parameters.

Existing technologies and methods for purifying silicon from impurities, such as refining by blowing the silicon melt with oxygen, zone melting, electrolysis in molten salts, sublimation of silicon monoxide and its reduction with magnesium and others do not provide the required degree of purification from impurities, are characterized as environmentally unsafe and energy-intensive. The Czochralski Method has proven itself to be quite effective [[2], [3], [4], [5], [6], [7], [8], [9]]. This refining method, although very expensive in terms of production costs, is still considered the most common in the production of semiconductor silicon [[10], [11], [12], [13], [14], [15]].

Methods

The experiments were carried out according to the following technological scheme:

1. Preparation of a hypereutectic alloy of silicon with aluminum, implemented in the following sequence:

1.1 melting silicon Kr1 in an induction furnace with a protective atmosphere (Nitrogen or carbon dioxide).

1.2 aluminum of Al1 grade (electrical) was loaded into a silicon melt at a temperature of 1415-1450°C, its concentration was adjusted to 20% (mass). A melt was obtained in which, upon cooling, crystallization began with the formation of silicon clusters.

1.3 when immersing a rotating rod made of pure silicon heated to a melt temperature of 660-690°C into the melt, the rotation speed was selected experimentally and amounted to 5-10 min^{-1}.

The process of silicon crystallization on the crystallizers was monitored visually; the duration of the crystallizer's stay in the melt did not exceed 30 minutes.

2. Analysis of the elemental composition of the resulting refined silicon was carried out using the X-ray fluorescence method on a scanning electron microscope with an analyzer at the Research Regional Engineering Laboratory "Structural and Biochemical Materials" at M. Auezov South Kazakhstan University, equipment used: Spekord V-80 and Superprobe 733-SCX.

Research Results and Discussion

This work studied the possibility of refining silicon in eutectic melts using the features of liquation processes and the limited solubility of melt components in the crystallizing phases of the eutectic, under the conditions of the beginning of silicon crystallization in the eutectic melt. The Silicon–Aluminum system with eutectic (Al 88% + Si 12%) melting at 577°C was chosen as the base material, Fig.1, [9].

This process of obtaining high-purity silicon has not yet been well studied and is of scientific and economic interest, since it can be carried out at relatively low temperatures, for example below 900°C. An important feature of eutectic melts is the stoichiometric content of components, which was the reason for the assumption of the molecular structure of eutectic melts [16].

Eutectic molecules are, in our opinion, compounds of silicon and aluminum clusters. Clusters of these components can be imagined if consider the crystal structure of aluminum and silicon (Fig.2).

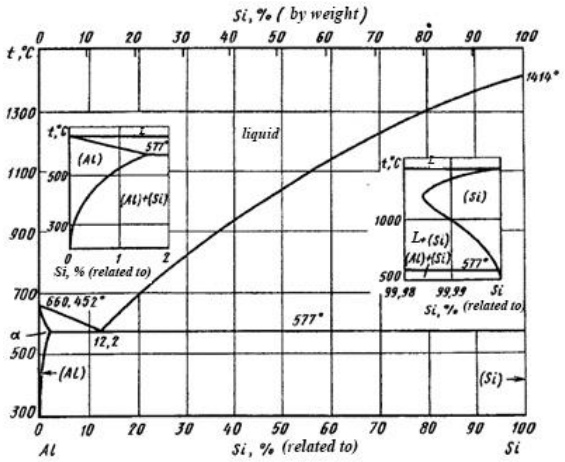

Figure 1 - Aluminum-silicon phase equilibrium diagram [9]

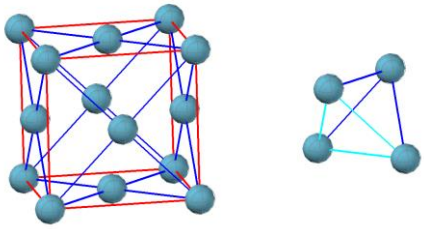

Crystal structure of aluminum
Atomic structure of cluster
a)

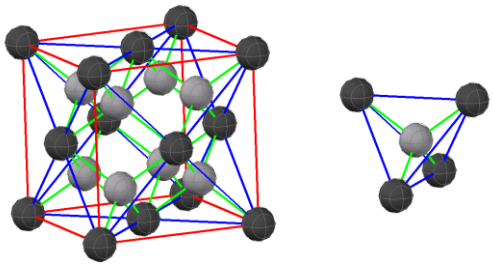

Crystal structure of silicon
Atomic structure of cluster
b)

Figure 2 - Crystal structure of aluminum and silicon atoms and atomic structure of clusters

Clusters in the melt are grouped into complex molecules according to the chemical composition of the eutectic 12.2% Si and 87.8% Al (mass per cent) [[16], [17], [18], [19]] (Fig.3).

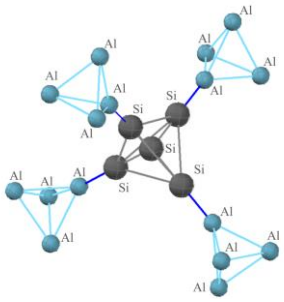

Figure 3 - Structure of a complex molecule of eutectic aluminum-silicon melt

This arrangement of the atomic eutectic melt structure ensures the density (specific gravity) of the eutectic melt close to the density of the crystallized eutectic alloy [[20], [21], [21], [22], [23], [24], [25]]. Figure 3 offers the reader the structure of the molecule of a eutectic aluminum-silicon melt. The main feature of the structure is that it consists of complex molecules of clusters of silicon atoms and clusters of aluminum atoms. The possibility of forming such complex molecules is explained by the geometric similarity of the clusters. The next reason for the formation of complexes is the almost identical density of the substance in the liquid and solid-crystalline states. The distinctive structure of the silicon cluster lies in the size of interatomic distances and the presence of the silicon atom with electronic bonds involved inside the cluster. This complicates the formation of crystallization nuclei and increases the stability of the liquid eutectic mixture of complex molecules and individual clusters of silicon and aluminum. Therefore, in eutectic melts of silicon and aluminum at temperatures below the liquidus temperature, clusters of silicon atoms are formed without admixtures of other atoms.

Figure 4 - Scheme of the atomic structure of a eutectic melt of silicon with aluminum (complex eutectic molecules and excess silicon clusters)

This is confirmed by the results of the scientific work of the authors, for example, at a temperature close to 900°C, crystallizing silicon has a purity of 99.99% (see an inset in the diagram in Fig. 1) [[16], [17], [20]].

By creating conditions for silicon crystallization, immersing crystallizer rods in the melt at a temperature 5-10°C below the liquidus temperature, we will ensure the deposition of silicon clusters on the surface of the silicon crystallizer. Silicon crystallization nuclei – silicon clusters in the eutectic melt provide a high rate of crystallization of high-purity polycrystalline silicon. If a crystallizer is used from a single crystal, it is possible to obtain monocrystalline silicon, but this is not a technically simple task and requires additional research. To regulate the rate of silicon crystallization, the surface temperature of the crystallizer is maintained within a specified range. Figure 5 shows a diagram of the refining installation and a photograph of a crystallizer with a crystallized layer of high-purity silicon. Complex molecules of silicon and aluminum clusters provide a high rate of crystallization; excess clusters in the hypereutectic melt crystallize on the surface of the crystallizer, maintaining a high degree of purity from harmful impurities.

For the continuity of the process, the melt is replenished with silicon clusters by dissolving the electrodes of the Aluminum – Silicon alloy and removing melts enriched with impurities from the refining zone. A flow process of hypereutectic melt through the crystallization zone of high-purity silicon is also provided. In this case, the secondary product can be used for casting parts from silumin. The main idea behind the new refining of silicon at temperatures below 900°C and above 5770°C will be widely used and useful for the production of products and alloys from silumin as an additional and efficient production of high-purity silicon.

Two options were tested: 1 – The process in a constantly renewed eutectic melt, that is, to grow high-frequency Silicon clusters on a crystallizer in a flow of always “new” eutectic melt. Growing crystalline silicon from a silumin melt – for a eutectic alloy of silicon with aluminum, ensures the filtration of impurities by the eutectic melt according to a mechanism similar to the process of zone melting [[9], [26]]. Impurities are pushed into the liquid phase, and the surface of the growing crystals on a rotating crystallizer is covered with clusters that form high-purity silicon crystallites. The basis for this process is the limited solubility of aluminum in silicon, which is confirmed by the authors [[16], [17], [20]]. Aluminum clusters act as a sorbent for impurities harmful to silicon. Movement of the surface of the crystallizing rod in the melt (rotation of the crystallizer rod) eliminates the accumulation of impurity atoms in the crystallization zone.

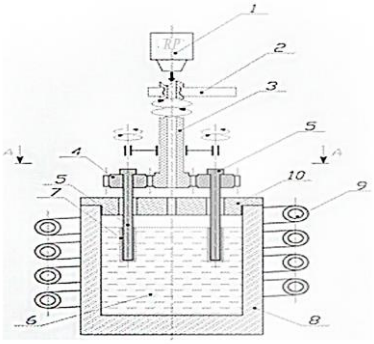

a)

b)

Figure 5 - Diagram of a laboratory refining installation

a) photograph of crystallizers with frozen refined silicon
b) 1 – radiation pyrometer; 2 – clutch with a manual drive lever; 3 – shaft gear with a through hole for transmitting rays of electromagnetic waves of light flux from the mirror of the melt bath to the radiation pyrometer; 4 – satellites (gears) for rotating the crystallizer rods; 5 – crystallizer rods; 6 – eutectic melt; 7 – frozen layer of refined silicon crystals; 8 – graphite crucible; 9 – inductor

The problem of removing accumulating impurities in the eutectic melt from the crystallization zone of refined silicon in crystallizers to ensure the minimum permissible concentration of impurities in the eutectic melt requires additional research and refinement of the technology [[27], [28], [29], [30], [31], [32], [33]].

The research results are shown in Table 1. The results show a significant increase in the degree of purity of the resulting polycrystalline silicon: from the original 97-98% Si to 99.95-99.99% Si. The degree of purity – the content of impurities in the polycrystalline silicon obtained after refining – is significantly influenced by:

- temperature range of the crystallization process on the crystallizer rod (Fig.4),

- rotation speed of the crystallizer rod, which ensures the renewal of the melt at the boundary between the crystallizer and the melt, excluding an increase in the concentration of impurities pushed

aside by growing crystallization centres into the liquid phase – eutectic melt.

Replacing the composition of the crystallizer bath and changing the fuse – the silicon rod coated with frozen high-purity silicon crystals – are very important factors influencing the quality of refining. These issues require careful study and research funds.

Table 1 - Elemental composition of metallurgical silicon and the resulting high-purity silicon by refining by crystallization from the eutectic melt

Sample name	Impurity content, % e				Note
	Ca	**Fe**	**P**	**B**	**Si**
MG-Si	0.016	0.28	0.0021	0.0030	99.69
Refining melt (original)	0.041	0.073	0.0007	0.0017	Melt: Si 20-30%, base: Al
Refining silicon	0.0008	Not detected	0.0003	0.0009	99.998 % Si
Refining melt (spent)	0.54	0.455	0.0615	0.0080	1.578% impurity

Conclusions

Conducted studies have shown the promise of using eutectic melts of silicon with aluminum as efficient in energy saving and relatively low process temperatures – below 900°C.

The possibility of using a similar process for growing silicon single crystals using a method similar to the Czochralski method cannot be ruled out, but this requires extensive research and funds to carry it out.

Research in this work revealed the need to study the refining ability of other eutectics with silicon and to create a technological process for refining silicon to silicon of “solar” quality using the selectivity of melts to absorb harmful impurities in high-purity silicon.

Acknowledgements. We express our gratitude and appreciation to the Research Regional Engineering Laboratory “Structural and Biochemical Materials” at M. Auezov South Kazakhstan University, where the analysis of the elemental composition of the resulting refined silicon was carried out using the X-ray fluorescence method on a scanning electron microscope with an analyzer, equipment used: Spekord V-80 and Superprobe 733-SCX.

***CRediT author statement*: A. Protopopov:** Conceptualization, Methodology, Software, Data curation, Writing-Original draft preparation. **M. Protopopov:** Visualization, Investigation. **Y. Suleimenov:** Supervision. **R. Altynbekov:** Software, Validation, Writing- Reviewing and Editing.

Cite this article as: Protopopov AV, Protopopov MA, Suleimenov EA, Altynbekov RF. Silicon refining by growing crystallites in a hypereutectic melt of aluminum with silicon. Kompleksnoe Ispolzovanie Mineralnogo Syra = Complex Use of Mineral Resources. 2025; 334(3):70-77. https://doi.org/10.31643/2025/6445.29

Алюминий мен кремнийдің эвтектикадан кейінгі балқымасында кристаллиттерді өсіру арқылы кремнийді тазарту

Протопопов А.В., Протопопов М.А., Сүлейменов Е.А., Алтынбеков Р.Ф.

М.Әуезов атындағы Оңтүстік Қазақстан университеті, Шымкент, Қазақстан

Мақала келді: *19 қаңтар 2024*
Сараптамадан өтті: *18 наурыз 2024*
Қабылданды: *15 шілде 2024*

ТҮЙІНДЕМЕ

Кремний-біздің планетамыздағы тіршілікті қамтамасыз етуде өте маңызды рөл атқаратын маңызды химиялық элемент. Бұл ең көп таралған химиялық элемент жердің барлық аймағында бар, оның мөлшері жер қыртысының массасының 27-30% құрайды. Оның жер қыртысындағы ең көп тараған қосылысы - кремний диоксиді, яғни кремнезем. Кремний диоксиді қазіргі электротехника үшін жартылай өткізгіш кремнийді алудың негізгі шикізат көзі болып табылады (диодтар, транзисторлар, фотоэлементтер, интегралдық схемалар өндірісі). Кремний арнайы материалтану саласында кеңінен қолданылады (арнайы болаттарды легирлеу, балқымаларды тазарту, алюминий-кремний қорытпаларын (силуминдер) алу). Өте таза кремнийдің құнын төмендетуге техникалық кремнийді тазарту

	процесінің температурасын төмендету арқылы қол жеткізуге болады. Бұл ғылыми жұмыста кремнийдің алюминиймен эвтектикалық балқымаларында кремнийді тазарту қарастырылады. Si-Al фазалық тепе-теңдік жүйесінің ликвидус температурасынан төмен эвтектикалық балқымалардағы кремнийдің кристалдануы кристаллизатордың бетіндегі кластерлерден кремнийдің кристалдану эмбриондарының - кремнийдің электродтарының (шыбықтарының) түзілуі арқылы жүреді. Мақалада өте таза кремний алу әдістері сипатталған және осындай әдістерді жүзеге асырудың ғылыми негіздемелері келтірілген. Өте таза кремнийді алудың ұсынылған әдісі әлі аз зерттелген және ғылыми және экономикалық қызығушылық тудырады, өйткені оны салыстырмалы түрде төмен температурада, мысалы, 900оС-тан төмен температурада жүзеге асыруға болады. Эвтектикалық балқымалардың маңызды белгісі – олардың молекулалық құрылымын болжауға себеп болған компоненттердің стехиометриялық құрамы. Эвтектикалық молекулалар, біздің ойымызша, кремний мен алюминий кластерлерінің қосылыстары.
	Түйін сөздер: кремний, алюминий, кластер, кристаллит, ликвация, кристалдану.
Протопопов Анатолий Всеволодович	***Авторлар туралы ақпарат:*** *Техника ғылымдарының докторы, профессор, М.Әуезов атындағы Оңтүстік Қазақстан университетінің «Композиттік материалдар мен металлургиялық процестердің жоғары температуралық синтезі» зертханасының меңгерушісі, Тәуке хан даңғылы, 5, 160000, Шымкент, Қазақстан. Email: awprotopopow@mail.ru*
Протопопов Максим Анатольевич	*М.Әуезов атындағы Оңтүстік Қазақстан университетінің «Композиттік материалдар мен металлургиялық процестердің жоғары температуралық синтезі» зертханасының ғылыми қызметкері, Тәуке хан даңғылы 5, 160000, Шымкент, Қазақстан. Email: promax80@gmail.com*
Сүлейменов Еркінбек Аятайұлы	*Техника ғылымдарының кандидаты, М.Әуезов атындағы Оңтүстік Қазақстан университетінің «Композиттік материалдар мен металлургиялық процестердің жоғары температуралық синтезі» зертханасының ғылыми қызметкері, Тәуке хан даңғылы 5, 160000, Шымкент, Қазақстан. Email: erkinbek.suleimenov@gmail.com*
Алтынбеков Рүстем Феликсұлы	*Т.ғ.к., доцент, М.Әуезов атындағы Оңтүстік Қазақстан университетінің Ғылыми-аналитикалық ақпарат орталығының бөлім меңгерушісі, Тәуке хан даңғылы, 5, 160000, Шымкент, Қазақстан. Email: rustik2030@ inbox.ru*

Рафинирование кремния выращиванием кристаллитов в заэвтектическом расплаве алюминия с кремнием

Протопопов А.В., Протопопов М.А., Сулейменов Е.А., Алтынбеков Р.Ф.

Южно-Казахстанский университет имени М. Ауэзова, Шымкент, Казахстан

Поступила: *19 января 2024*
Рецензирование: *18 марта 2024*
Принята в печать: *15 июля 2024*

АННОТАЦИЯ

Кремний – важнейший химический элемент, играющий очень важную роль для жизнеобеспечения на нашей планете. Нет ни одной области жизни на Земле, где бы ни присутствовал этот, самый распространенный химический элемент, его содержание составляет 27-30% от массы земной коры. Наиболее распространенная форма его присутствия в земной коре – это диоксид кремния, то есть кремнезем. Кремнезем — это основной сырьевой источник получения полупроводникового кремния для современной электротехники (изготовление диодов, транзисторов, фотоэлементов, интегральных схем). Широкое применение кремний получил в специальном материаловедении (легирование специальных сталей, рафинирование расплавов, получение алюминий-кремниевых сплавов (силуминов). Снижение себестоимости высокочистого кремния может быть обеспечено снижением температур процесса рафинирования технического кремния. В данной научной работе рассматривается осуществление рафинирования кремния в эвтектических расплавах кремния с алюминием. Кристаллизация кремния в заэвтектических расплавах ниже температуры ликвидус системы фазового равновесия Si-Al происходит формированием зародышей кристаллизации кремния из кластеров на поверхности кристаллизатора - электродов (стержней) из кремния с температурой ниже температуры ликвидус за эвтектическим расплавом. В статье расписаны способы получения кремния высокочистого и приводятся научные обоснования реализации такой задачи. Предлагаемый метод получения высокочистого кремния пока мало изучен и представляет научный и экономический интерес, так как может осуществляться при относительно низких температурах, например ниже 900оС. Важным признаком эвтектических расплавов является стехиометрическое содержание компонентов, что послужило причиной для предположения о молекулярном строении эвтектических расплавов. Молекулы эвтектики представляют собой, по нашему мнению, соединения кластеров кремния и алюминия.

Ключевые слова: кремний, алюминий, кластер, кристаллит, ликвация, кристаллизация.

Протопопов Анатолий Всеволодович	***Информация об авторах:*** *Доктор технических наук, профессор, заведующий лабораторией «Высокотемпературный синтез композиционных материалов и металлургические процессы» Южно-Казахстанского университета имени М. Ауэзова, 160000, пр-т Тауке хана, 5, Шымкент, Казахстан. Email: awprotopopow@mail .ru*
Протопопов Максим Анатольевич	*Научный сотрудник лаборатории «Высокотемпературный синтез композиционных материалов и металлургические процессы» Южно-Казахстанского университета им. М. Ауэзова, пр-т Тауке хана, 5, 160000, Шымкент, Казахстан. Email: promax80@gmail.com*
Сулейменов Эркинбек Аятаевич	*К.т.н., научный сотрудник лаборатории «Высокотемпературный синтез композиционных материалов и металлургические процессы» Южно-Казахстанского университета им. М. Ауэзова, пр-т Тауке хана 5, 160000, Шымкент, Казахстан. Email: erkinbek.suleimenov@gmail.com*
Алтынбеков Рустем Феликсович	*Кандидат технических наук, доцент, заведующий отделом Центра научно-аналитической информации Южно-Казахстанского университета имени М. Ауэзова, пр-т Тауке хана, 5, 160000, Шымкент, Казахстан. Email: rustik2030@inbox.ru*

References

[1] Lyakishev N P. Diagrammy sostoyaniya dvoynykh metallicheskikh sistem: Spravochnik [State diagrams of binary metallic systems: Handbook]. V 3-kh t. Moskva, Mashinostroenie [In 3 volumes. Moscow, Mechanical Engineering]. 1996, 996. (In Russ.).

[2] He Q, Wen J, Yang G, Xu F, Xu M, Chen Z. Impurity Aluminum Removal in Industrial Silicon by CaO-SiO2-CaF2 Slagging Refining. Silicon. 2023; 15:5445-5453. http://dx.doi.org/10.1007/s12633-023-02453-z

[3] Zhang ZH, Bian XF, Wang Yajun, Liu Xiangfa Refinement and thermal analysis of hypereutectic Al-25%Si alloy. Transactions of Nonferrous Metals Society of China. 2001; 11:374-377.

[4] Piątkowski J. Influence of Overheating Temperature on the Shape of Primary Silicon Crystals in Hypereutectic Al-Si Cast Alloys. Solid State Phenomena. 2013; 203-204:417-422. http://dx.doi.org/10.4028/www.scientific.net/ssp.203-204.417

[5] Eremin VP. Rafinirovanie tekhnicheskogo kremniya. Materialy soveshchaniya Si-2004 [Refining of technical silicon. Materials of the meeting SI-2004]. Irkutsk: Publishing House of the Institute of Geochemistry SB RAS. 2004, 27-34. (In Russ.).

[6] Cao J, Yang D, Wu J, Gu H, Cai X, Zeng Y. Study on Oxidization and Mass Transfer of Al from Si-Al Melt Using Top Oxygen Blowing Refining. Silicon. 2022; 14:9805-9812. http://dx.doi.org/10.1007/s12633-022-01672-0

[7] Nemchinova NV. Povedenie primesnykh elementov pri proizvodstve i rafinirovanii kremniya [Behavior of impurity elements during the production and refining of silicon]. Monograph. M.: Publishing House Academy of Natural Sciences. 2008, 237. (In Russ.).

[8] Calvo-Dahlborg M, Popel PS, Kramer MJ, Besser M, Morris JR, Dahlborg U. Superheat-dependent microstructure of molten Al–Si alloys of different compositions studied by small angle neutron scattering. Journal of Alloys and Compounds. 2013; 550:9-22. http://dx.doi.org/10.1016/j.jallcom.2012.09.086

[9] Bührig-Polaczek A, Michaeli W, Spur G. Handbuch Urformen. 2013. http://dx.doi.org/10.3139/9783446434066

[10] Gribov BG, Zinov'ev KV. Poluchenie vysokochistogo kremniya dlya solnechnykh elementov [Obtaining high-purity silicon for solar cells]. Inorganic, material. 2002; 39(7):775-785. (In Russ.).

[11] Pat.1857412 JP. Tokumaru Sh, Okazawa K, Kondo J, Okajima M. Silicon refining method. 2007.

[12] Pat. 2648436 RU. Andreev SP, Udalov YuP, Lavrov BA, Lavrov NN, Serzhanov GM. Sposob polucheniya poroshka kremniya vysokoi chistoty iz smesi dioksida kremniya i alyuminiya [A method for producing high-purity silicon powder from a mixture of silicon dioxide and aluminum]. 2018. (In Russ.).

[13] Pat. 2237616 RU. Karabanov SM, Trunin EB, Prikhod'ko VV. Sposob polucheniya kremniya solnechnogo kachestva [Method for producing solar grade silicon]. 2004. (In Russ.).

[14] Pat. 2159213 RU. Abdyukhanov IM, Abdyukhanov MA, Kuz'min YuA, Merkushkin VM. Sposob ochistki kremniya i ustroistvo dlya ego osushchestvleniya [Method for cleaning silicon and device for its implementation]. 2000. (In Russ.).

[15] Nepomnyashchikh A I. Kremnii dlya solnechnoi energetiki [Silicon for solar energy]. Izv. Tomsk Polytechnic University. 2000; 303(2):175-190. (In Russ.).

[16] Czochralski J. Ein neues Verfahren zur Messung der Kristallisationsgeschwindigkeit der Metalle. Zeitschrift für Physikalische Chemie. 1918; 92U(1):219-221. http://dx.doi.org/10.1515/zpch-1918-9212

[17] Ashuiko VA. Khimiya kompleksnykh soedinenii: kurs lektsii [Chemistry of complex compounds: a course of lectures]. Minsk: BGTU. 2011, 130. (In Russ.).

[18] Brodova IG, Popel' PS, Esin VO. Morfologicheskie osobennosti struktury i svoistv zaevtekticheskogo silumina. [Morphological features of the structure and properties of hypereutectic silumin]. Fizika metallov i metallovedenie [Physics of metals and metallurgy]. 1988; 65(4):1149-1154. (In Russ.).

[19] Marukovich EI, Stetsenko VYu, Stetsenko AV. Sovremennoye sostoyaniye teorii kristallizatsii metallicheskikh rasplavov [Current state of the theory of crystallization of metal melts]. Lit'ye i metallurgiya [Casting and metallurgy]. 2022; 12;(1):19-24. (In Russ.). http://dx.doi.org/10.21122/1683-6065-2022-1-19-24

[20] Bolshakov VI, Vorobiev VM, Krivusha LS, Tyuterev IA, Rott NA. O klasternoi modeli metallicheskikh rasplavov [On the cluster model of metal melts]. Vestnik Pridneprovskoi gosudarstvennoi akademii stroitel'stva i arkhitektury [Bulletin of the Dnieper State Academy of Construction and Architecture]. 2008; 5:125-137. (In Russ.).

[21] Filippov E.S. O vozmozhnom mekhanizme i posledovatel'nosti vozniknoveniya strukturnykh prevrashchenii v zhidkikh

splavakh, gallii i indii [On the possible mechanism and sequence of occurrence of structural transformations in liquid melts, gallium and India]. Izvestiya Vysshikh uchebnykh zavedenii. Chernaya metallurgiya [News of Higher Educational Institutions. Ferrous metallurgy]. 1973; 9:124-129. (In Russ.).

[22] Filippov E.S. Teoriya zhidkikh metallov, osnovannaya na predstavlenii sfer vzaimodeistviya [The theory of liquid metals based on the representation of the sphere of interaction]. Izvestiya Vysshikh uchebnykh zavedenii. Chernaya metallurgiya [News of Higher Educational Institutions. Ferrous metallurgy]. 1974; 7:101-110. (In Russ.).

[23] Anbu G, Nagarajan SG, Aravindan G, Srinivasan M, Ramasamy P. Influence of Additional Insulation Block on Melt-Crystal Interface Shape in Directional Solidification System for Growing High Quality mc-Silicon Ingot: a Simulation Investigation. Silicon. 2021; 13:1713–1722. http://dx.doi.org/10.1007/s12633-020-00572-5

[24] Presnyakov AA, Degtyareva AS, Aubakirova RK, Zhumartbaeva TV. Metallicheskie rasplavy, ikh zatverdevanie i kristallizatsiya [Metal melts, their solidification and crystallization]. Almaty: Gylym. 1994, 208. (In Russ.).

[25] Shakhnazarov KYu. Priznaki promezhutochnykh faz v sistemakh Al-Si, Fe-C i Al-Cu [Signs of intermediate phases in Al-Si, Fe-C and Al-Cu systems]. Bulletin of MSTU named after G.I. Nosova. 2016; 14(3):72-77. (In Russ.).

[26] Presnyakov AA, Degtyareva AS, Aubakirova RK, Zhumartbaeva TV. Metallicheskie rasplavy, ikh zatverdevanie i kristallizatsiya [Metal melts, their solidification and crystallization]. Almaty: Gylym. 1994, 208. (In Russ.).

[27] Petrov SC, Prigunova AG, Prigunov SV. Struktura zaevtekticheskikh siluminov pri modifitsirovanii rasplavov elektricheskim tokom [Structure of hypereutectic silumins during modification of melts by electric current]. Scientific information magazine MITOM. 2007; 1:43-52. (In Russ.).

[28] Ershov GS, Chernyakov VA. Stroenie i svoistva zhidkikh i tverdykh metallov [Structure and properties of liquid and solid metals]. Moskva: Metallurgiya. 1978, 248. (In Russ.).

[29] Voronkov VV. Aggregation of Point Defects in Silicon Crystals Growing from the Melt. Growth of Crystals. 1992; 18:157-167. http://dx.doi.org/10.1007/978-1-4615-3268-2_14

[30] Velyukhanov VP, Arkharov VI. Fizika metallov i metallovedenie [Physics of metals and metallurgy]. 1972; 33(2):303-307. (In Russ.).

[31] Prigunova AG, Mazur VI, Taran Yu N. Issledovanie struktury zhidkikh splavov Al-Si [Study of the structure of liquid Al-Si]. Zaevtekticheskie rasplavy. Metallofizika [Hypereutectic melts. Metal physics]. 1983; 5(1):88-94. (In Russ.).

[32] Spur G, Michaeli W, Bührig-Polaczek A. Handbuch Urformen. 2014. http://dx.doi.org/10.1007/978-3-446-43406-6

[33] Degtyareva AS, Dzhanysbaeva TA, Aubakirov EG, Khafizov EB, Khodareva TA. Strukturnye urovni metallicheskikh rasplavov [Structural levels of metal melts]. Tsvetnye metally [Non-ferrous metals]. 2006; 1:83-87. (In Russ.).

[34] Dahlborg U, Kramer M.J, Besser M, Morris JR, Calvo-Dahlborg M. Structure of molten Al and eutectic Al–Si alloy studied by neutron diffraction. Journal of Non-Crystalline Solids. 2013; 361:63-69. http://dx.doi.org/10.1016/j.jnoncrysol.2012.10.027

Crossref
DOI: 10.31643/2025/6445.30
Metallurgy

Technology for extraction of Pb, Cu, Zn from a feed based on lead cake from leached dust generated by reduction-oxidation blowing of melt

[1]Dosmukhamedov N.K., [2]Zholdasbay E.E., [2*]Argyn A.A., [2]Icheva Yu.B., [1]Klyshbekova Zh.E.

[1] Satbayev University, Almaty, Kazakhstan
[2] O.A. Baikonurov Zhezkazgan University, Zhezkazgan, Kazakhstan

** Corresponding author email: aidarargyn@gmail.com*

Received: *May 21, 2024*
Peer-reviewed: *June 25, 2024*
Accepted: *July 16, 2024*

ABSTRACT

The paper presents the theoretical basis and results of processing a mixture of complex types and compositions, based on lead cake, obtained after the preliminary removal of arsenic from dust and its subsequent leaching with sulfuric acid. The main goal of the technology is to involve the processing of substandard intermediate products of lead production together with lead cake and the selective extraction of non-ferrous metals into commercial products: copper into matte; lead - into rough lead: zinc - into slag. Choice of the composition of the feed charge was carried out taking into account the volumes obtained in production and is represented by the following structure, %: lead cake - 50; copper-lead matte – 40; quartz flux – 10. It has been established that the best results, ensuring high complex extraction of copper, lead, zinc and arsenic into the targeted smelting products, are achieved with a consumption of natural gas 1.4 times higher than its consumption from the stoichiometric required quantity (SRQ) for the reduction of lead compounds to metal lead. The optimal time for blowing the melt with natural gas is 15 minutes. The optimal oxygen consumption when blowing the intermediate matte obtained after the first stage was 1.1 times higher than its stoichiometric required amount (SRQ) for the oxidation of zinc and iron sulfide with their further transfer in the form of oxides to slag. The duration of matte blowing is 10 minutes. With the optimal established parameters, high technological indicators of the technology were achieved: extraction of lead into rough lead - 98.6%; copper in matte – 98.5%; zinc in slag – 94.1%.

Keywords: lead cake, feed charge, intermediate products, reduction blowing, oxidation blowing, copper, lead, zinc, extraction.

Information about authors:

Dosmukhamedov Nurlan Kalievich — *Candidate of Technical Sciences, Professor, Satbayev University, 050013, Almaty, 22 Satbayev St., Kazakhstan. Email: nurdos@bk.ru*

Zoldasbay Erzhan Esenbaiuly — *PhD, O.A. Baikonurov Zhezkazgan University, 100600, Zhezkazgan, 1b Alashahan st., Kazakhstan. Email: zhte@mail.ru*

Argyn Aidar Abdilmalikuly — *PhD, O.A. Baikonurov Zhezkazgan University, 100600, Zhezkazgan, 1b Alashahan st., Kazakhstan. Email: aidarargyn@gmail.com*

Icheva Yulianna Borisovna — *Candidate of Technical Sciences, O.A. Baikonurov Zhezkazgan University, 100600, Zhezkazgan, 1b Alashahan St., Kazakhstan.*

Klyshbekova Zhanar Erikovna — *Master of Sciences, Satbayev University, 050013, Almaty, 22 Satpayev St., Kazakhstan. Email: galamat3196@gmail.com*

Introduction

The dominant linear model in the production of non-ferrous metals from primary low-quality sulfide raw materials, although it no longer meets modern requirements in terms of environmental safety, nevertheless continues to function at its usual pace. Today it is no longer a secret to anyone that the pyrometallurgical production of copper, lead and copper, using technologies of the last century, is accompanied not only by low technological indicators but also by increasing volumes of substandard intermediate products and technogenic waste produced along the way. Finding rational, efficient technologies for their processing has no particular interest to manufacturers of basic products. The difficulty of processing this kind of raw material lies in the increased content of toxic arsenic in them, the presence of which determines the critical level of their impact on the environment and inhibits their further processing [[1], [2], [3], [4]].

Currently, the growth of substandard intermediate products is the main problem for non-ferrous metallurgy enterprises. Attempts to process them using existing technologies led to a decrease in technological, economic and environmental indicators of production. As a result, the compositions of technogenic waste of industry have

become greatly complicated, which has led to their significant accumulation, with all the ensuing negative social, economic and environmental consequences. The current situation at non-ferrous metallurgy enterprises requires a radical approach to solving these problems.

From this perspective, the circular economy model has a great interest, widely spread in the world economy, within the framework of the Zero concept of waste [5]. This approach is not new. In the practice of the economy of the Soviet Union, special attention was previously paid to the development of so-called “waste-free technologies”, which essentially solved the same problems as the circular economy model proposed in the West, where solving the problems of integrated use of raw materials and preserving a clean environment was at the forefront [6]. In our opinion, regardless of the nature of the use of these solutions to maintain resource efficiency and environmental safety, whether in the West or in the economy of the post-Soviet countries, these tasks today should determine the main trend in the development of the economy, regardless of its affiliation.

Materials characterized by a complex chemical composition include fine dust from copper and lead production. Their peculiarity is their multicomponent nature, %: 35-50 Pb; 5-7 Cu; 6-9 Zn; 4-6 Fe; 5-13 As; others. Minor deviations in the furnace operating conditions, the chemical composition of the concentrate and other factors from the specified parameters can significantly change the quantitative ratio of metals in the dust towards a deterioration in its composition [[7], [8], [9], [10], [11], [12]].

The value of dust is enhanced by the fact that, along with their high content of heavy non-ferrous metals and arsenic, they concentrate a significant amount of dual-use metals (Re, Os, Se, Sc, etc.), and could be used well as an additional source for their extraction. However, the high content of arsenic in dust (5-13%) hinders the development of new highly efficient technologies. A very simple solution for enterprises was to sell them to third parties, which, using not entirely rational technologies, in the pursuit of profit, extracting one or two main base metals, do not ensure the comprehensive extraction of metals that are strategic for the economy of Kazakhstan with high added value. This approach, where dust is one of the key sources for the production of Re, Sc, Os and other metals, does not seem entirely rational.

The material composition of dust depends mainly on the composition of the feedstock and technological smelting conditions. The unique polymetallic nature of the ores and concentrates of Kazakhstan, and the multi-component substandard intermediate products and technogenic wastes obtained during their processing, containing a wide range of valuable metals, inherently require the development of new, separate technology for their processing to ensure the complexity of the extraction of valuable metals.

There are several works in the scientific literature devoted to dust processing, each of which is distinguished by its originality in solving the problem of arsenic removal [[13], [14], [15], [16], [17], [18]].

When organizing a technology for processing dust using a hydrometallurgical method, it seems that the most acceptable way to remove arsenic from dust is at the initial stage of the technology. This will improve the technological performance of the processes that form the basis of the overall technology and reduce the consumption of reagents spent on the removal and disposal of arsenic. At the same time, high greening of the technology is ensured due to a significant reduction in the ecological influence on the environment and human health caused by arsenic.

The purpose of this article is the extraction of lead, copper and zinc from a feed composed of lead cake from the leaching of dust obtained after preliminary removal of arsenic by reduction roasting with natural gas.

A distinctive feature of the research is the development of a new technology for the complex extraction of lead, copper and zinc into targeted products from a charge composed of various substandard materials based on arsenic-free lead cake by sequentially blowing the melt with natural gas, then with oxygen. The minimum arsenic content in lead cake eliminates the need for complex, time-consuming sequential blowing of the melt to sublimate arsenic. This ensures maximum sublimation of arsenic into dust in the form of As2O3, complete oxidation of zinc and iron sulfides with subsequent conversion of their oxides into slag and the formation of matte with a high copper content (more than 50% Cu), which is easily reduced to blister copper.

Materials and research methods

Cake with the addition of converter slag, copper-lead matte and copper slips from lead production was used as the core of the complex feed charge. To calculate the rational composition of the charge, the results of comprehensive studies of the material composition of the feed materials and the forms of metals in them were used, obtained using an inductively coupled plasma mass spectrometer Agilent 7700 Series ICP-MS (USA), electron probe microanalyzer Superprobe 733 from JEOL (Japan) [[2], [8], [19]].

Mineralogical studies aimed at studying the surface structure of solid samples were carried out using a microscope Neofot (Carl Zeiss AG, Germany). Micro- and morphological analysis of the surface of individual samples was carried out using a JEOL scanning electron microscope EDS System (USA).

The compositions of the initial products forming the feed charge are given in Table 1.

The main methodological principle of the technology is a thermodynamic approach to describe the reduction-oxidation smelting of a balanced charge: lead cake and substandard sulfide intermediates (Table 1). The key core of the methodology is Big Data technology, which includes an iterative approach to calculating the quantitative ratios of the forming liquid phases: slag, matte and rough lead, depending on the composition and amount of source materials. The composition of the charge from various materials was carried out according to the sulfur content in the initial products, taking into account the production of matte with a high copper content. To obtain slag of optimal composition, ensuring minimal solubility of lead and copper in it, the required calculated amount of quartz flux was added to the charge [20].

Theoretical basis of technology

The interaction of charge components with natural gas and oxygen is based on a thermodynamic approach, including the establishment of quantitative ratios of the initial and resulting smelting products, the formation of liquid phases, etc.

By sequentially blowing the melt with natural gas to produce an intermediate matte, and then blowing it with oxygen, favourable conditions are created for the occurrence of basic physical and chemical processes: the enlargement of small particles of lead dissolved in the form of metal with the precipitation of lead in the form of rough lead; reduction of lead sulfide to metallic lead; destruction of intermetallic compounds of copper and iron (Me_xAs_y, Me_xSb_y) with maximum sublimation of arsenic and antimony into dust; oxidation of iron and zinc sulfides in the matte to their oxides, converting the latter into slag. The presence of residual lead sulfide in the melt inhibits the reduction of copper sulfide and other metals. This ensures the high quality of the resulting rough lead in terms of impurity content.

Considering that the main matrix of the charge is lead cake, consisting of lead, zinc and copper sulfates when developing the technology, we proceeded from the condition of ensuring their complete recovery by blowing the melt with natural gas at high temperatures (1200 °C).

During reductive blowing of the melt with natural gas, favourable conditions are created for the reduction of sulfates according to the reaction:

$$MeSO_4+CH_4 = MeO+CO_2\uparrow + SO_2\uparrow + H_2O\uparrow, \quad Me – Pb, Cu, Zn \qquad (1)$$

The resulting metal oxides interact with the components of sulfide materials (copper-lead matte, copper slips) according to reactions (2), and (3) to form liquid phases of rough lead and matte:

$$2PbO + PbS = 3Pb + SO_2\uparrow, \qquad (2)$$

$$Cu_2O + FeS = Cu_2S + FeO, \qquad (3)$$

Iron and zinc oxides interact with the flux and form a slag phase.

Metallic lead formed by reaction (2) will settle in the bottom phase. The main contribution to the

Table 1 - Chemical composition of initial products

Product Name	Cu	Pb	Zn	As	Sb	Fe	S	O	SiO_2	Others
Lead cake	0.41	87.53	0.11	0.05		0.58	0.78	8.24		2.3
Copper-lead matte	20.85	19.5	11.4	1.1	0.56	16.7	11.1	3.81		14.98
Converter slag	3.83	33.5	4.54	2.3	0.94	15.0		10.3	21.66	7.93
Copper slips	29.0	36.0	4.00	3.87	1.4		8.77			16.96

formation of metallic lead and the formation of the bottom phase will be made by reaction (2), the high rates of which are ensured by intense bubbling of the melt. Due to the absence of arsenic in lead cake, the need for long-term blowing of the melt with natural gas and oxygen is eliminated, which significantly increases the productivity of the technology as a whole.

Experimental part

For laboratory studies, the composition of the charge based on lead cake was calculated and prepared, %: lead cake – 50; copper-lead matte – 40; quartz flux – 10.

The choice and justification of the composition of the charge were carried out based on solving the problem of maximum involvement in the processing of substandard materials from lead production, taking into account the volumes obtained in production and the organization of their independent, separate smelting for high complex selective extraction of copper, lead and zinc from them.

The average composition of the charge was calculated taking into account the rational compositions of each product and the form of metals in them, is given in Table 2.

Experiments of reduction-oxidation melting of the charge were carried out at different flow rates of natural gas, oxygen and melt blowing time.

Installation diagram and experimental procedure. The experiments were carried out on a laboratory setup, the diagram of which is shown in Fig. 1.

It was not possible to organize continuous production of rough lead in laboratory conditions with sequential blowing of the melt with natural gas and oxygen, so the experiments were carried out in two stages.

Experimental methodology. All experiments were carried out at a constant temperature of 1200 °C. Initial sample – 200 g.

After thorough mixing, the initial mixture was loaded into an alundum crucible (9), which was placed in a quartz reactor (7) located in a tubular furnace (8). The reactor was plugged with a plug (6), cooled with water and equipped with two holes for the input and output of gases. The exhaust gases from the furnace entered the Drexel vessel with water (10). The temperature in the furnace was set and controlled by an automatic control and measuring unit (11). After the complete melting of the charge, the melt was blown through the tube (5), first with natural gas, then with oxygen, which was supplied from cylinders (1), and (2), respectively. The sequential supply of gases was carried out by a 2-way valve (4). The gas flow was regulated by rotameters (3).

Table 2 - Rational composition of the average charge

Compounds	Cu	Pb	Zn	Fe	S	As	Sb	SiO_2	O_2	Others	**Total:**
Cu_2S	2.54				0.64						**3.18**
$CuSO_4$	0.21				0.10				0.21		**0.51**
Cu	5.80										**5.80**
PbS		2.59			0.40						**2.99**
$PbSO_4$		0.60			0.09				0.19		**0.88**
PbO		43.23							3.34		**46.57**
Pb		5.21									**5.21**
ZnS			4.56		2.24						**6.80**
$ZnSO_4$			0.06		0.03				0.05		**0.14**
As_2O_5						0.03			0.01		**0.04**
FeS				2.03	1.16						**3.19**
$FeSO_4$				0.29		0.17			0.33		**0.79**
Fe_3O_4				4.00					1.52		**5.52**
Fe_3As_2				0.49		0.44					**0.93**
Fe_3Sb_2				0.16			0.22				**0.38**
SiO_2								7.48			**7.48**
Others										9.60	**9.60**
Total:	**8.55**	**51.63**	**4.61**	**6.97**	**4.66**	**0.63**	**0.22**	**7.48**	**5.65**	**9.60**	**100.0**

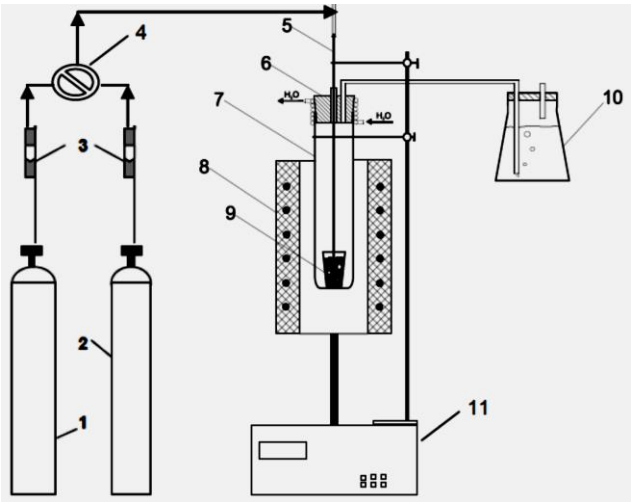

Figure 1 – Installation diagram for studying the distribution of Cu, Pb, Zn, and As during reduction-oxidation melting of the charge: 1 – natural gas cylinder; 2 – oxygen cylinder; 3 – rotameters RM-GS 004 KL4; 4 – 2-way valve; 5 – alundum tube for blowing the melt; 6 – plug with water cooling; 7 – quartz reactor; 8 – electric furnace Nabertherm 50/250/12 with temperature controller B 410; 9 – crucible with a sample; 10 – Drexel vessel ; 11 – control and measuring unit.

In the experiments, the influence of the consumption of natural gas, oxygen and the duration of blowing on the technological parameters of the smelting charge was determined. Natural gas consumption varied from 1 to 1.7, in fractions of the stoichiometric required amount (SRQ) for the complete reduction of lead from its sulfates and oxides. Melt blowing time – 5, 10, 15, 20 minutes.

At the first stage, upon reaching the required temperature, the melt was kept for 5 minutes to obtain a homogeneous melt, then the blowing tube was inserted and the melt was purged with natural gas for a specified time. Upon completion of the purging, the tube was removed from the melt, and the furnace was cooled in a stream of natural gas. After the furnace cooled, the crucible with the sample was removed from the quartz reactor, the smelting products were broken and separated: rough lead, matte and slag.

In the second stage, the intermediate matte obtained in the first stage was purged with oxygen. The procedure for conducting the experiments was the same as in the case of blowing the melt with natural gas. The experimental temperature of 1200 °C ensured the production of liquid slag with a minimum content of lead, copper and high, up to 16%, zinc. During the experiments, the optimal oxygen consumption was determined to ensure high extraction of lead, copper, zinc and arsenic into the targeted products.

The dust yield was calculated based on the difference between the amount of the initial sample and the sum of the amount of obtained smelting products.

Each experiment was repeated three times. The smelting products obtained after the experiments were subjected to comprehensive studies. The established results for the metal content in each product showed good agreement (error +/-0.81% abs.). Based on the results of averaged data on the yield of smelting products and the content of elements in each obtained product, the material balances of the reduction and oxidation stages of the melting of the charge, and then, the final material balance of the smelting of the charge under the conditions of reduction-oxidation blowing were calculated.

Laboratory experiments of reduction-oxidation smelting of the charge. The first stage of research included determining the optimal technological parameters for the reduction-oxidation melting of the charge.

The results of the experiments are presented in Fig. 2, 3, and 4 in the form of the dependence of the influence of natural gas consumption and blowing time on the extraction of copper, lead, zinc and arsenic.

The best results, ensuring high complex extraction of copper, lead, zinc and arsenic into the targeted smelting products, are achieved at a natural gas consumption 1.4 times higher than its consumption from the stoichiometric required quantity (SRQ) for the reduction of lead compounds to metallic lead. The optimal time for purging the melt with natural gas is 15 minutes.

The optimal oxygen consumption when blowing the intermediate matte obtained after the first stage was 1.1 times higher than its stoichiometric required amount (SRQ) for the oxidation of zinc and iron sulfide with their further transfer in the form of oxides to slag. The duration of matte purging is 10 minutes.

The results of the material balances of the reduction-oxidation melts of the charge, calculated based on the results of experiments performed at optimal parameters of blowing with natural gas and oxygen, are shown in Tables 3 and 4.

The final material balance of the charge processing technology is presented in Table 5.

During reduction smelting of the charge with natural gas, the yield of products was, % (of the total

charge): rough lead - 44.23; matte – 20.7; slag – 26.78; dust, gases – 2.1. Optimal slag composition, wt.%: 17 Fe; 27.41 SiO_2; 5.75 CaO, ensures minimal solubility of copper and lead in it, which significantly increases their extraction into matte and rough lead, respectively.

Mineralogical studies of the forms of copper and lead in the resulting slags showed their insignificant presence in the form of small inclusions of dissolved oxides. The established low copper contents in the slag (0.16%) and rough lead (0.12%) ensured the production of high quality rough lead - with a lead content of 99.52%. The recovery of lead into rough lead was 98.1%. At the same time, a high extraction of copper into matte was achieved – 98.5%. Despite the high performance, the resulting matte is characterized by a high content of zinc ~22% and iron – up to 11%. Studies of their forms in matte showed their presence in the form of sulfides. Although the resulting matte in terms of copper content in it (40.3% Cu) corresponds to the composition of factory mattes, the presence of zinc and iron sulfides in it deteriorates its quality. It should be expected that with further conversion of such mattes to blister copper, the costs of the process will increase significantly.

The obtained results indicate that it is not possible to obtain high-quality copper matte in one step of blowing the melt with natural gas. The fact is fully consistent with the thermodynamic laws of the physical and chemical processes mentioned above: when blowing the melt with natural gas, the thermodynamic probability of the reduction of lead compounds (sulfates, sulfides, oxides) with natural gas with the formation of rough lead is significantly higher than the reduction of zinc and iron sulfides. While lead compounds (sulfates, oxides, sulfides) are present in the melt, zinc and iron sulfides are not reduced by natural gas. As a result, those metals are concentrated in the obtained matte, which is fully confirmed by the results of the experiments (Table 3).

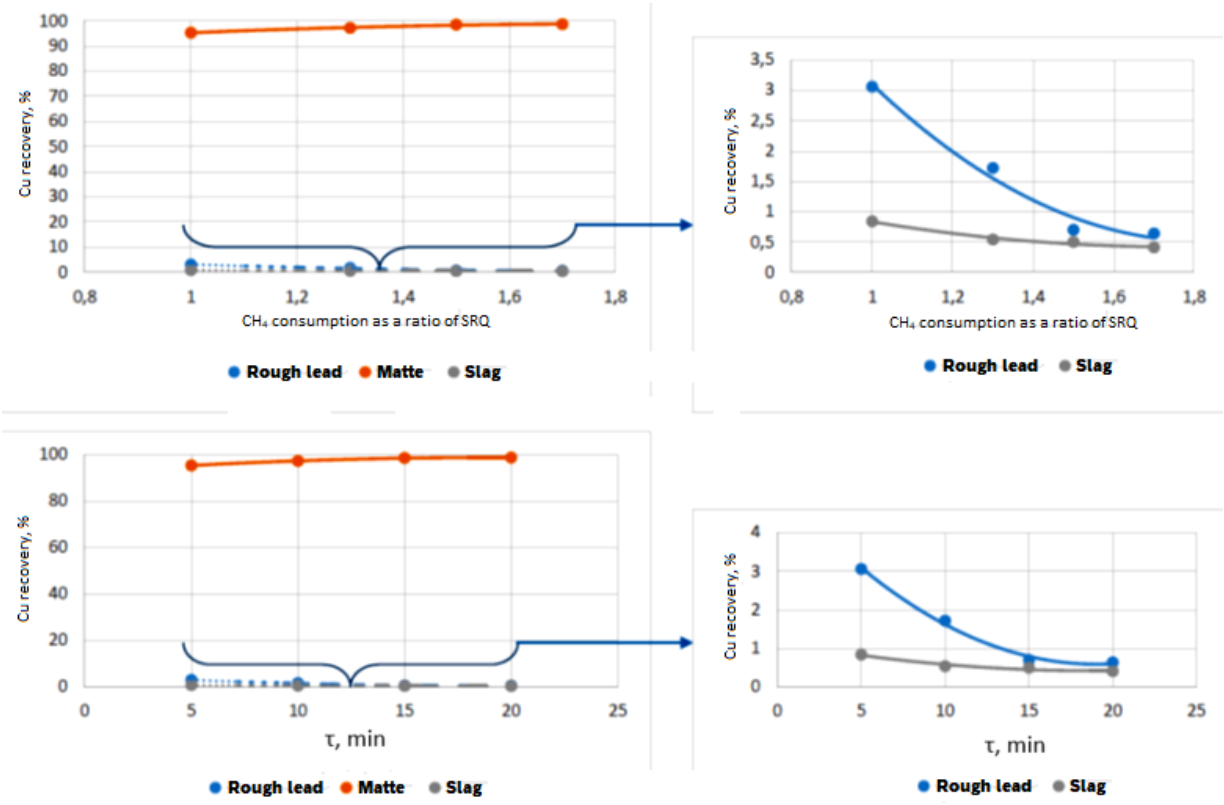

Figure 2 – Impact of natural gas consumption CH_4 (ratio of SRQ) and blowing time (τ, min) to extract copper into smelting products

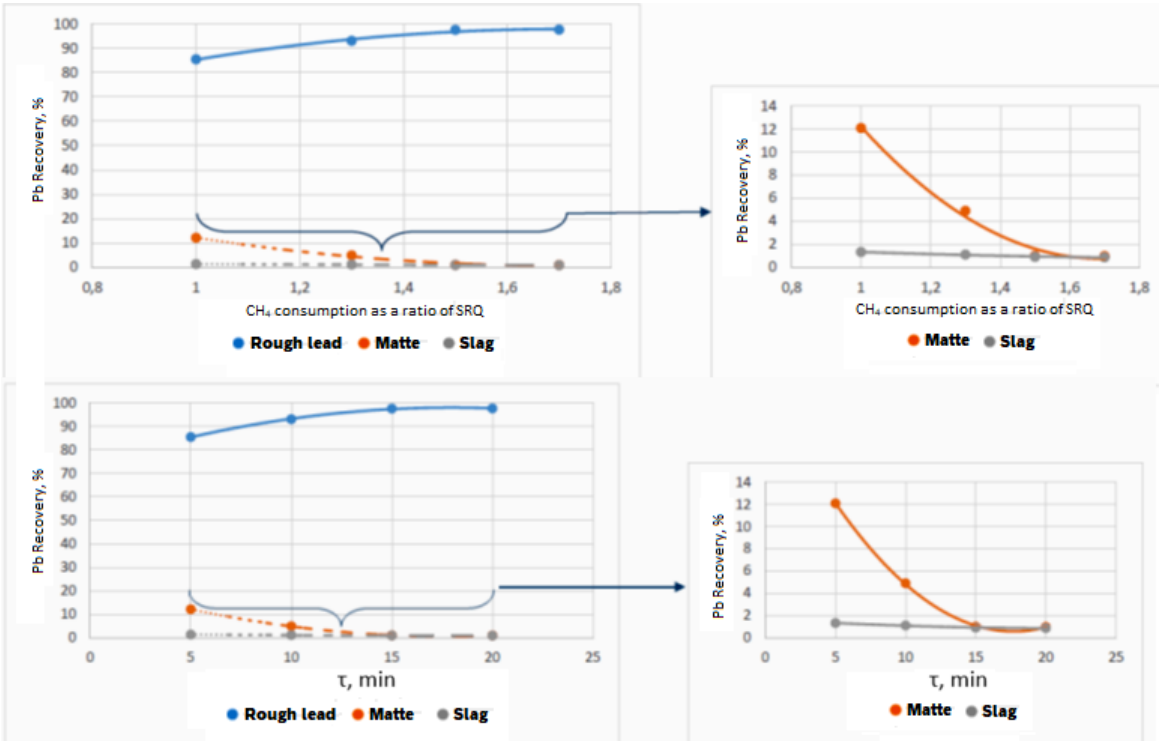

Figure 3 – Impact of natural gas consumption CH_4 (ratio of SRQ) and blowing time (τ, min) to extract lead into smelting products

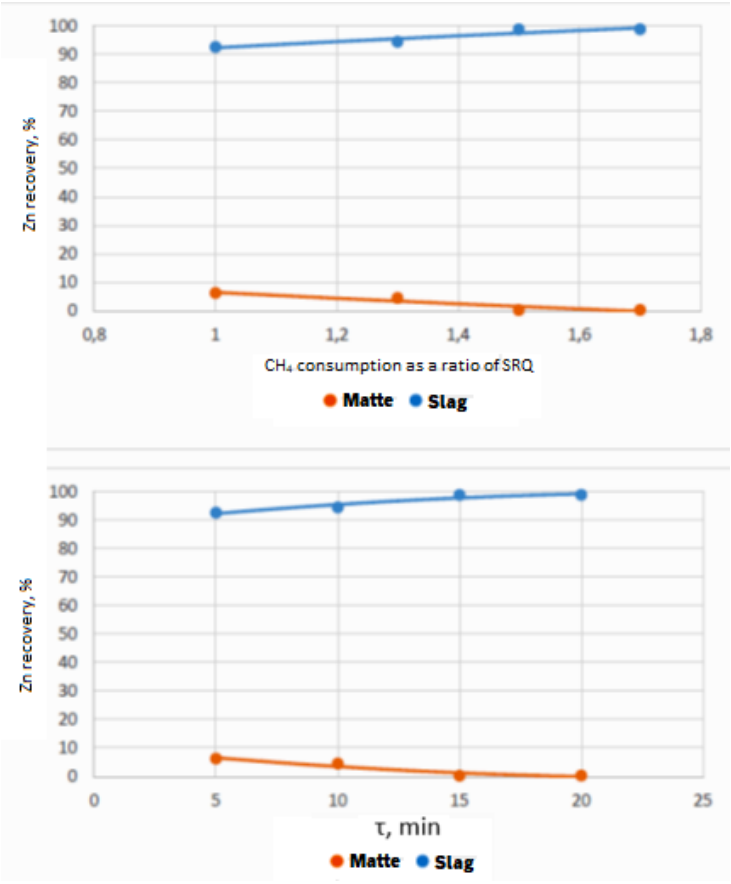

Figure 4 – Impact of natural gas consumption CH_4 (ratio of SRQ) and blowing time (τ, min) to extract zinc into smelting products

Table 3 - Material balance for reduction smelting of the charge with natural gas at optimal parameters: consumption of CH_4 is 1.4 times higher than its consumption from the SRQ for the reduction of lead compounds; blowing time – 15 minutes; T = 1200 °C

Name of the products	Qty		Cu			Pb			Zn			Fe			As		
	g.	%	I	II	III	I	II	III	I	II	III	I	II	III	I	II	III
Inlet:																	
Charge (feed)	200.00	99.10	17.09	8.54	100.0	103.25	51,63	100.0	9.23	4.61	100.0	13.94	6.97	100.0	0.93	0.93	100.0
Natural gas	1.82	0.90															
Total:	**201.82**	**100.0**	**17.09**		**100.0**	**103.25**		**100.0**	**9.23**		**100.0**	**13.94**		**100.0**	**0.93**		**100.0**
Outlet:																	
Rough lead	101.78	44.23	0.12	0.12	0.70	101.29	99.52	98.10									
Matte	41.80	20.71	16.86	40,34	98.89	0.72	1.73	0.70	9,12	21.81	98.77	4.64	11,11	33.3	0.03	0.07	3.0
Slag	54.01	26.76	0.05	0.03	0.11	0.83	1.53	0.80	0.02	0.04	0.23	9.19	17.01	65.9	0.02	0.03	2.0
Dust, gases	4.23	2.10	0.05	1.21	0.30	0.41	9.77	0.40	0.092	2.18	1.0	0.11	2.64	0.8	0.88	20.89	95.0
Total:	**201.82**	**100.0**	**17.09**		**100.0**	**103.25**		**100.0**	**9.23**		**100.0**	**13.94**		**100.0**	**0.93**		**100.0**

Sb			S			O			SiO_2			CaO			CH_4			Others			Total:
I	II	III	I	II	III	I	II	III	I	II	III	I	II	III	I	II	III	I	II	III	
Inlet:																					
0.5	0.5	100	9.7	9.7	100	11.3	11.3	100	14.9	14.9	100	3.1	3.1	100				16.1	8.02	100	200.0
															1.8	100	100				1.8
0.5		**100**	**9.7**		**100**	**11.3**		**100**	**14.9**		**100**	**3.1**		**100**	**1.8**		**100**	**16.1**		**100**	**201.8**
Outlet:																					
0.03	0.03	6.0																0.2	0.33	2.1	101.8
0.00	0.01	1.0	9.7	23	100													0.8	1.84	4.8	41.8
0.01	0.02	3.0				11.2	20.7	99.0	14.8	27.4	99.0	3.1	5.8	99.0				14.8	27.4	92.1	54.0
0.40	9.54	90				0.11	2.7	1.0	0.1	3.54	1.0		0.7	1.0	1.8	43.0	1000	0.2	3.80	1.0	4.2
0.45		**100**	**9.7**		**100**	**11.3**		**100**	**14.9**		**100**	**3.1**		**100**	**1.8**		**100**	**16.1**		**100**	**201.8**

I – quantity, g; **II –** content, %; **III –** extraction, %.

Table 4 - Material balance of oxidative smelting of intermediate matte with oxygen at optimal parameters: oxygen consumption - 1.1 times higher than its consumption from SRQ for the oxidation of FeS and ZnS ; purge time – 10 minutes; T = 1200 °C

Name of the products	Qty		Cu			Pb			Zn			Fe			As		
	G	%	I	II	III	I	II	III	I	II	III	I	II	III	I	II	III
Inlet:																	
Matte	41.80	59.64	16.86	40.34	100.0	0.72	1.73	100.0	9.11	21.81	100.0	4.64	11.11	100.0	0.028	0.07	100.0
Air	28.29	40.36															
Total:	**70.09**	**100.0**	**16.86**		**100.0**	**0.72**		**100.0**	**9.11**		**100.0**	**4.64**		**100.0**	**0.028**		**100.0**
Outlet:																	
Matte	29.96	42.74	16.83	56.18	99.80	0.22	0.72	30.0	0.45	1.52	5.0	4.50	15.03	97.0	0.028	0.09	100.0
Slag	8.83	12.60	0.03	0.38	0.20				8.66	98.04	95.0	0.14	1.58	3.0			
Dust, gases	31.30	44.65				0.50	1.62	70.0									
Total:	**70.09**	**100.0**	**16.86**		**100.0**	**0.72**		**100.0**	**9.11**		**100.0**	**4.64**		**100.0**	**0.028**		**100.0**

Sb			S			O			N_2			Others			Total:
I	II	III	I	II	III	I	II	III	I	II	III	I	II	III	
0.004	0.01	100.0	9.66	23,10	100.0							0.77	1.84	100.0	41.80
						5.94	21.0	100.0	22,35	79,0	100.0				28.29
0.004		**100.0**	**9.66**		**100.0**	**5.94**		**100.0**	**22,35**		**100.0**	**0.77**		**100.0**	**70.09**
0.004	0.01	100.0	7.24	24.17	75.0							0.68	2.26	88.0	29.96
															8.83
			2.41	7.71	25.0	5.94	18.98	100.0	22.35	71.40	100.0	0.09	0.30	12.0	31.30
0.004		**100.0**	**9.66**		**100.0**	**5.94**		**100.0**	**22.35**		**100.0**	**0.77**		**100.0**	**70.09**

I – quantity, g; **II –** content, %; **III –** extraction, %.

Table 5 – Summary material balance of reduction-oxidation smelting of the charge

Name products	Qty		Cu			Pb			Zn			Fe			As			Sb		
	G	%	I	II	III	I	II	III	I	II	III	I	II	III	I	II	III	I	II	III
Inlet:																				
In charge	200.0	86.9	17.1	8.5	100	103.3	51.6	100	9.2	4.61	100	13.9	6.97	100	0.9	0.9	100	0.5	0.5	100
Air	28.29	12.3																		
Natural gas	1.81	0.79																		
Total:	**230.1**	**100**	**17.1**		**100**	**103.3**		**100**	**9.2**		**100**	**13.9**		**100**	**0.9**		**100**	**0.5**		**100**
Outlet:																				
Rough lead	101.8	44.2	0.12	0.1	0.7	101.3	99.5	98										0.1	0.1	6.0
Matte	29.96	13.0	16.8	56	98.5	0.22	0.72	0.2	0.46	1.52	4.94	4.50	15.0	32.3	0.1	0.1	3.0	0.00	0.0	1.0
Slag	62.62	27.2	0.09	0.1	0.5	0.61	0.97	0.6	8.68	13.8	94.0	9.33	14.8	66.9			2.0	0.01	0.0	3.0
Dust, gases	35.74	15.5	0.05	0.1	0.3	1.14	3.18	1.1	0.09	0.26	1.0	0.11	0.31	0.8	0.8	2.5	97	0.40	1.1	94.0
Total:	**230.1**	**100**	**17.1**		**100**	**103.2**		**100**	**9.23**		**100**	**13.9**		**100**	**0.9**		**100**	**0.45**		**100**

S			O			N_2			SiO2			CaO			CH_4			Others			Total:
I	II	III	I	II	III	I	II	III	I	II	III	I	II	III	I	II	III	I	II	III	
Inlet:																					
9.66	9.66	100.0	11.30	11.3	65.55				14.96	14.96	100.0	3.14	3.14	100.0				16.05	8.02	100.0	200.0
			5.94	21.0	34.45	22.35	79.0	100.0													28.29
															1.82	100.0	100.0				1.82
9.66		**100.0**	**17.24**		**100.0**	**22.35**		**100.0**	**14.96**		**100.0**	**3.14**		**100.0**	**1.82**		**100.0**	**16.05**		**100.0**	**230.11**
Outlet:																					
																		0.34	0.33	2.10	101.78
7.24	24.17	75.0																0.68	2.26	4.22	29.96
			11.19	17.87	64.9				14.81	23.65	99.0	3.11	4.96	99.0				14.78	23.60	92.10	62.62
2.41	6.75	25.0	6.05	16.93	35.1	22.35	62.52	100.0	0.15	0.42	1.0	0.03	0.09	1.0	1.82	5.09	100.0	0.25	0.71	1.58	35.74
9.66		**100.0**	**17.24**		**100.0**	**22.35**		**100.0**	**14.96**		**100.0**	**3.14**		**100.0**	**1.82**		**100.0**	**16.05**		**100.0**	**230.11**

I – quantity, g; **II –** content, %; **III –** extraction, %.

Commercial, copper-rich matte is obtained in the second stage - by blowing the intermediate matte with oxygen, where the main amount of zinc and iron sulfides are oxidized to their oxides and turned into slag. In this case, the copper content in the matte increases from 40% to ~57% and zinc-rich slag is formed (Table 3).

From the results of the final material balance (Table 4) it is clear that when melting a charge using reduction-oxidation blowing, the yield of products is, % (of the total charge): rough lead - 44.5; copper matte – 13.0; slag – 27.2; dust and gases – 15.3.

Results of laboratory studies on joint smelting of lead cake with various substandard lead production materials fully confirm the provisions established in the theoretical part of the technology.

Based on the conducted research, technological regimes and optimal parameters for the joint processing of lead cake and copper-lead matte by two-stage reduction-oxidation blowing of the melt were recommended for practical application: with natural gas, then with oxygen:

– melt blowing time:

- natural gas – 15 minutes;
- oxygen – 10 min.

– gas consumption:

- CH_4 – 1.4 times, its consumption from the stoichiometric required amount (SRQ) for the reduction of lead compounds;
- oxygen – 1.1 times, its consumption from the stoichiometric required amount (SRQ) for the oxidation of zinc and iron sulfide.

– temperature – 1200 °C.

With the established optimal parameters, high technological indicators were achieved (Table 4):

– composition of rough lead, wt.%: 99.53 Pb; 0.12 Cu; 0.03 Sb.

– matte composition, wt.%: 56.2 Cu; 0.72 Pb; 1.52 Zn; 15.03 Fe; 24.17 S; 0.09 As.

– slag composition, wt.%: 14.89 Fe; 23.65 SiO2; 13.86 Zn; 0.14 Cu; 0.97 Pb.

– extraction of metals into targeted products:

- lead into rough lead – 98.6%;
- copper in matte – 98.5%;
- zinc to slag – 94.1%;
- arsenic and antimony in dust - up to 97 and 94%, respectively.

Conclusions

Based on the results of studies on the forms of metals in lead cake and substandard intermediate products of lead production, technological calculations were carried out for the layout of a charge of a new composition and laboratory experiments on its smelting under conditions of reduction-oxidation blowing. New data have been obtained on the complex selective extraction of Cu, Pb, Zn and As into the targeted smelting products.

Optimal conditions for melting the charge have been established: temperature – 1200 °C; blowing the melt with CH_4 – 15 min., oxygen – 10 min. High extraction of lead into rough lead was achieved – 98.6%; copper in matte – 98.5%; zinc to slag – 94.1%; arsenic and antimony into dust - up to 95 and 90%, respectively.

High-quality rough lead, matte and slag were obtained, which can easily be processed to produce commercial lead, copper and zinc using known technologies at minimal cost. The high copper content in the matte, more than 70%, will significantly reduce the costs of subsequent fire refining and electrolysis operations to obtain commercial copper cathodes.

Conflict of interest. On behalf of all authors, the corresponding author confirms that there is no conflict of interest.

CRediT author statement: **N. Dosmukhamedov:** Supervision, Conceptualization. **E. Zoldasbay:** Investigation, Data curation. **A. Argyn:** Methodology, Writing-Original draft preparation. **Y. Icheva:** Investigation, Software, Validation. **Zh. Klyshbekova:** Writing- Reviewing.

Acknowledgements. The research was carried out within the framework of grant funding from the Science Committee of the Ministry of Science and Higher Education of the Republic of Kazakhstan for 2023-2025 in the priority area “Geology, extraction and processing of mineral and hydrocarbon raw materials, new materials, technologies, safe products and designs” of the project AP19676951: “Development of resource-saving, combined technology for the complex processing of multicomponent non-ferrous metallurgy dust with the production of marketable products”.

Cite this article as: Dosmukhamedov NK, Zholdasbay EE, Argyn AA, Icheva YuB, Klyshbekova ZhE. Technology for extraction of Pb, Cu, Zn from a feed based on lead cake from leached dust generated by reduction-oxidation blowing of melt. Kompleksnoe Ispolzovanie Mineralnogo Syra = Complex Use of Mineral Resources. 2025; 334(3):78-90. https://doi.org/10.31643/2025/6445.30

Шаңды шаймалаудан алынған қорғасын қоқымы негізіндегі шикіқұрамнан балқыманы тотықсыздандырып-тотықтырып үрлеу арқылы Pb, Cu, Zn бөліп алу технологиясы

[1]Досмухамедов Н.К., [2]Жолдасбай Е.Е., [2]Арғын А.Ә., [2]Ичева Ю.Б., [1]Клышбекова Ж.Е.

[1]Сәтбаев университеті, Алматы, Қазақстан
[2]Ө.А. Байқоңыров атындағы Жезқазған университеті, Жезқазған, Қазақстан

Мақала келді: *21 мамыр 2024*
Сараптамадан өтті: *25 маусым 2024*
Қабылданды: *16 шілде 2024*

ТҮЙІНДЕМЕ

Жұмыста шаңнан мышьякты алдын ала алып тастап және оны күкірт қышқылымен шаймалағаннан кейін алынған қорғасын қоқымы негізіндегі шикіқұрамның түрі мен құрамы бойынша күрделі өңдеудің теориялық базасы мен нәтижелері келтірілген. Технологияның негізгі мақсаты – қорғасын қоқымымен бірге қорғасын өндірісінің кондициялық емес жартылай өнімдерін өңдеуге тарту және түсті металдарды тауарлық өнімдерге селективті бөліп алу: мысты – штейнге; қорғасынды – қара қорғасынға: мырышты – қожға. Шикіқұрамның құрамын таңдау олардың өндірісте шығатын көлемін ескере отырып жүзеге асырылды және мынадай құрылымда ұсынылды, %: қорғасын қоқымы – 50; мыс-қорғасынды штейн – 40; кварцты флюс – 10. Белгіленген балқыту өнімдеріне мыс, қорғасын, мырыш және мышьяк жоғары кешенді алынатын ең жақсы нәтижелерге қорғасын қосылыстарының металл қорғасынға дейін тотықсыздануын қамтамасыз ететін табиғи газды стехиометриялық қажетті мөлшерден (СНК) тұтынудан 1,4 есе жоғары тұтыну арқылы қол жеткізілетіні анықталды. Балқыманы табиғи газбен үрлеудің оңтайлы уақыты - 15 минут. Бірінші кезеңнен кейін алынған аралық штейнді үрлеу кезіндегі оттегінің оңтайлы шығыны мырыш пен темір сульфидінің тотығуы үшін оның стехиометриялық қажетті мөлшерінен (СНК) 1,1 есе жоғары болды, олар одан әрі оксидтер түрінде қожға көшеді. Штейнді үрлеу ұзақтығы – 10 минут. Белгіленген оңтайлы параметрлерде технологияның жоғары технологиялық көрсеткіштеріне қол жеткізілді: қорғасынның қара қорғасынға бөлінуі – 98,6%; мыстың штейнге – 98,5%; мырыштың қожға – 94,1%.

Түйін сөздер: қорғасын қоқымы, шикіқұрам, жартылай өнімдер, тотықсыздандырып үрлеу, тотықтырып үрлеу, мыс, қорғасын, мырыш, бөліп алу.

Авторлар туралы ақпарат:

Досмухамедов Нурлан Калиевич *Т.ғ.к., профессор, Satbayev University, 050013, Алматы, Сатпаев көш. 22, Казақстан. E-mail: nurdos@bk.ru*

Жолдасбай Ержан Есенбайұлы *PhD, Ө.А. Байқоңыров атындағы Жезқазған университеті, 100600, Жезқазған, Алашахан көш. 1б, Казақстан. E-mail: zhte@mail.ru*

Арғын Айдар Әбділмәлікұлы *PhD, Ө.А. Байқоңыров атындағы Жезқазған университеті, 100600, Жезқазған, Алашахан көш. 1б, Казақстан. E-mail: aidarargyn@gmail.com*

Ичева Юлианна Борисовна *Т.ғ.к., Ө.А. Байқоңыров атындағы Жезқазған университеті, 100600, Жезқазған, Алашахан көш. 1б, Казақстан*

Клышбекова Жанар Ериковна *Магистр, Satbayev University, 050013, Алматы, Сәтбаев көш. 22., Казақстан. Email: galamat3196@gmail.com*

Технология извлечения Pb, Cu, Zn из шихты на основе свинцового кека от выщелачивания пыли путем восстановительно-окислительной продувки расплава

[1]Досмухамедов Н.К., [2]Жолдасбай Е.Е., [2]Аргын А.А., [2]Ичева Ю.Б., [1]Клышбекова Ж.Е.

[1] Satbayev University, Алматы, Казахстан
[2]Жезказганский университет имени О.А. Байконурова, Жезказган, Казақстан

Поступила: *21 мая 2024*
Рецензирование: *25 июня 2024*
Принята в печать: *16 июля 2024*

АННОТАЦИЯ

В работе представлены теоретическая база и результаты переработки сложного по типу и составу шихты, составленной на основе свинцового кека, полученного после предварительного удаления из пыли мышьяка и последующего ее выщелачивания серной кислотой. Основная цель технологии – вовлечение на переработку некондиционных полупродуктов свинцового производства совместно со свинцовым кеком и селективное извлечение цветных металлов в товарные продукты: меди – в штейн; свинца – в черновой свинец: цинка – в шлак. Выбор компоновки шихты осуществлен с учетом получаемых их объемов на производстве и представлена следующей структурой, %: свинцовый кек – 50;

медно-свинцовый штейн – 40; кварцевый флюс – 10. Установлено, что наилучшие результаты, обеспечивающие высокое комплексное извлечение меди, свинца, цинка и мышьяка в целевые продукты плавки достигаются при расходе природного газа в 1,4 раза превышающем его расход от стехиометрического необходимого его количества (СНК) для восстановления соединений свинца до металлического свинца. Оптимальное время продувки расплава природным газом – 15 минут. Оптимальный расход кислорода при продувке промежуточного штейна, полученного после первой стадии, в 1,1 раза превышал его стехиометрическое необходимое количество (СНК) для окисления сульфида цинка и железа с дальнейшим переводом их в виде оксидов в шлак. Продолжительность продувки штейна – 10 минут. При установленных оптимальных параметрах достигнуты высокие технологические показатели технологии: извлечение свинца в черновой свинец – 98,6%; меди в штейн – 98,5%; цинка в шлак – 94,1%.

Ключевые слова: свинцовый кек, шихта, полупродукты, восстановительная продувка, окислительная продувка, медь, свинец, цинк, извлечение.

Досмухамедов Нурлан Калиевич	***Информация об авторах:*** *К.т.н., профессор. Satbayev University, 050013, Алматы, ул. Сатпаева 22, Казахстан. E-mail: nurdos@bk.ru*
Жолдасбай Ержан Есенбайулы	*PhD, Жезказганский университет имени О.А. Байконурова, 100600, Жезказган, ул. Алашахана 1б, Казахстан. E-mail: zhte@mail.ru*
Аргын Айдар Абдилмаликулы	*PhD, Жезказганский университет имени О.А. Байконурова, 100600, Жезказган, ул. Алашахана 1б, Казахстан. E-mail: aidarargyn@gmail.com*
Ичева Юлианна Борисовна	*К.т.н., Жезказганский университет имени О.А. Байконурова, 100600, Жезказган, ул. Алашахана 1б, Казахстан.*
Клышбекова Жанар Ериковна	*Магистр, Satbayev University, 050013, Алматы, ул. Сатпаева 22, Казахстан. Email: galamat3196@gmail.com*

References

[1] Kobayashi Y, Hirano S. Distribution and excretion of arsenic metabolites after oral administration of seafood-related organoarsenicals in rats. Metals. 2016; 6(10):231. https://doi.org/10.3390/met6100231

[2] Feng S, Che J, Zhang W, Zuo Y, Wang C, Ma B, Chen Y. A sustainable approach for recovering copper and zinc from copper smelting flue dust: Paving the path for waste reduction. Separation and Purification Technology. 2024; 342:127037. https://doi.org/10.1016/j.seppur.2024.127037

[3] Zhong DP, Li L, Tan C. Separation of arsenic from the antimony-bearing dust through selective oxidation using CuO. Metall. Mater. Trans. B. 2017; 48:1308-1314.

[4] Yang WC, Tian SQ, Wu JX, Chai LY, Liao Q. Distribution and behavior of arsenic during the reducing-matting smelting process. JOM. 2017. https://doi.org/10.1007/s11837-017-2332-8

[5] Vorotnikov AM, Lyzhin DN, Ipatova NS. Waste management system as an integral part of circular economy. Journal of economic research. 2018; 10:29-34.

[6] Takezhanov ST, Erofeev IE. Concept Complex of technical and technological development of non-ferrous metallurgy in Kazakhstan. Almaty: Publishing house Kitap. 2001.

[7] Orac D, Laubertova M, Piroskova J, Klein D, Bures R, Klimko J. Characterization of dusts from secondary copper production. J Min Metall Sect B – Metall. 2020; 56(2):221-228. https://doi.org/10.2298/JMMB190820011O

[8] Jabłońska M, Rachwał MF, Wawer M, Kądziołka-Gaweł M, Teper E, Krzykawski T, Smolka-Danielowska D. Mineralogical and Chemical Specificity of Dusts Originating from Iron and Non-Ferrous Metallurgy in the Light of Their Magnetic Susceptibility. Minerals. 2021; 11(2):216. https://doi.org/10.3390/min11020216

[9] Fry KL, Wheeler CA, Gillings MM, Flegal AR, Taylor MP. Anthropogenic contamination of residential environments from smelter As, Cu and Pb emissions: Implications for human health. Environmental Pollution. 2020; 262:114235. https://doi.org/10.1016/j.envpol.2020.114235

[10] González A, Font O, Moreno N. Copper flash smelting flue dust as a source of germanium. Waste Biomass Valor. 2017; 8:2121-2129. https://doi.org/10.1007/s12649-016-9725-8

[11] Chen J, Zhang W, Ma B, Che J, Xia L, Wen P, Wang Ch. Recovering metals from flue dust produced in secondary copper smelting through a novel process combining low temperature roasting, water leaching and mechanochemical reduction. Journal of Hazardous Materials. 2022; 430:128497. https://doi.org/10.1016/j.jhazmat.2022.128497

[12] Adrados A, Merchán M, Obregón A, Artola A, Iparraguirre JA, GM, Cortázar Eguizabal D, Demey H. Development of a sustainable metallurgical process to valorize copper smelting wastes with olive stones-based biochar. Metals. 2022; 12(10):1756. https://doi.org/10.3390/met12101756

[13] Li Q, Lai X, Liu Z, Chai F, Zhao F, Peng C, Liang Y. Thiourea-assisted selective removal of arsenic from copper smelting flue dusts in NaOH solution. Hydrometallurgy. 2024; 224:106246. https://doi.org/10.1016/j.hydromet.2023.106246

[14] Che J, Zhang W, Deen KM, Wang C. Eco-friendly treatment of copper smelting flue dust for recovering multiple heavy metals with economic and environmental benefits. Journal of Hazardous Materials. 2024; 465:133039. https://doi.org/10.1016/j.jhazmat.2023.133039

[15] Gao W, Xu B, Yang J, Yang Y, Li Q, Zhang B, Liu G, Ma Y, Jiang T. Comprehensive recovery of valuable metals from copper smelting open-circuit dust with a clean and economical hydrometallurgical process. Chemical Engineering Journal. 2021; 424:130411. https://doi.org/10.1016/j.cej.2021.130411

[16] Baniasadi M, Vakilchap F, Bahaloo-Horeh N, Mousavi SM, Farnaud S. Advances in bioleaching as a sustainable method for metal recovery from e-waste: A review. Journal of Industrial and Engineering Chemistry. 2019; 76:75-90. https://doi.org/10.1016/j.jiec.2019.03.047

[17] Gao W, Xu B, Yang J, Yang Y, Li Q, Zhang B, Liu G, Ma Y, Jiang T. Recovery of valuable metals from copper smelting open-circuit dust and its arsenic safe disposal. Resources, Conservation and Recycling. 2022; 179:106067. https://doi.org/10.1016/j.resconrec.2021.106067

[18] Shi T, He J, Zhu R, Yang B, Xu B. Arsenic removal from arsenic-containing copper dust by vacuum carbothermal reduction–vulcanization roasting. Vacuum. 2021; 189:110213. https://doi.org/10.1016/j.vacuum.2021.110213

[19] Chen Y, Zhu S, Taskinen P, Peng N, Peng B, Jokilaakso A, Liu H, Liang Y, Zhao Z, Wang Z. Treatment of high-arsenic copper smelting flue dust with high copper sulfate: Arsenic separation by low temperature roasting. Minerals Engineering. 2021; 164:106796. https://doi.org/10.1016/j.mineng.2021.106796

[20] Liu X, Wu F, Qu G, Zhang T, He M. Recycling and reutilization of smelting dust as a secondary resource: A review. Journal of Environmental Management. 2023; 347:119228. https://doi.org/10.1016/j.jenvman.2023.119228

Crossref
DOI: 10.31643/2025/6445.31
Metallurgy

Optimization of joint electric smelting of the Shalkiya sulfide ore and its beneficiation tailings with medium-silicon ferrosilicon production

[1]Shevko V.M., [1*]Makhambetova B.A., [2]Aitkulov D.K., [1]Badikova A.D.

[1]M. Auezov South Kazakhstan University, Shymkent, Kazakhstan
[2]National Center on complex processing of mineral raw materials of the Republic of Kazakhstan, Almaty, Kazakhstan

** Corresponding author email: mahanbetova@bk.ru*

Received: *May 22, 2024*
Peer-reviewed: *July 3, 2024*
Accepted: *July 17, 2024*

ABSTRACT

Flotation beneficiation of the Shalkiya deposit high-silicon sulfide ore, containing 4-6% of ∑ Pb and Zn, is ineffective, with the extraction of <80% of zinc and <60% of lead into the concentrate and the formation of up to 0.93 t of tailings per 1 ton of the ore. The paper presents the results of experimental studies on the processing of a mixture of the Shalkiya ore and its beneficiation tailings by electric smelting in the presence of coke, steel cuttings and magnetite concentrate, which acts as a sulfide oxidizer and iron supplier. The effect of coke and the iron replacement degree in magnetite concentrate with iron in steel cuttings on the silicon extraction in the alloy and its content in the alloy was studied using the method of planning experiments and their optimization. It was established that from 75 to 82.8% of silicon is extracted from the mixture into the silicon-containing alloy. The silicon content in the alloy varies from 30 to 44.2%. The formation of FeSi45 grade ferrosilicon, containing 41-47.7% of silicon, occurs during the smelting of the mixture of ore and tailings with a ratio of 1:1 in the presence of 26.8-33.0% of coke and the replacement of iron from magnetite concentrate with iron from steel cuttings from 19.4 to 97%. The sublimates formed during the electric smelting contain 25.2% of Zn and 11.7% of Pb. They are 9.4 times richer in ∑Zn and Pb compared to the base mixture.

Keywords: sulfide ore, beneficiation tailings, lead-zinc ore, electric smelting, zinc sublimate, ferrosilicon.

Information about authors:

Shevko Viktor Mikhaylovich — *Doctor of Technical Sciences, Professor, Department of Silicate Technology and Metallurgy, M. Auezov South Kazakhstan University, Tauke Khan Avenue, 5, 160002, Shymkent, Kazakhstan. E-mail: shevkovm@mail.ru*

Makhanbetova Baktygul Alimzhanovna — *Doctoral student of Department of Silicate Technology and Metallurgy, M. Auezov South Kazakhstan University, Tauke Khan Avenue, 5, 160002, Shymkent, Kazakhstan. E-mail: mahanbetova@bk.ru*

Aitkulov Dosmurat Kyzylbiyevich — *Doctor of Technical Sciences, Professor, Director of Scientific Research of National Center on complex processing of mineral raw materials of the Republic of Kazakhstan. Zhandosov st., 67, 050036, Almaty, Kazakhstan E-mail: aitkulov_dk@mail.ru*

Badikova Alexandra Dmitriyevna — *Doctoral student of Department of Silicate Technology and Metallurgy, M. Auezov South Kazakhstan University, Tauke Khan Avenue, 5, 160002, Shymkent, Kazakhstan. E-mail: sunstroke_91@mail.ru*

Introduction

Lead-zinc ores are divided into three classes according to their lead and zinc content: rich, containing >7% ∑Pb and Zn, ordinary - ∑Pb and Zn = 4-7%, and poor - ∑Pb and Zn = 2-4%. Based on the total reserves of zinc and lead, the ores are divided into rich (2-10 million tons), medium (0.5-2 million tons), and poor (<0.5 million tons) [1]. Based on this, the Shalkiya deposit sulfide ore with the total zinc and lead reserves of 5-8 million tons and containing 4.1-6% of ∑ Zn and Pb belongs to the category of rich with ordinary content [[2], [3]]. Ores of this category are mainly processed by hydrometallurgical method: beneficiation, roasting, leaching of the resulting cinder and then producing cathode zinc [[4], [5], [6], [7]]. Even though at least 90% of zinc-containing ores are processed using the hydrometallurgical method, taking into account flotation, and all of its stages are constantly being improved (from flotation to producing cathode zinc) [[8], [9], [10]], this method is associated with the formation of beneficiation tailings, and, as a rule, with an insufficiently high degree of zinc extraction into concentrate. The latter circumstance is quite often connected with the fact that in the process of ore crushing and grinding it is not possible to obtain relatively homogeneous grains of ore minerals, which differ in their

properties from the minerals of gangue; existing technologies and reagent regimes do not allow effectively process such ores and obtain required indicators [[11], [12], [13], [14], [15], [16], [17], [18], [19], [20], [21], [22], [23], [24]].

For this reason, the flotation beneficiation of the Shalkiya ore is characterized by low indicators. Thus, 70-77% of Zn (on average 73.5%) is extracted into the zinc concentrate with a content of 56% of Zn, and 49-56% of Pb (on average 52.5%) is extracted into the lead concentrate with a content of 45% of Pb. With an average content of 3.8% of Zn in the ore, the zinc concentrate mass formed from 1 ton of the ore is 1·0.038·0.735/0.56=0.0498 tons. With a concentration of 1.3% of Pb in the ore, the lead concentrate mass is 1·0.013·0.525/0.45=0.015 tons. The beneficiation tailings mass per 1 ton of the ore is 1-(0.0498+0.015)=0.93 tons. The number of tailings during the 8 years of the Shalkiya ore beneficiation is approximately 3 million tons. Therefore, the development of new, low-waste technologies for processing the Shalkiya ore and its beneficiation tailings is currently relevant. A distinctive feature of the Shalkiya ore and its tailings is a significant (40-60%) content of SiO_2 [[25], [26]]. Based on this, modern technology for processing the ore and tailings should provide for high zinc and lead extraction, and production of commercial silicon-containing products. By this, the authors of this paper propose a joint electrothermal processing of the Shalkiya ore and tailings with the extraction of zinc and lead into the gas phase and the production of silicon-containing ferroalloys. To obtain gaseous zinc, lead and silicon ferroalloy, the authors [27] propose the electric smelting of the mixture of ore and tailings in the presence of Fe_3O_4 with the implementation of the following reactions:

$$ZnS + Fe_3O_4 + 8C + 3SiO_2 = Zn_g + 3FeSi + SO_2 + 8CO; \quad (1)$$
$$PbS + Fe_3O_4 + C + 3SiO_2 = Pb_g + 3FeSi + SO_2 + 8CO; \quad (2)$$
$$FeS_2 + Fe_3O_4 + 6C + 3SiO_2 = 3FeSi + 2SO_2 + 6CO. \quad (3)$$

The effect of temperature on ΔG^0 and ΔH^0 of reactions 1-3 is shown in Figure 1 (the calculation was performed using the Equilibrium Compositions module of the HCS-10 software package [28]).

It can be seen that as the temperature increases, the reactions' equilibrium shifts to the right. The dependences of $\Delta G^0=f(T)$ for the reactions 1, 2, and 3, respectively, have the form:

$$\Delta G^0=2228.1-1.619T; \quad (4)$$
$$\Delta G^0=2166.1-1.569T; \quad (5)$$
$$\Delta G^0=2592.6-1.727T. \quad (6)$$

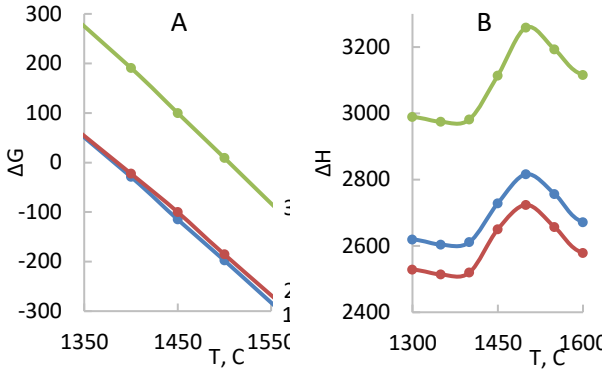

The numbers on the lines are the numbers of the reactions

Figure 1- Effect of temperature on ΔG^0 (a) and ΔH^0 (в) for reduction of Zn, Pb and Fe from sulfides

Based on the equations 4-6, it was determined (by $\Delta G^0=0$) that the first reaction becomes possible at a temperature of >1376.10C, the second at a temperature of >1380.60C, and the third at a temperature of >1501.20C. All the reactions under consideration are classified as endothermic. A more energy-consuming reaction is the interaction of pyrite with quartzite, Fe_3O_4 and carbon. The observed maximum on the dependence $\Delta H^0=f(T)$ is associated with the melting of FeSi. Earlier [[27], [29]] the authors published the results of a complete thermodynamic analysis of the formation of silicon-containing ferroalloys from the mixture of the Shalkiya ore and its beneficiation tailings and exploratory (preliminary) electrothermal smelting of silicon-containing alloys from the mixture.

This paper presents the results of experimental studies on the optimization of obtaining silicon-containing alloys from the mixture of the Shalkiya ore and its beneficiation tailings.

Experimental part

The electric smelting of the mixture of the Shalkiya ore and its beneficiation tailings (SHOT) with a mass ratio of 1:1 was carried out using a single-electrode arc furnace with a maximum power of 15 kV·A. The melting was carried out in a graphite crucible with a height of 12 cm and an internal diameter of 8 cm. The setup diagram and the experimental methodology were described by the authors earlier in [29].

The resulting alloy and sublimate were analyzed by SEM microscopy (a scanning electron microscope JSM-6490LV), gravimetric method. The content of lead and zinc was determined by the polarographic method according to [30]. The content of Si in the

alloy ($C_{Si(alloy)}$) was determined by its density (D, g/cm^3) by the formula (7):

$$C_{Si(alloy)}=252.405-101.848D+18.209D^2-1.243D^3 \quad (7)$$

The silicon extraction degree in the alloy ($\alpha_{(Si(alloy)}$) was determined by the ratio of the silicon mass in the alloy to the silicon mass in the charge. The studies were carried out by the method of mathematical planning of experiments using the second-order rotatable plans (Box-Hunter plan) [[31], [32]]. Based on the obtained experimental data, the regression equations were found for the effect of the coke amount (C, % of the SHOT mass) and the iron replacement degree in the magnetite concentrate with iron in the steel cuttings (γ, %) on $\alpha_{(Si(alloy)}$ and $C_{Si(alloy)}$. The adequacy of the regression equations was checked by the Fisher's criterion, the significance of the equation coefficients was checked by the Student's criterion. The experimental error did not exceed 5%. Based on the regression equations, 3D and planar images of the coke and γ effect on $\alpha_{(Si(alloy)}$ and $C_{Si(alloy)}$ were constructed.

Results and Discussion

The process was optimized by superimposing horizontal images $\alpha_{(Si(alloy)}$ =f(K, γ) and $C_{Si(alloy)}$= f(K, γ).

The chemical composition of the Shalkiya ore and its beneficiation tailings is shown in Table 1.

Table 1- Chemical composition of the Shalkiya ore and its beneficiation tailings, %

Component of the mixture	Content, %									
	ZnS	*PbS*	*FeS_2*	*SiO_2*	*$CaCO_3$*	*$MgCO_3$*	*Al_2O_3*	*Na_2O*	*K_2O*	*Fe_2O_3*
Ore	5.2	1.0	4.0	50.2	19.5	10.1	6.6	0.3	0.4	2.5
Tailings	2.5	0.8	3.1	60.1	17.06	8.9	2.2	0.5	0.6	3.2
Mixture	3.8	0.9	3.4	55.3	18.41	9.5	4.5	0.4	0.5	2.8

The ore and coke were used in 1-1.5 cm fractions. The beneficiation tailings were pelletized together with bentonite clay to 1-1.5 cm and dried at 150-160°C for 30 minutes. The magnetite concentrate obtained from the copper ore flotation tailings at the Balkhash plant was used as a raw material containing Fe_3O_4 and the following, by mass %: 86.0 of Fe_3O_4; 10.76 of SiO_2; 2.0 of CaO; 1.4 of Al_2O_3; 0.3 of MnO; 0.3 of K_2O; 0.2 of Na_2O; 0.4 of MgO; 0.017 of ZnO; 0.1 of PbO. The ash content in the coke was 13.0%, volatiles – 1.1%, moisture – 0.8%, S – 0.7%, and C – 84.5%. The steel cuttings contained 97.31% of Fe, 1.8% of C, 0.4% of Si, 0.2% of Mn, and 0.1% of Al.

Table 2 shows the matrix of the experiments and their results.

Table 2- Matrix of the experiments on the electric smelting of the Shalkiya ore and tailings mixture and their results

#	*Variables*				*Output parameter*			
	Coded		*Natural*		*$\alpha_{(Si(alloy)}$, %*		*$C_{(Si(alloy)}$, %*	
	X_1	*X_2*	*C, %*	*γ, %*	*Exp.*	*Calc.*	*Exp.*	*Calc.*
1	+	-	31.5	15	73.4	72.97	39.2	39.08
2	+	+	31.5	85	49.0	78.86	42	42.09
3	-	-	24.5	15	58.1	58.06	34.58	34.57
4	-	+	24.5	85	73.5	73.76	37.5	38.09
5	1.414	0	33	50	82.0	82.36	44.4	44.52
6	-1.414	0	23	50	68.4	68.21	39.1	35.51
7	0	1.414	28	100	74.3	74.17	38.1	37.71
8	0	-1.414	28	0	58.6	58.9	33.2	33.11
9	0	0	28	50	78.0	77.0	41.3	41.48
10	0	0	28	50	76.5	77.0	42	41.48
11	0	0	28	50	76.0	77.0	41.1	41.48
12	0	0	28	50	77.5	77.0	41.8	41.48
13	0	0	28	50	77.0	77.0	41.2	41.48

Based on the data in Table 2, the following regression equations were obtained:

$$\alpha_{(Si(alloy)} =-64.204+1.141\ \gamma+63.428\cdot10^{-1}\cdot C-42.694\cdot10^{-4}\gamma^2-69.877\cdot10^{-3}\cdot C^2-0.02\cdot C\cdot\gamma; \quad (8)$$

$$C_{Si(alloy)}=15.6+32.276\cdot10^{-2}\gamma-58.36\cdot C-24.767\cdot10^{-5}\ \gamma^2-10.204\cdot10^{-4}C\cdot\gamma. \quad (9)$$

Then, using the equations 8-9, 3D and planar images of $\alpha_{(Si(alloy)}=f(C,\ \gamma)$ and $C_{Si(alloy)}=f(C,\ \gamma)$ were constructed, shown in Figures 2-3.

It follows from Figure 2 that the minimum silicon extraction degree in the alloy is 45%, and the maximum is 82.8%. $\alpha_{(Si(alloy)}$ from 75 to 82.8% occurs in the presence of 15.0-33% of coke and 14.8-99.6% of γ, $\alpha_{(Si(alloy)}$ from 80 up to 82.3% occurs in the presence of 22.6-33% of coke and 31.5-81.0% of γ. At a constant value of γ, an increase in the amount of coke increases the silicon extraction in the alloy. The silicon concentration in the alloy varies from 30 to 44.2%. Moreover, the formation of FeSi45 grade ferrosilicon (41-44.7% of Si) occurs in the presence of 26.8-33% of coke and 19.4-97.2% of γ. At a constant value of γ, an increase in the amount of coke increases the silicon concentration in the alloy. The low silicon extraction degree in the alloy in the

absence of steel cuttings is associated with the foam formation during the magnetite reduction.

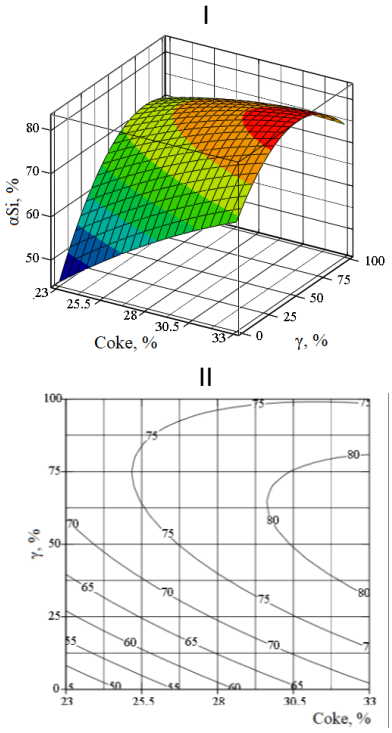

Image: I – 3D, II – planar

Figure 2- Effect of coke and iron replacement degree in the magnetite concentrate with iron in the steel cuttings on the silicon extraction degree in the alloy

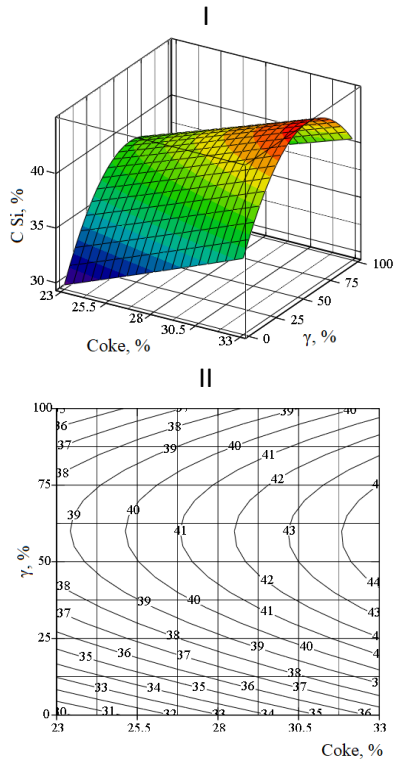

Image: I – 3D, II – planar

Figure 3- Effect of coke and iron replacement degree in the magnetite concentrate with iron in the steel cuttings on the silicon concentration in the alloy

Figure 4 shows a combined image picture of the dependence $\alpha_{(Si(alloy)}$=f(C, γ) and $C_{Si(alloy)}$=f(C, γ). Table 3 shows values of technological parameters in two areas, in the first area $C_{Si(alloy)}$=41-44.7% and $\alpha_{(Si(alloy)}$=75.1-82.6%, in the second area $\alpha_{(Si(alloy)}$=80.0-82.6% and $C_{Si(alloy)}$=42.6-44.7%.

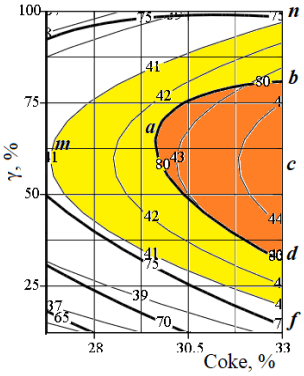

Figure 4- Combined image of the dependence $\alpha_{(Si(alloy)}$=f(C, γ) and $C_{Si(alloy)}$=f(C, γ)

Table 3- Values of technological parameters at the boundary points of two areas: 1 – with $C_{Si(alloy)}$≥91.0% and 2 – with $\alpha_{(Si(alloy)}$≥80%

Point in Figure 4	Technological parameters			
	Coke, %	*γ, %*	*$\alpha_{(Si(alloy)}$, %*	*$C_{Si(alloy)}$, %*
a	29.6	71.3	80.0	42.6
b	33.0	81.0	80.0	43.3
c	33.0	56.6	82.3	44.7
d	33.0	31.5	80.0	43.0
m	26.8	62.5	75.8	41.0
n	33.0	97.2	75.1	41.0
f	33.0	19.4	75.7	41.0

Figure 5 shows photos of ferroalloys smelted from ore and tailing mixtures with varying degrees of iron replacement in magnetite concentrate with iron in steel cuttings.

I – 33% of coke, γ=20.0%; II – 28.5% of coke, γ=75%

Figure 5- Photos of smelted ferroalloys

Figure 6 shows the SEM analysis of the alloy at γ=20%; Figure 7 shows the sublimates collected on the electric holder.

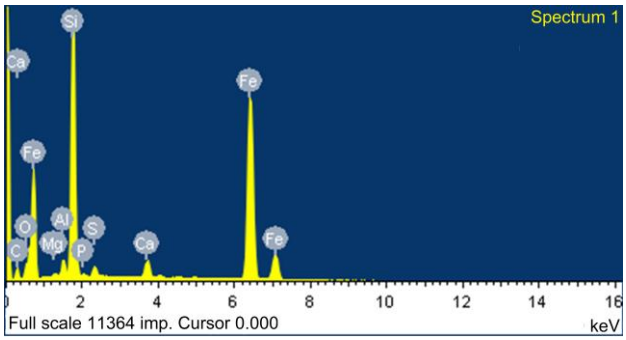

Element	Si	Fe	Al	Mg	P	S	Ca	O	C
Content, %	41.28	47.82	2.40	0.24	0.25	1.02	1.91	3.95	1.13

Figure 6- SEM analysis of the alloy

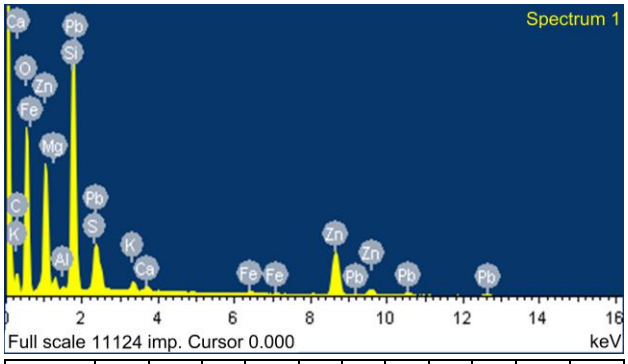

Element	Zn	Pb	Fe	Si	S	Ca	K	Al	Mg	C	O
Content, %	25.2	11.7	0.4	12.1	1.1	0.4	0.7	0.1	1.1	16.5	30.7

Figure 7- SEM analysis of the sublimates

The alloy containing 41.28% of silicon does not contain zinc or lead. In terms of silicon content, the alloy can be classified as FeSi45 grade ferrosilicon [33]. In the sublimates, into which 98.8% of Zn and 97.8% of Pb pass, the zinc content was 25.2% and the lead content was 11.7%. That is, the sublimates are a polymetallic concentrate, in which the zinc content is 8.1 times higher than in the base mixture, and the ∑ Zn and Pb is 9.4 times higher.

Conclusions

Based on the results obtained during the electric smelting of the mixture of ore and beneficiation tailings with coke, magnetite concentrate, and steel cuttings, the following conclusions can be drawn:

A high (75-82.8%) degree of silicon extraction in the alloy occurs when the mixture is smelted in the presence of 15-33% of coke and with 14.6-91.9% of iron replacement in the magnetite concentrate with iron in the steel cuttings.

The silicon concentration in the alloy varies from 30 to 44.2%. Moreover, the formation of FeSi45 grade ferrosilicon (41-44.7% of Si) occurs in the presence of 26.8-33% of coke and 19.4-97.2% of γ.

The main part of zinc (98.8%) and lead (97.81%) is extracted from the mixture into the sublimates, which contain 25.2% of Zn and 11.7% of Pb. The zinc concentration in the sublimates is 8.1 times higher than that in the base mixture, the zinc and lead sum concentration is 9.4 times higher.

Conflicts of interest. On behalf of all authors, the corresponding author states that there is no conflict of interest.

CRediT author statement: **V. Shevko:** Conceptualization, Formal Analysis, Software, Methodology, Investigation, Writing – original draft; **B. Makhambetova:** Project administration, Investigation, Writing – original draft; **D. Aitkulov:** Validation, Resources, Funding Acquisition, Writing – review & editing; **A. Badikova:** Investigation, Visualization, Writing – review & editing.

Acknowledgements. The research is funded by the Industry Committee of the Ministry of Industry and Construction of the Republic of Kazakhstan (Grant no. BR19777171).

Cite this article as: Shevko VM, Makhambetova BA, Aitkulov DK, Badikova AD. Optimization of joint electric smelting of Shalkiya sulfide ore and its concentration tailings to produce medium-silicon ferrosilicon. Kompleksnoe Ispolzovanie Mineralnogo Syra = Complex Use of Mineral Resources. 2025; 334(3):91-98. https://doi.org/10.31643/2025/6445.31

Орташа кремнийлі ферросилиций алу үшін Шалқия сульфидті кені мен оның байыту қалдықтарын біріктіріп электрмен балқытуды оңтайландыру

[1] Шевко В.М., [1] Маханбетова Б.А., [2]Айткулов Д.К., [1] Бадикова А.

[1] М.Әуезов атындағы Оңтүстік Қазақстан университеті, Шымкент, Қазақстан
[2] Қазақстан Республикасының минералдық шикізатты кешенді қайта өңдеу жөніндегі ұлттық орталығы, Алматы, Қазақстан

Мақала келді: *22 мамыр 2024*
Сараптамадан өтті: *3 шілде 2024*
Қабылданды: *17 шілде 2024*

ТҮЙІНДЕМЕ

Құрамында 4-6% ∑ Pb және Zn бар Шалқия кен орнының сульфидті жоғары кремнийлі кенін флотациялық байыту барысында <80% мырыш пен <60% қорғасынды концентратын алу тиімсіз және 1 тонна кенге шаққанда 0,93 т-ға дейін қалдық түзіледі. Мақалада Шалқия кенінің электрлік балқыту қоспасын және оны байыту қалдықтарын кокс, болат үгінділері және сульфидтерді тотықтырғыш және темір жеткізуші қызметін атқаратын магнетит концентратының қатысуымен өңдеудің тәжірибелік зерттеулерінің нәтижелері берілген. Тәжірибелерді жоспарлау және оларды оңтайландыру әдісін қолдана отырып, кремнийдің қорытпаға алынуына кокстың әсері және магнетит концентратындағы темірді болат үгінділеріндегі темірмен алмастыру дәрежесі және ондағы осы элементтің құрамы зерттелді. Қоспадан кремнийдің 75-тен 82,8%-ға дейін кремнийі бар қорытпаға алынатыны анықталды. Қорытпадағы кремний мөлшері 30-дан 44,2%-ға дейін өзгерді. Құрамында 41-47,7% кремнийі бар FeSi45 маркалы ферросилицийдің түзілуі 26,8-33,0% кокс қатысында және 1:1 кен мен оның байытылған қалдық қоспасын балқытқанда және магнетит концентратының темірін болат үгінділерімен 19,4-тен 97%-ға дейін алмастырғанда пайда болады. Электрлік балқыту кезінде түзілетін возгондар құрамында 25,2% Zn және 11,7% Pb болады. Олар бастапқы қоспамен салыстырғанда ∑Zn және Pb-ға 9,4 есе бай.

Түйін сөздер: сульфидті кен, байыту қалдықтары, қорғасын-мырыш кені, электрлік балқыту, мырыш возгоны, ферросилиций.

Шевко Виктор Михайлович — *Авторлар туралы ақпарат:* *Техника ғылымдарының докторы, Силикат технологиясы және металлургия кафедрасының профессоры, М.Әуезов атындағы Оңтүстік Қазақстан университеті, Тәуке хан даңғылы, 5, 160002. Шымкент, Қазақстан. E-mail: shevkovm@mail.ru*

Маханбетова Бактыгул Алимжановна — *Силикат технологиясы және металлургия кафедрасының докторанты, М.Әуезов атындағы Оңтүстік Қазақстан университеті, Тәуке хан даңғылы, 5, 160002. Шымкент, Қазақстан. E-mail: mahanbetova@bk.ru*

Айткулов Досмурат Кызылбиевич — *Техника ғылымдарының докторы, профессор, Қазақстан Республикасының минералдық шикізатты кешенді қайта өңдеу жөніндегі ұлттық ғылыми-зерттеу орталығының ғылыми жетекшісі, Жандосов көш., 67, 050036, Алматы, Қазақстан.E-mail: aitkulov_dk@mail.ru*

Бадикова Александра Дмитриевна — *Силикат технологиясы және металлургия кафедрасының докторанты, М.Әуезов атындағы Оңтүстік Қазақстан университеті, Тәуке хан даңғылы, 5, 160002. Шымкент, Қазақстан. E-mail: sunstroke_91@mail.ru*

Оптимизация совместной электроплавки сульфидной руды Шалкия и хвостов ее обогащения с получением среднекремнистого ферросилиция

[1] Шевко В.М., [1] Маханбетова Б.А., [2]Айткулов Д.К., [1] Бадикова А.

[1] Южно-Казахстанский университет имени М. Ауэзова, Шымкент, Казахстан
[2] Национальный центр по комплексной переработки минерального сырья Республики Казахстан, Алматы, Казахстан

Поступила: *22 мая 2024*
Рецензирование: *3 июля 2024*
Принята в печать: *17 июля 2024*

АННОТАЦИЯ

Флотационное обогащение сульфидной высококремнистой руды месторождения Шалкия, содержащей 4-6% ∑ Pb и Zn происходит не эффективно с извлечением в концентрат <80% цинка и <60% свинца и образованием на 1 т руды до 0,93 т хвостов. В статье приводятся результаты экспериментальных исследований переработки электроплавкой смеси руды Шалкия и хвостов ее обогащения в присутствии кокса, стальной стружки и магнетитового концентрата, выполняющего роль окислителя сульфидов и поставщика железа. Методом планирования экспериментов и их оптимизацией исследовано влияние кокса и степени замены железа магнетитового концентрата на железо стальной стружки на извлечение кремния в сплав и содержание в нем этого элемента. Установлено, что из смеси в кремнийсодержащий сплав извлекается от 75 до 82,8% кремния. Содержание кремния в сплав изменяется от 30 до 44,2 %. Образование ферросилиция марки FeSi45, содержащего 41-47,7% кремния происходит при плавке смеси руды и хвостов с отношением 1:1 в присутствии 26,8-33,0% кокса и заменой железа магнетитового концентрата на железо стальной стружки от 19,4 до 97%. Возгоны, образованные при электроплавке содержат 25,2% Zn и 11,7% Pb. Они богаче по ∑Zn и Pb в сравнении с исходной смесью в 9,4 раза.

	Ключевые слова: сульфидная руда, хвосты обогащения, свинцово-цинковая руда, электроплавка, цинковые возгоны, ферросилиций.
Шевко Виктор Михайлович	***Информация об авторах:*** *Доктор технических наук, профессор кафедры Технологии силикатов и металлургия, Южно-Казахстанского университета имени М. Ауэзова, проспект Тауке Хана, 5, 160002, Шымкент, Казахстан. Email: shevkovm@mail.ru*
Маханбетова Бактыгул Алимжановна	*Докторант кафедры Технологии силикатов и металлургия, Южно-Казахстанский университет им. М. Ауэзова, проспект Тауке хана, 5, 160002, Шымкент, Казахстан. E-mail: mahanbetova@bk.ru*
Айткулов Досмурат Кызылбиевич	*Доктор технических наук, профессор, научный руководитель Национального центра комплексной переработки минерального сырья Республики Казахстан, Жандосова, 67 050036, Алматы, Казахстан. E-mail: aitkulov_dk@mail.ru*
Бадикова Александра Дмитриевна	*Докторант кафедры Технологии силикатов и металлургия, Южно-Казахстанский университет им. М. Ауэзова, проспект Тауке хана, 5, 160002, Шымкент, Казахстан. E-mail: sunstroke_91@mail.ru*

References

[1] Tau-Ken Samruk. Shalkiya field (Electron resource) 2021. URL: https://tks.kz/mestorozhdenie-shalkiya/

[2] Yushina TI, Yergeshev AR, Dumov AM, Makavetskas AR. Study of the material composition of lead-zinc ore of the Shalkiya deposit in order to determine the possibility of its processing. Non-ferrous Metals. 2022; 53(2):8–14. https://doi.org/10.17580/nfm.2022.02.02

[3] Abuov MG, Freidin AM, Shalaurov VA. Technology for mining Shalkiya lead-zinc ore deposit. Journal of Mining Science. 1995; 31(3):208-215. https://doi.org/10.1007/bf02047670

[4] Chepushtanova T, Motovilov I, Merkibayev Y, Polyakov K, Gostu S. Flotation studies of the middling product of lead-zinc ores with preliminary sulfidizing roasting of oxidized lead and zinc compounds. Kompleksnoe Ispolzovanie Mineralnogo Syra = Complex Use of Mineral Resources. 2022; 323(4):77-83. https://doi.org/10.31643/2022/6445.43

[5] Tusupbayev NK, Kalugin SN, Tusupbayev SN, Semushkina LV, Turysbekov DK, Mukhanova AA, Mukhamedilova AM.Primeneniye modifitsirovannykh reagentov dlya usovershenstvovaniya tekhnologii flotatsionnogo obogashcheniya tonkovkraplennykh polimetallicheskikh rud [Application of modified reagents to improve flotation technology enrichment of finely disseminated polymetallic ores]. Kompleksnoe Ispolzovanie Mineralnogo Syra = Complex Use of Mineral Resources. 2013; 4:19-24. (in Russ.).

[6] Yessengaziyev A, Kenzhaliyev B, Berkinbayeva A, Sharipov R, Suleimenov E. Electrochemical extraction of Pb and Zn from a collective concentrate using a sulfur-graphite electrode as a cathode. Journal of Chemical Technology and Metallurgy. 2017; 52(5):975-980.

[7] Motovilov IY, Telkov SA, Barmenshinova MB, Nurmanova AN. Examination of the preliminary gravity dressing influence on the shalkiya deposit complex ore. Non-ferrous Metals. 2019; 47(2):3–8. https://doi.org/10.17580/nfm.2019.02.01

[8] Ubaydullayev AU. Tekhnologiya pererabotki kollektivnykh svintsovo-tsinkovykh kontsentratov [Technology for processing collective lead-zinc concentrates]. Tekhnicheskiye nauki: teoriya i praktika: materialy IV Mezhdunar. nauch. konf [Technical sciences: theory and practice: materials of the IV International. scientific conf]. Kazan, Russia. 2018, 36-38. (in Russ.).

[9] Moradi S, Monhemius J. Mixed sulphide–oxide lead and zinc ores: Problems and solutions. Minerals Engineering - MINER ENG. 2011; 24:1062-1076. https://doi.org/10.1016/j.mineng.2011.05.014

[10] Soltani F, Darabi H, Aram R, Ghadiri M. Leaching and solvent extraction purification of zinc from Mehdiabad complex oxide ore. Sci Rep. 2021; 11(1):1566. https://doi.org/10.1038/s41598-021-81141-7

[11] Tombal TD, Kurşun İ. Investigation of Zn recovery from Balıkesir Balya Pb-Zn ore by hydrometallurgical methods. Journal of the Faculty of Engineering and Architecture of Gazi University. 2024; 39(3):1541-1553. https://doi.org/10.17341/gazimmfd.1183600

[12] Krylova LN. Efficiency of Ozone Application for Extraction of Metals from Mineral Raw Materials. Russian Journal of Non-Ferrous Metals. 2022; 63(3):247-255. https://doi.org/10.3103/S1067821222030087

[13] Magdy Abdo D, Nasr El-Shazly A, Adel Hamza M. Effect of acidic and basic leachants on the synthesis of ZnO nanoparticles from Egyptian zinc ore, their optical/surface characteristics and photocatalytic performance. Materials Letters. 2024; 364:136377. https://doi.org/10.1016/j.matlet.2024.136377

[14] Li G, Zhang Z, Wei Q, Jiao F, Yang C, Li W, Qin W. Study on flotation recovery of typical carbon-bearing lead-zinc sulphide ore in Guizhou with pre-decarbonization. Geochemistry. 2024; 84(2):126096. https://doi.org/10.1016/j.chemer.2024.126096

[15] Chepushtanova T, Merkibayev Y, Mamyrbayeva K, Sarsenbekov T, Mishra B. Mechanism and technological results of sulfidation roasting of oxidized lead compounds. Kompleksnoe Ispolzovanie Mineralnogo Syra = Complex Use of Mineral Resources. 2024; 332(1):119-132. https://doi.org/10.31643/2025/6445.11

[16] Tusupbayev NK, Turysbekov DK, Semushkina LV, Mukhanova AA, Satylganova SB. Primeneniye modifitsirovannogo aeroflota i teplovogo rezhima pri flotatsii svintsovo-tsinkovykh rud mestorozhdeniya Shalkiya [Application of modified aeroflot and thermal regime in the flotation of lead-zinc ores of the Shalkiya deposit]. Kompleksnoe Ispolzovanie Mineralnogo Syra = Complex Use of Mineral Resources. 2014; 3:3-10. (in Russ.).

[17] Sharipov RK, Balgimbaeva UA, Suleimenov EN. Electrochemical Extraction of Pb and Zn from Raw Mineral Materials Using Sulfurgraphite Electrode. Minerals, Metals and Materials Series. 2020, 429-435. https://doi.org/10.1007/978-3-030-37070-1_37

[18] Semushkina L, Dulatbek T, Tusupbaev N, Nuraly B, Mukhanova A. The Shalkiya deposit finely disseminated lead-zinc ore processing technology improvement. Obogashchenie Rud. 2015; 2:8-14. https://doi.org/10.17580/or.2015.02.02

[19] Telkov ShA, Motovilov ITu, Barmenshinova MB, Abisheva ZS. Study of gravity-flotation concentration of lead-zinc ore at the Shalkiya deposit. Obogashchenie Rud. 2021; 6:9-15. https://doi.org/10.17580/or.2021.06.02

[20] Cheng L. Development of lead-zinc smelting technology in China. World of Metallurgy – ERZMETALL. 2017; 70(4):203-213.

[21] Fuls HF, Petersen J. Evaluation of processing options for the treatment of zinc sulphide concentrates at Skorpion Zinc. Journal of the Southern African Institute of Mining and Metallurgy. 2013; 113(5):423-434.

[22] Yang K, Sun Ch, Qu H, Shuo L, Luo Y, Zhang L, Ma A. Recovery of Zinc from Oxide-Sulphide Zinc Ore Through Oxidation and Chelation. In: Materials Engineering—From Ideas to Practice: An EPD Symposium in Honor of Jiann-Yang Hwang. The Minerals, Metals & Materials Series. Springer, Cham. 2021. https://doi.org/10.1007/978-3-030-65241-8_15

[23] Onukwuli OD, Nnanwube IA. Optimization of Zinc Recovery from Sphalerite Using Response Surface Methodology and Particle Swarm Optimization. Periodica Polytechnica Chemical Engineering. 2022; 66(1):20-29. https://doi.org/10.3311/PPch.17897

[24] Mütevellioğlu NA, Yekeler M. Beneficiation of Oxidized Lead-Zinc Ores by Flotation Using Different Chemicals and Test Conditions. Journal of Mining Science. 2019; 55:327-332. https://doi.org/10.1134/S1062739119025623

[25] Semushkina LV, Turysbekov DK, Mukhanova AA, Narbekova SM, Mukhamedilova AM. Pererabotka khvostov flotatsii rud kazakhstanskikh mestorozhdeniy s primeneniyem modifitsirovannogo flotoreagenta [Processing of ore flotation tailings from Kazakhstan deposits using a modified flotation reagent]. Kompleksnoe Ispolzovanie Mineralnogo Syra = Complex Use of Mineral Resources. 2018 ;1:3-11. (in Russ.).

[26] Shalkiya Mine Expansion Project. (Electron resource) 2021. (in Russ.). https://www.ebrd.com/documents/environment/48347-esmp-russian.pdf

[27] Pat. 36683 KZ. Sposob pererabotki vysokokremnistykh sul'fidnykh svintsovo – tsinkovykh rud [Method for processing high-silicon sulfide lead-zinc ores] Zharmenov AA, Abykaev N A, Shevko VM, Shkolnik VS, Aitkulov DK, Satkaliyev AM, Terlikbaeva AZ, Baisanov SO, Makhanbetova BA, Iskakov BO. Opubl. 05.04.2024, 14 (in Russ.).

[28] Roine A. HSC Chemistry, Metso:Outotec, Pori. (Electron resource) 2021. www.mogroup.com/hsc

[29] Shevko V, Makhanbetova B, Aitkulov D. Theoretical and experimental substantiation of obtaining an alloy from flotation tailings of lead-zinc sulfide ore. Physicochemical Problems of Mineral Processing. 2023; 59(1):161853. https://doi.org/10.37190/ppmp/161853

[30] State standard 13230 1-93. Ferrosilitsiy. Metody opredeleniya kremniya [Ferrosilicon. Methods for determining silicon] Minsk. 2021, 8 (in Russ.).

[31] Inkov AM, Tapalov T, Umbetov UU, Hu Wen Tsen V, Akhmetova KT, Dyakova ET. Metody optimizatsii: elektronnaya kniga [Optimization methods: e-book]. Shymkent: SKSU. 2003. (in Russ.).

[32] Akhnazarova SA, Kafarov BV. Metody optimizatsii eksperimenta v khimicheskoy promyshlennosti [Methods for optimizing experiments in the chemical industry]. Moscow: Higher School. 1978, 319. (in Russ.).

[33] State standard 1415-93. Ferrosilitsiy. Tekhnicheskiye trebovaniya i usloviya postavki [Ferrosilicon. Technical requirements and delivery conditions]. Moscow: Standartinform. 2011, 14. (in Russ.).

Crossref

DOI: 10.31643/2025/6445.32
Metallurgy

Development of an Enhanced Method for Copper Extraction from Sulfuric Acid Solutions

[1]Chepushtanova T.A., [1]Yessirkegenov M.I., [2]Nikoloski A. [*1]Merkibayev Y.S., [1] Altmyshbayeva A.Zh.

[1]Satbayev University, Almaty, Kazakhstan
[2]University of Murdoch, Australia

** Corresponding author email: y.merkibayev@satbayev.university*

Received: *May 29, 2024*
Peer-reviewed: *June 17, 2024*
Accepted: *August 9, 2024*

ABSTRACT

The paper presents a method for the extraction of copper from sulfuric acid solutions, which reduces the consumption of sulfuric acid, increases the extraction of copper and the quality of cathode copper, and reduces the undesirable formation of the third-phase crud. The main results of copper extraction, including 2-3 stepwise extraction of copper, are presented. The extraction is carried out by mixing sulfuric acid solutions with a solution of a chelating, selective extractant of the aldoxime group (10 vol.%) and separating the mixture by settling to obtain a copper-containing extract and extraction raffinate, with the suppression of the third phase-crud due to the dissolution of polymerized silicon bonds in the cruds with a monomeric polymer (H2C═CHC6H4SO3Na)n poly(4-sodium styrene sulfonate). This is achieved by adding 5 cm^3 of the polymer, influenced by the surfactant complex of sodium alkyl sulfonate, with an O/A ratio of 1:2 and a temperature of 20±5°C. Subsequent re-extraction of copper from the extract is carried out by mixing the extract with a sulfuric acid solution and separating the mixture by settling to obtain a copper-containing re-extraction and an extractant solution. The re-extract is purified from impurities, and copper is extracted electrically from the purified re-extract to obtain cathode copper and waste electrolyte. A method for calculating the technical and economic choice of an extraction apparatus has also been developed.

Keywords: SX-EW; copper; solvent extraction; crud, intensifying method; sulfuric acid solutions

Information about authors:

Chepushtanova Tatyana Aexandrovna — *Candidate of Technical Sciences, PhD, Head of Department Metallurgical processes, heat engineering and technology of special materials, Associate Professor, Mining and Metallurgical Institute, Satbayev University, Almaty, Kazakhstan. Email: T.Chepushtanova@satbayev.university*

Yessirkegenov Meirbek Ibragimovich — *Master's degree, PhD student of the Head of Department Metallurgical Processes, Heat Engineering and Technology of Special Materials, Mining and Metallurgical Institute, Satbayev University, Almaty, Kazakhstan. Email: m.yessirkegenov@satbayev.university*

Nikoloski Aleksandar — *Professor of University of Murdoch, Australia. Email: A.Nikoloski@murdoch.edu.au*

Merkibayev Yerik Serikovich — *PhD, head of laboratories of the Head of Department Metallurgical Processes, Heat Engineering and Technology of Special Materials, Mining and Metallurgical Institute, Satbayev University, Almaty, Kazakhstan. Email: y.merkibayev@satbayev.university*

Altmyshbayeva Aliya — *Senior Lecturer, мaster's degree of the Head of Department Metallurgical Processes, Heat Engineering and Technology of Special Materials, Mining and Metallurgical Institute, Satbayev University, Almaty, Kazakhstan. Email: a.altmyshbayev@satbayev.university*

Introduction

Today, producing energy from renewable sources requires significantly more copper than producing energy from traditional sources. For example, an offshore wind farm may require five times more copper than a coal-fired power plant. Copper is also used in the manufacture of wind turbine cables to connect elements of complex installations (particularly deep-sea cables) and to transmit power to shore. Increasing demand from renewable energy sources, which require large amounts of copper, is driving the development of new technologies and the intensification of existing copper extraction technologies. KAZ Minerals Group achieved record copper production of 403 kt in 2023, up 6% from 2022, driven by increased production at Aktogay following the launch of its second world-class sulphide concentrator in 2022. Management's constant focus on operational

improvement resulted in all ore processing plants exceeding design capacity throughout the year.

Methods that solve the problem of intensifying the extraction process and reducing the consumption of reagents are relevant. There is a method for the extraction of copper from sulfuric acid solutions, which includes extraction by mixing sulfuric acid solutions with a solution of a cation-exchange organic selective extractant and subsequent separation of the mixture by settling to obtain a copper soda hot extract and raffinate extraction [1]. The process is characterized by the formation of three phases: raffinate, extract, and the third phase - crud, which is concentrated in the extract as a separate phase. Re-extraction of copper from the extract is carried out by mixing the extract with a solution of sulfuric acid, followed by separation of the mixture by settling to obtain a copper-containing re-extraction and extractant solution. The re-extract is then purified by flotation with subsequent filtration or coalescence, and copper is electroextracted from the purified re-extract to obtain copper cathode and spent electrolyte. The spent electrolyte is used for copper re-extraction.

The technical result is a reduction in sulfuric acid consumption, increased copper extraction, reduced copper losses with waste solutions, and improved quality of copper cathode. The disadvantage of this method is that it does not provide for the suppression or reduction of the third phase - crud, containing various types of impurities, with silicon as the main component at 17.58% and above. This reduces the extraction of copper and affects the quality of commercial copper during electroextraction due to the use of the extractant LIX 984N, a ketoxime derived from a ketone. In the IR spectrum of this extractant, there are bands of stretching vibrations of C-H aliphatic hydrocarbons at 2957, 2926, 2871, 2856 cm-1, deformation vibrations of aliphatic hydrocarbons δ(CH3), δ(CH2) at 1464, 1378 cm-1, and stretching vibration ν(OH) at 3374 cm-1, aimed specifically at selectivity for copper rather than other metals in the liquid phase.

The interaction in the D2EHPA - $In2(SO_4)_3$ - $Fe_2(SO_4)_3$ - $Ti2(SO_4)_3$ - $ZnSO_4$ - H_2O system was studied, showing that the basis of cruds is the salt InR3, resulting from the secondary interaction of indium ions in solution with compounds formed in the extract [[2], [3]]. The formation of interphase suspensions containing osmium during the extraction of rhenium from acid wash solutions in copper production was examined. Secondary interaction of salts with compounds formed in the extract also occurs when the extractant contains iron and titanium [4], [[5], [6], [7]], [[8], [9], [10], [11], [12]]. This interaction greatly contributes to crud formation in the raffinate when in contact with the original indium-containing solution.

Methods for selecting extractants of the ACORGA class are discussed in works considering the suppression of iron and silicon impurities [[13], [14], [15], [16], [17]]. These works propose mechanisms for silicon polymerization, albeit with different initial solution compositions and preparation histories than those considered in the present study.

Let's consider the factors influencing the efficiency of extractors. The operation of the extraction apparatus depends on many technological parameters, controlled and uncontrolled. To carry out the process under optimal conditions, it is necessary to determine the values of the controlled parameters at which, considering the existing limitations, the most advantageous technological regime would be ensured. The efficiency of the extraction apparatus is influenced not only by the mode of the process carried out in it but also by the correct choice of the structural type of the apparatus itself, which contributes to the achievement of the specified technological parameters [18].

Continuous action devices are subject to various requirements, the main ones being: 1) maximum productivity and work intensity; 2) low energy consumption during operation; 3) high degree of extraction of valuable components; 4) simplicity of the device and low cost of production; 5) ease of control and automatic regulation. Currently, devices of mainly two types are used in practice: periodic and continuous, and the use of continuous devices is more effective due to their greater productivity and the possibility of automated control of their operation. Batch-type devices are usually used in industries with small volumes of reacting phase flows [[19], [20], [21], [22]].

The operation of extraction equipment is characterized by a close relationship between its productivity, quality, and the cost of the products produced since the cost depends on the optimal time for the actual residence of the raw materials in the apparatus. If raw materials are unjustifiably delayed in the devices, the overall productivity of the equipment decreases, the cost of production increases, and in some cases, the quality of the

products may decrease. An unjustified reduction in the residence time of raw materials in devices, although it increases the overall productivity of the equipment, reduces the efficiency of using raw materials and the volume of the device, and also leads to a deterioration in product quality [[23], [24]].

Thus, when choosing the type of continuous extractor, it is necessary, first of all, to consider the residence time of the phase flows in the apparatus to achieve the specified economic efficiency of the process being carried out. Having information about the residence time of flow elements in the apparatus, it is possible to assess the operating efficiency of the apparatus itself, i.e., determine the proportion of the apparatus volume occupied by particles kept in the apparatus for a given time interval, the value of which was determined earlier in the process of laboratory or pilot-scale tests in periodic devices.

The purpose of the research was to develop a method for intensifying the extraction of copper from sulfuric acid solutions of the Aktogay deposit and to develop a technique for the technical and economic assessment of the choice of extraction apparatus.

Materials and Methods

The research focused on investigating copper extraction processes using different extractants. The main object of study was a productive copper-containing sulfate solution, commonly referred to as PLS (Pregnant Leach Solution). This solution was obtained through processing ore derived from the Aktogay deposit, with a solution pH of approximately 1.7.

Methods of Analysis: Analytical methods were employed to analyze the samples in this study. The quantitative determination of major elements in brines was conducted using an Optima 8300DV inductively coupled plasma atomic emission spectrometer and a PFP 7 flame photometer (Jenway, England).

Infrared absorption spectra were recorded using an Avatar 370 IR-Fourier spectrometer across the range of 400 - 4000 cm-1 from capillary layers in KRS-5 windows. The experimental setup included the “Transmission E.S.P.” attachment. Data processing was performed using OMNIC 6 software, along with electronic libraries including HR Aldrich FT-IR Collection Edition II (containing 18,454 spectra) and Aldrich Organometallic, Inorganic, Boron, Deuterium Compounds (consisting of 632 spectra) published by Nicolet Instrument Corp. in 1995. In cases where information was not available in the electronic libraries, literary sources were consulted.

X-ray fluorescence analysis was carried out using an Axios PANalytical wavelength dispersive spectrometer (Netherlands). X-ray phase analysis was performed using a D8 ADVANCE diffractometer (BRUKER AXS GmbH, Germany) equipped with Cu Kα radiation, a tube voltage of 40 kV, and a current of 40 mA. Data processing of the obtained diffraction patterns and calculation of interplanar distances were accomplished using EVA software. Sample interpretation and phase identification were achieved using the Search/Match program, utilizing the PDF-2 database from the International Center for Diffraction Data (ICDD, USA).

Extraction Experiment Procedure: Extraction experiments were conducted under controlled room temperature conditions of 20 ± 5°C. Temperature stability was ensured using a LOIP-105A thermostat. The investigation focused on studying the volume ratio of the organic and aqueous phases, ranging from 1:2 to 1:10 with a step size of 2. The contact time between phases was determined based on the time-dependent behaviour of the copper distribution coefficient (DCu), set at 5 minutes. The extraction process was carried out in conventional separatory funnels, followed by phase separation through settling. Aqueous solutions were filtered through a designated paper filter labelled "red ribbon" before sampling for analysis. Mechanical mixing was employed to achieve homogenization of the phases. Depending on the experimental objectives, the resulting solutions were analyzed for their copper content.

Materials. The results of the chemical analysis of a sample of the productive solution are presented in Table 1.

Table 1 – Chemical composition of the initial solution, g/dm^3

Cu	Fe	Mo	Mn	Zn	Al	Ca	Mg
1.25	4.23	-	1.47	0.16	29.10	0.69	12.98
Si	Co	Ni	Cr	Cd	P	Pb	H_2SO_4
0.51	0.033	0.007	0.002	0.0017	0.55	0.02	2.22

As shown in Table 1, the concentration of copper in the solution is 1.25 g/dm³, while sulfuric acid has a concentration of 2.22 g/dm³. The concentrations

of aluminum, magnesium, total iron, calcium, and phosphorus are 29.1, 12.98, 4.23, 0.69, and 0.55 g/dm³, respectively. Silicon is also present in the solution with a concentration of 0.51 g/dm³. Other elements in the solution have relatively low levels.

To determine the composition of the solid residue obtained after evaporating the sulfuric acid solution to wet salts, X-ray fluorescence analysis (XRF) was performed. Table 2 presents the results of the XRF analysis of the solid residue.

Table 2 - Content of elements in solid residue

Element	Content, %	Element	Content, %
O	59.394	Ti	0.067
Na	0.346	V	0.008
Mg	3.818	Mn	0.386
Al	4.883	Fe	5.048
Si	0.304	Co	0.014
P	0.296	Ni	0.016
S	14.984	Cu	0.746
Cl	0.263	Zn	0.073
K	0.019	Y	0.004
Ca	0.114	Th	0.013

According to Table 2, the residue contains significant amounts of aluminum (4.9%), magnesium (3.8%), and iron (5.1%). The sulfur content is approximately 15%, which can be attributed to the presence of metal sulfates in the solution. The presence of the $SO4^{2-}$ group is confirmed by infrared (IR) analysis of a sample of the productive solution.

In the spectrum, absorption bands corresponding to water are observed at wave numbers of ν(OH) 3368 cm^{-1} and δ(HOH) 1647 cm^{-1}. The presence of the $SO4^{2-}$ group is evidenced by absorption bands at wave numbers 1108, 979, 671, and 620 cm^{-1}. The band with a peak at a wave number of 698 cm-1 corresponds to the manifestation of deformation vibrations of Me-O-H.

Based on the results obtained from chemical, infrared spectroscopic, and X-ray fluorescence (XRF) analyses, it can be concluded that the productive solution contains silicates of aluminum, magnesium, iron, and calcium, in addition to sulfates. These silicates are the primary components responsible for the formation of impurities. However, the solid residue has a relatively low silicon content of approximately 0.3%. This suggests that insoluble hydroxides, such as $Al(OH)_3$ and $Fe(OH)_3$, which are generated through the hydrolysis of metal salts in the original sulfuric acid solution, may also contribute to the presence of impurities.

To further investigate the process and optimize the extraction of copper, different classes of extractants were tested, including ketoximes (derivatives of ketones) and aldoximes (derivatives of aldehydes). The goal was to identify the most effective extractant for suppressing the formation of copper during the extraction process.

Results

Selecting an Extractant to Reduce Crud Formation During the Extraction of Copper from Sulfuric Acid Solutions.

The copper extraction method is carried out from leaching solutions of oxidized, sulfide, or sulfide-oxidized copper ore or flotation copper concentrate, derived from productive solutions obtained after percolation leaching. At least 5 dm³ of a representative batch of the productive solution is filtered, with a solution pH of approximately 1.7. Purified solutions are collected in a separate container to study their chemical and material composition and conduct further research.

The copper concentration in the solution was 1.25 g/dm³ or less, and sulfuric acid was 2.22 g/dm³. The concentrations of aluminum, magnesium, total iron, calcium, and phosphorus are 29.1, 12.98, 4.23, 0.69, and 0.55 g/dm³, respectively. In addition to these elements, silicon is also present in the solution at a concentration of 0.51 g/dm³. The remaining elements have relatively low content.

The productive solution contained, in addition to sulfates, silicates of aluminum, magnesium, iron, and calcium. Silicates are the main crud-forming components. The silicon content in the solid residue can be approximately 0.3%. Therefore, the crud-forming components can also be insoluble hydroxides $Al(OH)_3$ and $Fe(OH)_3$, which are formed in the original sulfuric acid solution due to the hydrolysis of salts of these metals.

The choice of extractant during the extraction process largely depends on its extraction ability and the initial concentration of the metal in the process solutions. Other important parameters for the effective operation of extraction technology are the low solubility of the extractant in the aqueous phase, its chemical stability under operating conditions, which ensures low losses of the

extractant, the possession of acceptable values of the flash point and viscosity of the extract (to ensure effective phase separation), as well as the commercial availability of reagents.

Extraction is carried out at room temperature (20 ± 5°C). Temperature regulation and consistency are ensured by a thermostat (LOIP-105A). The ratio of the volumes of the organic and aqueous phases is controlled in the range of 1:2 to 1:10, with a step of 2; the phase contact time is established based on the time dependence of the copper distribution coefficient (DCu) – 5 minutes. Separatory funnels are used to carry out the extraction process. Phase separation is carried out by settling. Before sampling for analysis, aqueous solutions after extraction are filtered through a paper filter marked “red ribbon.” Mixing of the phases is carried out mechanically. Depending on the task, the resulting solutions are analyzed for copper content.

The volume ratio of extractant and diluent is 10-20% to 80-90%. Aliphatic kerosene is used as a diluent. The organic phase is a solution of 10 vol.% of the studied extractants in kerosene, previously purified.

Two classes of extractants are used as reagents for the extraction of copper from acidic leaching solutions: ketoximes and aldoximes. However, it is necessary to take into account the selectivity of elements of these extractants, as well as the formation of the third phase - crud.

The extractant used in this work is ACORGA M5774, which is a modified aldoxime (5-nonyl salicylaldoxime). A distinctive feature of the IR spectrum of the ACORGA M5774 extractant is the presence of a stretching vibration of the carbonyl group ν(C=O) – 1736, 1712 cm-1. In the range of 1400-1000 cm-1, vibrations of the C–O–H group appear. The band at a wave number of 1271 cm-1 also falls into the range of –C–N– vibrations in compounds of the type: ArNHR.

A productive sulfuric acid solution is used, containing 1.25 g/dm³ Cu and 2.22 g/dm³ H2SO4. Table 1 presents the results of the influence of the extractant ACORGA M5774 and the O/A phase ratio on the formation of cruds and the extraction of copper from the productive solution.

When extracting copper with aldoxime ACORGA M5774 from a productive solution at a phase ratio O/A = 1:2, the degree of copper extraction into the extract is approximately 67%. An increase in the O/A ratio towards the aqueous phase during extraction leads to a significant decrease in the degree of copper extraction; at O/A = 1:4, the extraction into the extract decreases to 17.44%.

Extraction is characterized by the formation of three phases: raffinate, extract, and cruds, which are concentrated in the extract as a separate phase. When using the extractant ACORGA M5774, regardless of the O/A ratio, the phases divide quickly. However, with an increase in O/A, the amount of cruds in the organic matter decreases, so at an O/A of 1:10, only a small amount of sediment is formed.

Table 3 - Effect of the extractant ACORGA M5774 and the O: A phase ratio on the formation of cruds and the extraction of copper from the productive solution

№	O: A*	Content Cu in raffinate, g/dm³	Extraction, %		Note
			raffinat	extract	
1	3	4	5	6	7
1	1:2	0.412	32.96	67.04	Extraction at O:A 1:2: the raffinate is transparent, brown in color. The organic matter contains a marsh-colored sediment. Phase separation time is 5 minutes.
2	1:4	1.032	82.56	17.44	Extraction at O: A 1:4: after filtration, the colour of the raffinate is dark brown with a greenish tint.
3	1:6	1.250	100.0	-	Extraction at O: A 1:6: after filtration, the colour of the raffinate is dark brown with a greenish tint.
4	1:8	1.250	100.0	-	Extraction at O: A 1:8: phase separation occurs quickly. The raffinate was filtered, its colour is dark green. No precipitate formed in this sample.
5	1:10	1.250	100.0	-	Extraction at O: A 1:10: phases separate well. Raffinate is brownish-greenish in colour. A precipitate is observed in the organic phase.

O: A* - ratio of organic phase to aqueous

At higher pH values, the solution turns yellow due to hydrolysis, and if the pH is above 2-3, further condensation occurs, and the formation of colloidal gels begins, eventually forming a reddish-brown precipitate of hydrated iron(III) oxide.

The content of the main components in the third phase, in percentages, is silicon 17.58%, nickel 3.13%, total iron 2.31%, aluminum 2.14%, and magnesium 2.023%. The remaining elements have relatively low content. Two compounds predominate in the crud sample: alunogen

$[Al(H_2O)_6]2(SO_4)_3$ $(H_2O)_5$ (28.3%) and quartz SiO2 (28.1%). There is a small amount of the compound nuyakasite (7.6%), a complex silicate of iron and aluminum with sodium and silicon oxide of variable composition (3.9%).

Analysis of IR spectroscopic data confirms that during the copper extraction operation, the formation of crud leads to the loss of the extractant. Thus, we can draw the following conclusion that in most cases, the main components of crud are:

Silicic acid is contained in solutions in the form of colloidal particles, which cannot be isolated even by careful filtration, and inorganic sulfates.

Solid compounds present in aqueous solutions: ore material, metal oxides and hydroxides, etc.

The next stage of extraction is to use an alternative method that helps suppress the third phase (crud) formation during the copper extraction process by adding a monomeric polymer, poly(sodium 4-styrene sulfonate), with the chemical formula $(H_2C{=}CHC_6H_4SO_3Na)n$. The sulfonate ion contains the functional group $-S(=O)_2-O-$. The general formula is RSO2O−, where R is a radical; sodium alkyl sulfonate functionally acts as a surfactant.

When this additive is used in the form of a monomeric polymer, the formation of crud in settling tanks is reduced, thereby increasing the volume available for flows of productive sulfuric acid solutions (PLS) and organics, which directly leads to an increase in plant productivity. The process of liquid extraction in the presence of silicon dioxide in PLS solutions is challenging; however, with the addition of the monomeric polymer poly(sodium 4-styrene sulfonate), stable operation of the process is observed with a pronounced decrease in the formation of the third phase.

Table 4 - Extraction of PLS solution with the addition of $(H_2C{=}CHC_6H_4SO_3Na)_n$

Name extractant	O:W	Volume of raffinate, cm^3	Volume of extract, cm^3	Concentration of Cu in raffinate, g/dm^3	Recovery, into extract, %
ACORGA M 5774	1:2	82	43	0.947	24

Table 4 presents the results of the copper extraction process in the presence of the additive (H2C═CHC6H4SO3Na)n to reduce the formation of crud. Copper extraction is carried out using the extractant ACORGA M5774 – 10 vol.% with the addition of the additive (H2C═CHC6H4SO3Na)n in an amount of 5 cm^3.

When extracting with the extractant ACORGA M5774 and the additive $(H_2C{=}CHC_6H_4SO_3Na)n$, the phases separate quickly, but the raffinates remain turbid. The raffinates are left to settle for a day and then filtered through a red ribbon filter. The resulting raffinates are pure transparent solutions, without sediment, and have a light brown colour with a yellowish tint.

The rich organic phase is filtered separately through a blue ribbon filter. Filtration proceeds quickly, and there is no sediment on the filter. The amount of sediment is sharply reduced and becomes ultradispersed.

The use of a reagent to reduce the formation of crud $(H_2C{=}CHC_6H_4SO_3Na)n$ in an amount of 5 cm^3 in a productive sulfuric acid solution before it is subjected to the liquid extraction operation leads to a significant reduction in the formation of interfacial crud.

The use of surfactants to reduce the formation of the third phase - crud - allows several problems to be solved: returning the extractant and copper-containing solution to circulation and reducing the number of cruds sent for disposal.

Thus, the optimal technological parameters of extraction with the process of reducing the formation of the third phase - crud - are as follows: ACORGA M5774 extractant is used at a concentration of 10 vol.%. Kerosene is used as a diluent. The O/A ratio is 1:2, temperature 20-25°C, process duration 5 minutes, and phase settling time 1 day. The volume of the additive $(H_2C{=}CHC_6H_4SO_3Na)n$ is 5 cm^3. The pH value of the initial solution should be between 1.5 and 3.0, which helps prevent the decomposition of the organic phase and avoids the formation of various types of precipitation that can contaminate the organic phase and prevent phase separation, reducing the technical characteristics of the process. To increase the degree of extraction, extraction and re-extraction are carried out in several stages (2-3), determined by the concentration of copper in the raffinate and extractant after extraction.

Development of a technique for technical and economic assessment of the choice of extraction apparatus.

The economic efficiency of using an extraction apparatus is determined, on the one hand, by the achieved degree of extraction of the substance, and

on the other hand, by the costs of conducting the process. To assess the economic efficiency of using this type of extraction apparatus, an optimality criterion is used, which depends on the cost per unit volume of interacting phases at the entrance to and exit from the apparatus, the compositions and volumetric flow rates, operating costs (energy costs for ensuring the movement of flows and heat exchange, costs for depreciation of equipment, labour costs, etc.). Conditional cost savings (Sc) and present income (Ip) can be used as optimality criteria. Conditional cost savings are determined using one of the following equations:

$$S_c = (C_p - C)\,Q \qquad S_c = C_p Q - (C_f + C_v)$$

$$S_c = R_{ex} C_{ex} - R_{en} C_{en} - C_t \quad (1)$$

Where,

C_p - planned cost

C - actual cost

S_c - conditional cost savings

I_p - present income

Q- quantity of product produced

C_f - fixed costs

C_v - variable costs

R_{en} - volumetric flow rates at the entrance

R_{ex} - volumetric flow rates at the exit

C_{en} - cost per unit volume of interacting phases at the entrance

C_{ex} - cost per unit volume of interacting phases at the exit

C_t - total costs associated with equipment operation

Where C_p, C planned and actual compared cost of products; Q - quantity of product produced; C_f - fixed production costs that do not depend on productivity and quality of management; C_v - variable costs determined by the productivity and quality of the technological process; R_{en}, R_{ex} - volumetric flow rates at the entrance to and exit from the apparatus; C_{en}, C_{ex} - cost per unit volume of interacting phases at the entrance to the apparatus and exit from it; C_t - total costs associated with equipment operation.

Another quantitative measure of the technical and economic effect of using an extractor is the present income, equal to the difference between the income from the sale of commercial products and the total present costs and determined per unit of output

$$I'_p = (\sum_{i=1}^{N} P_i - C_v)\mathrm{O} - \mathrm{E}C_i = (\sum_{i=1}^{N} P_i - C_v)\mathrm{O} - (C_i/P_p) \quad (2)$$

or the total present income from the release of all products

$$I'_p = \sum_{i=1}^{N} P_i O_i - C_v - \mathrm{E}C_i \quad (3)$$

Here P_i - price of 1 product: O - annual output of product i; E - standard investment efficiency ratio; C_i - capital investment; P_p - standard payback period; O - annual output of all products. The value of the reduced income is one of the most universal criteria for optimality since it indicates both the volume of production and the quality of products, as well as operating and capital costs. The maximum amount of present income is achieved at a minimum cost or present costs, or a maximum profit.

$I`_p$ - present income, equal to the difference between income from the sale of commercial products and total present costs and determined per unit of output

P_i - price of 1 product

O - annual output of product i

E - standard investment efficiency ratio

C_i - capital investment

P_p - standard payback period

Dependency (VIII.35) can be rewritten in a video

$$I'_p = (\sum_{i=1}^{N} \bar{E}_i\,(\tau) O_i \mathrm{H}_i - C_{0\Sigma})\mathrm{B}_\mathrm{o} - (C_i/P_p) \quad (4)$$

Where $\bar{E}_i\,(\tau)$- extraction; O_i. — conditional production of commercial products per unit of raw materials (with complete extraction); $C_{0\Sigma}$ costs of processing a unit of raw materials; P_o raw material productivity.

If the volume of output is strictly determined, then to carry out technical and economic calculations, you can use the average value of the reduced costs per unit of output:

$$I_p = C_v + (\frac{C_i}{\mathrm{O}P_p}) \quad (5)$$

Optimizing the process when using dependencies (VIII.33)-(VIII.37) comes down to finding the maximum of the optimality criterion I_p

when using dependency (VIII.36) and its minimum when using dependency (VIII.37).

In the case of a sufficiently low price of the obtained by-products, the reduced income can be determined by the formula:

$$I_p = P_t O - [\frac{P_r O}{E(\mathrm{i})} + C_{var} O + C_{fix}] \qquad (6)$$

where, P_r, P_t - total price per unit of raw materials and target product; C_{var} - variable costs per unit of product produced; C_{fix} - fixed costs per unit of time.

An increase in the value of Ppr can be achieved by regulating the following factors:

1) Improving the conditions of the process (with unchanged installation productivity;

2) Making additional capital investments when an increase in output leads to an increase inI_p i.e., when d C_{fix} /dE(i) < $P_r O/ E^2$(i), or in the case of an increase in productivity and volume of marketable products;

3) Increasing the productivity of the installation.

4) Increasing product yield and reducing variable costs (especially the cost of raw materials, heat, and energy costs).

If variable and fixed costs are much higher than the cost of raw materials (i.e. $C_{var}O+C_{fix}$>> $P_r O/ E(\tau)$), then they should be reduced to a minimum, and the extractor productivity should be increased to a maximum value, provided that the depreciation of the apparatus significantly affects total fixed costs.

In the case where the cost of raw materials significantly exceeds other costs (i.e. $P_r O/ E(\tau)$>> $C_{var}O+C_{fix}$) the output value at the installation should be maximized by improving the process conditions.

In general, when searching for an optimality criterion in practice, it is necessary to vary various independent variables, the limit values of which are determined by technological conditions. Optimization of continuous devices is achieved in two ways: static (in which they strive to carry out the process with maximum efficiency according to the optimized criterion at each moment in time) and dynamic (in which the process is subject to frequent disturbances and practically proceeds in a dynamic mode).

Since solving the problem of achieving the maximum value of the optimality criterion in a general form is impossible, in practice the optimum is found according to one or, in rare cases, two or three indicators, which may include productivity, degree of extraction, cost, product yield, etc. Other main variables that can be changed to optimize an industrial extractor are the process temperature, the type of extractor, the reaction time and the residence time of the material in the apparatus, the concentration of reagents, the number of apparatuses in the cascade, etc. For multi-stage devices, the selected indicator is optimized for each link, moving from the next stage to the previous one.

Conclusion

A method has been developed for the extraction of copper from sulfuric acid solutions, which reduces sulfuric acid consumption, increases copper extraction and the quality of cathode copper, and reduces the formation of the third phase (crud). Crud, which is concentrated as a separate phase in the extract along with the raffinate, negatively affects phase separation, copper extraction, and the removal of non-ferrous metal impurities. The introduction of the monomeric polymer poly(4-sodium styrene sulfonate) ((H2C═CHC6H4SO3Na)n) into the process dissolves and destroys polymerized silicon bonds in crystals, enhancing the process by more than 25%.

After completing calculations to optimize all compared options for using the extraction apparatus, preference is given to the option that corresponds to the maximum value of Ppr, found for the optimal values of the studied independent technological parameters. If the values of Ppr for the compared options differ slightly from each other, preference is given to the option characterized by better working conditions, a shorter payback period, and improved flow organization of the reacting phases.

Conflicts of interest. On behalf of all authors, the corresponding author states that there is no conflict of interest.

CRediT author statement: **T. Chepushtanova:** Conceptualization, Visualization, Writing draft preparation, Investigation. **M. Yessirkegenov, A. Nikoloski, Y. Merkibayev:** Methodology, Data curation. **Y. Merkibayev, A. Altmyshbayeva**: Reviewing and Editing, Investigation.

Acknowledgements: This study was funded by the Science Committee of the Ministry of Science and Higher Education of the Republic of Kazakhstan, № AP19175411.

Cite this article as: Chepushtanova TA, Yessirkegenov MI, Nikoloski A, Merkibayev YS, Altmyshbayeva AZh. Development of an Enhanced Method for Copper Extraction from Sulfuric Acid Solutions. Kompleksnoe Ispolzovanie Mineralnogo Syra = Complex Use of Mineral Resources. 2025; 334(3):99-109. https://doi.org/10.31643/2025/6445.32

Күкірт қышқылы ерітінділерінен мысты алудың жетілдірілген әдісін жасау

[1]Чепуштанова Т.А., [1]Есиркегенов М.И., [2]Николоский А., [1*]Меркибаев Е.С., [1]Алтмышбаева А.Ж.

[1]Сәтбаев Университеті, Алматы, Қазақстан
[2] Мюрдока Университеті, Австралия

Мақала келді: *29 мамыр 2024*
Сараптамадан өтті: *17 маусым 2024*
Қабылданды*: 9 тамыз 2024*

ТҮЙІНДЕМЕ

Мақалада күкірт қышқылының ерітінділерінен мысты алу әдісі ұсынылған, ол күкірт қышқылының шығынын азайтады, мыстың алынуын және катодты мыстың сапасын арттырады, сонымен қатар үшінші фаза-крадтың қажетсіз түзілуін азайтады. Мыс алудың негізгі нәтижелері, соның ішінде 2-3 сатылы мыс алу келтірілген. Күкірт қышқылды ерітінділерді хелаттаушы, селективті экстрагент альдоксимдер тобынан (10 көлем. %) ерітіндімен араластыру және қоспаны тұндыру арқылы мыс құрамды экстракт және экстракциялық раффинат алу арқылы экстракция жүргізіледі. Крадтағы полимерленген кремний байланыстарын мономерлі полимер (H2C═CHC6H4SO3Na)n поли (4-натрий стиролсульфонаты) пайдаланып еріту арқылы үшінші фаза-крадтың пайда болуын азайтады. Бұл натрий алкилсульфонатының ПАВ кешенінің әсерінен, О/А қатынасы 1:2 және температура 20±5°С болғанда 5 см³ полимер қосу арқылы жүзеге асырылады. Құрамында мыс бар реэкстракт және экстрагент ерітіндісін алу үшін экстрактты күкірт қышқылының ерітіндісімен араластырып, одан кейін қоспаны тұндырып бөлу арқылы жүзеге асырылады. Реэкстракт қоспалардан тазартылады және катодты мыс пен пайдаланылған электролитті алу үшін тазарған реэкстрактан мыс электролиттік жолмен алынады. Сондай-ақ, экстракциялық аппаратты техникалық және экономикалық таңдау әдісі әзірленді.

Түйін сөздер: SX-EW; мыс; экстракциялау; крад; интенсификация әдісі; күкірт қышқылды ерітінділер.

Авторлар туралы мәліметтер:

Чепуштанова Татьяна Александровна *Қауымдастырылған профессор, т.ғ.к., Металлургиялық процестер, жылу техникасы және арнайы материалдар технологиясы кафедрасының меңгерушісі, Тау-кен металлургия институты, Сәтбаев Университеті, Алматы, Қазақстан. Email: t.chepushtanova@satbayev.university*

Есиркегенов Мейрбек Ибрагимович *Докторант, Металлургиялық процестер, жылу техникасы және арнайы материалдар технологиясы кафедрасы, Тау-кен металлургия институты, Сәтбаев Университеті, Алматы, Қазақстан. Email: m.yessirkegenov@satbayev.university*

Николоский Александр *Мердок университетінің профессоры, Австралия. Email: A.Nikoloski@murdoch.edu.au*

Меркибаев Ерик Серикович *PhD, Металлургиялық процестер, жылу техникасы және арнайы материалдар технологиясы кафедрасының оқу зертханаларының меңгерушісі, Тау-кен металлургия институты, Сәтбаев Университеті, Алматы, Қазақстан. Email: y.merkibayev@satbayev.university*

Алтмышбаев Алия *Аға оқытушы, магистр, Металлургиялық процестер, жылу техникасы және арнайы материалдар технологиясы кафедрасы, Тау-кен металлургия институты, Сәтбаев Университеті, Алматы, Қазақстан. Email: a.altmyshbaev@satbaev.university*

Разработка усовершенствованного метода извлечения меди из сернокислых растворов

[1]Чепуштанова Т.А., [1]Есиркегенов М.И., [2]Николоский А., [1*]Меркибаев Е.С., [1]Алтмышбаева А.Ж.

[1]Satbayev University, Алматы, Казахстан
[2]Университет Мюрдока, Австралия

Поступила: *29 мая 2024*
Рецензирование: *17 июня 2024*
Принята в печать: *9 августа 2024*

АННОТАЦИЯ

В статье представлен метод извлечения меди из сернокислых растворов, который снижает потребление серной кислоты, увеличивает извлечение меди и качество катодной меди, а также уменьшает нежелательное образование третьей фазы (крада). Основные результаты извлечения меди, включая 2-3 этапное извлечение меди, представлены. Извлечение осуществляется путем смешивания сернокислых растворов с раствором хелатирующего, селективного экстрагента группы альдоксимов (10 об.%) и разделения смеси путем отстаивания для получения медьсодержащего экстракта и экстракционного раффината, с подавлением третьей фазы (крада) за счет растворения полимеризованных кремниевых связей в крудах с использованием мономерного полимера (H2C═CHC6H4SO3Na)n поли(4-натрий стиролсульфоната). Это достигается добавлением 5 см³ полимера, под влиянием комплекса ПАВ из алкилсульфоната натрия, с соотношением О/В = 1:2 и температурой 20±5°С. Последующая реэкстракция меди из экстракта проводится путем смешивания экстракта с раствором серной кислоты и разделения смеси путем отстаивания для получения медьсодержащего реэкстракта и раствора экстрагента. Реэкстракт очищается от примесей, и медь извлекается электролитически из очищенного реэкстракта для получения катодной меди и отработанного электролита. Также разработан метод расчета технического и экономического выбора экстракционного аппарата.

Ключевые слова: SX-EW; медь; жидкостная экстракция; крад; метод интенсификации; сернокислые растворы.

Информация об авторах:

Чепуштанова Татьяна Александровна *Ассоциированный профессор, кандидат технических наук, PhD доктор, заведующая кафедрой Металлургические процессы, теплотехника и технология специальных материалов, Горно-металлургический институт, Satbayev University, Алматы, Казахстан. Email: t.chepushtanova@satbayev.university*

Есиркегенов Мейрбек Ибрагимович *Докторант «Металлургические процессы, теплотехника и технология специальных материалов», Горно-металлургический институт, Satbayev University, Алматы, Казахстан. Email: m.yessirkegenov@satbayev.university*

Николоский Александр *Профессор Университета Мердока, Австралия. Email: A.Nikoloski@murdoch.edu.au*

Меркибаев Ерик Серикович *PhD, Металлургические процессы, теплотехника и технология специальных материалов, Горно-металлургический институт, Satbayev University, Алматы, Казахстан. Email: y.merkibayev@satbayev.university*

Алтмышбаев Алия *Старший преродователь, магистр,Металлургические процессы, теплотехника и технология специальных материалов, Горно-металлургический институт, Satbayev University, Алматы, Казахстан. Email: a.altmyshbaev@satbaev.university*

References

[1] Pat. 2339713 RU. МПК C22B 15/00, C22B 3/30. Opubl. 27.11.2008, bull. 33.

[2] Pat. 2178342 RU. МПК B03B 7/00, C22B 3/04, C22B 3/26. Opubl. 20.01.2002, bull. 2.

[3] Zagorodnyaya A N, Abisheva Z S, Sadykanova S E, Bobrova V V, & Sharipova A S. The characterisation and origins of interphase substances (cruds) in the rhenium solvent extraction circuit of a copper smelter. Hydrometallurgy. 2010; 104(2):308-312. https://doi.org/10.1016/j.hydromet.2010.05.013

[4] Panda S, Parhi P K, Pradhan N, Mohapatra U B, Sukla L B, & Park K H. Extraction of copper from bacterial leach liquor of a low grade chalcopyrite test heap using LIX 984N-C. Hydrometallurgy. 2012; 121-124:116-119. https://doi.org/10.1016/j.hydromet.2012.03.008

[5] Nobahar A, Melka A B, Pusta A, et al. A New Application of Solvent Extraction to Separate Copper from Extreme Acid Mine Drainage Producing Solutions for Electrochemical and Biological Recovery Processes. Mine Water Environ. 2022; 41:387-401. https://doi.org/10.1007/s10230-022-00858-7

[6] Shakibania S A, Mahmoudi A, Mokmel M, & Rashchi F. The effect of chloride ions on copper solvent extraction from sulfate-chloride medium using LIX 984N. Minerals Engineering. 2020; 156:106498. https://doi.org/10.1016/j.mineng.2020.106498

[7] Chepushtanova TA, Merkibayev YS, Mamyrbayeva K K, Sarsenbekov T, & Mishra B. Mechanism and technological results of sulfidation roasting of oxidized lead compounds. Kompleksnoe Ispolzovanie Mineralnogo Syra=Complex use of mineral resources. 2025; 332(1):119-132. https://doi.org/10.31643/2025/6445.11

[8] Cole P. Understanding aqueous-in-organic entrainment in copper solvent extraction. J. S. African Institute of Mining and Metallurgy. 2016; 116(6):525-531. http://dx.doi.org/10.17159/2411-9717/2016/v116n6a6

[9] Kenzhaliev BK, Kvyatkovsky SA, Kozhakhmetov S M, Sokolovskaya L V, Semenova A S. Depletion of waste slag of balkhash copper smelter. Kompleksnoe Ispolzovanie Mineralnogo Syra = Complex Use of Mineral Resources; 2018; 306(3):45-53. (in Russ.). https://doi.org/10.31643/2018/6445.16

[10] Bochevskaıa E G, Abısheva Z S, Sharıpova A S, & Sargelova E A. Obrazovanıe osmıısoderjaıh mejfaznyhvzvesеı prı ekstraktsıı renıia ız promyvnoı kısloty mednogoproızvodstva. Izvestıia Natsıonalnoı Akademıı Naýk[Formation of organic compounds containing

meiotic fluids by extracting the extracted product from the industrial acidity of honey production. Report by the National Academy of Sciences.]. Shemistry and technology. 2022; 3(452):42-56. (in Russ.).

[11] Solvent Extraction Principles and Practice, Revised and Expanded, by Jan Rydberg, Michael Cox, Charles Musikas, and Gregory R. Choppin was published on March 3, 2004.

[12] Agarwal S, Ferreira A E, Santos S M C, Reis M T A, Ismael M R C, & Correia M J N. Separation and recovery of copper from zinc leach liquor by solvent extraction using ACCORGA M5640. International Journal of Mineral Processing. 2010; 97(1-4):85-91. https://doi.org/10.1016/j.minpro.2010.08.009

[13] Alguacil F J, Cobo A, & Alonso M. Copper separation from nitrate/nitric acid media using ACCORGA M5640 extractant: Part I: solvent extraction study. Chemical Engineering Journal. 2002; 85(2-3):259-263. https://doi.org/10.1016/S1385-8947(01)00166-8

[14] Chepushtanova T, Yessirkegenov M, Mamyrbayeva K, Akcil A, & Gaipov T. Extraction of Copper from Pregnant Leach Solution (PLS) and Reduction of Crud Formation. Mineral Processing and Extractive Metallurgy Review. 2024, 1-13. https://doi.org/10.1080/08827508.2024.2340545

[15] Chepushtanova TA, Yessirkegenov MI, Mamyrbayeva KK, Merkibayev YS. Investigations of extraction of copper and crud formation components of productive solution of Almaly deposit. Non-ferrous Metals. 2023; 54(1):11-19 https://doi.org/10.17580/nfm.2023.01.02

[16] Li X H, Zhou G Y, Huang S T, & Wen J K. Effect of Bioleaching Microorganisms and Solid Ore Particles on Formation of Interfacial Crud in Solvent Extraction Plants. Advanced Materials Research. 2013; 825:335-339. https://doi.org/10.4028/www.scientific.net/AMR.825.335

[17] Autef A, Joussein E, Gasgnier G, & Rossignol S. Role of the silica source on the geopolymerization rate. Journal of Non-Crystalline Solids. 2012; 358:2886-2893. https://doi.org/10.1016/j.jnoncrysol.2012.07.015

[18] Watling H R. Chalcopyrite hydrometallurgy at atmospheric pressure: 1. Review of acidic sulfate, sulfate–chloride and sulfate–nitrate process options. Hydrometallurgy. 2013; 140:163-180. https://doi.org/10.1016/j.hydromet.2013.09.013

[19] Ferreira A E, Agarwal S, Machado R M, Gameiro M L F, Santos S M C, Reis M T A, Carvalho J M R. Extraction of copper from acidic leach solution with ACCORGA M5640 using a pulsed sieve plate column. Hydrometallurgy. 2010; 104(1):66-75. https://doi.org/10.1016/j.hydromet.2010.04.013

[20] Petersen J. Heap leaching as a key technology for recovery of values from low-grade ores – A brief overview. Hydrometallurgy. 2016; 165(1):206-212. https://doi.org/10.1016/j.hydromet.2015.09.001

[21] Pat. (11) 2 339 713(13) C1 RU. Sposob ekstraktsiimedı ız sernokıslyh rastvorov [Method of extracting medicine from sulfite seeds]. Bulletin, Opubl. 27.11.2008, bull.33.

[22] Jumadilov T, Abilov Z, Grazulevicius J, Zhunusbekova N, ...Agibayeva L, Akimov A. Mutual activation and sorption ability of rare cross-linked networks in intergel system based on polymethacrylic acid and poly-4-vinylpyridine hydrogels in relation to Lanthanum ions. Chemistry and Chemical Technology. 2017; 11(2):188-194.

[23] Yelubay M, Yerzhanova D, Bakibaev A, ...Amitova A, Aitkaliyeva G. Selection of an Effective Activating Agent for Coke Production Waste. Polish Journal of Environmental Studies. 2024; 33(1):467-476. https://doi.org/10.15244/pjoes/171656

[24] Sperline RP, Song YE, Freiser Ma H. Organic constituents of cruds in Cu solvent extraction circuits: I. Separation and identification of diluent-soluble compounds. Hydrometallurgy. 1998; 50(1):1-21. https://doi.org/10.15244/pjoes/171656

Crossref
DOI: 10.31643/2025/6445.33
Earth Sciences

Evaluation of modern methods and techniques for calculating parameters during coal bed degassing

[1] Rabatuly M., [1]Demin V.F., [1]Kenetaeva A.A., [2]Steflyuk Yu.Yu., [3]Toshov J.B.

[1] A. Saginov Karaganda Technical University, Karaganda, Kazakhstan
[2] Management of special maintenance and gasification, Coal Department of JSC Qarmet, Karaganda, Kazakhstan
[3] Islam Karim Tashkent State Technical University, Tashkent, Republic of Uzbekistan

** Corresponding author email: mukhammedrakhym@mail.ru*

Received: *August 7, 2024*
Peer-reviewed: *August 8, 2024*
Accepted: *August 26, 2024*

ABSTRACT

The modern strategy for the development of underground coal mining in the Karaganda basin provides for the development of the concept of reforming the mining fund, ensuring a high level of concentration and intensification of mining operations with increasing the load on the treatment face to 5-6 thousand tons per day. At the same time, the main deterrent factor is the high methane content of the coal seams of the basin, which reaches 30-40 m3/t of coal. The high gas content of the coal seams being developed and their satellites is one of the main causes of methane explosions in mines, leading to violations of the technological regime and irretrievable loss of life. The problem of degassing minefields has always been and is among the priority areas that require prompt solutions. Gas dynamic phenomena and sudden methane emissions are accompanied by human casualties, and large material and financial losses, and are 25-30% of the cause of the total number of accidents that occurred in coal mines of the CIS countries in the last decade. The article evaluates progressive methods of degassing high-gas-bearing, explosive formations to reduce the methane content and ensure the safety of the operation of coal mines in the Karaganda region, taking into account modern experience and achievements in this field.

Keywords: *methane, gas flow rate, gas output, methane abundance, coal mines, degassing, mining technology, minefields, gas dynamic phenomena, formation.*

Information about authors:

Rabatuly Mukhammedrakhym *Ph.D., Senior lecturer of the Department of Development of Mineral Deposits of Karaganda Technical University, 100027, The Republic of Kazakhstan, Karaganda, Ave. Nursultan Nazarbayev, 56. E-mail: mukhammedrakhym@mail.ru; ORCID ID: https://orcid.org/0000-0002-7558-128X*

Demin Vladimir Fedorovich *Doctor of Technical Sciences, Professor of the Department of Development of Mineral Deposits of Karaganda Technical University, Karaganda, Kazakhstan. E-mail: vladfdemin@mail.ru; ORCID https://orcid.org/0000-0002-1718-856X*

Kenetaeva Aigul Akanovna *lecturer of Karaganda Technical University, Master of Engineering and Technology specialty "Mining", Karaganda, Kazakhstan. E-mail: aigul_tate@bk.ru; ORCID: https://orcid.org/0000-0001-7943-3279*

Steflyuk Yuri Yurievich *Chief Engineer of Management of special maintenance and gasification, , Coal Department of JSC "Qarmet", 100012, The Republic of Kazakhstan, Karaganda, Saransk highway, 10. E-mail: steflyuk@mail.ru; ORCID ID: https://orcid.org/0000-0002-7240-0447*

Toshov Javokhir Buriewicz *Doctor of Technical Sciences, Professor of Tashkent State Technical University named after Islam Karim, 100095 Republic of Uzbekistan, Tashkent, Almazar district, Universitetskaya street 2. E-mail: j.toshov@tdtu.uz; ORCID ID: https://orcid.org/0000-0003-4278-1557*

Introduction

The mine gases of the coal seams of the Karaganda coal basin contain methane, carbon dioxide, nitrogen, hydrogen sulfide, hydrogen and heavy hydrocarbons. The Dolinskaya and Karaganda formations are characterized by the highest gas content. At depths of more than 400-500 m in the Karaganda basin in the developed formations of the Karaganda formation, the amount of gas reaches 22-25 m^3/t, increasing in the Sherubainurinsky and Tenteksky districts to 25-27 m^3/t. The methane content of coal seams increases with the depth of their occurrence [1].

Unlike oil and gas reservoirs, most coal seams are characterized by lower values of natural porosity, filtration and diffusion permeability. The natural permeability of coal seams is low and in the conditions of the Karaganda basin, it is (10-50)×10-4 milliDarsi (mDa) [2].

The deeper the coal seams sink into the subsurface, the more gas they contain, but at the

same time, their gas permeability and methane flow rate from drilled degassing wells decrease. In this regard, there is a need for artificial directional effects on coal seams to intensify their gas recovery. These include such methods as hydraulic fracturing (sufficiently high methane production rates from hydraulic fracturing wells have been recorded – up to 5-7 m^3/min), hydraulic fracturing, hydrochloric acid treatment (a decrease in the gas content of mine workings by 30-70% has been achieved), torpedoing in wells, hydraulic pulse treatment, interval fracturing and several other modifications of the intensifying effect for the growth of coal gas recovery [3].

Currently, an integrated method of artificial degassing has been developed and implemented at the mines, including the simultaneous use of several methods and schemes of degassing from methane sources: preliminary degassing of the reservoir under development, degassing of under- and over-worked formations (satellites) and the developed space: underground wells drilled above the mounting chamber, counter wells, wells above collapse domes and vertical wells from the surface; gas extraction from a particularly explosive formation d6 through wells drilled from field unloading workings, etc. [4]. Currently, work is actively being carried out on advance degassing preparation from unloading field workings of a particularly explosive formation d6 is being carried out in the field of the Kazakhstanskaya mine, with drilling of ascending degassing wells through a particularly explosive coal pack.

Experimental part

In the mines of the Karaganda basin, degassing of converging coal seams, worked-out spaces and host gas-bearing rocks with the help of wells drilled from the surface is widely used. The location of the well is chosen in such a way that after the end of drilling and casing of the well, the area of its intersection with the reservoir under development is located in the coal massif at a distance of more than 30 m ahead of the lava. The well should cross the reservoir under development and go deeper into the soil rocks by 3-5 m. The casing of vertical wells is carried out with steel pipes with a diameter of at least 100 mm. The lower part of the casing is located 3 - 5 m above the roof of the formation. In the areas of intersection of the adjacent overlying layers, the casing pipes are perforated with holes with a diameter of 15-20 mm with a length of this pipe of 20 m for each of the layers.

The mouth of the vertical well is sealed to the first from the surface of the coal seam, but not less than 10 m long. At the same time, the methane flow rate through wells increases, and the service life of vertical and underground degassing wells increases. The gas is sucked out at a discharge of at least 150 mmHg. The efficiency of degassing the methane release source at a distance between wells of 60-70 m is 60-80% and at a distance of 70-100 m - 50-60%.

Analytical studies show that with an increase in the load on the lava to 3,000 - 4,000 tons per day or more, the optimal values of the lava length of at least 200-250 m and the excavation column up to 1,500-2,000 m increase [5].

One of the promising areas of improvement is the work on the early degassing of coal seams by hydro-pneumatic action through wells drilled from the earth's surface. The intensification of reservoir gas recovery is based on the methodology of B. Moscow State Mining University (now MISIS) (Figure 1). During the period of application of this method, 152 wells were processed at the mines of the Karaganda coal basin (Table 1) with subsequent hydraulic fracturing and more than were extracted 100 million tons m^3 of methane.

When processing the d6 formation in the field of the Kazakhstanskaya mine (Figure 2), the following technological schemes for early degassing of coal seams have been developed and implemented: pneumohydraulic action; hydrodynamic action using the effect of self-sustaining destruction of coal; pneumohydraulic action with exposure to working fluid; exposure using foaming substances, pneumohydraulic action using the effect of aeration of working fluid; hydro-impact using a water hammer [[6], [7]].

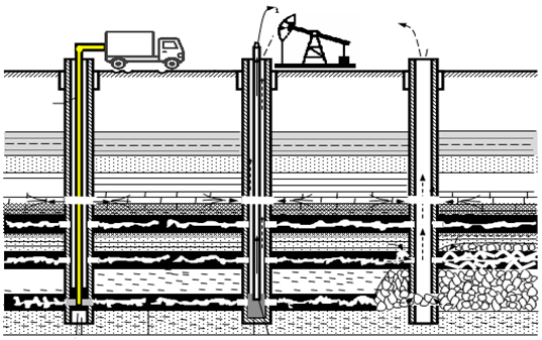

Figure 1 - Advance degassing of coal seams by hydro-pneumatic action through wells drilled from the surface

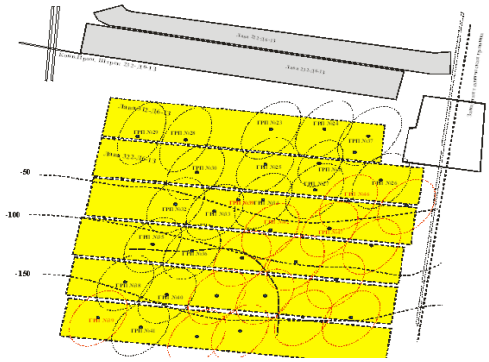

Figure 2 - The scheme of early degassing of the d6 formation in the field of the Kazakhstanskaya mine

The increase in the depth of coal seam mining determines the need to improve the technology of early degassing of minefields and methane extraction through wells drilled from the surface. At the same time, along with the positive aspects, such as separation in time and space of mining and degassing operations; the possibility of processing significant coal reserves through a well; achieving stable methane flows with a concentration of over 90%, there are also several negative factors and manifestations [8]. These include insufficient reliability of the method (with the same parameters of impact on the formation, the volumes of methane extraction from the treated areas vary significantly); lack of technical means to control the process of hydraulic impact on the formation and subsequent opening of natural cracks; no reliable relationship has been revealed between the parameters of reservoir treatment, its characteristics and methane extraction indicators [9].

To increase the reliability and efficiency of the method, it is necessary to change the approach to carrying out work on the early degassing preparation of minefields by methodically substantiating the parameters of artificial impact on the coal seam from the earth's surface. It is most advisable to improve the method of pneumohydro-separation of a coal seam, which is the most technologically advanced and effective method of exposure, using powerful high-performance compressors that provide a rate of injection of a gaseous working agent of more than 80 m3/min. A feature of the pneumatic hydroelectric effect on the coal seam is an increase in the phase permeability of the formation for gas, regardless of the mode of air introduction into the array, and a decrease in the sorption capacity of coal for methane when heating the formation, due to the chemical reaction of oxygen in the air with coal, when compressed air is injected into the coal seam at a rate exceeding the natural intake of the formation. The main parameters of pneumatic hydraulic separation include: the number of injection cycles; injection volume; injection rate; expected pressure, distance between wells.

The effectiveness of the impact of the method of pneumohydro separation of a coal seam from the earth's surface is estimated by the coefficient of pick-up:

$$K_n = \frac{q \cdot P_{at}}{\delta \cdot P_3} \quad (1)$$

where q - is the rate of air injection into the reservoir, m^3/sec;

P_{at} - atmospheric pressure, MPa;

δ - is a coefficient that takes into account the conditions of opening the formation, the properties of the formation and the injected air, δ = 0.05-0.15;

P_3 - is the pressure at the bottom of the well, MPa.

Pneumohydro separation is carried out in cycles with an increase in the rate by 20-25% and an increase in the volume of injection of the gaseous agent by 10-15% in each subsequent cycle.

At the end of each cycle, the air is kept in the reservoir until the pressure stabilizes, and then the gas mixture is released until the pressure drops at the wellhead of the Py = 0.1 MPa. The number of cycles is assumed to be equal to the number of natural crack systems (n).

With an assumed radius of pneumatic separation of the R_{pd}, equal to 125 m, the total amount of air injected into the coal seam Q is determined by the formula:

$$Q = \frac{\pi \cdot R_э^{n^2} \cdot h \cdot m_e \cdot K \cdot P_c^p}{z \cdot P_\delta \cdot P_б \cdot \frac{T_{ai}}{T_{form}}} \quad (2)$$

where h - is the reservoir capacity, m;

m_e - is the effective porosity of the formation, %;

K - is a coefficient that takes into account the filtration and reservoir properties of the coal seam and host rocks, K = 1.8 - 3.2;

R_{cp} - the expected average pressure of compressed air in the pneumatic separation zone:

$$P_c^n = \frac{P_p + P_{form}}{2} \quad (3)$$

where P_p - is the pressure of the pneumatic separation of the formation, MPa; $P_p = \sigma_1 - P_{form} + \sigma_p$, here σ_1 is the vertical rock pressure, MPa;

P_{form} - reservoir pressure, MPa;

σ_p - is the tensile strength of coal, MPa;

z - is the coefficient of super-compressibility of air;

P_b - barometric pressure, MPa;

T_{ai} - the temperature of the injected air, Co;

T_{pl} - reservoir temperature, Co.

R_{cp} is the expected average pressure of compressed air in the area of pneumatic dismemberment.

During pneumohydroaction, sequential processes of hydraulic fracturing of the reservoir with a working fluid with compressed air injection occur. The technology provides for the separation of the formation by aerated working fluid due to the simultaneous injection of liquid and gaseous agents at a rate exceeding the natural permeability of the formation. In this case, the injection of aerated liquid is carried out according to the pressure, injection, which must be at least:

$$P_н = 0{,}025H + \sigma_p \quad (4)$$

where H - is the depth of the formation, m;

σ_p - is the tensile strength of coal, MPa.

At the end of the injection cycle, the degassing well is kept hermetically closed for 3 to 7 days. until the pressure drops at the wellhead to the value of reservoir pressure. Then the well is opened and a cyclic self-discharge of water occurs. At the same time, air bubbles contribute to the removal of the working fluid from the filter pores and cracks [[10], [11]].

In order to increase the efficiency of methane extraction from the formation of coal seams, the treatment of each formation of the formation begins with a hydropneumatic rupture of the downhole zone, which is then washed and strengthened with a solid filler, and the treatment of the formation continues in the mode of hydropneumatic separation, while the treatment of the subsequent formation of the formation begins after the output of the treated formation to a stable water and gas flow mode, and the processing parameters are determined by the following calculation formulas:

- in case of hydro-pneumatic rupture of the downhole zone of the formation, the volume of injection of the working fluid:

$$Q_{wf} = K R_{dz}^2 \cdot h \cdot n_e; \text{ м}^3; \quad (5)$$

- the volume of injection of solid filler to secure the downhole area:

$$V_3 = 2\pi R_{da}^2 \cdot h \cdot d \cdot L_{bl} \cdot K_p, \text{ м}^3 \quad (6)$$

where K - is a coefficient that takes into account the degree of filling of fracturing cracks with solid filler, K = 0.4 - 0.8; K = 0.4 - with maximum filling of cracks, K = 0.8 - with no or minimal filling of cracks;

R_{dz} - is the radius of the downhole zone of the formation, m;

h - is the reservoir capacity, m;

n - is the effective porosity of the formation, in fractions of a unit;

d - is the effect of a hydraulic fracturing crack, m;

L_{bl} - the size of the coal block in the downhole zone, m;

K_l - is the coefficient of loosening of the solid filler;

H - is the depth of the formation, m;

σ - is the tensile strength of coal, MPa;

R_e - is the effective radius of hydraulic action, m.

Calculated parameters were obtained for the possible absolute volume of drained methane from the depth of vertical degassing wells at different distances between them (from 50 to 250 m).

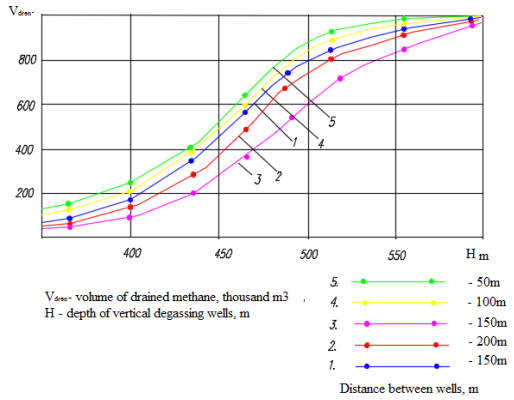

Figure 3 - Calculated parameters for the possible absolute volume of drained methane from the depth of vertical degassing wells at different distances between them (from 50 to 250 m)

It is known from world practice that in some cases, various intensifying methods of influencing the coal seam are used to increase the efficiency of degassing in underground mines [[12], [13], [14]].

One of the methods of progressive intensification of gas release during reservoir degassing is the point-to-point hydraulic fracturing of a coal seam, in which the formation is processed in fixed sections along the length of the well (Figure 4, a).

For the production of hydraulic fracturing, the machine drills degassing wells to a predetermined depth. After the end of drilling and flushing (no screw drilling) before drilling the well with the drilling machine 1, a sealing device consisting of two (or several) sealers 4 is introduced using rods 2.

The ratio of the lengths of the sealers is selected taking into account that water breaks into the well and occur in the direction of its bottom. A valve device 5 is placed between the sealers to supply water to the well (Figure 4, b).

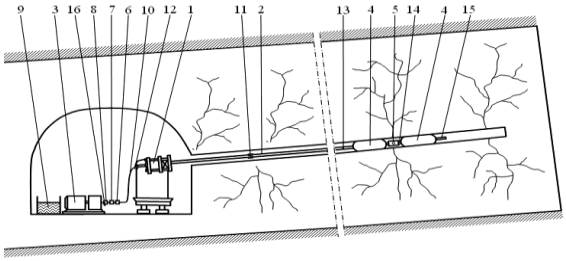

1 – drilling rig (SBG-1m); 2 – drilling rods; 3 – high–pressure pumping unit; 4 – sealers; 5 – valve device; 6 – pressure gauges; 7 – flow meter; 8 – three-way tap; 9 – water tank; 10 - high-pressure hose; 11 - seal ring; 12 – adapter to the drill rods; 13 – adapter from the drill rods to the sealer; 14 – adapter from the sealer to the valve device; 15 – plug to the sealer; 16 – adapter from the three-way tap to the hoses

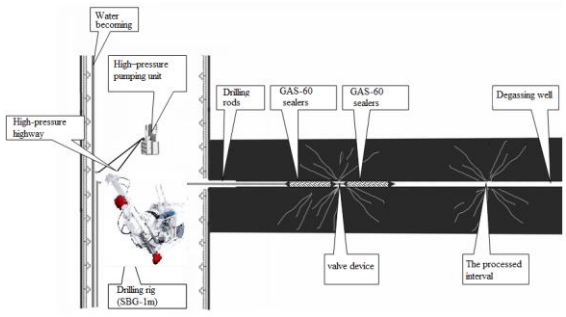

Figure 4 - The scheme of conducting inter-interval hydraulic fracturing of a coal massif through reservoir wells

After installing the sealing device in a given area, a high-pressure pump 3 is turned on and waterfalls along the rods at a rate of 20-50 l/min, which expands the sealers. When the maximum liquid pressure is exceeded (at least 2-3 MPa), the valve opens automatically in the valve device, and water enters the well cavity located between adjacent sealers. The pressure and flow of water are constantly monitored with a pressure gauge and a water meter. After supplying the calculated amount of water or a drop in liquid pressure, the pump is stopped and the water is lowered from the rods and sealers using a three-way crane, carrying out depressurization of the well (Figure 5).

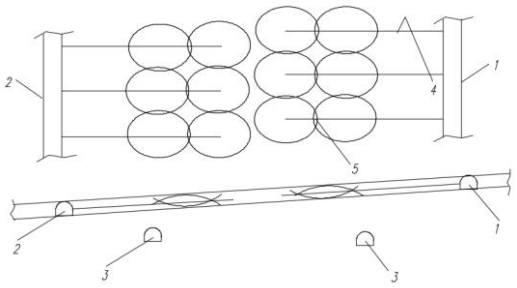

1 – conveyor belt of overlying lava;
2 – conveyor belt of prepared lava;
3 – field production; 4 – hydraulic fracturing wells;
5 – Overlaying adjacent zones of interval hydraulic fracturing.

Figure 5 - The scheme of hydraulic fracturing using two seals

Then, the sealing device is moved with the help of rods and a drilling machine in the direction of the wellhead and installed in such a way that the end of the sealer closest to the bottom of the well is located at the boundary of the rupture zone with the movement of sealing elements along the well to a length equal to the length of both sealers and the valve device.

After installing the sealing device on a new section of the well, the processing process is repeated. In this sequence, sections of the coal massif are processed along the entire length of the well until the near end of the sealer approaches the wellhead at a distance of up to 15 m.

Despite the low pump performance in case of intermittent hydraulic fracturing (2.4 - 5.0 m3/min) compared with hydraulic fracturing from the surface (270 m3/min), hydraulic fracturing of the coal massif, as shown by the positive results of work in mine conditions, occurs within a radius of up to 10 m from the treated well. Calculations show that with intermittent hydraulic fracturing, the specific injection rate per 1 ton of processed coal reserves is 1.5 times higher than with hydraulic fracturing, and therefore, at this rate of fluid supply, hydraulic fracturing can occur within a radius of up to 10 m from the fracturing well (Figure 5, Table 1) [15].

Table 1 – Comparative parameters and indicators for different modes of hydraulic action on the formation

Type of action	The weight of the equipment used	Pressure, MPa	Injection rate, m3/h	The radius of the hydraulic action, m	Total volume of liquid, m3	Processed stocks in the specified radius,t	Specific injection rate per 1 ton of reserves, 10-4m3/(h*t)
Hydropneumor separation of a coal seam from the surface	Over 10	20-25	270	130	10000	297.3	9.1
Hydraulic fracturing from underground workings	3.0	20-25	40	30	200	28.1	14.2
Point-to-point hydraulic fracturing	0.4-0.6	20-25	2.4	10	2	1.8	13.0

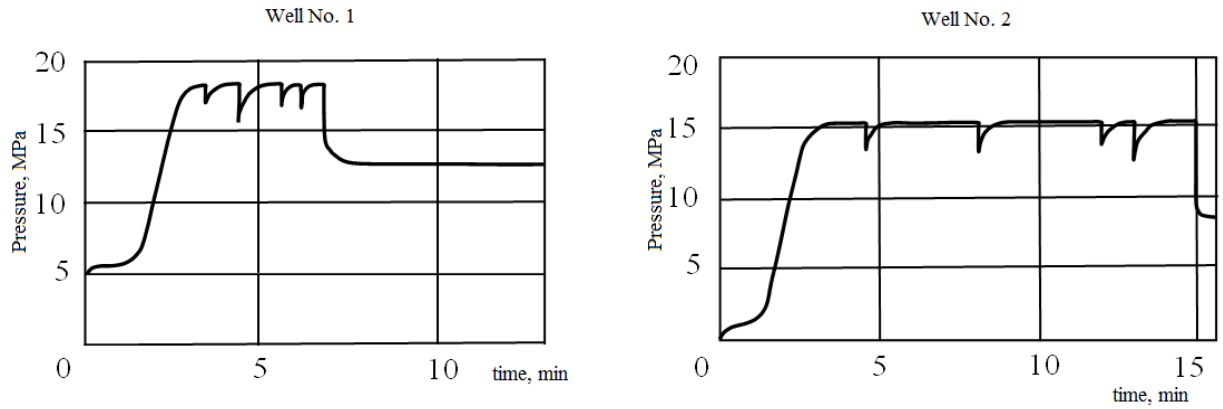

Figure 6 - Change in fluid pressure during well interval processing

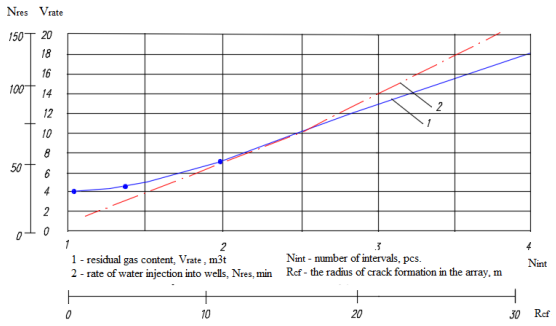

Figure 7 - The change in the rate of water injection into wells and the residual gas content of the coal seam, depending on the amount of applied hydraulic fracturing at the radius of crack formation in the massif

The main controlled parameter for the process of hydraulic fracturing of a coal massif is the liquid pressure according to the readings of a pressure gauge mounted on the discharge side of a high-pressure pump (Figure 6). High liquid pressure and its sharp drop indicate the formation of hydraulic fracturing cracks in the coal massif. The time spent on processing the formation in one interval is 7-15 minutes.

The rate of water injection into wells and, accordingly, the residual gas content of the coal seam is determined depending on the number of hydraulic fractures at the radius of formation (propagation) of cracks in the massif – Figure 7.

When choosing the type of pump for hydraulic fracturing, it is necessary that existing cracks open and new cracks form during its operation.

The formation of a tearing force by is performed according to the formula 16]:

$$P_r=(1-v)\,(2q_{\infty}+\sigma_s) \qquad (7)$$

where Pr - is the liquid pressure required for the formation of vertical cracks during hydraulic fracturing of a coal seam, MPa;

v - is the Poisson's ratio;

q_{∞} - lateral mountain pressure, MPa;

σ_s - is the tensile stress of coal, MPa.

In mine conditions, hydraulic fracturing was performed at the mine named after Lenin of the Karaganda coal basin from conveyor and ventilation bremsbergs 4.05 d6-1b (depth from the surface 672.7 - 822.2 m).

The conducted studies have established that for the conditions of the Karaganda coal basin, the lateral mountain pressure does not exceed 15-20% of the vertical pressure and it can be determined by the formula [17]

$$q_{\infty}=0,2\gamma H \quad (8)$$

where γ - is the volume weight of the overlying rocks, t/m^3;

H - is the depth of the formation, m.

After being reduced to a single measurement system (with an average density of carbon-bearing rocks γ = 2.5 t/m^3), formula (8) will take the form:

$$q_{\infty}=0,005H \quad (9)$$

At a depth of 700 m, the lateral mountain pressure value will be q_{∞} = 3.5 MPa.

For the d6 formation, the value of the Poisson's ratio is in the range v = 0.1 - 0.3, and the breaking force for coal is σ_s =9.1 - 40 MPa. Substituting the initial data into formula (7), it turns out that the value of the liquid pressure for hydraulic fracturing at a depth of 700 m (mining operations will be carried out at this depth) is in the range of 16-20 MPa [18].

The rate of liquid supply to the coal seam is a very important parameter of hydraulic fracturing, since the higher the injection rate, the greater the radius of influence of hydraulic fracturing, and vice versa. In the case of underground hydraulic fracturing with an injection rate of 30-40 m^3/h through a reservoir well with a length of 70-100 m (with a sealing length of 40 m), the specific flow rate is 0.5 - 0.8 m^3/h. m.

In the mode of intermittent hydraulic fracturing with a rate of 2.4 m^3/h at a well interval of 0.3 - 0.4 m, the specific flow rate of liquid is 6 - 8 m^3/hr. m, i.e., an order of magnitude higher.

Therefore, at low flow rates (about 2.4 m^3/h), it is also possible to get cracks in the coal mass if the liquid acts on a small interval of the well [[19], [20]].

The injection rate and the fracking radius are interrelated parameters. At a water flow rate of 0.5 - 2 m^3/h or less through reservoir wells, natural cracks do not open, but only water is filtered into the reservoir with its humidification. Therefore, for the formation of non-closing cracks during hydraulic fracturing at a considerable distance from the well, it is advisable to use pumps with the highest possible performance.

In case of intermittent underground hydraulic fracturing in the Karaganda basin, when liquid is supplied to the reservoir at a rate of 30-50 l/min, the opening of existing and the formation of new cracks in the coal massif occurs within a radius of up to 10 m from the place where the liquid exits the valve device of the treated well. For hydraulic fracturing within a radius of 20 m, it will be necessary to increase the injection rate by 4 times and bring it to 60-100 liters/min.

In case of underground hydraulic fracturing, when a large amount of water is supplied to the coal mass per unit of time, first of all, the liquid also moves through large cracks. Under the influence of the "water wedge" there is an increase in the gaping of large cracks with simultaneous closure of cracks with a small gape due to movements and compaction of the coal mass between the cracks.

At the initial moment of water supply in the coal massif adjacent directly to the bottom of the well, the zone through which the liquid moves in the coal will generally represent a spherical radial flow resembling an ellipsoid. After the liquid reaches the roof and soil, the impact zone takes the form of a truncated ellipsoid. With the further movement of liquid from the well, the radial flow takes the form of a cylinder of a certain radius with a generator equal to the reservoir capacity.

The total amount of injected liquid QB (m^3) in each well interval is calculated using the formula:

$$Q_B = \frac{2}{3}\pi R_G^2 \, m_P K_{cap}, \quad (10)$$

where R_G - is the radius of propagation of hydraulic fracturing cracks, m;

m_P - full capacity of the coal seam;

K_{cap} - the coefficient of filling the coal massif with liquid, during hydraulic fracturing, is assumed to be in the range of 0.001 - 0.002.

Processing time of one interval - the estimated operating time of the t_r pump for processing is defined as the ratio of the calculated amount of water QB to the pumping rate q_p, assumed to be equal to the pump capacity

$$t_{\Gamma} = \frac{Q_B}{q_H}, \quad (11)$$

For wells drilled through the reservoir, the distance between the treatment intervals is selected so that the zones do not overlap, i.e. the sealing device after the completion of the injection cycle must be moved at least the full length of the two sealers. In this case, the number of processing intervals is determined by the formula:

$$N = \frac{L_{well} - 20}{L_G}, \qquad (12)$$

where N - is the number of processing intervals;
L_{well} - the length of the well, m;
L_G is the length of the sealing device, m.

The number 20 indicates the extent of the degassing zone near the reservoir preparatory work for the rise or fall of the formation.

The experimental installation for hydraulic fracturing was tested in the landfill conditions of the Special Mine Installation and Degassing Department, and experimental work in underground conditions was carried out at the Abayskaya mine along the k10 formation at a depth of 510 m. The calculated fluid pressure at which the opening of existing fractures and the formation of new fractures for this depth should occur is 16.5 MPa. Hydraulic fracturing occurs at a liquid pressure of 15-18 MPa, close to the design pressure. To determine the methane flow rate from the treated wells, a packer (a device designed to separate 2 zones of the borehole and isolate the inner space of the production column from the impact of the borehole environment) and a measuring device were used, with the help of which it was established that the productivity of 1 cubic meter of the well as a result of interval treatment increased from 0.1-0.3 to 1.031.5 m^3/day *m, i.e. an average of 7 times [17].

Results and Discussions

The increase in the depth of coal seam mining determines the need to improve the technology of early degassing of mine fields and methane extraction through wells drilled from the surface. Along with the positive aspects: separation in time and space of mining and degassing operations; the possibility of processing significant coal reserves through a well; achieving stable methane production rates with a concentration of over 90%, there are also a number of negative factors. These include: insufficient reliability of the method (with the same parameters of impact on the formation, the volumes of methane extraction from the treated areas vary significantly); lack of technical means to control the process of hydraulic impact on the formation and subsequent opening of natural cracks; no reliable relationship between the parameters of formation treatment, its characteristics and methane extraction indicators has been revealed.

When pneumohydrogenation acts on a coal seam, the phase permeability of the formation for gas increases, regardless of the mode of air introduction into the array, and the sorption capacity of coal for methane decreases when the formation is heated, due to the chemical reaction of oxygen in the air with coal. A method for calculating the parameters of pneumohydro-separation of a coal seam from the surface is presented.

Conclusion

To increase the reliability and efficiency of the method, it is necessary to change the approach to carrying out work on the advance degassing of mine fields from the earth's surface. It is most advisable to improve the method of pneumohydro-separation of a coal seam, which is the most technologically advanced and effective method of exposure, using powerful high-performance compressors that provide a rate of injection of a gaseous working agent of more than 80 m^3 / min. During pneumohydrogenation, successive processes of hydraulic fracturing of the reservoir with a working fluid and subsequent air injection occur. The technology provides for the separation of the formation by aerated working fluid due to the simultaneous injection of liquid and gaseous agents at a rate exceeding the natural permeability of the formation.

Intensification of gas release during reservoir degassing in underground conditions is recommended to be carried out by inter-interval hydraulic fracturing of a coal seam, in which the formation is processed on fixed sections of the well. The calculation method, operational parameters and indicators are recommended for various modes of hydroelectric action on the coal seam in underground conditions during intermittent hydraulic fracturing of the coal seam. The article discusses the characteristics of the mine gases of the coal seams of the Karaganda coal basin, the features of their gas content and methods of

artificial degassing. Studies show that with an increase in the depth of coal seams, the gas content increases, but their natural permeability and methane flow rate decrease, which requires the use of various technologies to intensify gas recovery, such as hydraulic fracturing, hydraulic fracturing and other methods. The article also presents data on the effectiveness of various methods of artificial impact on coal seams, which emphasizes the need for further improvement of these technologies to increase methane production and ensure the safety of mining operations.

CRediT author statement: **M. Rabatuly**: Conceptualization, Methodology, Software. **V. Demin**: Data curation, Writing-Original draft preparation. **A. Kenetaeva**: Visualization, Investigation. **Yu. Steflyuk**: Supervision. **J. Toshov**: Software, Validation.

Cite this article as: Rabatuly M, Demin VF, Kenetaeva AA, Steflyuk YuYu, Toshov JB. Evaluation of modern methods and techniques for calculating parameters during coal bed degassing. Kompleksnoe Ispolzovanie Mineralnogo Syra = Complex Use of Mineral Resources. 2025; 334(3):110-120. https://doi.org/10.31643/2025/6445.33

Көмір қабаттарын газсыздандыру кезінде параметрлерді есептеудің заманауи тәсілдері мен әдістерін бағалау

[1]Рабатұлы М, [1]Демин В.Ф., [1]Кенетаева А.А., [2]Стефлюк Ю.Ю., [3]Тошов Ж.Б.

[1] А. Сағынов атындағы Қарағанды техникалық университеті, Қарағанды, Қазақстан
[2]Арнайы қызмет көрсету және газсыздандыру басқармасы, Qarmet АҚ көмір департаменті, Қарағанды, Қазақстан
[3] Ислам Кәрім атындағы Ташкент мемлекеттік техникалық университеті, Ташкент, Өзбекстан

Мақала келді: *7 тамыз 2024*
Сараптамадан өтті: *8 тамыз 2024*
Қабылданды: *26 тамыз 2024*

ТҮЙІНДЕМЕ
Қарағанды бассейнінде жерасты көмір өндіруді дамытудың заманауи стратегиясы шахта қорын реформалау тұжырымдамасын әзірлеуді, тау-кен жұмыстарын шоғырландырудың және қарқындатудың жоғары деңгейін қамтамасыз етуді, жүктемені тәулігіне 5-6 мың тоннаға дейін жеткізуді көздейді. Бұл жағдайда негізгі шектеуші фактор бассейндегі көмір қабаттарының метанының жоғары болуы болып табылады, ол критикалық түрде 30 - 40 м3/т көмірге (орта есеппен 18 - 25 м3/т) жетеді. Өндірілетін көмір қабаттары мен олардың серіктерінің жоғары газдылығы кеніштердегі метан жарылысының негізгі себептерінің бірі болып, технологиялық режимнің бұзылуына және адам өліміне әкеліп соқтырады. Кен орындарын газсыздандыру мәселесі әрқашан жедел шешуді талап ететін басым бағыттардың бірі болды және болып қала береді. Газ-динамикалық құбылыстар мен метанның кенеттен бөлінуі адам өлімімен, үлкен материалдық және қаржылық шығындарға әкеледі және соңғы онжылдықта ТМД елдерінің көмір шахталарында орын алған апаттардың жалпы санының 25-30% құрайды. Мақалада осы саладағы заманауи тәжірибе мен жетістіктерді ескере отырып, метанды азайту және Қарағанды облысындағы көмір шахталарының қауіпсіз жұмысын қамтамасыз ету үшін жоғары газды, жарылу қаупі бар түзілімдерді газсыздандырудың прогрессивті тәсілдеріне баға берілді.

Түйін сөздер: метан, газ дебиті, газ бөліну, метанның көп болуы, көмір шахталары, газсыздандыру, тау-кен технологиясы, шахта алаңдары, газ-динамикалық құбылыстар, қабат.

Авторлар туралы ақпарат:

Рабатұлы Мұхаммедрахым — *PhD докторы, Әбілқас Сағынов атындағы Қарағанды техникалық университетінің Пайдалы қазбалар кенорындарын игеру кафедрасының доцент м.а., 100027, Нұрсұлтан Назарбаев 56, Қарағанды, Қазақстан. E-mail: mukhammedrakhym@mail.ru; ORCID ID: https://orcid.org/0000-0002-7558-128X*

Демин Владимир Федорович — *Техника ғылымдарының докторы, Әбілқас Сағынов атындағы Қарағанды техникалық университетінің Пайдалы қазбалар кенорындарын игеру кафедрасының профессоры, 100027, Нұрсұлтан Назарбаев 56, Қарағанды, Қазақстан. E-mail: vladfdemin@mail.ru; ORCID https://orcid.org/0000-0002-1718-856X*

Кенетаева Айгуль Акановна — *Техника ғылымдарының магистрі, Әбілқас Сағынов атындағы Қарағанды техникалық университетінің Геология және пайдалы қазбалар кен орындарын барлау кафедрасының оқытушысы, 100027, Нұрсұлтан Назарбаев 56, Қарағанды, Қазақстан. E-mail: aigul_tate@bk.ru; ORCID: https://orcid.org/0000-0001-7943-3279*

Стефлюк Юрий Юрьевич — *PhD докторы, Арнайы қызмет көрсету және газсыздандыру басқармасы, «Qarmet» АҚ көмір департаменті бас Инженері, 100012, Саран тас жолы, 10. Қарағанды, Қазақстан. E-mail: steflyuk@mail.ru; ORCID ID: https://orcid.org/0000-0002-7240-0447*

Тошов Жавохир Буриевич — *Техника ғылымдарының докторы, Ислам Карим атындағы Ташкент мемлекеттік техникалық университетінің профессоры, 100095, Алмазар ауданы Университетская көшесі 2, Ташкент, Өзбекстан. E-mail: j.toshov@tdtu.uz; ORCID ID: https://orcid.org/0000-0003-4278-1557*

Оценка современных способов и методик расчета параметров при дегазации угольных пластов

[1]Рабатұлы М, [1]Демин В.Ф., [1]Кенетаева А.А., [2]Стефлюк Ю.Ю., [3]Тошов Ж.Б.

[1] Карагандинский технический университет имени А. Сагинова, Караганда, Казахстан
[2] Управление спецшахтмонтаж дегазация, Угольный департамент АО Qarmet, Караганда, Казахстан
[3] Ташкентский государственный технический университет имени Ислама Карима, Ташкент, Узбекистан

Поступила: *7 августа 2024*
Рецензирование: *8 августа 2024*
Принята в печать: *26 августа 2024*

АННОТАЦИЯ
Современная стратегия развития подземной добычи угля в Карагандинском бассейне предусматривает развитие концепции реформирование шахтного фонда, обеспечения высокого уровня концентрации и интенсификации горных работ с доведением нагрузки на очистной забой до 5 - 6 тыс. тонн в сутки. При этом основным сдерживающим фактором является высокая метаноносность угольных пластов бассейна, которая критически достигает 30 - 40 м^3/т (в среднем 18 - 25 м^3/т) угля. Высокая газоносность разрабатываемых угольных пластов и их спутников является одной из главных причин взрывов метана на шахтах, приводящих к нарушениям технологического режима и безвозвратным человеческим жертвам. Проблема дегазации шахтных полей всегда была и стоит в ряду первоочередных направлений, требующих оперативного решения. Газодинамические явления и внезапные выделения метана сопровождаются человеческими жертвами, большими материальными и финансовыми потерями, являются на 25-30 % причиной общего числа аварий, произошедших на угольных шахтах стран СНГ в последнее десятилетие. В статье произведена оценка прогрессивных способов дегазации высокогазоносных, выбросоопасных пластов для снижения метаноносности обеспечения безопасности эксплуатации угольных шахт Карагандинского региона с учетом современного опыта и достижений в этой области.

Ключевые слова: метан, дебит газа, газоотдача, метанообильность, угольные шахты, дегазация, технология горных работ, шахтные поля, газодинамические явления, пласт.

Информация об авторах:

Рабатулы Мухаммедрахым
Доктор PhD, и.о. доцента кафедры Разработки месторождений полезных ископаемых Карагандинского технического университета имени Абылкаса Сагинова, 100027, пр. Нурсултана Назарбаева, 56, Караганда, Казахстан. E-mail: mukhammedrakhym@mail.ru; ORCID ID: https://orcid.org/0000-0002-7558-128X

Демин Владимир Федорович
Доктор технических наук, профессор кафедры «Разработки месторождений полезных ископаемых» Карагандинского технического университета имени Абылкаса Сагинова, 100027, пр. Нурсултана Назарбаева, 56, Караганда, Казахстан. E-mail: vladfdemin@mail.ru; ORCID https://orcid.org/0000-0002-1718-856X

Кенетаева Айгуль Акановна
Магистр технических наук кафедры «Геология и разведка месторождений полезных ископаемых» Карагандинского технического университета имени Абылкаса Сагинова, 100027, пр. Нурсултана Назарбаева, 56, Караганда, Казахстан. E-mail: aigul_tate@bk.ru; ORCID: https://orcid.org/0000-0001-7943-3279

Стефлюк Юрий Юрьевич
Доктор PhD, главный инженер Управление спецшахтмонтаж дегазация, Угольный департамент АО «Qarmet», 100012, Саранское шоссе, 10, Караганда, Казахстан. E-mail: steflyuk@mail.ru; ORCID ID: https://orcid.org/0000-0002-7240-0447

Тошов Жавохир Буриевич
Доктор технических наук, профессор Ташкентского государственного технического университета имени Ислама Карима, 100095, Алмазарский район улица Университетская 2, Ташкент, Узбекистан. E-mail: j.toshov@tdtu.uz; ORCID ID: https://orcid.org/0000-0003-4278-1557

References

[1] Rabatuly M, Musin RA, Demin VF, Usupaev ShE, Kenetaeva AA. Improving the efficiency of methane extraction from coal seams. Kompleksnoe Ispolzovanie Mineralnogo Syra = Complex Use of Mineral Resources. 2023; 324(1):5-11. https://doi.org/10.31643/2023/6445.01

[2] Drizhd NA, Rabatuly M, Aleksandrov AYu, Balniyazova G, Zhunis G. The results of the development of pilot wells in the sherubainurinsky site of the Karaganda coal Basin. Ugol. 2020; 6:36-40. http://dx.doi.org/10.18796/0041-5790-2020-6-36-40

[3] Demin V, Khalikova E, Rabatuly M. Research into mine working fastening technology in the zones of increased rock pressure behind the longwall face to ensure safe mining operations. Mining of Mineral Deposits. 2024; 18(1). https://doi.org/10.33271/mining18.01.027

[4] Zepeng W, Zhaolong G, Ruihui L, Haoming W, Shihui G. Effects of acid-based fracturing fluids with variable hydrochloric acid contents on the microstructure of bituminous coal: An experimental study. Energy. 2022; 244(PA):122621. https://doi.org/10.1016/j.energy.2021.122621

[5] Zou G, Zhang Q, Peng SJin C, Che Y. Influence of geological factors on coal permeability in the Sihe coal mine. 2022; 9. International Journal of Coal Science and Technology. https://doi.org/10.1007/s40789-022-00475-3

[6] Imashev A, Suimbayeva A, Zhunusbekova G, Zeitinova Sh, Kuttybayev A, Mussin A. Research into stress-strain state of the mass under open pit with a change in the open-pit bottom width. Mining of Mineral Deposits. 2022; 16(3):61-66. https://doi.org/10.33271/mining16.03.061

[7] Kenetayeva AA, Kenetayeva ZhK, Tokusheva ZhT, Rabatuly M. Methane content of coal seams of Karaganda basin. Mater. 3th internat. conf. Cognitive Robotics. Tomsk. 2018, 1-5. https://doi.org/10.1088/1757-899X/516/1/012020

[8] Petrov AA, Nikolayev NI. Rezultaty issledovaniya vliyaniya zhidkostey-razrushiteley na polimermineralnuyu filtratsionnuyu korku [Results of the study of the effect of liquid destroyers on the polymer-mineral filter cake]. Nedropolzovaniye [Subsoil use]. 2021; 21(2):58-63. (in Russ.). https://doi.org/10.15593/2712-8008/2021.2.2

[9] Solar J. Sizing the thickness of the coated insulation against methane leakage coming out of bedrock. Applied Mechanics and Materials. 2014. https://doi.org/10.4028/www.scientific.net/AMM.501-504.2327

[10] Drizhd NA, Rabatuly M, Kenetayeva AA, Steflyuk YuYu. Metody intensifikatsii gazootdachi ugolnykh plastov Gornyy zhurnal Kazakhstana. 2021; 10:8-12. https://doi.org/10.48498/minmag.2021.198.10.001

[11] Plaksin M S, Rodin R I. Improvement of degasification efficiency by pulsed injection of water in coal seam. IOP Conf. Ser.: Earth Environ. Sci. 2019; 377:012052. https://doi.org/10.1088/1755-1315/377/1/012052

[12] Maussymbayeva AD, Yurov VM, Rabatuly M, Rakhimova GM. Assessment Of The Influence Of The Surface Layer Of Coals On Gas-Dynamic Phenomena In The Coal Seam. Naukovyi Visnyk Natsionalnoho Hirnychoho Universytetu. 2024; 2. https://doi.org/10.33271/nvngu/2024-2/005

[13] Inkin O, Tishkov V, Dereviahina N, Sotskov V. Integrated analysis of geofiltrational parameters in the context of underground coal gasification relying upon calculations and modeling. Ukrainian School of Mining Engineering. 2018. https://doi.org/10.1051/e3sconf/20186000035

[14] Pat. 2022/0131.2 KZ. Sposob otsenki absolyutnoy pronitsayemosti v protsesse pri burenii skvazhin [A method for assessing absolute penetration in the process of well drilling]. Rabatuly M. Opubl. 17.02.2022, bull. 7212. (in Russ.). https://cloud.mail.ru/attaches/16554580951242976274%3B0%3B1?folder-id=0&x-email=mukhammedrakhym%40mail.ru&cvg=f

[15] Bodden WR, Ehrlichb R. Permeability of coals and characteristics of desorption tests: Implications for coalbed methane production. International Journal of Coal Geology. 1998; 1-4:333-347. https://doi.org/10.1016/S0166-5162(97)00039-6

[16] Zhang S, Tang S, Zhang D, Fan G, & Wang Z. Determination of the Height of the Water-Conducting Fractured Zone in Difficult Geological Structures: A Case Study in Zhao Gu No. 1 Coal Seam. Sustainability. 2017; 9(7):1077. https://doi.org/10.3390/su9071077

[17] Tutak M, & Brodny J. Predicting Methane Concentration in Longwall Regions Using Artificial Neural Networks. International Journal of Environmental Research and Public Health. 2019; 16(8):1406. https://doi.org/10.3390/ijerph16081406

[18] Portnov VS, Filimonov EN, Mausymbayeva AD. et al. Otsenka gazonosnosti plasta k10 v usloviyakh Sherubaynurinskogo uchastka na osnove dannykh fakticheskogo gazovydeleniya [Assessment of gas content of the K10 formation in the conditions of the Sherubaynurinsky site based on actual gas emission data]. Kompleksnoe Ispolzovanie Mineralnogo Syra = Complex Use of Mineral Resources. 2016; 2:3-10. (in Russ.). https://kims-imio.kz/wp-content/uploads/2018/03/ilovepdf_com-3-10.pdf

[19] Ma Y, Nie B, He X, Li X, Meng J, & Song D. Mechanism investigation on coal and gas outburst: An overview. International Journal of Minerals, Metallurgy and Materials. 2020; 27(7):872-887. https://doi.org/10.1007/s12613-019-1956-9

[20] Cun Zhang, Shihao Tu, Min Chen, Lei Zhang. Pressure-relief and methane production performance of pressure relief gas extraction technology in the longwall mining. Journal of Geophysics and Engineering. 2019; 14(1):77-89. https://doi.org/10.1088/1742-2140/14/1/77

[21] Kamarov RK, Akhmatnurov DR, Mussin RA, Zamaliyev NM. Setting the volume and location of the gas collectors of abandoned coal mines. Naukovyi Visnyk Natsionalnogo Hirnychoho Universytetu, Dnepropetrovsk. 2018; 2:5-11. http://www.nvngu.in.ua/jdownloads/pdf/2018/02/NVNGU02_2018_Kamarov-1.pdf

[22] Drizhd NA, Mussin RA, Alexandrov A Ju. Improving the Technology of Hydraulic Impact Based on Accounting Previously Treated Wells. International science and technology conference Earth science. IOP Conf. Series: Earth and Environmental Science. 2019; 272:022031. https://iopscience.iop.org/article/10.1088/1755-1315/272/2/022031/pdf

МАЗМҰНЫ
СОДЕРЖАНИЕ
CONTENTS

ENGINEERING AND TECHNOLOGY

METALLURGY

EARTH SCIENCES

Техникалық редакторлар:
Г.К. Қасымова, Н.М.Айтжанова, Т.И. Қожахметов

Компьютердегі макет:
Г.К. Қасымова

Дизайнер:
Г.К. Қасымова, Н.М.Айтжанова

Металлургия және кен байыту институты
050010, Қазақстан Республикасы, Алматы қаласы, Шевченко к-сі, 29/133

Жариялауға 26.08.2024 жылы қол қойылды

Технические редакторы:
Г.К. Касымова, Н.М. Айтжанова, Т.И. Кожахметов

Верстка на компьютере:
Г.К. Касымова

Дизайнер:
Г.К. Касымова, Н.М.Айтжанова

Институт металлургии и обогащения
050010, г. Алматы, Республика Казахстан. ул. Шевченко, 29/133

Подписано в печать 26.08.2024г.

Technical editors:
G.K. Kassymova, N.M. Aitzhanova, T.I. Kozhakhmetov

The layout on a computer:
G.K. Kassymova

Designer:
G.K. Kassymova, N.M. Aitzhanova

Institute of Metallurgy and Ore Benficiation
050010, Almaty city, the Republic of Kazakhstan. Shevchenko str., 29/133

Signed for publication on 26.08.2024